

**Formal and Conceptual Development of Density
Functional Theory (DFT) Based Reactivity Descriptors
and Their Applications to Understand Kinetic and
Thermodynamic Aspects of a Chemical Reaction**

THESIS

Submitted in partial fulfillment
of the requirements for the degree of
DOCTOR OF PHILOSOPHY

By

Amrit Sarmah

Under the Supervision of
Prof. Ram Kinkar Roy, Ph.D.



**BIRLA INSTITUTE OF TECHNOLOGY AND SCIENCE
PILANI (RAJASTHAN) INDIA**

2015

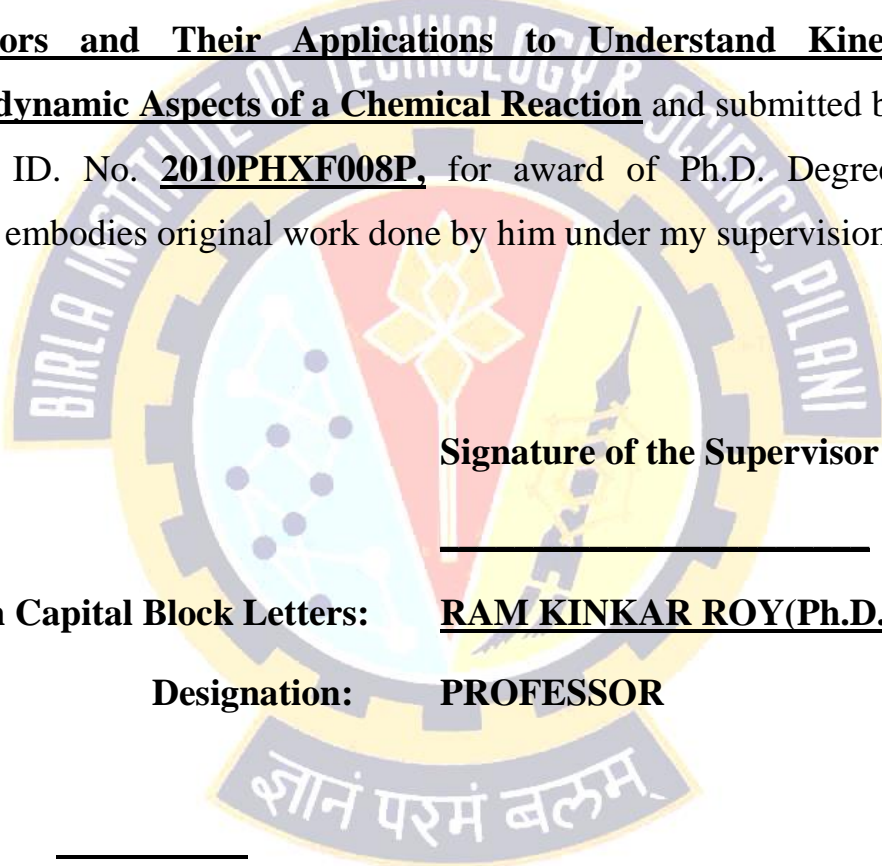


*Dedicated to My Family and
Teachers*

**BIRLA INSTITUTE OF TECHNOLOGY & SCIENCE
PILANI RAJASTHAN**

CERTIFICATE

This is to certify that the thesis entitled **Formal and Conceptual Development of Density Functional Theory (DFT) Based Reactivity Descriptors and Their Applications to Understand Kinetic and Thermodynamic Aspects of a Chemical Reaction** and submitted by **Amrit Sarmah** ID. No. **2010PHXF008P**, for award of Ph.D. Degree of the Institute, embodies original work done by him under my supervision.



Signature of the Supervisor

Name in Capital Block Letters: **RAM KINKAR ROY(Ph.D.)**

Designation: **PROFESSOR**

Date: _____

Acknowledgment

I would like to start the main body of the thesis by switching from plural to singular construction and express my gratitude to the people who provide some form of assistance in making of this work.

I would like to express my special appreciation and thanks to my supervisor Prof. Ram Kinkar Roy, for his guidance, understanding, patience, and most importantly, his tremendous mentorship.

It is an immense pleasure to acknowledge Prof. A. K. Chandra, for his creative comments and suggestions in different academic and non-academic purposes throughout the period. He is an amazing personality. I would like to thank his unbounded motivation and encouragement to fulfill my destiny and hope it will continue forever.

Many other people have taught me or played some role in my scientific education. I would like to thank members of my doctoral advisory committee, Prof. S. C. Sivasubramanian and Dr. Inamur R. Laskar for their cooperation and timely suggestions. Indeed, it is a pleasure to extend my sincere gratitude to all the faculty members of Department of Chemistry BITS Pilani, for their excellent teaching and enthusiastic corporation throughout my doctoral study.

I am grateful to all my collaborators including Prof. Subit K. Saha, Dr. Inmur R. Laskar and Dr. Chandan Mukharjee (IIT, Guwahati) for their trust and belief on our potentials.

I appreciate Vice Chancellor, Prof. B. N. Jain, Director, Prof. G. Raghurama, Dean, ARD, Prof. S. K. Verma and Associate Dean, Prof. Hemant R. Jadhav for providing the required infrastructure and research facilities.

Departmental staff members assisted me in various ways while carrying out this work. I would like to thank Pushplataji, Sardar-Ramji, Sureshji, Mahipalji, Raguveerji, Sureshji (CPU) and many others for their unconditional support.

I am thankful to past and current lab members Dr. Soumen Saha, Rituparna Bhattacharjee, Amar Singh, Captain Rituraj Singh along with all the research scholars of the Department of Chemistry specially, Dr. Amit Tiwari, Sonu, Dr. Kameshwar Rao, Dr. Manoj Kumar, Kashi, Ashok Sharma, Rajesh Bhatt for their unbounded love and

charming company. Their ready-to-help attitude and everlasting friendship will always be appreciated.

The Financial Assistance from DST-India as well as UGC-BSR Fellowship is thankfully acknowledged.

Words are inadequate to express gratitude towards my family. My parents and two brothers Alok and Amor are the source of inspiration and courage in every ups-and-down of my life. I feel proud to say that they are the finest peoples in earth. It's an opportunity to thank my in-laws, especially Priyakshi and Uddipana, bunches of wonderful peoples who provide endless support at every instance. All my relatives deserve heartfelt of thanks as they put their trust on me. These phrases will remain incomplete without mentioning the contribution of a special figure, Dr. Smritakshi Phukan Sarmah, my wife and best friend. She is the true architect behind this glory. Every achievement of this thesis is the result of her prayers, encouragement, and love.

Finally, I am thankful to the Supreme Power of Universe, almighty *God* for his/her unparalleled grace that leads me toward the ultimate goal through the lows and highs of my PhD journey. I am thankful, for your love and care.

Thank you all.

BITS Pilani

February, 2015

Amrit Sarmah

ABSTRACT

Present thesis contains Density Functional Reactivity Theory based interesting findings on some of the chemically and biologically important systems. The fundamental objective of the thesis is to introduce Comprehensive Decomposition Analysis of Stabilization Energy, CDASE (Bagaria *et al. Phys. Chem. Chem. Phys.*, 2009, **11**, 8306-8315) scheme as a cost-effective and alternative solution (to some extent) for rigorous computational studies. CDASE scheme is proposed on the argument that in a particular reactive interaction (between comparable sized donor and acceptor systems) the mutual effect of interacting species cannot be ignored while, evaluating their individual energy components.

A concise review of literature, objectives and motivation behind the present work are discussed in the initial part of the thesis. The basic foundation of Density Functional Theory (DFT) and conceptual Density Functional Theory is also revisited in the introduction chapter.

Chapter II explores the anti-cancer activity of cisplatin drug in molecular level using CDASE scheme. The interaction of cisplatin with individual nucleobases along with the two Watson-Crick base pairs were critically analyzed from the different CDASE scheme based parameters. This provides a better understanding on the specific target of cisplatin like drugs inside human cell.

Chapter III deals with the formulation of a scientific protocol (albeit qualitative) for the application of protecting agents against cisplatin drug. Through comparison of earlier experimental findings available in the literature with the CDASE scheme based theoretical results, we have tried to make a reasonable prediction on the suitable combination of cisplatin drug and the protecting agent.

Chapter IV contains an interesting application of CDASE scheme on nanoscience. The kinetic and the thermodynamic aspects of the interaction of nucleobases as well as Watson-Crick base pairs (AT and GC) with SWCNTs (Single Walled Carbon Nanotube) are evaluated on the basis of different scheme based parameters. The trend of interaction generated by reactivity parameters follow the experimentally and theoretically verified order, $G \succ A \succ T \succ C \succ U$, observed in earlier studies. Additionally, binding energy

calculations (conventional approach) are also performed on some of the chosen systems using ONIOM QM:MM approach to support the CDASE scheme based findings.

In chapter V, the effect of variation in sizes and symmetries of smaller fullerene (C_{32}) on their mode of interaction with semi-conducting SWCNT in the formation of hybrid carbon NanoBud is explored. CDASE scheme based findings along with the conventional *ab-initio* computations provides a better understanding on the energetic stability of hybrid nanostructures.

Different factors associated with the stability of interaction between gold clusters and nucleobases are assayed using density functional reactivity theory (DFRT) based CDASE scheme in chapter VI. The observed interaction trend of nucleobases with Au_n clusters found to follow the order $G \succ A \succ C \succ T \succ U$ showing convincing correlation between theoretical findings and experimental results.

The use of CDASE scheme to predict the most stable H-bonded adduct structure is a new aspect of the thesis, which we have reported in chapter VII. Urea and m-Nitrobenzoic acid are able to form stable adducts through hydrogen bonding interaction in different solvent systems. In the theoretical investigation we have picked-up the three possible orientations of adduct and use DFRT based CDASE scheme to determine the most stable H-bonded structure.

Finally, in chapter VIII the results and conclusions of the investigations presented in the earlier chapters are summarized. Areas that require further exploration are identified and accordingly, future scope of work is presented.

LIST OF ABBREVIATIONS AND SYMBOLS

α	Polarizability
A	Adenine
AT	Adenine-Thymine
BLYP	Becke exchange and Lee-Yang-Parr correlation functional
B3LYP	Becke three parameter Lee-Yang-Parr functional
χ	Electronegativity
C	Cytosine
cc-pVDZ	Correlation consistent polarized Valence Double Zeta (basis set)
cc-pVTZ	Correlation consistent polarized Valence Triple Zeta (basis set)
CDASE	Comprehensive Decomposition Analysis of Stabilization Energy
CI	Configuration Interaction
ΔE_{SE}	Stabilization energy
$G^\#$	Free energy of activation
ΔN	Electron transfer
$S^\#$	Activation entropy
DFT	Density Functional Theory
DFRT	Density Functional Reactivity Theory
DMM	Density Matrix Minimization
DNA	Deoxyribonucleic Acid
DNP	Double Numeric with Polarization
E	Energy
E_a	Activation energy
$E[\rho]$	Total electronic energy
EA	Electron Affinity
EEM	Electronegativity Equalization Method
$E_{xc}[\rho]$	Exchange correlation energy
$f(\rho)$	Fukui function
$F[\rho]$	Hohenberg Kohn universal Functional
FC	Frozen Core
FF	Fukui Function

FMM	Fast Multiple Methods
G	Guanine
GC	Guanine-Cytosine
GGA	Generalized Gradient Approximation
GTO	Gaussian Type Orbital
η	Chemical hardness
$\eta(\bar{r})$	Local hardness
$k(\eta)$	Atomic local hardness
$\eta(\bar{r}, \bar{r}')$	Hardness kernel
h	Planck's constant
$h(\bar{r})$	Hardness potential
$h(k)$	Atomic hardness potential
HIV	Human Immunodeficiency Virus
HOMO	Highest Occupied Molecular Orbital
HPA	Hirshfeld Population Analysis
HSAB	Hard and Soft Acid and Base
IP	Ionization Potential
$J(\rho)$	Coulombic interaction energy
K	Equilibrium constant
k	Rate of reaction
k_B	Boltzmann constant
LDA	Local Density Approximation
LRD	Local Reactivity Descriptors
LSDA	Local Spin Density Approximation
LUMO	Lowest Unoccupied Molecular Orbital
μ	Chemical potential
MEDLA	Molecular Electron Density Lego Assembler
MEF	Molecular Electrostatic Field
MESP	Molecular Electrostatic Potential
MPA	Mulliken Population Analysis
MPn	Møller Plesset perturbation theory of order n

MPP	Minimum Polarizability Principle
N	Total number of electrons
NOA	Natural Orbital Analysis
P_k	Gross electronic population of atom k in the molecule
PEP	Phosphoenolpyruvate
PMH	Principle of Maximum Hardness
PWC	Perdew-Wang Correlation functional
PW91	Perdew-Wang (1991) correlation functional
q_k	Effective atomic charge
QSAR	Quantitative Structure Activity Relationship
\vec{r}	Electronic position
RHF	Restricted Hartree Fock
$\rho(r)$	Electron density
ROHF	Restricted Open-shell Hartree-Fock
S	Global softness
S_N2	Bimolecular nucleophilic substitution
$s(\vec{r})$	Local softness
$s(k)$	Condensed-to-atom local softness
$s(\vec{r}, \vec{r}')$	Softness kernel
SP-DFT	Spin-Polarized Density Functional Theory
STO	Slater Type Orbital
T	Thymine
T	Temperature
$T_k(\rho)$	Electronic kinetic energy
TFD	Thomas-Fermi-Dirac theory
TS	Transition State
UHF	Unrestricted Hartree Fock
U	Uracil
w	Global electrophilicity index
$w(\vec{r})$	Local electrophilicity index
$v(\vec{r})$	External potential

$V_{ee}[\rho]$	Electron-electron repulsion energy
$v_{xc}(\vec{r})$	Exchange correlation potential
Ψ	Electronic wave function
ZPE	Zero Point Energy

Table of Contents

Certificate	
Acknowledgements	
Abstract	
List of Abbreviations and Symbols	
List of Tables	i-vi
List of figures	vii-viii
Chapter I: General Introduction	1-49
1.1. Basic Foundations of Quantum Mechanics	3
1.1.1. The Electronic Structure Problem	3
1.1.2. Born-Oppenheimer (BO) Approximation	4
1.1.3. The Hartree Approximation	5
1.1.4. Slater Determinants	5
1.1.5. The Hartree-Fock Approximation	6
1.1.6. Post-Hartree-Fock Methods	7
1.2. A Brief Overview on the Historical Development of Density Functional Theory	8
1.2.1. Thomas-Fermi-Dirac Approximation	9
1.2.2. Hohenberg-Kohn Theorem	10
1.2.3. The Kohn-Sham (KS) Ansatz	12
1.2.4. Exchange-Correlation Functionals	13
1.3 Time-dependent DFT	16
1.4 Conceptual Density Functional Theory	16
1.4.1. DFT Based Reactivity Descriptors	16
(i) Global Reactivity Descriptors	17
(ii) Theoretical treatment of qualitative concepts	20
(iii) Local Reactivity Descriptors	23
1.4.2. Electronegativity and Associated Principles	27
1.5 Comprehensive Decomposition Analysis of Stabilization Energy (CDASE) Scheme	29
1.6 Applications of Density Functional Theory: Motivation behind the Present Thesis	32
1.7 Organization of Thesis	38
References	42
Chapter II: Understanding the Preferential Binding Interaction of Aqua-cisplatin with Nucleobase Guanine over Adenine: A Density Functional Reactivity Theory Based Approach	50-69
2.1 Introduction	50
2.2 Computational Details	52
2.3 Results and Discussion	53

2.3.1 Application of CDASE scheme to understand the relative stability of adducts formed by aqua-cisplatin and purine bases	54
(i) On the basis of global electrophilicity (Δw) values	55
(ii) On the basis of positive energy component ($\Delta E_{B(A)}$) values	55
(iii) On the basis of negative energy component ($\Delta E_{A(B)}$) values	56
(iv) On the basis of charge transfer (ΔN) values	57
(v) On the basis of overall stabilization energy ($\Delta E_{SE(AB)}$) values	57
2.3.2 Identification of the Donor and Acceptor on the Basis of CDASE Scheme	57
2.4 Conclusions	58
References	61
Tables	64
Chapter III: A Density Functional Reactivity Theory (DFRT) Based Approach to Understand the Interaction of Cisplatin Analogues with Protecting Agents	70-106
3.1 Introduction	70
3.2 Implemented Computational Techniques	73
3.3 Results and Discussion	74
3.3.1 Strategy for choosing the best possible protecting agent against a particular cisplatin analogue	74
3.3.2 Interaction of different cisplatin analogues with DNA	76
3.3.3 Relative strength of interaction of protecting agents with cisplatin analogues as well as active biomolecules	79
(i) On the basis of difference in global electrophilicity (Δw) values	80
(ii) On the basis of positive energy component ($\Delta E_{B(A)}$) values	82
(iii) On the basis of charge transfer (ΔN) values	84
(iv) On the basis of negative energy component ($\Delta E_{A(B)}$) values	86
(v) On the basis of overall stabilization energy ($\Delta E_{SE(AB)}$) values	88
3.3.4 Synchronization of the data generated by different reactivity parameters and use of the strategy proposed in Sec. 3.3	89
3.4 Conclusions	90
References	93
Tables	96

Chapter IV: Understanding the Interaction of Nucleobases with Chiral Semi-conducting Single-Walled Carbon Nanotubes (SWCNTs): An Alternative Theoretical Approach Based on Density Functional Reactivity Theory (DFRT) 107-131

4.1	Introduction	107
4.2	Adopted Models and Computational Methodology	110
4.3	Results and Discussion	111
	(a) Evaluation of the five CDASE scheme based parameters in explaining interaction between nucleobases and SWCNTs	112
	(i) Role of global electrophilicity Δw values	112
	(ii) Role of positive energy component (i.e., $\Delta E_{B(A)}$)	112
	(iii) Role of charge transfer values (i.e., ΔN)	114
	(iv) Role of negative energy component (i.e., $\Delta E_{A(B)}$)	115
	(v) Role of overall stabilization energy (i.e., $\Delta E_{SE(AB)}$)	115
	(b) ONIOM (QM:MM) calculation for the interaction between SWCNT and nucleobases	117
4.4	Conclusion	119
	References	122
	Table	126

Chapter V: A DFT Based Approach to Understand the Effect of Fullerenes Symmetry on the Kinetic, Thermodynamic and Structural Properties of Carbon NanoBuds 132-162

5.1	Introduction	132
5.2	Computational Details	135
5.3	Results and Discussion	137
	(A) Kinetics and thermodynamics of NanoBud formation	137
	(a). Kinetics of NanoBud formation using CDASE based parameters	
	(i) On the basis of (Δw) values	137
	(ii) Using the positive energy component (i.e., $\Delta E_{B(A)}$)	138
	(b) Thermodynamics of NanoBud formation using CDASE based parameters	139
	(i) On the basis of charge transfer (ΔN) values	139
	(ii) On the basis of negative energy component, (i.e., $\Delta E_{A(B)}$)	140
	(iii) On the basis of overall stabilization energy, (i.e., $\Delta E_{SE(AB)}$)	141
	(B) (i) Comparison of conventional binding energy (BE) values and geometrical parameters to assess the relative stabilities of NanoBuds	142
	(ii) Synchronous transit-guided quasi-Newton (STQN) Transition State (TS) optimization of the NanoBud structures to evaluate activation energy involved in the hybrid	

nano-structure formation	146
(C) Atom Centered Density Matrix Propagation (ADMP)	
molecular dynamics simulation study on hybrid NanoBud structures	148
5.4 Conclusion	150
References	152
Tables	155
Chapter VI: Interaction Between Small Atomic Gold Clusters and Nucleobases: A Combined Theoretical Approach	163-197
6.1 Introduction	163
6.2 Computational Techniques	165
6.3 Results and Discussion	167
6.3.1 Understanding the interaction between gold-clusters and DNA bases using CDASE scheme based parameters	167
(i) Evaluation of the kinetics of interaction between gold-cluster and nucleobases	168
(a) On the basis of their difference in global electrophilicity (Δw) values	168
(b) On the basis of the values of positive energy component ($\Delta E_{B(A)}$)	169
(c) On the basis of charge transfer (ΔN) values	169
(ii) Evaluation of thermodynamics of interaction between gold-cluster and nucleobases	170
(a) On the basis of the values of the negative energy component ($\Delta E_{A(B)}$)	170
(b) On the basis of overall stabilization energy ($\Delta E_{SE(AB)}$) values	172
6.3.2 Conventional binding energy calculation for selected gold-clusters and nucleobase composite systems	173
6.3.3: Synchronous transit-guided quasi-Newton (STQN) Transition State (TS) calculation for some selected composite systems formed by gold-clusters and nucleobase	176
6.3.4: TDDFT analysis to determine the nature of electronic excitations in gold cluster-DNA composite systems	177
6.4 Conclusions	178
References	180
Tables	184
Chapter VII: On The Complimentarity of CDASE-Scheme and Supermolecular Approach	198-216
7.1 Introduction	198
7.2 Computational Details and Complementarity of CDASE Scheme and Supermolecular Approach	199
7.3 Results and Discussion	
A. Most stable structure from supermolecular approach	202

B. The most stable structure from DFT based stabilization energy	203
C. CDASE-scheme based energy components and prediction of donor and acceptor	204
7.4 Conclusion	205
References	207
Tables	209
CHAPTER VIII: SUMMARY AND CONCLUSIONS	217-224
8.1 General Conclusions	217
8.2 Specific Conclusions	218
8.3 Future Scope of Work	222
References	224

List of Publications

Brief Biography of Supervisor

Brief Biography of Candidate

List of Tables

- 2.1** The difference between the global electrophilicity values (*i.e.*, Δw) (in kcal/mol) of the chosen aqua-cisplatin and nucleobases. Three different levels of theories (HF/LanL2DZ, MP2/LanL2DZ and B3LYP/LanL2DZ for the platinum complexes and HF/6-31G(d,p), MP2/6-31G(d,p) and B3LYP/6-31G(d,p) for nucleobases) are used to generate the w values. 64
- 2.2** $\Delta E_{B(A)}$ values (in kcal/mol) corresponding to the adduct formation process between aqua-cisplatin and nucleobases. The required parameters are generated at three different levels of theories (HF/LanL2DZ, MP2/LanL2DZ and B3LYP/LanL2DZ for aqua-cisplatin and HF/6-31G(d,p), MP2/6-31G(d,p) and B3LYP/6-31G(d,p) for nucleobases) 65
- 2.3** $\Delta E_{A(B)}$ values (in kcal/mol) corresponding to the adduct formation process between aqua-cisplatin and nucleobases. The required parameters are generated at three different levels of theories (HF/LanL2DZ, MP2/LanL2DZ and B3LYP/LanL2DZ for aqua-cisplatin and HF/6-31G(d,p), MP2/6-31G(d,p) and B3LYP/6-31G(d,p) for nucleobases) 66
- 2.4** The amount of charge transferred (ΔN) in the process of adduct formation between aqua-cisplatin and nucleobases. Relevant parameters are generated at three different levels of theories (HF/LanL2DZ, MP2/LanL2DZ and B3LYP/LanL2DZ for aqua-cisplatin and HF/6-31G(d,p), MP2/6-31G(d,p) and B3LYP/6-31G(d,p) for nucleobases) 67
- 2.5** Stabilization energy values ($\Delta E_{SE(AB)}$) generated for different mode of interactions between aqua-cisplatin and nucleobases. The relevant parameters are generated at three different levels of theories (HF/LanL2DZ, MP2/LanL2DZ and B3LYP/LanL2DZ for the aqua-cisplatin and HF/6-31G(d,p), MP2/6-31G(d,p) and B3LYP/6-31G(d,p) for nucleobases) 68
- 2.6** Prediction of the direction of charge (ΔN) transfer using CDASE scheme based parameters 69
- 3.1** Five CDASE scheme based parameters namely, ΔW , $\Delta E_{B(A)}$, ΔN , $\Delta E_{A(B)}$, and $\Delta E_{SE(AB)}$ calculated for the interaction of 12 different cisplatin analogues with DNA. Method used for cisplatin analogues is B3LYP/LanL2DZ, whereas for nucleobases it is B3LYP/6-31 G(d,p) 96
- (a)** Computed CDASE scheme based parameters for the interaction between cisplatin analogues and individual purine bases adenine (A) and guanine (G) 96
- (b)** Computed CDASE scheme based parameters for the interaction between cisplatin analogues and W-C single base pair unit 98
- (c)** Computed CDASE scheme based parameters for the interaction

	between cisplatin analogues and double base pair unit	99
(d)	Computed CDASE scheme based parameters for the interaction between cisplatin analogues and triple base pair unit	100
3.2	Earlier reported experimental as well as theoretical studies which are relevant to understand the mode of interaction of some promising protecting agents (chosen in the present study) against platinum based anticancer drugs	101
3.3	The difference between global electrophilicity (ΔW) values (in kcal mol ⁻¹) for different combinations of cisplatin analogues (acceptor, A) and protecting agents (donor, B)	102
3.4	The values of the positive energy component, $\Delta E_{B(A)}$, (in kcal/mol) for different combinations of cisplatin analogues (considered as A) and protecting agents (considered as B)	103
3.5	A qualitative comparison between the experimental rate constant (k) with the computed $\Delta E_{B(A)}$ values	103
3.6	The charge transfer (ΔN) values for different combinations of chosen cisplatin analogues (considered as A) and protecting agents (considered as B)	104
3.7	The values of the negative energy component, $\Delta E_{A(B)}$ (in kcal/mol), for different combinations of cisplatin analogues (considered as A) and protecting agents (considered as B)	105
3.8	The values of the overall stabilization energy, $\Delta E_{SE(AB)}$ (in kcal/mol) for different combinations of cisplatin analogues (considered as A) and the protecting agents (considered as B)	106
4.1	The values of the global electrophilicity difference, ΔW (in kcal mol ⁻¹) for different combination of chosen SWCNTs (considered as acceptor, A) and nucleobases (considered as donor, B)	126
4.2	The values of positive energy component, $\Delta E_{B(A)}$ (in kcal mol ⁻¹) for different combination of chosen SWCNTs (considered as acceptor, A) and nucleobases (considered as donor, B)	127
4.3	CDASE scheme based charge transfer, ΔN values for different combination of chosen SWCNTs (considered as acceptor, A) and nucleobases (considered as donor, B)	128
4.4	The values of the negative energy component, $\Delta E_{A(B)}$ (in kcal mol ⁻¹) for different combination of chosen SWCNTs (considered as acceptor, A) and nucleobases (considered as donor, B)	129
4.5	The values of overall stabilization energy, $\Delta E_{SE(AB)}$ (in kcal mol ⁻¹) for different combination of chosen SWCNTs (considered as acceptor, A)	

	and nucleobases (considered as donor, B)	130
4.6	Binding Energies (kilocalories per mole) of SWCNT-Nucleobase Complexes at ONIOM (B3LYP/6-31G(d):UFF) Level of Theory	131
5.1	Difference in global electrophilicity (Δw) values (in kcal/mol) of interacting fullerenes (considered as acceptor, A) and SWCNTs (considered as donor, B). The values are calculated at the B3LYP/6-31G(d)//B3LYP/3-21G level	155
5.2	Positive energy component ($\Delta E_{B(A)}$) values (in kcal/mol) for different combinations of fullerenes (considered as acceptor, A) and SWCNTs (considered as donor, B). The values are calculated at the B3LYP/6-31G(d)//B3LYP/3-21G level.	156
5.3	Charge transfer (ΔN) values for different combinations of fullerenes (considered as acceptor, A) and SWCNTs (considered as donor, B). The values are calculated at the B3LYP/6-31G(d)//B3LYP/3-21G level.	157
5.4	Negative energy component ($\Delta E_{A(B)}$) values (in kcal/mol) for different combinations of fullerenes (considered as acceptor, A) and SWCNTs (considered as donor, B). The values are calculated at the B3LYP/6-31G(d)//B3LYP/3-21G level.	158
5.5	Overall stabilization energy ($\Delta E_{SEA(B)}$) values (in kcal/mol) for different combinations of fullerenes (considered as acceptor, A) and SWCNTs (considered as donor, B). The values are calculated at the B3LYP/6-31G(d)//B3LYP/3-21G level.	159
5.6	(a) Calculated binding energies (in kcal/mol), average bond lengths and bond angles values at the common attached site for six hybrid NanoBuds. The values are calculated through optimization at B3LYP/ 3-21G level with addition to an energy correction at B3LYP/ 6-31G (d) level.	160
	(b) Calculated binding energies (in kcal/mol), average bond lengths and bond angles values at the common attached site for six hybrid NanoBuds. The values are calculated through optimization at M06/ 3-21G level with addition to an energy correction at M06/ 6-31G (d) level.	161
5.7	Calculated STQN TS energy barrier values (in kcal/mol) for six hybrid NanoBuds generated at B3LYP and M06 level	162
5.8	Calculated relative energy values (in kcal/mol) for six isomers of C32 fullerenes generated at B3LYP/3-21G and M06/3-21G level.	162
6.1	(a). Calculated values of the global electrophilicity difference (Δw) (in kcal mol ⁻¹) for different combination of Au _n clusters (considered as acceptor, A) and nucleobases (considered as donor, B). The values are calculated at B3PW91 method using SDD basis sets for gold atoms and 6-31G(d,p) for other atoms.	184
	(b) Calculated values of the global electrophilicity difference (Δw) (in kcal mol ⁻¹) for different combination of Au _n clusters	

-
- (considered as acceptor, A) and nucleobases (considered as donor, B).
The values are calculated at M06 method using SDD basis sets
for gold atoms and 6-31G(d,p) for other atoms 184
- 6.2** (a). Values of the positive energy component, $\Delta E_{B(A)}$, (in kcal/mol)
calculated for different combination of Au_n clusters (considered as acceptor, A)
and nucleobases (considered as donor, B). The values are calculated at B3PW91
method using SDD basis sets for gold atoms and 6-31G(d,p) for other atoms.185
(b) Values of the positive energy component, $\Delta E_{B(A)}$, (in kcal/mol)
calculated for different combination of Au_n clusters (considered as acceptor, A)
and nucleobases (considered as donor, B). The values are calculated at M06
method using SDD basis sets for gold atoms and 6-31G(d,p) for other atoms.185
- 6.3** (a) Charge transfer (ΔN) values calculated for different combination
of Au_n clusters (considered as acceptor, A) and nucleobases (considered as
donor, B). The values are calculated at B3PW91 level using SDD basis
sets for gold atoms and 6-31G(d,p) for other atoms. 186
(b) Charge transfer (ΔN) values calculated for different combination
of Au_n clusters (considered as acceptor, A) and nucleobases (considered as
donor, B). The values are calculated at M06 level using SDD basis
sets for gold atoms and 6-31G(d,p) for other atoms. 186
- 6.4** (a) Values of the negative energy component, $\Delta E_{A(B)}$, (in kcal/mol)
calculated for different combination of Au_n clusters (considered as acceptor, A)
and nucleobases (considered as donor, B). Values are calculated at B3PW91 level
using SDD basis sets for gold atoms and 6-31G(d,p) for other atoms. 187
(b) Values of the negative energy component, $\Delta E_{A(B)}$, (in kcal/mol)
calculated for different combination of Au_n clusters (considered as acceptor, A)
and nucleobases (considered as donor, B). Values are calculated at M06 level
using SDD basis sets for gold atoms and 6-31G(d,p) for other atoms. 187
- 6.5** (a) Values of the overall stabilization energy, $\Delta E_{SE(AB)}$, (in kcal/mol)
calculated for different combination of Au_n clusters
(considered as acceptor, A) and nucleobases (considered as donor, B).
The values are calculated at B3PW91 level using SDD basis sets for gold atoms
and 6-31G(d,p) for other atoms. 188
(b) Values of the overall stabilization energy, $\Delta E_{SE(AB)}$, (in kcal/mol)
calculated for different combination of Au_n clusters (considered as acceptor, A)
and nucleobases (considered as donor, B). The values are calculated at
M06 level using SDD basis sets for gold atoms and 6-31G(d,p)
for other atoms. 188
- 6.6** Comparison of the CDASE scheme based stabilization energy
($\Delta E_{SE(AB)}$) values at B3PW91 method (using SDD basis sets for Au₄ clusters

	and 6-31G(d) for other atoms) with the desorption energies obtained TPD and RAIR spectroscopic techniques.	189
6.7	Computed binding energy values at B3PW91/GenECP-SDD (gold) U 6-31G (d) (DNA bases) level. The values are for the nanocomposites formed between Au ₄ and Au ₆ clusters and five nucleobases along with the two W-C base pairs.	189
6.8	Computed STQN TS energy values at B3PW91/GenECP-SDD (gold) U 6-31G+(d) (DNA bases) level. The values are for the transition states formed between Au ₄ and Au ₆ clusters with five nucleobases and also two W-C base pairs	189
6.9	Vertical excitation energies calculated for lowest singlet states of Au ₄ -nucleobase complex at B3PW91/GenECP-SDD (gold) U 6-31G+(d) (DNA bases) level.	190
6.10	Vertical excitation energies calculated for lowest singlet states in Au ₆ -DNA complex at B3PW91/GenECP-SDD (gold) U 6-31G+(d) (DNA bases) level	191
6.11	Pictorial representation of FMOs for the Au ₄ cluster-nucleobase and Au ₆ cluster-nucleobase complexes along with the major individual atomic orbital contributions to it	192
7.1	Interaction Energy values of the three probable binary (1:1) structures formed between Urea (U) and m-Nitrobenzoic acid (m-NBA) using HF/6-31G(D,P) and MP2/6-31G(D,P) methods	210
7.2	Relevant geometrical and electronic parameters of the three probable <i>H</i> – bonded structures of the binary (1:1) complex using HF/6-31G(D,P) and MP2/6-31G(D,P) methods	210
7.3	Energy values of the three probable binary (1:1) structures formed between Urea (U) and m-Nitrobenzoic acid (m-NBA) in presence of solvents	211
7.4	Charge transfer from Urea (U) to m-Nitrobenzoic acid (m-NBA) in the three probable binary (1:1) structures formed between U and m-NBA in gas phase and in presence of solvents using HF/6-31G(D,P) and MP2/6-31G(D,P) methods using supermolecular approach	212
7.5	DFT-based charge transfer (ΔN) from Urea (U) to m-Nitrobenzoic acid (m-NBA) in the three probable binary (1:1) structures formed between U and m-NBA in gas phase and in presence of solvents using Koopmanns' approximation at HF/6-31G(D,P) and MP2/6-31G(D,P) levels	213
7.6	DFT-based stabilization energy values (ΔE_{SE}) of the three probable binary (1:1) structures formed between Urea (U) and m-Nitrobenzoic acid (m-NBA) in gas phase and in presence of solvents at HF/6-31G(D,P) and MP2/6-31G(D,P) method	214

-
- 7.7** CDASE-scheme based study of the direction of charge transfer (ΔN) between Urea (U) and m-Nitrobenzoic acid (m-NBA) in the binary (1:1) structure in gas phase as well as in presence of solvents using Koopmanns' approximation. The values are generated at HF/6-31G(D,P) level 215
- 7.8** CDASE-scheme based study of the direction of charge transfer (ΔN) between Urea (U) and m-Nitrobenzoic acid (m-NBA) in the binary (1:1) structure in gas phase as well as in presence of solvents using Koopmanns' approximation. The values are generated at MP2/6-31G(D,P) level 216

LIST OF FIGURES

2.1	A probable mechanistic scheme for the hydrolysis of cisplatin and its interaction with nucleobases	51
2.2	Optimized structures of aqua-cisplatin and purine bases	53
3.1	Name and structure of different cisplatin analogues used in the present study	73
3.2	Name and structure of eight promising protecting agents considered for the present study	74
3.3	Structure of the methyl capped DNA base pairs optimized at B3LYP/6-31G(d,p) level of theory	78
3.4	Graphical representation of the difference of global electrophilicity (Δw) values for different combinations of cisplatin analogues and protecting agents.	80
3.5	Graphical representation of the values of positive energy component ($\Delta E_{B(A)}$) for different combinations of cisplatin analogues and protecting agents.	83
3.6	Graphical representation of the charge transfer (ΔN) values for different combinations of cisplatin analogues and rescue agents	85
3.7	Graphical representation of the values of negative energy component ($\Delta E_{A(B)}$) (in kcal/mol) for different combinations of cisplatin analogues and rescue agents.	87
3.8	Graphical representation of the values of overall stabilization energy ($\Delta E_{SE(AB)}$) (in kcal/mol) for different combinations of cisplatin analogues and rescue agents.	88
4.1	Optimized structure [at B3LYP/6-31G(d) level of theory] of Me-capped nucleobases and base pairs.	110
4.2	Selected higher and lower level region for the implementation of QM/MM ONIOM model calculation in the four SWCNTs	116
4.3	Geometries of the optimized structures for nucleobase-SWCNT complexes at ONIOM (B3LYP/6-31G(d):UFF) level.	117
4.4	Graphical representation of the variation in binding energy values for nucleobase-SWCNT complexes computed at ONIOM (B3LYP/6-31G(d):UFF) level.	119
5.1	Structures of six C ₃₂ fullerenes having different point group symmetries (optimized at B3LYP/6-31G(d)//B3LYP/3-21G level)	135
5.2	Hybrid NanoBud structures generated through (2+2) and (6+6) cycloaddition between SWCNT (7,5) and (7,6) with C ₃₂ fullerene	141
5.3	Three different type of sites available in C ₃₂ fullerene for 2+2 cycloaddition with SWCNT	142
5.4	Structures of the six hybrid NanoBuds generated by the attachment	

	of fullerene through its three different sites on the surface of CNT (7,5)	143
5.5	HOMO-LUMO representation of the six hybrid NanoBud structures	145
5.6	A qualitative pictorial representation of the TS energy barriers for six hybrid NanoBuds generated from STQN calculation at B3LYP/3-21G* level	148
5.7	Graphical representation of snapshots for continuous change in total energy throughout the ADMP-MD simulation (at PM3MM level) for six hybrid NanoBuds	150
6.1	Optimized structures of the gold-clusters at B3PW91/SDD level	165
6.2	Optimized structures of the methyl capped nucleobases and the W-C base pairs at B3PW91/6-31+G(d) level	166
6.3	optimized structures of the nanocomposites formed between methyle-capped nucleobases as well as W-C base pairs with Au ₄ and Au ₆ clusters. The method used is B3PW91/ [GenECP-SDD (for gold atoms)/6-31G(d)(for other atoms)].	173
7.1	Initial structures drawn in CHEM-3D program and optimized at MOPAC/AM1	200
7.2	Final optimized structures at RHF/6-31G (d, p) and further re-optimized at MP2/6-31G (d,p) level using Gaussian03 program	201

Chapter I

Introduction

1. Introduction:

The primary objective of chemical science is to explore and understand different types of reactive and non-reactive interactions. In the contemporary research it is possible to perform extensive investigation on the various aspects of chemical reactions such as progress, speed, transition state, etc. at the molecular level with the development of sophisticated experimental and theoretical techniques.^{1,2} In the last one decades or so theoretical and computational chemistry has experienced exceptional progress to complement almost all kinds of experimental studies, with a corresponding theoretical method which are intertwined and supportive to each other. In the present scenario, there exist a large number of theoretical approaches to understand the properties associated with the electronic level modulation for a particular interaction. In a particular reactive interaction, stability of the final product is the subject of fundamental interest in chemistry. Basically, the two major theoretical approaches (based on quantum mechanics) for investigating the stability of the reaction products and reaction mechanisms are the studies of energetics and reactivity descriptors. While energetic study provides the information of preferable reaction products by using the energy minimization principle as well as studying the activation energies, the reactivity descriptors provide us information about the probable site of attack by a reactant to a substrate. Thus, in one sense the studies of energetics and reactivity descriptors are complimentary to each other.

In the past few decades, a number of theoretical methodologies have been developed for the precise understanding of chemical reactivity. Among these *Ab-initio* level treatments like Frontier Molecular Orbital (FMO),^{3,4} Molecular electrostatic Potential (MEP),⁵⁻⁹ Electron Localization Function (ELF)^{10,11} etc., have been proposed and extensively used to explain the wide variety of reactions. In a similar note, introduction of empirical principles such as the hard and soft acids and bases (HSAB),¹²⁻¹⁴ Electronegativity equalization method (EEM),¹⁵⁻¹⁹ etc. also provide significant contribution to rationalize chemical phenomena. However, with the development of powerful and sophisticated computer hardware the empirical nature of the approaches need a major upgradation to become a worthy theoretical tool. To uphold the expectations of theoretical chemists a branch of Density Functional Theory (DFT),²⁰⁻³² called

“Conceptual DFT (CDFT)” or “Chemical Reactivity Theory” or Density Functional Reactivity Theory (DFRT), was initiated by Robert G. Parr. This initiative leads to a completely different way of understanding chemical interactions through certain specifically designed parameters based on both chemical and physical consequences. The initial works of Parr and co-workers, and later stage a large community of theoretical chemists provided significant contribution to develop theoretical foundation for formal definitions of empirical concepts.³³⁻⁴³ Conceptual DFT devised an effective quantitative principle to predict the most stable state of a chemical system termed as ‘principle of maximum hardness’ (PMH).⁴⁴⁻⁵³

The computational advantage of DFT originates with the fact that the electron density has three spatial coordinates, regardless of the number of electrons in the chemical system. The main idea of DFT is to describe a many-body interacting system via its particle density and not via its many-body wavefunction. Its significance is to reduce the $3N$ degrees of freedom of the N -body system to only three spatial coordinates through its particle density. This significantly reduces the computational cost for a particular calculation. Thus, DFT allows the calculation of structures and properties for even large molecular systems. Not only does DFT provide computational advantages over wavefunction based theory, but also readily defines the parameters such as electronegativity, hardness, softness etc. and reactivity indices such as the Fukui function, frontier orbitals, etc., which are always of interest to chemists. Over the past two decades, DFT has been the most successful and widely used *Ab-initio* method in the areas like quantum chemistry, condensed-matter physics, and computational physics, etc. In many cases, the results of DFT calculations for various chemical and biological systems agreed quite satisfactorily with experimental data, especially with better approximations for the exchange correlation energy functional since the 1990s. In fact, in the present scenario specific theoretical findings are becoming a potential lead to setup and design a particular experiment. Also, the computational costs are relatively low compared to traditional ways which were based on the complicated many-electron wavefunction, such as Hartree-Fock theory^{54,55} and its descendants such as Moller-Plesset perturbation theory,⁵⁶ Coupled Cluster Method,⁵⁷ etc.

The objective of the research work presented herein is to study kinetic and thermodynamic aspects associated with a particular reactive interaction using density functional reactivity theory. In this exploratory process, the fundamental of quantum mechanics has been discussed initially (Section 1.1). The basic foundation of DFT is elaborated in Section 1.2. Section 1.3 consists of a short review on the contemporary development of Conceptual DFT. In Section 1.4, we describe more recent developments enabling evaluation of the structural stability of the product formed during a reactive interaction. A systematic orientation of the thesis is presented at the end of this introductory chapter.

1.1 Basic foundation of Quantum Mechanics:

In this thesis, we have proposed a systematic study to investigate the development and application of Conceptual Density Functional Theory based reactivity descriptors. We have tried to provide some new insights on few interesting chemical interactions through a conceptual DFT based study with the additional support from conventional DFT. The research work is an attempt to understand the thermodynamic, kinetic and electronic aspects of different reactive interactions between chemical and biological systems. Therefore, it is important to dedicate a brief discussion on different approaches that allow us to model such complex systems.

1.1.1 The Electronic Structure Problem

A major goal of electronic structure calculations is to solve the non-relativistic time-independent Schrodinger equation,⁵⁸

$$\hat{H}\Psi = E\Psi \quad 1.01$$

where \hat{H} is the Hamiltonian for a system consisting of M nuclei and N electrons which are described by position vectors R_A and r_i , respectively. The distance between the i-th electron and the A-th nucleus is $r_{iA} = |r_i - R_A|$; The distance between i-th and j-th electron is $r_{ij} = |r_i - r_j|$, and the distance between the A-th nucleus and B-th nucleus is $R_{AB} = |R_A - R_B|$. In atomic units (energy in Hartree and length in Bohr), \hat{H} can be expanded as:

$$\hat{H} = - \sum_{i=1}^N \frac{1}{2} \nabla_i^2 - \sum_{A=1}^M \frac{1}{2M_A} \nabla_A^2 - \sum_{i=1}^N \sum_{A=1}^M \frac{Z_A}{r_{iA}} + \sum_{i=1}^N \sum_{j>i}^N \frac{1}{r_{ij}} + \sum_{A=1}^M \sum_{B>A}^M \frac{Z_A Z_B}{R_{AB}} \quad 1.02$$

In the above equation, M_A is the ratio of the mass of nucleus A to the mass of an electron and Z_A is the atomic number of nucleus A. The ∇_i^2 and ∇_A^2 are the Laplacian operators. The first two terms in Eq. (1.02) are for the kinetic energy of the electrons and the nuclei, respectively. The third term represents the Coulomb attraction between electrons and nuclei. The fourth and fifth terms represent the repulsion between electrons and between nuclei, respectively.

1.1.2 Born-Oppenheimer (BO) Approximation:

The Born-Oppenheimer approximation⁵⁹ plays a vital role in electronic structure calculations. The underlying rationalization of this approximation is that the mass of nuclei are much heavier than electrons. Even for the lightest nucleus, a proton, its mass is approximately 1800 times larger than the electron. Thus in most cases the nuclei move much more slowly than electrons. Hence, in many cases, one can consider the electrons are moving in a field produced by the fixed nuclei. This is the qualitative rationalization to separate the movement of electrons and nuclei. Under the Born-Oppenheimer approximation, the second term in Eq. (1.02) is neglected, and the final term, the repulsion between nuclei, can be treated as a constant for a fixed configuration of the nuclei. The remaining terms in Eq. (1.02) are called the electronic Hamiltonian, (\hat{H}_{elec})

$$\hat{H}_{elec} = - \sum_{i=1}^N \frac{1}{2} \nabla_i^2 - \sum_{i=1}^N \sum_{A=1}^M \frac{Z_A}{r_{iA}} + \sum_{i=1}^N \sum_{j>i}^N \frac{1}{r_{ij}} \quad 1.03$$

The solution to a Schrodinger equation involving the electronic Hamiltonian,

$$\hat{H}_{elec} \Psi_{elec} = E_{elec} \Psi_{elec} \quad 1.04$$

is the electronic wave function,

$$\Psi_{elec} = \Psi_{elec}(r_i, R_A) \quad 1.05$$

which describes the motion of the electrons and explicitly depends on the electronic coordinates (r_i) but parametrically on the nuclear coordinates (R_A).

The difficulties in solving Eq. (1.05) lies in the electron-electron interaction, $\frac{1}{r_{ij}}$, which includes all the quantum effects of the electrons. Despite the intractable nature of these interactions, many approximate methods have been developed to solve Schrodinger-like equations. However, the Slater determinant will be introduced first due to its fundamental role in many aspects of electronic structure theory.

1.1.3 The Hartree Approximation:

Hartree-Fock (HF) method⁶⁰ is a major breakthrough in the context of solving the electronic Schrodinger equation that results from the time-independent Schrodinger equation after invoking the Born-Oppenheimer approximation. Hartree-Fock approximation often paves the way toward more accurate calculations in modern quantum chemistry.

Basically, we know how to solve the electronic problem for the simplest atom, hydrogen, which has only one electron. We imagine that perhaps if we added another electron to hydrogen, to obtain H^- , then it might be reasonable to start of pretending that the electrons don't interact with each other (i.e., that $V_{ee} = 0$). If that was true, then the Hamiltonian would be separable, and the total electronic wavefunction $\Psi(r1; r2)$ describing the motions of the two electrons would just be the product of two hydrogen atom wavefunctions (orbitals), $\Psi_H(r1) \Psi_H(r2)$.

Obviously, without considering the electronic repulsions, it becomes a very crude approximation. However, we have to take the initiative somewhere, and it seems that best plausible way to start with a wavefunction of the general form

$$\Psi_{HP}(r_1, r_2, \dots, r_N) = \phi_1(r_1)\phi_2(r_2) \dots \phi_N(r_N) \quad 1.06$$

which is known as a Hartree Product.

The functional form of the Hartree product wave function has a major drawback: it fails to satisfy the antisymmetry principle, which states that a wavefunction describing fermions should be antisymmetric with respect to the interchange of any set of space-spin coordinates.

1.1.4 Slater Determinants:

Electrons are fermions and has to obey the Pauli exclusion principle. According to this the wave function of electrons should be antisymmetric with respect to the interchange of the coordinates x of any two electrons,

$$\Phi(X_1, \dots, X_i, \dots, X_j, \dots, X_N) = -\Phi(X_1, \dots, X_j, \dots, X_i, \dots, X_N) \quad 1.07$$

Slater determinants nicely satisfy this antisymmetric condition through an appropriate linear combination of Hartree products, which are the non-interacting electron wave functions. For example, in a two electron case if we put electron one in χ_i and electron two in χ_j , we will have,

$$\Phi_{12}(x_1, x_2) = \chi_i(x_1)\chi_j(x_2) \quad 1.08$$

Again, if we put electron one in χ_j and electron two in χ_i we will have,

$$\Phi_{21}(x_1, x_2) = \chi_i(x_2)\chi_j(x_1) \quad 1.09$$

By taking the linear combination of Eq. 1.08 and Eq. 1.09,

$$\Phi(x_1, x_2) = 2^{-1/2}[\chi_i(x_1)\chi_j(x_2) - \chi_i(x_2)\chi_j(x_1)] \quad 1.10$$

Where, $2^{-1/2}$ is the normalization factor. It is seen that the antisymmetry has been retained by interchanging coordinates of the electrons:

$$\Phi_{12}(x_1, x_2) = -\Phi_{21}(x_2, x_1) \quad 1.11$$

It is possible to express the antisymmetric wave function of Eq. (1.10) in a determinant form,

$$\Phi(x_1, x_2) = 2^{-1/2} \begin{vmatrix} \chi_i(x_1) & \chi_j(x_1) \\ \chi_i(x_2) & \chi_j(x_2) \end{vmatrix}$$

and this is called Slater determinant.⁶¹

1.1.5 The Hartree-Fock Approximation:

The Hartree-Fock method⁶⁰ is a very first attempt to approximately solve the electronic Schrodinger equation, assuming that the wavefunction can be approximated by a single Slater determinant made up of single spin orbital per electron. We know that the Slater determinant with the lowest energy is as close as we can get to the true wavefunction for the assumed functional form of a single Slater determinant. The Hartree-Fock method determines the set of spin orbitals, which minimize the energy and give us this best single determinant.

It is necessary to minimize the Hartree-Fock energy expression with respect to changes in the orbitals $\chi_i \rightarrow \chi_i + \delta\chi_i$. Through variational procedure, we try to ensure

that χ is orthonormal. This can be obtained using Lagrange's method of undetermined multipliers, where we assume a functional \mathcal{L} defined as

$$\mathcal{L}[\{\chi_i\}] = E_{HF}[\{\chi_i\}] - \sum_{ij} \epsilon_{ij} (\langle i|j \rangle - \delta_{ij}) \quad 1.12$$

where ϵ_{ij} are the undetermined Lagrange multipliers and $\langle i|j \rangle$ is the overlap between spin orbitals i and j , i.e.,

$$\langle i|j \rangle = \int \chi_i^*(x) \chi_j(x) dx \quad 1.13$$

Setting the first variation $\mathcal{L} = 0$, and working through some algebra, we eventually arrive at the Hartree-Fock equations defining the orbitals:

$$\begin{aligned} h(x_1) \chi_i(x_1) + \sum_{j \neq i} \left[\int dx_2 |\chi_j(x_2)|^2 r_{12}^{-1} \right] \chi_i(x_1) - \sum_{j \neq i} \left[\int dx_2 \chi_j^*(x_2) \chi_i(x_2) r_{12}^{-1} \right] \chi_j(x_1) \\ = \epsilon_i \chi_i(x_1) \end{aligned} \quad 1.14$$

where ϵ_i is the energy eigenvalue associated with orbital χ_i .

The Hartree-Fock equations can be solved either numerically (exact Hartree-Fock), or they can be solved in the space spanned by a set of basis functions (Hartree-Fock-Roothan equations). In both cases, the solutions depend on the orbitals. Hence, it is important to guess some initial orbitals and then refine our guesses iteratively. Due this reason, Hartree-Fock is known a self-consistent-field (SCF) approach.

1.1.6 Post-Hartree-Fock Methods:

The major inconvenience in the Hartree-Fock method is the complete ignorance of correlations between electrons with opposite spin (beyond exchange). Following Lowdin⁶², it is very common to define the energy associated with the missing electron correlation energy as:

$$E_{corr} = E_{exact} - E_{HF} \quad 1.15$$

where, E_{exact} is the exact energy of the system and E_{corr} is thus the missing energy associated with correlations in the exact many body ground state wave function. E_{corr} should be negative as E_{HF} is always the upper bound of the E_{exact} . The missing correlation energy is typically a very small fraction of the total energy. However, it has significant contribution to many systems of physical and chemical interest. For example, the restricted Hartree-Fock method cannot describe the dissociation of H_2 into two open-

shell H atoms. Alternatively, almost one fourth of the strength of hydrogen bonds between water molecules comes from correlations beyond HF.⁶³

Post-Hartree-Fock methods in quantum chemistry aim to improve on Hartree-Fock by taking account of electron correlation. These methods include configuration interaction (CI),⁶⁴ Moller-Plesset perturbation theory,⁶⁵ and coupled cluster.⁶⁶ In CI methods, a linear combination of Slater determinants rather than one single Slater determinant (as used in Hartree-Fock) is used to approximate the wave function. Moller-Plesset perturbation theory, as the name suggests, treats electron correlation in perturbative way. Whereas, in coupled cluster method, the electron correlation is handled through use of a so-called cluster operator.

1.2 A Brief Overview on the Historical Development of Density Functional Theory:

In the preceding section, we have discussed different ways to approximately solve the electronic Schrodinger equation such as the Hartree-Fock method. The similarity between different approximation methods is that they all rely on the many body wave function as a central quantity. Indeed, once the wave function is known, it is possible to determine the energy and all related properties of the system. However, the wave function itself is a complicated quantity as it depends on $3N$ spatial variables together with the spin variable, where N is the number of electrons in the system. This severe drawback limits the system sizes that can be treated with wave function based methods. Certainly, systems with tens of thousands of atoms and relatively large basis sets are beyond reach for most practical studies with wave function based methods.

Density Functional Theory (DFT)⁶⁷ differs from the wave function based methods by using the electron density ($\rho(r)$) as the central quantity. The advantage of using the electron density over the wave function is the much-reduced dimensionality. Regardless of the number of electrons in the system, the density is always three-dimensional. This enables DFT to be applied to much larger systems, hundreds or even thousands of atoms become possible. Partly for this reason, DFT has become the most widely used electronic structure approach today. In this section, we will discuss the basic foundation of DFT.

Authoritative and comprehensive discussions of DFT can be found in wide ranges of excellent review articles.⁶⁸⁻⁷⁰

1.2.1 Thomas-Fermi-Dirac Approximation

The history of using the electron density rather than the wave function begins with the early work of Thomas and Fermi.^{71,72} First, let us define the electron density,

$$\rho(r) = N \int \dots \int |\Psi(x_1, x_2, \dots, x_N)|^2 dx_1 dx_2 \dots x_N \quad 1.16$$

$\rho(r)$ determines the probability of finding any of the N electrons within the volume r but with arbitrary spin while the other $N - 1$ electrons have arbitrary positions and spin in the state represented by Ψ . This is a nonnegative simple function of three variables, x , y , and z , integrating to the total number of electrons,

$$\int \rho(r) dr = N \quad 1.17$$

In Thomas-Fermi theory, the kinetic energy of electrons are derived from the quantum statistical theory based on the uniform electron gas, but the interaction between electron-nucleus and electron-electron are treated classically. Within this model, the kinetic energy of the electrons is defined as,

$$T[\rho] = C_F \int \rho^{5/3}(r) dr \quad 1.18$$

with

$$C_F = \frac{3}{10} (3\pi^2)^{2/3} = 2.871 \quad 1.19$$

From the above equation, the approximation is made that the kinetic energy only of the electron depends exclusively on the electron density. By adding the interaction between electron-nucleus and electron-electron into Eq. (1.18), a total energy in terms of electron density is obtained,

$$E_{TF}[\rho(r)] = A_1 \int \rho(r)^{5/3} dr + \int \rho(r) V_{\text{ext}}(r) dr + \frac{1}{2} \iint \frac{\rho(r)\rho(r')}{|r - r'|} dr dr' \quad 1.20$$

The second and third terms are the electron-nucleus and electron-electron interactions, respectively.

The importance of this simple Thomas-Fermi model is not how well it performs in computing the ground state energy and density but more as an illustration that the energy can be determined purely using the electron density.

1.2.2 Hohenberg-Kohn Theorem

Modern density-functional theory was born in 1964 with the paper of Hohenberg and Kohn.⁷³ The two key results of this paper are:

- (i) *a one to one mapping between external potential and electron density was established;*
- (ii) *it was shown that the ground state density can be found by using a variational principle.*

The first part was proved in a simple and extremely elegant manner using the principle of *reductio ad absurdum* (i.e., a method of disproving a proposition by showing that its inevitable consequences would be absurd), and this is derived for a non-degenerate system. Suppose there is a collection of electrons enclosed into a box influenced by an external potential $v(r)$. It is assumed that we know the electron density of this system and it also determines $v(r)$ and thus all properties. If there is another external potential $v'(r)$ which differs from $v(r)$ by more than a constant that can also give the same electron density $\rho(r)$ for the ground state, then there will be two different Hamiltonians \hat{H} and \hat{H}' whose ground state electron density is the same but the normalized wave function Φ and Φ' would be different. In that instance we will have,

$$\begin{aligned} E_0 &< \langle \Phi' | \hat{H} | \Phi' \rangle = \langle \Phi' | \hat{H}' | \Phi' \rangle + \langle \Phi' | \hat{H} - \hat{H}' | \Phi' \rangle \\ &= E'_0 + \int \rho(r) [v(r) - v'(r)] dr \end{aligned} \quad 1.21$$

where E_0 and E'_0 are the ground-state energies for \hat{H} and \hat{H}' , respectively. Similarly, we can get,

$$\begin{aligned} E'_0 &< \langle \Phi | \hat{H}' | \Phi \rangle = \langle \Phi | \hat{H} | \Phi \rangle + \langle \Phi | \hat{H}' - \hat{H} | \Phi \rangle \\ &= E_0 - \int \rho(r) [v(r) - v'(r)] dr \end{aligned} \quad 1.22$$

Adding Eq. 1.21 and 1.22,

$$E_0 + E'_0 < E'_0 + E_0 \quad 1.23$$

This is an obvious contradiction. So there are no two different external potentials that can give the same $\rho(r)$. Thus $\rho(r)$ uniquely determines $v(r)$ and all ground-state properties.

Now it is possible to write the energy E explicitly as a function of the electron density $\rho(r)$:

$$\begin{aligned} E[\rho] &= T[\rho] + T_{ne}[\rho] + V_{ee}[\rho] \\ &= \int \rho(r)v(r)dr + F_{HK}[\rho] \end{aligned} \quad 1.24$$

where,

$$F_{HK}[\rho] = T[\rho] + V_{ee}[\rho] \quad 1.25$$

It is worth mentioning here that $F_{HK}[\rho]$ is only dependent on ρ and independent from any external potential $v(r)$. Thus $F_{HK}[\rho]$ is a universal functional of ρ .

The second Hohenberg-Kohn theorem demonstrates that the ground state energy can be obtained variationally, with the density that minimizes the total energy being the exact ground state density. This is expressed as:

$$E_0[\rho_0] \leq E_v[\rho] \quad 1.26$$

where $E_v[\rho]$ is the energy functional of Eq. (1.24). Following from the first part of the theorem, suppose the ground state wave function is Φ and its related electron density is ρ . Thus the ρ uniquely defined the external potential $v(r)$. If there is another wave function Φ' with an arbitrary variation from Φ and its electron density is ρ' , then we can obtain,

$$\langle \Phi' | \hat{H}' | \Phi' \rangle = \int \rho'(r)v(r)dr + F_{HK}[\rho'] = E[\rho'] \geq E[\rho] \quad 1.27$$

So the energy will reach the minimum providing the electron density is the ground-state electron density.

Although HK theorems put particle density $\rho(r)$ as the basic variable, it is still impossible to calculate any property of a system because the universal functional $F[\rho(r)]$ is unknown. This difficulty was overcome by Kohn and Sham⁷⁴ in 1965, who proposed the well known Kohn-Sham ansatz.

1.2.3 The Kohn-Sham (KS) Ansatz

It is the Kohn-Sham (KS) ansatz⁷⁴ that puts Hohenberg-Kohn theorems into practical use and makes DFT calculations possible with even a single personal computer. This is part of the reason that DFT became the most popular tool for electronic structure calculations. The KS ansatz was so successful that Kohn was honored with the Nobel Prize in chemistry in 1998.

From the Hohenberg-Kohn theorem, the ground-state energy of a particular system can be determined by minimizing the energy functional,

$$E[\rho] = \int \rho(r)v(r)dr + F_{HK}[\rho] \quad 1.28$$

Kohn and Sham recognized that the principle failure of Thomas-Fermi theory basically resulted from the bad description of the kinetic energy. To encounter this problem they decided to re-introduce the idea of one-electron orbitals and approximate the kinetic energy of the system by the kinetic energy of non-interacting electrons. This establishes the basic foundation of Kohn-Sham DFT which is the one-electron Schrodinger-like equation expressed as:

$$\left(-\frac{1}{2}\nabla^2 + v(r) + \int \frac{\rho(r')}{|r-r'|} dr' + v_{xc}(r)\right)\phi_i = \varepsilon\phi_i \quad 1.29$$

Here ϕ are the Kohn-Sham orbitals and the electron density is expressed by,

$$\rho(r) = \sum_i^N |\phi_i|^2 \quad 1.30$$

The terms on the left side of Eq. (1.29) are the kinetic energy of the non-interacting reference system, the external potential, the Hartree potential, and exchange-correlation potential, respectively. The ε is the energy of the Kohn-Sham orbital. In addition, the exchange-correlation potential can be expressed as:

$$v_{xc}(r) = \frac{\delta E_{xc}[\rho]}{\delta \rho(r)} \quad 1.31$$

Here, $E_{xc}[\rho]$ is the exchange-correlation functional. Furthermore, we can define an effective potential (v_{eff}) which is,

$$v_{eff} = v(r) + \int \frac{\rho(r')}{|r-r'|} dr' + v_{xc}(r) \quad 1.32$$

From this we can write the Eq. 1.29 in more compact form,

$$\left(-\frac{1}{2}\nabla^2 + v(r) + v_{eff}\right)\phi_i = \varepsilon\phi_i \quad 1.33$$

This indicates, Hartree-Fock like single particle equation, which requires to be solved iteratively. Finally, the total energy can be determined from the resulting density through

$$E = \sum_i^N \varepsilon_i - \frac{1}{2} \iint \frac{\rho(r)\rho(r')}{|r-r'|} dr dr' + E_{xc}[\rho] - \int v_{xc}(r)\rho(r)dr \quad 1.34$$

Equations (1.33), (1.30), and (1.31) are the celebrated Kohn-Sham equations. Note that the v_{eff} depends on $\rho(r)$ through Eq. (1.32). Henceforth the Kohn-Sham equation must

be solved self-consistently. Initially the computation begins with an initial guess of the electron density, construct the v_{eff} from Eq. (1.32), and then determine the Kohn-Sham orbitals. Based on these orbitals, a new density is obtained from Eq. (1.30) and the cycle is continued until convergence is achieved. Finally, the total energy of the system will be calculated from Eq. (1.34) with the final electron density. If each term in the Kohn-Sham energy functional was known, we would be able to obtain the exact ground state density and total energy. Unfortunately, there is one unknown term, the exchange-correlation (xc) functional (E_{xc}). E_{xc} includes the non-classical aspects of the electron-electron interaction along with the component of the kinetic energy of the real system different from the fictitious non-interacting system. Since E_{xc} is not known exactly, we have to make necessary assumption to approximate it.

1.2.4 Exchange-Correlation Functionals

“Density functional theory is in principle exact! But, in practice approximations have to be made.”

Prof. W. Kohn

Oct. 14, 1997

Laboratoire de Chimie Theorique

Universite Pierre et Marie Curie

Paris, France

The KS ansatz successfully maps the original interacting many-body system onto a set of independent single-particle equations and makes the problem much easier. In the meantime, without knowing the exact form of the exchange-correlation energy functional $E_{XC}[\rho(r)]$,⁷⁵ the KS equations are unsolvable. Although the exact exchange-correlation energy functional $E_{XC}[\rho(r)]$, should be very complicated, simple but successful approximations to it have been made, which not only predict various properties of many body systems reasonably well but also greatly reduce computational costs, leading to the wide use of DFT for electronic structure calculations.⁷⁶

(a) The Local-Density Approximation (LDA): This is simplest approximation, and can be written as

$$E^{xc-LDA}[\rho(r)] = \int \rho(r) \varepsilon^{xc-unif}(\rho(r)) d(r) \quad 1.35$$

where $\varepsilon^{xc-unif}$ is the exchange-correlation energy per particle of the homogeneous electron gas of density $(\rho(r))$, i.e. the exchange-correlation energy density is taken to be that of a uniform electron gas of the same density. The exchange energy is known exactly and the correlation energy is obtained by fitting to the many-body studies of Gell-Mann and Brueckner and Ceperly and Alder.^{77,78} Modern LDA functionals tend to be exceedingly similar, differing only in how their correlation contributions have been fitted to the many-body free electron gas data. The Perdew-Zunger (PZ)⁷⁹, Perdew-Wang (PW)⁸⁰, and Vosko-Wilk-Nusair (VWN)⁸¹ functionals are all common LDA functionals. Strictly, the LDA is valid only for slowly varying densities. Indeed LDA works surprisingly well and much current understanding of metal or semiconductor (Si or GaAs) surfaces comes from LDA simulations. A partial rationalization of the success of LDA is provided by the observation that it satisfies a number of so-called sum rules.⁸²⁻⁸⁵

(b) The Generalized Gradient Approximation (GGA): These are the second generation functionals in which the gradient of the density, $\nabla\rho(r)$, at each coordinate is taken into account as well as the density itself:

$$E^{xc-GGA}[\rho(r)] = \int \rho(r) \varepsilon^{xc-unif}(\rho(r)) \nabla\rho(r) d(r) \quad 1.36$$

Thus GGAs are "semi-local" functionals, comprising corrections to the LDA while (again) ensuring consistency with known sum rules. For many properties, for example geometries and ground state energies of molecules, GGAs can yield better results than the LDAs. Although for the properties of metals and their surfaces, GGA results are not necessarily superior to LDA results. The most widely used GGAs in surface physics are the PW91⁸⁶ functional, and its close relative PBE.⁸⁷

(c) The Meta-GGAs: These are the third generation functionals (third rung of Jacob's ladder) and use the second derivative of the density, $\nabla^2\rho(r)$, and or kinetic energy densities, $\tau_\sigma(\rho(r)) = 1/2 \sum_i |\nabla\phi_i|^2$, as additional degree of freedom. In gas phase studies of molecular properties meta-GGAs, such as the TPSS⁸⁸ functional have been shown to offer improved performance over LDAs and GGAs. However, aside from some benchmark studies of bulk materials and jellium surfaces, these functionals have not yet been exploited largely in the solid state.

(d) The Hybrid Functionals: These fourth generation functionals add “exact exchange” from Hartree-Fock theory to some conventional treatment of DFT exchange and correlation. The most widely used, particularly in the quantum chemistry community, is the B3LYP^{89,90} functional which employs three parameters, a_{1-3} (determined through fitting to experiment) to control the mixing of the HF exchange and density functional exchange and correlation. It takes the following form:

$$E^{xc} = E^{x-LDA} + a_1(E^{x-HF} - E^{x-LDA}) + a_2\Delta E^{x-GGA} + a_3\Delta E^{c-GGA} \quad 1.37$$

Reformulating this to eliminate two parameters leads to an equation of the form

$$E^{xc} = E^{x-GGA} + a(E^{x-HF} - E^{x-GGA}) \quad 1.38$$

and setting $a = 1/4$ (based on the grounds of perturbation theory⁹¹) leads to a class of functionals with only as many parameters as their underlying GGAs. If PBE is the GGA used in Eq. (1.37) we arrive at the hybrid PBE0 functional.⁹² Another popular hybrid functional worth mentioning here is BH&HLYP,⁹³ which has 50% Hartree-Fock exchange. Such functionals have been shown to offer noticeably improved performance over LDA and GGA functionals for the calculation of gas phase properties of molecules and band gaps in solids.

1.3 Time-dependent DFT:

The many-electron wavefunction of a nonrelativistic many-electron system in a time-dependent external potential $v(r, t)$ must satisfy the time-dependent Schrödinger equation,

$$\hat{H}(t)\Psi(r_1\sigma_1, r_1\sigma_1, \dots \dots \dots r_N\sigma_N) = i\frac{\partial}{\partial t}\Psi(r_1\sigma_1, r_1\sigma_1, \dots \dots \dots r_N\sigma_N, t) \quad 1.39$$

where the time-dependent Hamiltonian takes the form,

$$\hat{H}(t) = -\frac{1}{2}\sum_i \nabla_i^2 + \frac{1}{2}\sum_{i \neq j} \frac{1}{|r_i - r_j|} + \sum_i v(r_i, t) \quad 1.40$$

In the stationary case, we have the kinetic energy operator \hat{T} , the Columbic electron-electron interaction energy operator \hat{W} , and the potential energy operator $\hat{V}(t)$ of the electrons in the time-dependent potential $v(r, t)$. In 1984 Runge and Gross⁹⁴ derived the analog of the Hohenberg-Kohn theorem for time-dependent systems by establishing a one-to-one mapping between time-dependent densities and time-dependent potentials for a given initial state.

1.4 Conceptual Density Functional Theory

In the late 1970s and early 1980s an additional branch of DFT has been emerged termed as “conceptual DFT” by its protagonist, Robert G. Parr.³⁶ Concentrating on the basic principle of DFT, i.e., the electron density is the fundamental quantity for describing atomic and molecular ground states, Parr and co-workers, and later on a large community of theoretical chemists (physicists also), were able to provide sharp definitions for some of the fundamental chemical concepts those are well known and had been in use for many years in various branches of chemistry (electronegativity being the most prominent example), thus affording their calculation and quantitative use. “Conceptual DFT”^{36,40,43} concentrates on the extraction of chemically relevant concepts and principles from DFT. The central quantities of Conceptual DFT are the so called response functions or reactivity descriptors.^{14,33-50}

1.4.1 DFT Based Reactivity Descriptors:

The fundamental response functions are divided into three categories: global, local, and nonlocal. The global quantities describe global responses against global perturbations. Such quantities do not depend on the spatial position \vec{r} within the molecular framework, but characterize the entire system as an entity. Hence, they do not contain any information about regioselectivity. The local descriptors (i.e., \vec{r} dependent) are associated to global/local responses of the system against local/global perturbations. These quantities are therefore suitable to describe the molecular selectivity because they vary locally from one position to another in a molecule. Therefore, the local reactivity descriptors are key in making predictions about regioselectivity. The nonlocal indices (i.e., quantities depending of two or more spatial positions, \vec{r} , \vec{r}' , etc.) are associated to local responses as a result of local perturbations. Nonlocal reactivity descriptors either measure a molecule’s polarization with respect to its environment or the change in polarization associated with electron transfer. All these descriptors provide us a status to understand experimental observations in an elegant way.

(i) Global Reactivity Descriptors:

Electronegativity^{92,95} and hardness⁹⁸ are the two important global reactivity descriptors. In order to understand the nature of the chemical bonds, Pauling⁹² first

defined the electronegativity as “the power of an atom in a molecule to attract electrons to itself”. When there is a difference in the electronegativity values of atoms forming a molecule, there will be a flow of electrons.⁹²⁻⁹⁴ Because electronegativity is not a experimental observable, there are various definitions⁹⁵ of it having respective merits and demerits.

A quantum thermodynamic definition of electronegativity has been provided by Gyftopoulos and Hatsopoulos⁹⁶ by considering the atom or molecule as a member of grand canonical ensemble where the energy (E) and the number of electrons (N) are continuous function and all other properties of the ensemble are written in terms of these two variables. The chemical potential of the ensemble can be written as

$$\mu = \frac{\partial E}{\partial N}, \text{ at constant entropy} \quad 1.41$$

As the electrochemical potential measures the escaping tendency of electrons, the electron attracting power should be its negative. Hence, electronegativity is defined as

$$\chi = -\mu = -\frac{\partial E}{\partial N}, \text{ at constant entropy} \quad 1.42$$

which is a continuous function of the number of electrons and temperature (Θ).

Due to electron, attracting property of atoms, electrons flows from the atoms with lower electronegativity to the atom with higher electronegativity, leading to the equalization of electronegativity⁹⁷ in the molecule.

However, in many cases electronegativity difference alone cannot account for the stability of the molecules. For example, according to the electronegativity criterion, the CsF molecule should be much stable compared to LiF. But the reaction enthalpy data indicates that LiI and CsF will react to form CsI and LiF. In order to predict the direction of acid base reaction and to account for the stability of the products, Pearson introduced two parameters “hardness” and “softness” in the vocabulary of chemistry. The qualitative definitions of hard and soft acid and bases are follows⁹⁸⁻¹⁰³

Hard acid: acceptor atoms with small size, high positive charges, low polarizability, and the absence of easily excitable outer electrons (e.g., H^+ and Li^+).

Hard bases: donor atoms with small size, low polarizability, high electronegativity, having empty orbitals with large energy and are hard to oxidize (e.g., NH_3 , OH).

Soft acids: acceptor atoms with large size, low positive charge, and bearing easily excitable outer electrons (e.g., I₂, Pd²⁺).

Soft bases: donor atoms with high polarizable, low electronegativity, having low-lying orbitals and easy to oxidize.

The classification is purely empirical and based on the observations of bond energy, equilibrium constant, rate constant and other experimental data.¹⁰⁴ These experimental observations finally leads to the prediction of simple but important principle, which states that hard acid will prefer to bind with hard base and soft acid will prefer to bind with soft base for both thermodynamic and kinetic reasons. This empirical principle known as “hard-soft acid-base” (HSAB) principle.⁹⁸⁻¹⁰³ It is also been argued that hard-hard reactions are governed by charge controlled interactions and soft-soft interactions are covalent type. Different studies on reactivity suggest that soft molecules are more reactive compared to the corresponding harder counterparts. Hence, isomeric molecules having higher hardness are found to be more abundant in nature than having lower hardness values. This leads to the principle of maximum hardness, which states¹⁰⁴ that “there seems to be a rule of nature that molecules arranged themselves so as to be as hard as possible. In attempt to quantify the concept of hardness and softness, Pearson proposed a relation that correlates the stability of molecules with hardness and softness as well as inherent strength of acid and bases. The stability constant of a reaction is given by¹⁰⁴:

$$-p^k = S_A S_B + \sigma_A \sigma_B \quad 1.43$$

where S_A and S_B are the inherent strength of acid and bases whereas σ_A and σ_B are softness factors. The HSAB principle has been criticized by Drago *et al.*^{105(a)} who pointed out that although the strength of acid and bases are considered in Eq. 1.43, the HSAB principle explained molecular stability solely in terms of softness and hardness, and neglect the effect of acid-base strength in the molecule formation. Drago *et al.*^{105(a)} proposed a relation to measure the enthalpy change in terms of the parameters, which measures the strength of hard and soft species as:

$$-\Delta H = C_A C_B + E_A E_B \quad 1.44$$

where the first term measures the covalent contribution to the enthalpy change whereas second term measures the corresponding electronic contribution. Here, C parameters are

identified^{105(a)} with softness and E parameters are identified with hardness. However, it is suggested^{105(b)} that the contradiction in the theories of Pearson^{98,100-103} and Drago *et al.*^{105(a)} are basically due to the difference in the approach in understanding the acid-base reactions. Drago *et al.* used E and C parameter in Eq. 1.44 to study the reaction of two species where the solvation effect is minimized or absent, whereas Pearson's theory considered the competition between forward and backward reactions in the acid-base equilibrium.

Although the qualitative concepts such as electronegativity and hardness have been found to be useful in understanding various reactions they are not taken very seriously until recently because they did not have legitimate theoretical genesis. Rigorous quantitative definition and method for calculations¹⁰⁶⁻¹⁰⁸ of electronegativity, hardness and related quantities such as chemical potential, local hardness, softness, Fukui function, etc. have been provided within density functional theory (DFT).

(ii) *Theoretical treatment of qualitative concepts:*

In DFT, the Lagrange multiplier associated with the normalization constraints is identified as chemical potential (μ), maintaining the analogy with an ordinary thermodynamic system¹⁰⁹ viz,

$$\mu = \left(\frac{\partial E}{\partial \rho} \right)_{v(\vec{r})} \quad 1.45$$

Where E is the total energy and $v(\vec{r})$ is the external potential. Chemical potential defined in Eq. 1.45 can be interpreted as the escaping tendency of the electrons analogous to the chemical potential of the macroscopic system.¹⁰⁹ The chemical potential of a N electron system can as well be written as a partial derivative of energy with respect to the number of electrons because

$$\int \rho d\vec{r} = N \quad 1.46$$

The definition of Iczkowski and Margrave¹¹⁰ identifies electronegativity (χ) as the slope of energy vs. N plot. Thus, μ can be shown to be equivalent to the negative of electronegativity as¹⁰⁹

$$-\chi = \int \left(\frac{\partial E}{\partial \rho} \right)_v \left(\frac{\partial \rho}{\partial N} \right)_v d\vec{r} = \left(\frac{\partial E}{\partial N} \right)_v = \mu \quad 1.47$$

The finite difference approximation of the partial derivative $\left(\frac{\partial E}{\partial N}\right)_v$ gives the equivalence of χ defined within DFT with that given by Mulliken,⁹⁵ that is,

$$-\mu = \chi = \frac{I+A}{2} \quad 1.48$$

The ground state energy curve as a function of N is continuous and shows a series of straight line segments.¹¹¹ The slope of E vs. N plot shows discontinuity at integral number of N. Thus, at zero temperature limit, the chemical potential for neutral species is obtained by taking the average of limits of the $Z < N$ and $Z > N$ curves and is written as:¹¹¹

$$\mu = -I \text{ for } Z - 1 < N < Z \quad 1.49(a)$$

$$\mu = -\frac{I+A}{2} \text{ for } Z = N \quad 1.49(b)$$

$$\mu = A \text{ for } Z < N < Z + 1 \quad 1.49(c)$$

where Z is the nuclear charge.

It should be noted that the correct definition of μ is difficult to evaluate and, for all practical purposes, μ is calculated simply as $\mu = \left(\frac{\delta E}{\delta \rho}\right)_v$ without any serious error as it has been shown that¹¹²:

$$\left(\frac{\delta E}{\delta \rho}\right)_{N,v} \left(\frac{\delta E}{\delta \rho}\right)_v = C; C \text{ being a constant.}$$

Electronegativity (χ) or chemical potential (μ), ionization potential (I) and electron affinity (A) can be computed for electronic system from the Kohn-Sham (KS) equation, which has been extended by Janak¹¹³ and others¹¹⁴⁻¹¹⁶ using $\chi\alpha$ method¹¹⁷. In this approach, one gets a meaning for orbital energy as:

$$\varepsilon_i = \frac{\partial E_i}{\partial n_i} \quad 1.50$$

where n_i is the occupation number:

$$N = \sum_i n_i$$

Now the integration of above equation between limits N and N+1 gives electron affinity for a species:

$$-A = E_{N+1} - E_N = \int_0^1 \varepsilon_{LUMO}(n) dn \quad 1.51$$

ϵ_{LUMO} is the energy of the lowest unoccupied molecular orbital. In Eq. 1.50 the occupation number n has been assumed to vary continuously.

In *Ab initio* theory, I and A can be approximated as the negative energies of HOMO and LUMO, respectively, using Koopmans' theorem. In this framework, the electronegativity is the negative of HOMO-LUMO energy average and written as¹¹⁸

$$-\chi = \mu = \frac{1}{2}(\epsilon_{HOMO} + \epsilon_{LUMO}) \quad 1.52$$

The curvature of E vs. N curve has been equated with hardness¹⁰⁶, another important parameter for understanding structure and reactivity. The absolute hardness is given as:

$$\eta = \frac{I-A}{2} \quad 1.53$$

Hardness can be equated to the second term in the Taylor series expansion of energy^{14,119}:

$$\eta = \frac{1}{2} \left(\frac{\partial^2 E}{\partial N^2} \right)_v = \frac{1}{2} \left(\frac{\partial \mu}{\partial N} \right)_v \quad 1.54$$

and would be always positive as the E vs.N curve is convex in nature. It can be interpreted as the resistance of the chemical potential of a system to change with the number of electrons.^{106,120} The finite difference approximation of Eq. 1.54 leads to Eq. 1.53, which is the energy change ΔE of a species in disproportionation reaction of the type:



$$\Delta F = I - A$$

In *Ab initio* wave function pictures using Koopmans' theorem, η became half of the energy gap between HOMO and LUMO as¹¹⁸:

$$\eta = \frac{1}{2}(\epsilon_{LUMO} - \epsilon_{HOMO}) \quad 1.56$$

This definition, like previous ones, has a direct consequence on the reactivity theories as large HOMO-LUMO gap satisfy reluctance of the system to take or give up electrons. For insulators or semiconductors, band gap is taken as the measure of η .

The inverse of hardness is softness, which is given as¹²¹

$$S = \frac{1}{2\eta} = \left(\frac{\partial N}{\partial \mu} \right)_v \quad 1.57$$

The concept of softness is associated with polarizability. The larger the chemical system the softer it will be. This correlation of softness with polarizability can be found directly from a bond charge model¹²²⁻¹²⁵ where softness is found to be proportional to the internuclear distance of molecules. To extend this definition to open system, consider the particular system is the member of a grand canonical ensemble with well-defined parameters $\mu, v(\vec{r})$ and temperature, θ . Now the definition of softness within the ensemble can be written in terms of different fluctuation formulas¹²⁶:

$$S = \left(\frac{\partial \langle N \rangle}{\partial \mu} \right)_{v, \theta} = \frac{1}{k\theta} [\langle N^2 \rangle - \langle N \rangle^2] \quad 1.58$$

where k is the Boltzmann constant. This statistical thermodynamic definition or charge fluctuation formula of softness relates it with bond index and volume.¹²⁷ It is worth noting that in a contemporary theoretical development, Parr *et al.*¹²⁸ defined another important global reactivity descriptor, electrophilicity index w as:

$$w = \frac{\mu}{2\eta} \quad 1.59$$

This measures the propensity of electrophilic attack and is used¹²⁸ in understanding the reactivity of the human immunodeficiency virus type I (HIV-I) nucleocapsid protein p7 (NCp7) when reacted with variety of electrophilic agents.

(iii) *Local Reactivity Descriptors:*

As the global reactivity descriptors are proposed to understand the overall reactivity of a system, the reactivity of a particular site within the system of interest can be explored through local quantities such as electron density $[\rho(\vec{r})]$, Fukui function $[f(\vec{r})]$ ¹²⁹ local softness¹²⁶ local hardness.^{130,131} The dependence of these local quantities on reaction coordinate reflects the usefulness of these quantities in predicting the site selectivity of a chemical reaction. The most important local descriptor is the density $\rho(\vec{r})$ itself, the basic variable of DFT¹³¹ given as:

$$\rho(\vec{r}) = \left(\frac{\delta E[\rho]}{\delta v(\vec{r})} \right)_N \quad 1.60$$

The definition of Fukui function is given by¹²⁹

$$f(\vec{r}) = \left(\frac{\partial \rho}{\partial N} \right)_v = \left(\frac{\delta \mu}{\delta v(\vec{r})} \right)_N \quad 1.61$$

Such that $\int f(\vec{r}) d\vec{r} = 1$

This definition of $f(\vec{r})$ is obtained by considering the change in energy and chemical potential when a system goes from one ground state to another, viz.,

$$dE = \mu dN + \int \rho(\vec{r}) dv(\vec{r}) d\vec{r} \quad 1.62$$

$$d\mu = 2\eta dN + \int f(\vec{r}) dv(\vec{r}) d\vec{r} \quad 1.63$$

and by application of a Maxwell relation in Eq. 1.63. The extent of reaction can be given by $d\mu$ from Eq. 1.63. It can be predicted that the reaction would be favored in a direction of increasing $f(\vec{r}) dv(\vec{r}) d\vec{r}$ at a particular site. As the slope of $\rho(\vec{r})$ vs. N curve has discontinuity for integral number of N, three types of Fukui functions can be defined, which separately accounted for electrophilic, nucleophilic and radical attack at a particular reaction site. Using finite difference and frozen core approximations, these three functions can be written as:

$$f^+(\vec{r}) = \left(\frac{\partial \rho}{\partial N}\right)_v^+ \cong \rho_{N+1}(\vec{r}) - \rho_N(\vec{r}) \approx \rho_{LUMO}(\vec{r}) \text{ [For nucleophilic attack]}$$

$$f^-(\vec{r}) = \left(\frac{\partial \rho}{\partial N}\right)_v^- \cong \rho_N(\vec{r}) - \rho_{N-1}(\vec{r}) \approx \rho_{HOMO}(\vec{r}) \text{ [For electrophilic attack]}$$

$$f^0(\vec{r}) = \left(\frac{\partial \rho}{\partial N}\right)_v^0 \cong \frac{1}{2}(\rho_{N+1}(\vec{r}) - \rho_{N-1}(\vec{r})) \approx \frac{1}{2}(\rho_{LUMO}(\vec{r}) + \rho_{HOMO}(\vec{r}))$$

[For neutral attack]

The above equations provide a correspondence between this local parameters and the frontier orbital theory of chemical reactions¹³² and thus justifies the nomenclature of Fukui (frontier) function. A large value of f^+ , f^- or f^0 at a particular site denotes the high probability of electrophilic, nucleophilic, or radical attack to take place at that site.

The expression for condense Fukui function for the i^{th} atom in a molecule can be obtained by considering the finite difference approximation and Mulliken's population analysis scheme as^{133,134}:

$$f_i^+ = q_i(N + 1) - q_i(N) \quad \text{[For nucleophilic attack]}$$

$$f_i^- = q_i(N) - q_i(N - 1) \quad \text{[For electrophilic attack]}$$

$$f_i^0 = \frac{1}{2}[q_i(N + 1) - q_i(N - 1)] \quad \text{[For radical attack]}$$

Because electron number can be continuous in the extended version of Kohn-Sham theory¹¹³, Fukui function may be determined as derivatives. The explicit forms for f^+ and f^- can be given in this formalism as¹³⁵:

$$f^+ = |\phi_{LUMO}(\vec{r})|^2 + \sum_{i=1}^N \frac{\partial}{\partial N} |\phi_i(\vec{r})|^2$$

$$f^- = |\phi_{HOMO}(\vec{r})|^2 + \sum_{i=1}^{N-1} \frac{\partial}{\partial N} |\phi_i(\vec{r})|^2$$

where ϕ is the spatial orbital of neutral atom. Prescriptions for calculation of Fukui function using a variation technique¹³⁶ and a gradient expansion¹³⁷ is also provided.

The tendency of particular site to involve in “frontier-controlled”¹³⁸ interaction, where frontier orbital density plays important roles, is given by a local softness parameter, Local softness is defined as¹²⁶:

$$s(\vec{r}) = - \left(\frac{\delta N}{\delta v(\vec{r})} \right)_{\mu} = \left(\frac{\partial \rho}{\partial \mu} \right)_{\nu} \quad 1.64$$

and its integrates to global softness as:

$$s = \int s(\vec{r}) d\vec{r} \quad 1.65$$

Local softness is related to Fukui function, which may be defined as a normalized local softness by the following formula:

$$s(\vec{r}) = \left(\frac{\partial \rho(\vec{r})}{\delta \mu} \right)_{\nu} = \left(\frac{\partial \rho}{\partial N} \right)_{\nu} \left(\frac{\partial N}{\partial \mu} \right)_{\nu} = f(\vec{r})s \quad 1.66$$

The information of Fukui function can be obtained from local softness although the reverse is not true.³⁶

To obtain the reciprocal relation between local quantities similar to Eq. 1.57, Berkowitz and Parr¹³⁹ defined two local kernels, which integrates to give local softness and local hardness. Softness kernel is defined as¹³⁹:

$$-s(r, r') = \frac{\delta \rho(\vec{r})}{\delta u(\vec{r}')} = \frac{\delta \rho(\vec{r}')}{\delta u(\vec{r})} \quad 1.67$$

where the modified potential $u(\vec{r})$ has the form:

$$u(\vec{r}) = v(\vec{r}) - \mu = - \frac{\delta F[\rho]}{\delta \rho(\vec{r})} \quad 1.68$$

for which derivatives $\frac{\delta\rho(\vec{r})}{\delta u(\vec{r}')}$ as well as $\frac{\delta u(\vec{r})}{\delta\rho(\vec{r}')}$ exist. Local softness is obtained from softness kernel simply as:

$$s(\vec{r}) = \int s(\vec{r}, \vec{r}') d\vec{r}' \quad 1.69$$

Hardness kernel is defined as:

$$-2\eta(\vec{r}, \vec{r}') = \frac{\delta u(\vec{r})}{\delta\rho(\vec{r}')} = \frac{\delta u(\vec{r}')}{\delta\rho(\vec{r})} \quad 1.70$$

Hardness kernel is the inverse of softness kernel in the sense:

$$2 \int s(\vec{r}, \vec{r}') \eta(\vec{r}, \vec{r}'') d\vec{r}' = \delta(\vec{r} - \vec{r}'') \quad 1.71$$

Local hardness cannot be obtained from hardness kernel by simple integration.

But the relation exists as:

$$\eta(\vec{r}) = \frac{1}{N} \int \eta(\vec{r}, \vec{r}') \rho(\vec{r}') d\vec{r}' \quad 1.72$$

Inserting the expression for $\eta(\vec{r}, \vec{r}')$ from Eq. 1.70 into Eq. 1.72, we get $\eta(\vec{r})$ as¹³⁰:

$$\eta(\vec{r}) = \frac{1}{2N} \int \frac{\delta^2 F[\rho]}{\delta\rho(\vec{r})\delta\rho(\vec{r}')} \rho(\vec{r}') d\vec{r}' \quad 1.73$$

These quantities are reciprocals in the sense that:

$$2 \int \eta(\vec{r}) s(\vec{r}) d\vec{r} = 1 \quad 1.74$$

To obtain another definition of $\eta(\vec{r})$, we write $d\mu$ as^{130(a)}

$$d\mu = 2 \int \eta(\vec{r}) d\rho(\vec{r}) + \frac{1}{N} \int \rho(\vec{r}) dv(\vec{r}) d\vec{r}' \quad 1.75$$

which gives:

$$\eta(\vec{r}) = \frac{1}{2} \left(\frac{\delta\mu}{\delta\rho} \right)_v \quad 1.76$$

It should be noted that the definition of local hardness has inherent ambiguity in it.¹⁴⁰ The local hardness defined above requires a variation of $\rho(\vec{r})$, keeping $v(\vec{r})$ constant, which seems to be ambiguous because $v(\vec{r})$ and $\rho(\vec{r})$ are independent as has been proven by Hohenberg and Kohn.^{73,141}

Local hardness integrates to give global hardness¹³⁰ in a way similar to that of hardness kernel:

$$\eta = \int \eta(\vec{r}) f(\vec{r}) d\vec{r} \quad 1.77$$

1.4.2 Electronegativity and Associated Principles:

The theoretical background of electronegativity and related concepts generated intense excitement among global community of chemists primarily because it can be evaluated in terms of experimental ionization potential and electron affinity¹⁴² as well as through density functional calculations.^{120,143-146} The systematic study on this topic revealed newer aspects such as relation between electronegativity and diamagnetic shielding¹⁴⁷ and high temperature superconductivity,¹⁴⁸⁻¹⁵² application of electronegativity difference in classifying the crystal structure of a binary solid,¹⁵³ explanation of alloy formation,¹⁵⁴ etc. Several other studies¹⁵⁵⁻¹⁵⁷ involved quantitative dependence of electronegativity on atomic number Z . It was shown¹⁵⁶ that in each group, electronegativity shows a periodic behavior and, at large Z , it is approximately $\sim Z^{1/3}$. The dependence of binding energy values of neutral atom has also been studied.¹⁵⁸

The density functional theory not only provided a rigorous definition of electronegativity but also a basis of Sanderson's electronegativity equalization and geometrical mean principle.⁹⁷ Moreover, in the chemical system of interest, electron will be distributed in such a way that the electronegativity of the orbitals will be equal to electronegativity of the system, that is,

$$\mu = \frac{\partial E}{\partial n_i} \text{ for all } i; \sum_i n_i = N \quad 1.78$$

where n_i is the occupancy of the i^{th} natural orbital. In recent years, Prof. R. G. Parr along with other pioneers provide significant contributions to find a suitable solution for the dependence of charge flow on electronegativity difference.^{47,109,159-164} Without remaining confined to any theoretical framework, Politzer and Weinstein¹⁶³ proved the validity of the principle of equalization of electronegativity for any arbitrary region of space in a molecule.

As the charge, transfer leads to the formation of a new molecule, the molecular electronegativity, after equalization can be obtained from isolated atoms' electronegativity values by the Sanderson's geometrical mean law⁹⁷ as:

$$\chi_{AB\dots N} = (\chi_A^0 \chi_B^0 \dots \dots \chi_N^0)^{1/N} \quad 1.79$$

where $\chi_{AB\dots N}$ is the electronegativity of a polyatomic molecule and $\chi_A^0 \chi_B^0 \dots \dots \chi_N^0$ are the isolated atoms' electronegativities. The sufficient condition for the validity of Eq.

1.79 is that the energy of atoms should be an exponentially decay function of the number of electrons¹⁰⁹:

$$E(N) \cong E(Z)\exp[-\gamma(N - Z)] \quad 1.80$$

or equivalently,

$$\chi = \chi^0 \exp[-\gamma(N - Z)] \quad 1.81$$

which agrees to the supposition that atomic energy is quadratic function of the number of electrons.¹⁶⁵ In Eq. 1.80 and 1.81 the decay parameter ($\gamma = \frac{I}{A}$) is found to be more or less constant for all atoms and has a approximate value of 2.2.

The concept of equalization of electronegativity can be applied to determine various properties of atoms and molecules. Using this concept, one can define the different atomic radii¹⁶⁶⁻¹⁷⁰ which are the measures of binding property of atoms. The electronegativity equalization principle gives a scheme for calculating the amount of charge transfer and partial charges on atom in a molecule. For diatomic molecule AB, the energy and chemical potential can be written as the following Taylor expansion¹⁴:

$$E_A = E_A^0 - \chi_A \Delta N_A + \eta_A \Delta N_A^2 + \dots \dots \dots A \equiv A, B \quad 1.82$$

and

$$-\chi_A = \frac{\partial E_A}{\partial N_A} = -\chi_A^0 + 2\eta_A \Delta N_A + \dots \dots \dots A \equiv A, B \quad 1.83$$

Truncation of Taylor expansion Eq. 1.82 after second-order variation may be shown to be legitimate because the third-order derivative is often small,¹⁷¹ which is, however, not always true.¹⁷² Application of EEP gives:

$$\chi_A = \chi_B$$

which implies,

$$\Delta N = \frac{\chi_B^0 - \chi_A^0}{2(\eta_A + \eta_B)} \quad 1.84$$

and
$$\Delta E = -\frac{(\chi_B^0 - \chi_A^0)^2}{4(\eta_A + \eta_B)} \quad 1.85$$

From Eq. 1.84 and 1.85, it can be seen that charge transfer is dependent on the first order of electronegativity difference, and stabilization energy has a second-order dependence on electronegativity difference. Eq. 1.84 and 1.85 predict that the charge transfer process will be hindered by the hardness sum.¹¹⁹ This model is only a crude model and Eq. 1.84

gives connectivity-independent charge transfer for atoms in polyatomic molecules, which are not always acceptable. This model can be improved by taking into consideration change in the molecular environment. Considering electrostatic interaction between atoms in a molecule, an improved expression for the amount of charge transfer can be given, which depends on intermolecular distance γ as:¹⁷³

$$\Delta N = (\chi_B^0 - \chi_A^0) / \left[\left(\frac{\partial \chi_A}{\partial N_A} \right)_{N_A=Z_A} + \left(\frac{\partial \chi_B}{\partial N_B} \right)_{N_B=Z_B} + 2/r \right] \quad 1.86$$

The charges calculated from different orbital electronegativity equalization scheme is found to exhibit good correlations with ESCA or NMR shifts¹⁷⁴ and could differentiate between different isomers present in structurally different phases.¹⁷⁵ These methods are also used¹⁷⁴⁻¹⁷⁶ to study electronegativity and charge distribution in solids. Connectivity-dependent charges¹⁷⁷ calculated this way^{178,179} have been found to be adequate in explaining charge transfer in donor-acceptor atoms.¹⁸⁰ Concepts of bond electronegativity and bond hardness have also been introduced¹⁸⁴⁻¹⁸⁸ in providing a model of covalent bonding in molecules.

It has been realized by Parr and Pearson^{14,119} that electronegativity alone is not sufficient to account all facts of a chemical process and another parameter, hardness, is necessary. Whereas electronegativity is the tangent to E vs. N curve, the corresponding curvature has been identified as hardness, which has been discussed in the earlier subsection.

1.5 Comprehensive Decomposition Analysis of Stabilization Energy:

Parr and Pearson¹⁴ derived the expression of energy lowering due to electron transfer (ΔN) from a species B to another species A as,

$$\Delta E = (E_A - E_A^0) + (E_B - E_B^0) = (\mu_A^0 - \mu_B^0)\Delta N + \frac{1}{2}(\eta_A + \eta_B)(\Delta N)^2 + \dots \quad 1.87$$

where, $\Delta N = N_A - N_A^0 = N_B^0 - N_B$ (which indicates that B is electron donor and A is electron acceptor). The terms E_A^0 and E_B^0 denote the energies of systems A and B, respectively, before the electron transfer. Similarly, E_A and E_B denote the corresponding quantities after the electron transfer. The reactivity descriptors μ and η are known as chemical potential and chemical hardness, respectively, of the two species.

Maximum flow of electrons can be characterized by applying the chemical potential equalization principle (i.e. $\mu_A = \mu_B$ or $\chi_A = \chi_B$, here, χ denotes the electronegativity parameter and $\mu = -\chi^{33}$) when,

$$\frac{\Delta E}{\Delta N} = 0 \quad 1.88$$

Implying,

$$\Delta N = \frac{\mu_B^o - \mu_A^o}{(\eta_A + \eta_B)} \quad 1.89$$

which yields stabilization energy E_{SE} to be as,

$$\Delta E_{SE} = -\frac{(\mu_B^o - \mu_A^o)^2}{2(\eta_A + \eta_B)} \quad 1.90$$

here, the operational definition of μ and η (analytical definitions are, $\mu = \left(\frac{\delta E}{\delta N}\right)_v$ and $\eta = \left(\frac{\delta^2 E}{\delta N^2}\right)_v$, where v is external potential) are provided by the finite difference approximation¹⁴ as,

$$\mu = -\frac{1}{2}(IP + EA) \quad 1.91$$

and

$$\eta = \frac{1}{2}(IP - EA) \quad 1.92$$

where, IP and EA are first vertical ionization potential and electron affinity, respectively. The IP and EA values can be generated either by separately calculating energy values of the neutral and ionic species (in the geometry of the neutral species) or through the Koopmanns' approximation¹⁸⁹ within the molecular orbital theory, wherein IP and EA can be obtained from the frontier orbital energies (i.e., $HOMO$ and $LUMO$ energy) as,

$$-E_{HOMO} = IP \quad 1.93$$

$$-E_{LUMO} = EA \quad 1.94$$

where, $HOMO$ and $LUMO$ represent the Highest Occupied Molecular Orbital and Lowest Unoccupied Molecular Orbital, respectively. Therefore, on the basis of frontier orbitals, we can write,

$$\mu = \frac{1}{2}(E_{HOMO} + E_{LUMO})$$

$$\eta = \frac{1}{2}(E_{LUMO} - E_{HOMO})$$

From Eq. 1.90 it is obvious that ΔE_{SE} value will always be negative in the process of spontaneous flow of electrons from one species to another. Therefore, this expression of stabilization energy can be used to explain the most favorable interaction between two chemical systems. However, the spontaneity of electron flow from B (i.e. donor) to A (i.e., acceptor) cannot be predicted from the negative value of ΔE_{SE} alone (because in the numerator of Eq. 1.90 the square term will always be positive and denominator is always positive, making ΔE_{SE} always negative). This information can be extracted from Eq. 1.89. If from eqn. 1.89 the value of ΔN is positive then electron flow is spontaneous from B to A, otherwise it is in the reverse direction.

In a recent paper Roy and collaborators¹⁹⁰ have shown that not only ΔN , but also components of ΔE_{SE} can provide important information regarding the direction of electron transfer when (i) two systems, A and B, form a complex AB and (ii) when A and B go further to react and give different products (i.e., $A + B \Rightarrow [AB]^\ddagger \Rightarrow C + D$). In case (ii) whether the reaction is spontaneous or required some external assistance, could also be predicted from these energy components. As the present thesis work is based on the type (i), (i.e., $A + B \Rightarrow AB$), interactions, it will be interesting to know how these energy components also (apart from ΔN -value) can predict the donor and acceptor species in the process of complex formation. These can be done if we analyze the expressions of energy components as obtained from Eq 1.87. From Eq.1.87 we see,

$$\begin{aligned} \Delta E_{B(A)} &= (E_B - E_B^0) = (-\mu_B^0)\Delta N + \frac{1}{2}(\eta_B)(\Delta N)^2 \\ &= \Delta N(-\mu_B^0 + \frac{1}{2}\eta_B \Delta N) \end{aligned} \quad 1.95$$

i.e.,

$$\Delta E_{B(A)} = \frac{\mu_B^o - \mu_A^o}{\eta_A + \eta_B} \left[-\mu_B^o + \frac{1}{2}\eta_B \left(\frac{\mu_B^o - \mu_A^o}{\eta_A + \eta_B} \right) \right] \quad 1.96$$

and

$$\Delta E_{A(B)} = (E_A - E_A^0) = (\mu_A^0)\Delta N + \frac{1}{2}(\eta_A)(\Delta N)^2$$

$$= \Delta N(\mu_A^0 + \frac{1}{2}\eta_A \Delta N) \quad 1.97$$

i.e.,

$$\Delta E_{A(B)} = \frac{\mu_B^0 - \mu_A^0}{\eta_A + \eta_B} \left[\mu_A^0 + \frac{1}{2}\eta_A \left(\frac{\mu_B^0 - \mu_A^0}{\eta_A + \eta_B} \right) \right] \quad 1.98$$

From Eq. 1.96 it is obvious that the value generated from the square-bracketed term will be positive only if ΔN is a positive quantity (because μ_B^0 is a negative and η_B is a positive quantity). Now, ΔN is positive only if electrons flow from B to A (then only $\Delta N = N_B^0 - N_B$ positive quantity). Again, positive ΔN value causes a positive $\Delta E_{B(A)}$ value. Thus, positive $\Delta E_{B(A)}$ value also indicates that B is the donor and A is acceptor. Similar argument reveals that $\Delta E_{A(B)}$ will be negative quantity when B is donor and A is acceptor and electron transfer from B to A causes the complex $[AB]$ more stable than the two individual species. If ΔN and $\Delta E_{B(A)}$ are negative and $\Delta E_{A(B)}$ is positive then, however, A is actually the donor and B is the acceptor in the complex.

1.6 Applications of Density Functional Reactivity Theory: Motivation behind the Present Thesis

The fundamental basis of chemical science is the chemical interactions. Chemistry is the science to explore the process of new bond formation through the breaking of old one. Indeed, chemical science encounters hundreds of thousands of different chemical interactions such as substitution, addition (including pericyclic reactions), elimination, and rearrangements. The thermodynamic and kinetic aspects are significantly important to determine the overall stability of product in a particular chemical reaction. While, the thermodynamic parameters determines overall stability of products (either large decrease in Gibbs free energy implies or large value of the equilibrium constant, K). On the other hand, kinetic parameters latter determine how fast it will take place (a small free energy of activation value or a larger rate constant, k , at a given temperature).

In the contemporary research, application of DFT to understand the mechanism of various chemical and biological interactions is a routine practice. Density Functional Theory offers great deal of flexibility and accountability to the *Ab initio* calculation at a

reasonable computational cost. The formulation of energy based global reactivity descriptors have been found to provide promising insights in analyzing the reactivity along with the stability of the molecular systems. Indeed that helps to understand the reaction mechanisms of diverse classes of chemical process. However, the conventional DFT based approaches have some major set-back in the cost-effective computational study on large systems (like DNA and carbon nanotube). In the present thesis, we have projected the proposed DFRT based CDASE scheme as an effective alternative to understand the thermodynamic and kinetic aspects of diverse reactive interaction (both chemical and biological) at a reasonably low computational cost combined with adequate modeling techniques.

The interaction of metal containing anti-cancer drug cisplatin¹⁹¹ with DNA is a largely explored area of research for long time. Numerous experimental studies and theoretical calculations are dedicated to understand the DNA binding activity of cisplatin drug.¹⁹² In a recent study Baik *et al.*¹⁹³ revealed the importance of H-bonding and strong electrostatic interaction on the stability of adducts formed between cisplatin drugs and purine bases. The thermodynamics and kinetics for the monofunctional binding of the antitumor drug cisplatin, (cis-diamminedichloroplatinum(II)), to a purine base site of DNA were studied computationally using guanine and adenine as model reactants. A dominating preference for initial attack at the N7-position of guanine is established experimentally, which is a crucial first step for the formation of a 1,2-intrastrand cross-link of adjacent guanine bases that leads to bending and unwinding of DNA. Biak *et al.* concluded that these structural distortions are ultimately responsible for the anticancer activity of cisplatin. Mantri and co-workers¹⁹⁴ performed an extensive modeling study on the bifunctional binding of the anticancer drug cisplatin to two adjacent nucleobases in DNA using density functional theory. Previous experimental studies revealed that cisplatin binding to adjacent guanine and adenine is sensitive to nucleobase sequence. Whereas AG 1,2-intrastrand cross-links are commonly observed, the analogous GA adducts are not known. Mantri *et al.*¹⁹⁴ particularly emphasized on understanding this directional preference by constructing a full reaction profile using quantum chemical simulation methods. Monofunctional and bifunctional cisplatin adducts were generated, and the transition states that connect them were located for the dinucleotides d(pApG)

and d(pGpA), assuming that initial platination takes place at the guanine site. The computer simulations reveal a significant kinetic preference for formation of the AG over the GA adduct.

The quest for nanoscale structures with practical applications is rapidly passing from the realm of dreams to reality. The combination of nanoscale structures deriving from solids, such as carbon nanotubes or silicon nanowires, with biologically important structures, such as DNA or polypeptides, is particularly intriguing since it opens the door to novel bio and nanotechnology applications. In an interesting study, DFT has been extensively used to investigate the properties of Carbon nanotubes (CNT) in recent times. Functionalization of CNT is the first step towards its application in various fields. Significant number of publications are appeared discussing the possibility of DNA functionalizing CNTs.¹⁹⁵⁻¹⁹⁹ However, the modulation in physical and chemical properties of DNA-CNT conjugate basically controlled by the nature of interaction between individual nucleobases and CNT. The interaction between the π -orbitals of nucleobases and SWCNTs play a crucial role during the physisorption process of nucleobases on SWCNTs. An extensive DFT based *Ab initio* electronic structure calculations have been performed for single-walled carbon nanotube, single-stranded DNA molecule, and DNA wrapped carbon nanotube considering in all cases vacuum conditions and water solvent conditions by Bobadilla and Seminario.²⁰⁰ It is observed that in vacuum, decrease in the band-gap is mainly responsible for the metallic behavior of DNA- CNT nanocomposite. In water medium, an energy shift is produced in the HOMO and LUMO energy levels for the hybrid structure. Here, the breaking of electronic symmetry in carbon nanotube in presence of DNA molecule is the possible explanation for the above observation. In a recent development, Lu et al.²⁰¹ used density functional theory (DFT) calculations to study the interaction of an infinitely long (periodic) DNA molecule with an array of nanotubes, and showed that simultaneous charge flow through CNT and DNA is possible. The particular interest of Lu et al. lies in the fact that conduction can be controlled by gating the DNA-right lead contact, while the current changes direction from the CNT orientation (into which electrons are injected) to the DNA orientation (from which electrons are extracted). Moreover, the outcome of Lu and

co-workers introduced DNA-CNT composite as one of the effective tool for DNA sequencing.

Very recently, Density Functional Theory based calculations were found to have significant impact on the design and development of hybrid nanostructures. These hybrid nanomaterials have significant importance in the next generation electronic as well mechanical devices.^{202,203} In a contemporary study, Wu *et al.* have investigated structural, electronic, chemical, and field-emission properties of Carbon NanoBuds (CNB) using density functional theory.²⁰⁴ It is observed that relative stabilities of Carbon NanoBuds depend on the nature of cycloaddition reaction (2+2 or 6 +6), through which, fullerene can be attached to the outer surface of nanotube. The computed reaction path (from kinetic data) shows that the formation of Carbon NanoBud entails a high energy barrier in both forward and backward reactions, indicating that CNBs are significantly stable at room temperature. In a subsequent study, He and co-workers explored the structural stability and electronic properties of carbon NanoBud, where a C₆₀ molecule covalently attaches or embeds in an armchair carbon nanotube using DFT.²⁰⁵ The findings of their study suggest that CNBs exhibit either metallic or semiconducting conductivity and depends on the mode of covalent bonding interaction between C₆₀ and the CNT, as well as size of the CNT.

The possibilities of employing DNA as a template have opened up new avenues for the synthesis of nanomaterials pushing the cost and size limit imposed by the conventional top-down approaches like optical lithography. The interaction of DNA with metal nanoparticles finds diverse applications in the recent advancements of nanobiotechnology.²⁰⁶⁻²¹⁰ Of particular interest is the DNA– gold interaction which forms the basis of several diagnostics applications. For all these diverse applications, understanding the binding of DNA bases adenine (A), thymine (T), guanine (G), and cytosine (C) with gold is of central importance. Recent experimental studies showed that DNA bases, adenine (A), thymine (T), guanine (G), and cytosine (C), interact with Au surfaces in a specific and sequence-dependent manner.²¹¹ Kryachko et al. have recently investigated the nature of the DNA-gold interaction in order to understand the differential affinity of the nucleobases to gold.²¹² On the basis of high-level DFT computations, they have shown that the DNA bases are able to form covalent bond with gold clusters through their

nitrogen or oxygen atoms. It is further demonstrated that, together with the formation of an anchoring Au-N or Au-O bond, the DNA base-gold cluster complexes are stabilized by a nonconventional N-H--Au type of hydrogen bond.²¹² Such a direct and specific bonding offers an interesting alternative to thiolated DNA because of its increased stability and could therefore be useful to prepare DNA molecules tagged with gold clusters at specific locations.

The nonbonding interactions are extremely significant in both chemical and biological systems. Hydrogen bonds²¹³ are one of the principal inter-molecular forces. These strong interactions are critical, for example, in ionic clusters and nucleation, in electrolytes, ion solvation, and acid-base chemistry, in the structures of ionic crystals, surfaces, silicates, and clays, in surface adsorption, and in self-assembly in supramolecular chemistry and molecular crystals. A vast variety of supramolecular assemblies owe their well-defined structure to the existence of adjacent hydrogen bond donor and acceptor units at complementary constituent parts. With such wide-ranging roles, the fundamental properties of H-bonding interactions need to be understood. The energetics of hydrogen bonding interactions cannot be isolated and quantified in the condensed phase. However, these interactions can be isolated and studied quantitatively in gas phase. These studies lead to a fundamental understanding of relations between hydrogen bond strength and molecular structure.²¹⁴ Lukin *et al.* extensively performed DFT based calculations in the rational design of hydrogen-bonded building blocks.²¹⁵ In another study, Riley *et al.* investigated the role of hydrogen bonding interactions in the structural stability of biomacromolecules. They have observed that the interaction is quite different than those played by solvation effects because the presence of certain binding motifs that commonly occur in proteins and DNA (as well as other biomolecular structures), lead to very stable interactions.²¹⁶

Thus, the above discussion provides a glimpse of the enormous scope of DFT based modeling techniques to understand different chemical and biological phenomena. Usually the conventional *Ab initio* calculation on a large size system is computationally intensive. The development of theoretical methodology to reduce the computational cost is always demanding. Present thesis work is a part of our initiative to develop DFT based formalism to study relatively large and interesting chemical and biological interactions

with minimum computational cost justified through relevant experimental evidence. We have proposed that CDASE formalism is a computationally cost effective solution for the intensive quantum mechanical calculations with wide range of applicability e.g., the drug-DNA interaction hybrid nanosystems and crystal structure. It is possible to evaluate three specific parameters, kinetics, amount of charge transfer and thermodynamic stability for a particular interaction from a single CDASE scheme based computation and the theoretical outcomes can be correlated to the experimental findings of that particular system. This significantly reduce the excessive amount of calculations involved in the conventional approaches and that is also with reasonable accuracy.

1.7 Organization of the Thesis

The present Ph. D. dissertation concentrates on the development of computationally cost-effective formalism on the basis of conceptual density functional theory (DFT) based global reactivity descriptors and their applications to provide important insights into the thermodynamics, kinetics and mechanism of reactive interactions. More importantly, our goal is to establish methodical correlation between experimental data and theoretical findings to investigate the reactivity of molecular systems in a qualitative way. Additionally, conventional computational approaches are also implemented to justify reliability of the results obtained from newly proposed methodology.

Chapter I (the present chapter) gives an overview of the present research work, theoretical background, limitations, and advantages of the DFT-based global and local reactivity descriptors along with the related principles, on which these descriptors are based on. An elaborate discussion on “Comprehensive Decomposition Analysis of Stabilization Energy” (CDASE) scheme is also included in the chapter. We discuss in detail the recent developments and applications relevant to the objective of the thesis. This chapter also presents objectives and organization of the work.

Interaction of cisplatin drug (very well known anti-cancer agent) with DNA is one of the highly explored areas in chemistry for last few decades. So far, there is limited numbers of report that explain this interesting phenomenon through conceptual DFT

based reactivity descriptors. In chapter II, we have provided an extensive study on the interaction of aqua-cisplatin (which is the active component of the anti-cancer drug cisplatin) with the two purine nucleobases adenine and guanine. For the first time, we have used proposed CDASE scheme to understand the energetic of such interactions which is very important from the medical point of view.

Although, cisplatin and its analogues have unprecedented success rate against different types of cancer cell-lines, the toxic side-effects of cisplatin drugs are found to be a serious concern for their chemotherapeutic applications. In chapter III, we try to model a scientific protocol for the application of protecting agents against a particular cisplatin analogue to inhibit the toxic side-effects associated with the application of cisplatin drug. Taking the consideration of three major interactions i.e., Cisplatin-DNA, Cisplatin-Protecting agent, and Protecting agent-Active biomolecule, we have suggested some qualitative predictions on the effectiveness of protecting agents against the different cisplatin drugs. Without going through computationally intensive conventional *ab-initio* approaches, proposed CDASE scheme seems to be quite effective to model this kind of complex interactions in the biological medium. On the basis of our theoretical findings, it is possible to predict the most suitable protecting agents against a particular cisplatin analogue. It is encouraging to note that our theoretical predictions are correlated well with the available experimental data.

Due to the quantum confinement effect, carbon based nanostructures exhibit some extraordinary electronic properties and it is one of the most extensively explored research area for the last two decades. Chapter IV, contains a detailed study on the interaction of Singled-Walled Carbon Nanotubes (SWCNT) with different nucleobases. We have explicitly analyzed the kinetic and thermodynamic parameters associated with the interaction between SWCNT DNA. Five CDASE scheme based parameters are calculated for the interaction of nucleobases guanine, adenine, cytosine, thymine, and uracil along with the standard Watson-Crick base pairs AT and GC with eight different CNTs. In this particular study we have implemented the QM:MM based ONIOM model for binding energy calculation to justify the CDASE scheme based findings in case of nanosystems.

Extending the application of CDASE scheme for nanosystems, chapter V, is an attempt to design some hybrid nanostructures and analyze the stability and electronic properties of the proposed NanoBud systems. We have combined the fullerene and SWCNT in a single framework structure known as carbon NanoBud, where the fullerene molecule is attached to the surface of SWCNT through covalent bonding. We have considered C_{32} fullerenes having six different point group symmetries and three different conformations of SWCNTs namely armchair, zigzag and chiral as our model systems. The impact of both fullerene and SWCNT symmetry on the stability of hybrid nanostructure, NanoBud has been analyzed through CDASE scheme based parameters along with conventional binding energy and transition state calculations. We have reported the computer simulated IR spectrums for two hybrid systems to distinguish the structural variation. Molecular Dynamics (MD) simulation is also performed to assess the dynamic stability of the NanoBud structure. It is observed that the attachment of higher symmetry fullerene improves the overall structural stability of the NanoBud system. However, the covalent bonding sites of the fullerene through which it can attach to the surface of SWCNT is equally important for the stability of hybrid framework.

Chapter VI, contains a detailed investigation on the interaction of small gold clusters interaction with DNA. The tunable electronic properties of the gold nanoparticles and DNA composite system finds some sophisticated applications for the development of instrumentation in the contemporary progress of nanobiotechnology. The thermodynamic and kinetic aspects associated to the interaction of metal clusters with nucleobases are assessed using Density Functional Reactivity Theory (DFRT) based CDASE scheme. To obtain more details about the complexation between small gold clusters and nucleobases, conventional binding energy (BE) and transition state (TS) calculations are also performed at B3LYP and MP2 level. It is observed that the interaction between Au_n clusters and nucleobases follows the order $G > A > C > T > U$. It is observed that the GC base pair interaction with Au_n clusters is energetically favorable than that of the AT pair. Additionally, TDDFT calculations are performed on some selected gold-DNA composite to understand the photophysical behavior of those systems. TDDFT analysis predicts significantly high MLCT character for the Au_n -DNA nanocomposite.

The relative stability of the H-bonded crystal structures are analyzed using CDASE scheme in chapter VII. Complementarity of the proposed CDASE scheme and the conventional supermolecular approach is tested in the present study. The most stable binary (1:1) molecular complex formed between urea (U) and m-nitrobenzoic acid (m-NBA) is chosen as a test case. Interaction energy values generated from supermolecular approach show that the most stable binary structure is formed through double H-bonding. Stabilization energy values, generated by the CDASE scheme and derived from the CDFT based reactivity descriptors of the individual components (i.e. Urea and m-NBA) in the overall geometry of the molecular complex, fully supports the outcome of the supermolecular approach.

Finally, chapter VIII presents summary of the outcomes and conclusions of the research presented in this thesis. Particular areas that require further exploration are identified and accordingly, future scope of work is highlighted.

References:

1. P. Wolohan, W. J. Welsh, R. M. Friedman, and J. R. Ebner *Transition State Modeling for Catalysis*, Chapter 20, 1999 **721**, 259.
2. H. Cheng, D. B. Reiser, P. M. Mathias, K. Baumert, S. W. Dean, Jr. *Computer-Aided Molecular Design*, 1995, **589**, 359.
3. (a) K. Fukui, T. Yonezawa, H. Shingu, *J. Chem. Phys.*, 1952, **20**, 722. (b) K. Fukui, T. Yonezawa, C. Nagata, H. Shingu, *J. Chem. Phys.*, 1954, **22**, 1433.
4. (a) K. Fukui, *Theory of orientation and stereoselection*, Springer, Berlin, Heidelberg, New York, 1973. (b) K. Fukui, *Science*, 1987, **218**, 747. *Angew. Chem. Int. Ed.*, 1992, **31**, 187.
5. R. Bonaccorsi, E. Scrocco, J. Tomasi, *J. Chem. Phys.*, 1970, **52**, 5270.
6. P. Politzer, *J. Chem. Phys.*, 1980, **72**, 3027.
7. P. Politzer, *J. Chem. Phys.*, 1980, **73**, 3264.
8. In *Chemical Applications of Atomic and Molecular Electrostatic Potentials*, ed. P. Politzer, D. G. Truhlar, Plenum: New York, 1981.
9. J. Tomasi, R. Bonaccorsi, R. Cammi, *Theoretical Models of Chemical Bonding*, Maksic, R., Ed. Springer: Berlin, 1990, 230.
10. A. D. Becke, K. E. Edgecombe, *J. Chem. Phys.*, 1990, **92**, 5397.
11. A. Savin, O. Jepsen, J. Flad, O. Andersen, H. Preuss, H. von Schnering,
12. R. G. Pearson, *J. Am. Chem. Soc.*, 1963, **85**, 3533.
13. R. G. Pearson, *Hard and Soft Acids and Bases*, Dowden, Hutchinson & Ross, Stroudsburg, PA, 1973.
14. R. G. Parr, R. G. Pearson, *J. Am. Chem. Soc.*, 1983, **105**, 7512.
15. R. T. Sanderson, *Science*, 1951, **114**, 670.
16. G. Klopman, *J. Chem. Phys.*, 1965, **43**, S124.
17. N. C. Baird, J. M. Sichel, M. A. Whitehead, *Theor. Chim. Acta.*, 1968, **11**, 38.
18. R. T. Sanderson, *Chemical Bonds and Bond Energy*, 2nd edn., Academic Press, New York, 1976
19. N. K. Ray, L. Samuels, R. G. Parr, *J. Chem. Phys.*, 1979, **70**, 3680.
20. P. Hohenberg, W. Kohn, *Phys. Rev. B*, 1964, **136**, 864.
21. W. Kohn, L. J. Sham, *Phys. Rev. A*, 1965, **140**, 1133.
22. A. S. Bamzai, B. M. Deb, *Rev. Mod. Phys.*, 1981, **53**, 95.

-
23. S. K. Ghosh, B. Deb, *Phys. Rep.*, 1982, **92**, 1.
 24. R. Dreizler, E. Gross, *Density functional theory: an approach to the quantum many-body problem*, Springer-Verlag Berlin, 1990.
 25. T. Ziegler, *Chem. Rev.*, 1991, 91, 651.
 26. E. J. Baerends, O. V. Gritsenko, *J. Phys. Chem. A*, 1997, **101**, 5383.
 27. W. Koch and M. Holthausen, *A chemist's guide to density functional theory*, Wiley. Vch Weinheim, 2000.
 28. P. W. Ayers, W. Yang, in *Computational Medicinal Chemistry for Drug Discovery*, ed. P. Bultinck, H. De Winter, W. Langenaeker and J. P. Tollenaere, Marcel Dekker Inc: Basel, 2004, pp. 89.
 29. R. G. Parr, *J. Chem. Sci.*, 2005, **117**, 613.
 30. K. Capelle, *Brazilian Journal of Physics*, 2006, **36**, 1318.
 31. A. J. Cohen, P. Mori-Sanchez, W. Yang, *Science*, 2008, **321**, 792.
 32. J. P. Perdew, A. Ruzsinszky, L. A. Constantin, J. Sun, G. B. I. Csonka, *J. Chem. Theory Comput.*, 2009, **5**, 902.
 33. R. G. Parr, R. A. Donnelly, M. Levy, W. E. Palke, *J. Chem. Phys.*, 1978, **68**, 3801.
 34. R. G. Parr, *Annu. Rev. Phys. Chem.*, 1983, **34**, 631.
 35. R. F. Nalewajski, *J. Phys. Chem.*, 1985, **89**, 2831.
 36. R. G. Parr and W. Yang, *Density-Functional Theory of Atoms and Molecules*, Oxford University Press, New York, 1989.
 37. R. G. Parr, W. Yang, *Annu. Rev. Phys. Chem.*, 1995, **46**, 701.
 38. H. Chermette, *J. Comput. Chem.*, 1999, **20**, 129.
 39. P. Geerlings, F. De Proft, *Int. J. Mol. Sci.*, 2002, **3**, 276.
 40. P. Geerlings, F. De Proft, W. Langenaeker, *Chem. Rev.*, 2003, **103**, 1793.
 41. M. H. Cohen, A. Wasserman, *J. Phys. Chem. A*, 2007, **111**, 2229.
 42. J. L. Gázquez, *J. Mex. Chem. Soc.*, 2008, **52**, 3.
 43. *Chemical reactivity theory: a density functional view*, ed. P. K. Chattaraj, CRC, 2009.
 44. R. G. Pearson, *J. Chem. Educ.*, 1987, **64**, 561.
 45. R. G. Pearson, *Acc. Chem. Res.*, 1990, **23**, 1.
 46. R. G. Parr, P. K. Chattaraj, *J. Am. Chem. Soc.*, 1991, **113**, 1854.
 47. R. G. Pearson, W. E. Palke, *J. Phys. Chem.*, 1992, **96**, 3283.
 48. S. Pal, N. Vaval, R. K. Roy, *J. Phys. Chem.*, 1993, **97**, 4404.
 49. R. G. Pearson, *Acc. Chem. Res.*, 1993, **26**, 250.
 50. P. W. Ayers, R. G. Parr, *J. Am. Chem. Soc.*, 2000, **122**, 2010.
 51. A. K. Chandra, T. Uchimaru, *J. Phys. Chem. A*, 2001, **105**, 3578.
 52. M. Torrent-Sucarrat, J. M. Luis, M. Duran, M. Sola, *J. Am. Chem. Soc.*, 2001, **123**, 7951.

-
53. (a) K. R. S. Chandrakumar, S. Pal, *Int. J. Mol. Sci.*, 2002, **3**, 324. (b) M. Torrent.Sucarrat, J. M. Luis, M. Duran, M. Sola, *J. Chem. Phys.*, 2002, **117**, 10561. (c) P. W. Ayers, *Faraday Discuss.*, 2007, **135**, 161.
54. D. R. Hartree, *Proc. Cam. Phil. Soc.*, 1928, **24**, 89.
55. V. Z. Fock, *Z. Phys.*, 1930, **61**, 209.
56. G. Chałasiński, M. M. Szczęśniak *Chem. Rev.*, 2000, **100**, 4227.
57. M. Head-Gordon, T. Van Voorhis, S. R. Gwaltney, Edward F. C. Byrd *Low-Lying Potential Energy Surfaces*, 2002, **828**, 93.
58. E. Schrödinger, *Phys. Rev.*, 1926, **28**, 1049.
59. M. Born, R. Oppenheimer, *Ann. Phys.*, 1927, **84**, 457.
60. A. Szabo, N. S. Ostlund, *Modern Quantum Chemistry*. Mineola, New York: Dover Publishing (1996).
61. J. Slater, H. C. Verma, *Physical Review* 1929, **34**, 1293.
62. P. O. Lowdin, *Adv. Chem. Phys.* 1959 **2**, 207.
63. B. Santra, A. Michaelides, M. Scheoer, *J. Chem. Phys.* 2007, **127**, 184104.
64. S. C. Sherrill, C. David; Schaefer III, F. Henry, "The Configuration Interaction Method: Advances in Highly Correlated Approaches". In Löwdin, Per-Olov. *Advances in Quantum Chemistry* 34, 1999, San Diego: Academic Press. pp. 143–269.
65. Chr. Møller, M. S. Plesset, *Phys. Rev* 1934, **46**, 618.
66. G. D. Purvis, R. J. Bartlett (1982) *The J. Chem. Phys.* 1982, **76**, 1910.
67. M. R. Dreizler, E. K. U. Gross, *Density Functional Theory: An Approach to the Quantum Many-Body Problem* (Springer, Berlin, 1990).
68. R. G. Parr, *Ann. Rev. Phys. Chem.* 1983, **34**, 631.
69. T. Ziegler, *Chem. Rev.* 1991, **91**, 651.
70. R. O. Jones, O. Gunnarsson, *Rev. Mod. Phys.* 1989, **61**, 689.
71. L. H. Thomas, *Proc. Camb. Phil. Soc.* 1927, **23**, 542.
72. E. Fermi, *Rend. Accad. Lincei.* 1927, **6**, 602.
73. P. Hohenberg, W. Kohn, *Phys. Rev.* 1964, **136**, B864.
74. W. Kohn, L. J. Sham, *Phys. Rev.*, 1965, **140**, A1133.
75. R. O. Jones, *Introduction to Density Functional Theory and Exchange-Correlation Energy Functionals*. Published by: Computational Nanoscience: Do It Yourself! J. Grotendorst, S. Blugel, D. Marx (Eds.), 2006.
76. R. G. Parr, *Chemical Hardness*, Wiley-VCH, Weinheim, 1997
77. M. Gell-Mann, K. A. Brueckner, *Phys. Rev.* 1957, **106**, 364.
78. D. M. Ceperley, B. J. Alder, *Phys. Rev. Lett.* 1980, **45**, 566.
79. J. P. Perdew, A. Zunger, *Phys. Rev. B*, 1981, **23**, 5048.
80. J. P. Perdew, Y. Wang, *Phys. Rev. B*, 1991, **45**, 13244.
81. S. J. Vosko, L. Wilk, M. Nusair, *Can. J. Phys.* 1980, **58**, 1200.
82. O. Gunnarsson, B. I. Lundqvist, *Phys. Rev. B*, 1976, **13**, 4274.

-
83. O. Gunnarsson, M. Jonson, B. I. Lundqvist, *Sol. Stat. Comm.*, 1977, **24**, 765.
 84. T. Ziegler, A. Rauk, E. J. Baerends, *Theor. Chim. Acta* 1977, **43**, 261.
 85. K. Burke, J. P. Perdew, M. Ernzerhof, *J. Chem. Phys.*, 1998, **109**, 3760.
 86. J. P. Perdew, K. Burke, Y. Wang, *Phys. Rev. B*, 1992, **54**, 16533.
 87. J. P. Perdew, K. Burke, M. Ernzerhof, *Phys. Rev. Lett.* 1996, **77**, 3865.
 88. J. M. Tao, J. P. Perdew, V. N. Staroverov, G. E. Scuseria, *Phys. Rev. Lett.* 2003, **91**, 146401.
 89. A. D. Becke, *J. Chem. Phys.* 1993, **98**, 5648.
 90. C. Lee, W. Yang, R. G. Parr, *Phys. Rev. B* 1988, **37**, 785.
 91. J. P. Perdew, M. Ernzerhof, K. Burke, *J. Chem. Phys.* 1996, **105**, 9982.
 92. L. Pauling, *J. Chem. Phys.* 1932, **54**, 3570.
 93. A. D. Becke, *J. Chem. Phys.* 1993, **98**, 1372.
 94. E. Runge, E. K. U. Gross, *Phys. Rev. Lett.* 1984, **52**, 997.
 95. R. S. Mulliken, *J. Chem. Phys.* 1934, **2**, 782.
 96. E. P. Gyftopoulos, G.N. Hatsopoulos, *Proc. Natl. Acad. Sci. USA* 1968, **60**, 786.
 97. (a) R. T. Sanderson, *Science* 1951, **114**, 670.
(b) R. T. Sanderson, *Science* 1952, **116**, 41.
(c) R. T. Sanderson, *J. Chem. Edu.* 1952, **29**, 539.
 98. (a) R. G. Pearson, J. Songstad, *J. Am. Chem. Soc.* 1963 **85** 3533. (b) R. G. Pearson, *Science* 1966, **151**, 172.
 99. R. G. Pearson, J. Songstad *J. Am. Chem. Soc.* 1967, **89**, 1827.
 100. R. G. Pearson, *J. Chem. Educ.* 1968, **45**, 581.
 102. R. G. Pearson, *Inorg. Chem.* 1972, **11**, 3146.
 103. R. G. Pearson *Theoretical Models of Chemical Binding: Part II*. In: Z. B. Maksic, ed. Berlin: Springer-Verlag, 1990:45.
 104. R. G. Pearson, *Bonding Energetics in Organometallic Compounds, Chapter 17*, 1990, 428, 251-262. ACS Symposium Series.
 105. (a) R. S. Drago, G. C. Vogel, T. E. Needham, *J. Am. Chem. Soc.* 1971, **93**, 6014.
(b) J. E. Huheey, *Inorganic Chemistry*, 2nd Edition, Oxford Univ. Press, 1979.
 106. R. G. Parr *J. Chem. Educ.*, 1967, **44**, p A162
 107. P. K. Chattaraj, *J. Indian Chem. Soc.* 1992, **69**, 173.
 108. H. J. Chermette, *J. Comput. Chem.* 1999, **20**, 129.
 109. R. G. Parr, L. J. Bartolotti, *J. Am. Chem. Soc.*, 1982, **104**, 3801.
 110. R. P. Iczkowski, J. L. Margrave, *J. Am. Chem. Soc.* 1961, **83**, 3547.
 111. J. P. Perdew, R. G. Parr, M. Levy, J. L. Bladuz, *Phys. Rev. Lett.* 1982, **49**, 1691.
 112. R. G. Parr, L. J. Bartolotti, *J. Phys. Chem.*, 1983, **87**, 2810.
 113. J. F. Janak, *Phys. Rev. B*, 1978, **18**, 7165.
 114. J. P. Perdew, A. Zunger, *Phys. Rev. B* 1981, **23**, 5048.
 115. J. Harris, *Int. J. Quantum Chem.* 1979, **13**, 189.
 116. M. S. Gopinathan, M. A. Whitehead, *Isr. J. Chem.*, 1980, **19**, 209.

-
117. J. C. Slater, *Phys. Rev.*, 1951, **81**, 385.
118. R. G. Pearson, *Proc. Natl. Acad. Sci. USA*, 1986, **83**, 8440.
119. (a) P. K. Chattaraj, H. Lee, R. G. Parr, *J. Am. Chem. Soc.*, 1991, **113**, 1855.
(b) A. Cedillo, P. K. Chattaraj, R. G. Parr, *Int. J. Quantum Chem.*, 2000, **77**, 403.
120. R. J. Kostyk, M. A. Whitehead, *J. Mol. Struct. (Theochem)*, 1991, **203**, 83.
121. W. Yang, R. G. Parr, *Proc. Natl. Acad. Sci., USA*, 1985, **82**, 6723.
122. (a) A. Pasternak, *Chem. Phys.* 1997, **26**, 101.
(b) A. Pasternak, *J. Chem. Phys.* 1980, **73**, 539.
123. R. G. Parr, R. F. Borkman, *J. Chem. Phys.* 1968, **49**, 1055.
124. R. G. Parr, G. Siman, *J. Chem. Phys.* 1971, **55**, 4197.
125. P. Politzer, *J. Chem. Phys.*, 1970, **52**, 2157.
126. (a) Y. Simón-Manso, P. Fuentealba, *J. Phys. Chem. A*, **1998**, *102*, 2029. (b) L. T. Nguyen, F. De Proft, M. C. Amat, V. L. Gregory, P. W. Fowler, P. Geerlings, *J. Phys. Chem. A*, 2003, **107**, 6837. (c) A. K. Chandra, P. Geerlings, M. T. Nguyen, *J. Org. Chem.*, 1997, **62**, 6417.
127. P. Pitansg, M. Giambiagi, M. S. De. Gimbiagi, *Chem. Phys. Lett.*, 1986, **128**, 411.
128. R. G. Parr, L. von Szentpaly, S. Liu. *J. Am. Chem. Soc.*, 1999, **121**, 1922.
129. (a) R. G. Parr, W. Yang, *J. Am. Chem. Soc.*, 1984, **106**, 4049.
(b) P. W. Ayers, M. Levy, *Theor. Chem. Acc.* 2000, **103**, 353.
(c) W. Yang, W. J. Mortier, *J. Am. Chem. Soc.* 1986, **108**, 5708.
130. (a) M. Berkowitz, S. K. Ghosh, R. G. Parr. *J. Am. Chem. Soc.*, 1985, **107**, 6811.
(b) S. Saha, R. K. Roy, *J. Phys. Chem. B*. 2007, **111**, 9664. (c) S. Saha, R. K. Roy, *J. Phys. Chem. B*. 2008, **112**, 1884. (d) S. Saha, R. K. Roy. *Phys. Chem. Chem. Phys.* 2008, **10**, 5591.
131. (a) R. G. Parr, W. Yang, *Annu. Rev. Phys. Chem.*, 1985, **46**, 107. (b) J. L. Reed, *J. Phys. Chem. A*, 1997, **101**, 7396. (c) W. Langenaeker, F. de Proft, P. Geerlings, *J. Phys. Chem.*, 1995, **99**, 6424. (d) J. L. Reed, *J. Phys. Chem. A*, 1997, **101**, 7401.
(e) H. Bögel, S. Hansen, U. Laube, *J. Chem. Inf. Comput. Sci.*, 1997, **37**, 316. (f) T. Mineva, E. Sicilia, N. Russo, *J. Am. Chem. Soc.*, 1998, **120**, 9053.
132. (a) T. Helgaker, S. Coriani, P. Jørgensen, K. Kristensen, J. Olsen, K. Ruud, *Chem. Rev.*, 2012, **112**, 543. (b) D. G. Truhlar, R. Steckler, M. S. Gordon, *Chem. Rev.*, 1987, **87**, 217. (c) R. K. Roy, *J. Phys. Chem. A* 2004, **108**, 4934. (d) R. K. Roy, V. Usha, J. Paulovic, K. Hirao *J. Phys. Chem. A* 2006, **109**, 4601. (e) R. K. Roy, V. Usha, B. K. Patel, K. Hirao, *J. Comput. Chem.* 2006, **27**, 773. (f) R. K. Roy, P. Bagaria, S. Naik, V. Kavala, B. K. Patel, *J. Phys. Chem. A* 2006, **110**, 2181. (g) P. Bagaria, R. K. Roy *J. Phys. Chem. A* 2008, **112**, 97.
133. (a) W. Yang, W. J. Mortier, *J. Am. Chem. Soc.* 1986, **108**, 5708. (b) P. Fuentealba, E. Florez, W. Tiznado, *J. Chem. Theory Comput.*, 2010, **6**, 1470. (c) R. Flores-Moreno, *J. Chem. Theory Comput.*, 2010, **6**, 48. (d) E. Osorio, M. B. Ferraro, O. B. Oña, C. Cardenas, P. Fuentealba, W. Tiznado, *J. Chem. Theory Comput.*, 2011,

-
- 7, 3995.
- (e) H. Fujimoto, N. Koga, K. Fukui, *J. Am. Chem. Soc.*, 1981, **103**, 7452.
134. C. Lee, W. Yang, R. G. Parr, *J. Mol. Struct. (Theochem)*, 1988, **163**, 305.
135. W. Yang, R. G. Parr, R. Pucci, *J. Chem. Phys.* 1984, **81**, 2862.
136. P. K. Chattaraj, A. Cedillo, R. G. Parr, *J. Chem. Phys.* 1995, **103**, 7645.
137. P. K. Chattaraj, A. Cedillo, R. G. Parr, *J. Chem. Phys.* 1995, **103**, 10620.
138. G. Klopman, *J. Am. Chem. Soc.*, 1968, **90**, 223.
139. M. Berkowitz, R. G. Parr, *J. Chem. Phys.* 1988, **88**, 2554.
140. M. K. Harbola, P. K. Chattaraj, R. G. Parr, *Isr. J. Chem.*, 1991, **321**, 395.
141. B. B. Laird, R. B. Ross, and T. Ziegler, *Chemical Applications of Density-Functional Theory*, Chapter 1, **1996**, pp 1-17, *ACS Symposium Series*, Volume 629.
142. R. G. Pearson, *Inorg. Chem.* 1988, **27**, 734.
143. L. J. Bartolotti, S. R. Gadre, R. G. Parr, *J. Am. Chem. Soc.*, 1980, **102**, 2945.
144. J. Robles, L. J. Bartolotti, *J. Am. Chem. Soc.*, 1984, **106**, 3723.
145. S. Manoli, M. A. Whitehead, *J. Chem. Phys.* 1984, **81**, 841.
146. K. S. Lackner, G. Zweig, *Phys. Rev. D.* 1983, **28**, 1671.
147. N. K. Ray, R. G. Parr, *J. Chem. Phys.*, 1980, **73**, 1334.
148. S. Balasubramaniam, K. J. Rao, *Solid State Commun.*, 1989, **71**, 979.
149. D. A. Nepala, J. M. McKay, *Physica, C*, 1989, **158**, 65.
150. G. Luo, R. Y. Wang, *J. Phys. Chem. Solid*, 1989, **50**, 931.
151. S. Ichikawa, *J. Phys. Chem.*, 1989, **93**, 7302.
152. T. K. Ghanty, S. K. Ghosh. *J. Mol. Struct. (Theochem)*, 1992, **274**, 83.
153. S. Shankar, R. G. Parr, *Proc. Natl. Acad. Sci. USA*, 1984, **82**, 264.
154. J. A. Alonso, L. A. Girifalco, *Phys. Rev. B*, 1979, **19**, 3889.
155. N. H. March, R. G. Parr, *Proc. Natl. Acad. Sci. USA*, 1980, **77**, 6285.
156. J. L. Gazquez, A. Vela, M. Galvan, *Phys. Rev. Lett.*, 1986, **56**, 2606.
157. J. L. Gazquez, A. Vela, E. Ortiz, A. Vek, In: R. Erdahl, Jr. V. H. Smith, eds. *Density Matrix and Density Functionals*, Dordrecht: Reidel, 643-662.
158. P. K. Chattaraj, A. Mukherjee, M. P. Das, B. M. Deb, *Proc. Indian. Natl. Acad. Sci.* 1986, **96**, 231.
159. R. G. Parr, *Int. J. Quantum Chem.* 1984, **26**, 687.
160. W. E. Palke, *J. Chem. Phys.* 1980, **72**, 2511.
161. M. P. Gause, *J. Chem. Phys.* 1981, **75**, 828.
162. J. L. Reed, *J. Chem. Phys.* 1981, **75**, 148.
163. P. Politzer, H. Weinstein, *J. Chem. Phys.* 1979, **71**, 4218.
164. T. Leyssens, P. Geerlings, D. Peeters, *J. Phys. Chem. A*, 2006, **110**, 8872.
165. R. P. Iczkowski, J. L. Margrave, *J. Am. Chem. Soc.* 1961, **83**, 3547.
166. P. Politzer, R. G. Parr, D. R. Murphy, *J. Chem. Phys.*, 1983, **79**, 3859.
167. R. G. Boyd, G. E. Markus, *J. Chem. Phys.*, 1981, **75**, 5885.

-
168. L. C. Balbas, J. A. Alonso, L. V. Vega, *Z. Phys.* 1986, **D1**, 215.
169. B. M. Deb, R. Singh, N. Sukumar, *J. Mol. Struct. (Theochem)*, 1992, **259**, 121.
170. S. Nath, S. Bhattacharjee, P. K. Chattaraj, *J. Mol. Struct. (Theochem)*, 1995, **331**, 267.
171. P. Funtealba, R. G. Parr, *J. Chem. Phys.* 1991, **94**, 5559.
172. P. K. Chattaraj, *J. Ind. Chem. Soc.* 1993, **70**, 103.
173. L. C. Balbas, J. A. Alonso, H. E. Las, *Mol. Phys.*, 1983, **48**, 981.
174. (a) W. J. Mortier, K. A. van Genechten, J. Gasteiger, *J. Am. Chem. Soc.*, 1985, **107**, 829.(b) J. Gasleiger, M. Marsili, *Tetrahedron*, 1980, **36**, 3219.(c) W. J. Mortier, S. K. Ghosh, S. Shankar, *J. Am. Chem. Soc.*, 1986, **108**, 5063.
(d) K. A. van Genechten W. J. Mortier, P. Geerlings, *J. Chem. Phys.*, 1987, **86**, 5063.
175. F. Bertant, *J. Phys. Radium*, 1952, **13**, 499.
176. P. P. Ewald, *Ann. Phys.* 1921, **64**, 253.
177. T. K. Ghanty, S. K. Ghosh, *J. Mol. Struct. (Theochem)*, 1992, **274**, 83.
178. W. Yang, C. Lee, S. K. Ghosh, *J. Chem. Phys.* 1985, **89**, 5412.
179. T. K. Ghanty, S. K. Ghosh, *J. Chem. Phys.* 1991, **95**, 6512.
180. V. Gutmann, *The Donor-Acceptor Approach to Molecular Interaction*. New York: Plenum, 1978.
184. A. S. Bamzai, B. M. Deb, *Rev. Mod. Phys.* 1981, **53**, 91.
185. S. K. Ghosh, R. G. Parr, *Theor. Chim. Acta.* 1987, **72**, 379.
186. T. K. Ghanty, S. K. Ghosh, *Inorg. Chem.* 1992, **31**, 1951.
187. T. K. Ghanty, S. K. Ghosh, *J. Chem. Soc. Chem. Comm.* 1992, **1**, 1502.
188. S. K. Ghosh, *Int. J. Quantum Chem.* 1994, **49**, 239.
189. T. A. Koopmans, *Physica.* 1933, **1**, 104.
190. P. Bagaria, S. Saha, S. Murru, V. Kavala, B. Patel, R. K. Roy, *Phys. Chem. Chem. Phys.* 2009, **11**, 8306.
191. B. Rosenberg, L. Van Camp, T. Krigas *Nature* 1965, **205**, 698.
192. S. E. Sherman, S. J. Lippard, *Chem. Rev.* 1987, **87**, 1153.
193. M. H. Baik, R. A. Friesner, S. J. Lippard, *J. Am. Chem. Soc.*, 2003, **125**, 14082.
194. Y. Mantri, S. J. Lippard, M. H. Baik. *J. Am. Chem. Soc.* 2007, **129**, 5023.
195. R. J. Chen, Y. G. Zhang, D. W. Wang, H. J. Dai, *J. Am. Chem. Soc.* **2001**, **123**, 3838.
196. Dinadayalane, T. C.; Leszczynski, J. *Toward Nanomaterials: Structural, Energetic and Reactivity Aspects of Single-Walled Carbon Nanotubes*. In *Nanomaterials: Design and Simulation* ; Balbuena, P. B.; Seminario, J. M., Eds.; Elsevier: Amsterdam, 2006; pp 167.
197. A. Bianco, M. Prato, *Adv. Mater.* 2003, **15**, 1765.
198. R. Satio, G. Dresselhause and M. Dresselhause, *Physical Properties of Carbon Nanotubes*; Imperial College Press: London, UK, 2003.

-
199. P. Singh, S. Campidelli, S. Giordani, D. Bonifazi, Abiancoand M. Prato, *Chem. Soc. Rev.* 2009, **38**, 2214.
 200. A. D. Bobadilla, J. M. Seminario *J. Phys. Chem. C* 2011, **115**, 3466.
 201. Lu, G.; Maragakis, P.; Kaxiras, E. *Nano Lett.* 2005, **5**, 897.
 202. Drexler, K. E. *Nanosystems: Molecular Machinery, Manufacturing and Computation* Wiley, **1992**.
 203. B. W. Smith, M. Monthieux, D. E. Luzzi, *Nature* 1998, **396**, 323.
 204. X. J. Wu, X. C. Zeng, *ACS Nano* 2008, **2**, 1459.
 205. H. He, B. C. Pan, *J. Phys. Chem. C* 2009, **113**, 20822.
 206. M. J. Tarlov, A. B. Steel, *Biomolecular Films: Design, Function, and Applications*; Marcel Dekker: New York, 2003; Vol. 111
 207. R. Muller, A. Csoki, J. M. Kohler, W. Fritzsche, *Nucleic Acids Res.* 2000, **28**, e91.
 208. C. M. Niemeyer, *Angew. Chem., Int. Ed.* 2001, **40**, 4129.
 209. M. C. Pirrung, *Angew. Chem., Int. Ed.* 2002, **41**, 1276.
 210. R. Bashir, *Superlattices Microstruct.* 2001, **29**, 1.
 211. L. M. Demers, M. Ostblom, H. Zhang, N. H. Jang, B. Liedberg, C. A. Mirkin, *J. Am. Chem. Soc.* 2002, **124**, 11248.
 212. E. S. Kryachko, F. Remacle *J. Phys. Chem. B* 2005, **109**, 22746.
 213. L. Pauling, *The Chemical Bond: A Brief Introduction to Modern Structural Chemistry* Cornell University Press: Ithaca, NewYork, 1967
 214. C. A. Deakyne, In *Molecular Interactions*; Scheiner, S., Ed.; John Wiley: New York, 1997
 215. O. Lukin, J. Leszczynski, *J. Phys. Chem. A*, 2002, **6**, 6775.
 216. K. E. Riley, M. Pitonak, J. Cerny, P. Hobza, *J. Chem. Theory Comput.* 2010, **6**, 66.

Chapter II

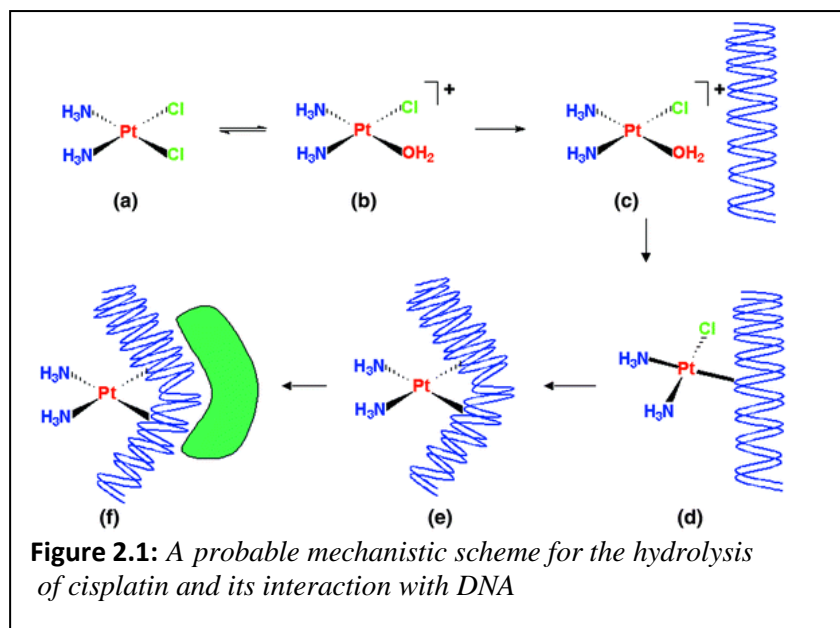
Understanding the Interaction of Aqua-
cisplatin with Nucleobase Guanine over
Adenine: A Density Functional Reactivity
Theory Based Approach

2.1 Introduction:

Design and development of a new generation of metal-containing anti-cancer drugs attributes an emerging area of research in recent times.¹ In the last four decades remarkable achievements in the field of cancer treatment have been observed with the introduction of various metal-containing anti-cancer agents.² It is conspicuous that an adequate understanding of the biological pathways that differentiate between carcinogenic states from the normal healthy states is important to design an effective anti-cancer agent that is selective for the cancer cells, without affecting normal cells. Since its discovery by Rosenberg *et al.*³ in 1964, cisplatin (cis-[PtCl₂(NH₃)₂]) has been credited with greater recognition as one of the most widely used, anti-cancer drug to date.⁴⁻⁷ This was one of the successful developments of metal-containing anti-cancer agent, which is widely used to treat testicular, ovarian, head, neck and small cell lung cancer^{8,9} (with excellent cure rate up to 90%).^{1,10-12} To make a better understanding of the anti-cancer activity of cisplatin the researcher explores the interaction mechanism of the drug with DNA bases (Fig 2.1).^{7,13,14,26a} The anti-tumor activity of cisplatin originated from its interaction with guanine bases (specifically at N-7 position) in genomic DNA.^{15,16} Initial attachment of cisplatin with guanine generates mono-functional adduct, which in turn is closed by formation of intrastrand or interstrand crosslinking^{17,18} with N-7 position of another purine base of DNA.^{19,20} Another mode of binding is DNA-protein crosslinking. As the leaving group (-Cl or -OH₂)²¹ are in cis orientation, the intrastrand crosslinking between two adjacent purine bases is more preferred over interstrand one. Again, the most abundant intrastrand adduct is of GpG type and ApG cross-link being the next major adducts formed.^{22,23}

Over the past few years, many theoretical studies have been reported on the hydrolysis of cisplatin²⁴⁻²⁶ and its analogs (both in semi empirical and *ab-initio* levels) as well as mode of interactions of these drugs with purine bases.^{27,28} These theoretical studies put some new insights to the origin of anticancer activity of cisplatin drug. Wysokinski *et al.* performed a DFT (Density Functional Theory) based study²⁹ to compare the structural properties and vibrational spectra of cisplatin and its analogue carboplatin. Another useful study by Baik *et al.*¹⁹ revealed the importance of H-bonding and strong electrostatic interaction on the stability of adduct formation between cisplatin

drugs and purine bases. The nature of the transition state generated in the process of substitution of two labile chloride ligands of cisplatin by water and guanine has been theoretically investigated by Chaval *et al.*^{24(a)} In a recent study Mantri *et al.*^{26(a)} adopted DFT based approach to explore the bifunctional binding interaction of cisplatin with DNA. Using classical molecular dynamics simulation technique Carloni *et al.*^{24(f)} studied the interaction of cisplatin with 1, 2-d(GpG) sequence of DNA. Solvent effects on the reactivity of different cisplatin analogues has been investigated by Sarmah *et al.*^{24(d)} using density functional theory based reactivity descriptors. An elaborate study on the stability of DNA bases in presence of square planar platinum complexes has been reported by Zeizinger *et al.*^{27(a)}



In last three decades a series of reactivity descriptors^{30,31} have been proposed within the framework of density functional reactivity theory (DFRT).^{32,33} Reactivity descriptors such as chemical potential (μ)^{34(c)} (i.e., the negative of electronegativity), chemical hardness^{34(a)} (η), global electrophilicity index,^{35,36} nucleophilicity,³⁷ electrofugality and nucleofugality,³⁸ etc. are known as global reactivity descriptors, which represent properties of a molecule as a whole. The local reactivity descriptors, which have the potential to describe relative reactivity (or site selectivity) are Fukui function $[f(r^-)]$,^{34(b,d)} local softness $[s(r)]$, local hardness $[\eta(r)]$,³⁹⁻⁴¹ etc.

An explicit study on different components of stabilization energy values, derived on the basis of DFT based reactivity descriptors, can produce worthy information about the kinetics and thermodynamics of chemical reactions. In a very recent study Sarmah *et al.*⁴³ have shown that (by using already proposed Comprehensive Decomposition Analysis of Stabilization Energy (CDASE)-scheme⁴²) components of stabilization energy (in terms of donor and acceptor) as well as charge transfer values can be used to determine the most stable adduct formed through weak non-bonding interaction. Saha *et al.*⁴⁴ performed an exclusive study to understand the interaction between different diens and dinophiles in Diels-Alder cycloaddition reaction using CDASE scheme based formalism.

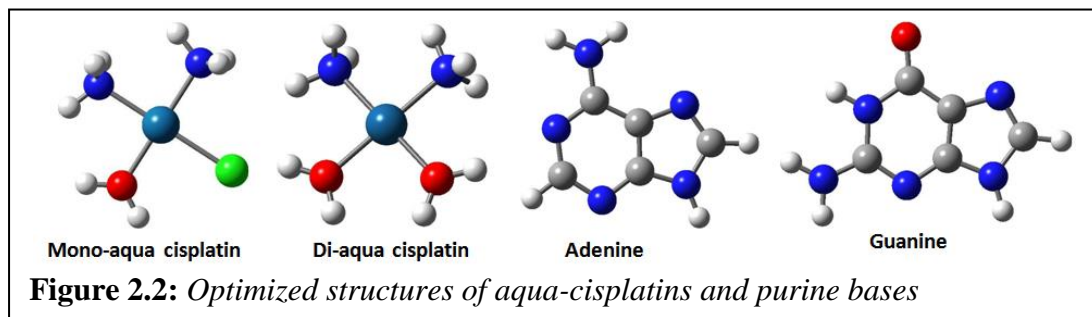
However, the focus of our present study is on the reliability of the CDASE scheme in extracting some information on an important biological phenomena and that is drug-DNA interaction. It is well known that hydrolysis of cisplatin to form mono-aqua and di-aqua complexes (by the replacement of chloride ligands with water molecules) is necessary for the activation of relatively inert platinum (II) complexes.^{26(a)} However, an ultimate mechanistic pathway regarding the competitive interaction of these two reactive species (*i.e.*, mono-aqua and di-aqua complex of cisplatin) with DNA bases is yet to be explored. Whether both of these complexes are equally reactive or one of them are more dominant as precursor in the interaction of cisplatin with DNA-bases requires an in-depth study. CDASE scheme based stabilization energy components, augmented by careful modeling technique, are expected to throw some light on this important aspect of cisplatin therapy.

Thus, the entire discussion emphasizes the worthiness of the proposed CDASE scheme in explaining interaction of aqua-cisplatin with purine bases, which is expected to open up extensive future applications of this scheme in exploring the activity of other kinds of drugs with DNA. Towards the end, some possible limitations of the CDASE scheme (as adopted in the present study) and its probable refinements are highlighted.

2.2 Computational Details:

In our computational model, two hydrolyzed products of cisplatin [Pt(NH₃)₂Cl₂] are chosen as acceptors (A) and these are the mono-aqua complex ([Pt(NH₃)₂ClH₂O]⁺)

and the di-aqua complex ($[\text{Pt}(\text{NH}_3)_2(\text{H}_2\text{O})_2]^{2+}$). The two DNA bases, adenine and guanine, are chosen as donor systems (*i.e.*, B). The three dimensional (3D) structures of aqua-cisplatin as well as purine bases are shown in Fig 2.2.



All the structures were generated with Gauss View^{45(a)} visualization program. The geometries of adenine and guanine are generated at RHF⁴⁶, MP2⁴⁷, and B3LYP^{48,49} level using 6-31G (d, p) basis set.⁵⁰⁻⁵² However, for aqua-cisplatins although the levels remain same (*i.e.*, RHF, MP2, and B3LYP) the basis set used is LanL2DZ⁵³ (with effective core potential, ECP^{54,55}). Use of LanL2DZ basis sets is a common practice for system containing atoms of higher atomic number (Pt in case of cisplatin), because in this way, chemically inert core electrons can be taken care and at the same time computational cost will also be reduced.^{56(a-c)} All the above methods are as implemented in the Gaussian 03 package.^{45(b)} Vertical ionization potential (IP) and electron affinity (EA) values are only considered in the present study and these are generated from separate single point calculations for neutral, cationic and anionic systems. While restricted level of theories (like as RHF/6-31G (d,p), RMP2/6-31G(d,p)) were used for the neutral systems, unrestricted level (such as UHF/6-31G(d,p), UMP2/6-31G(d,p)) were adopted for the calculations of ionic systems. All calculations are performed in the gas phase.

2.3 Results and Discussion:

To understand exact structures of the mono-functional adducts formed between aqua-cisplatin and purine bases¹⁶ a theoretical study was carried out by Baik et al.¹⁹ They observed that thermodynamic preference (in terms of binding free energy in solution) for the adduct formation of mono-aqua cisplatin with guanine is increased by 4.6 kcal/mol over that of adenine (in gas phase this difference is even higher *i.e.*, 17.3 kcal/mol). The

same value for di-aqua cisplatin (as an electrophile) is 10.8 kcal/mol (in gas phase this preference is by 26.17 kcal/mol), indicating the adducts formed by guanine and di-aqua cisplatin is the most stable one.

Baik et al.¹⁹ attributed the observed trend of stabilities to the following factors:

- (1) A stronger H-bonding interaction between amino H of cisplatin and exocyclic oxygen atom of guanine.
- (2) A stronger electrostatic interaction between the interacting aqua complexes of cisplatin and the nucleobase guanine.

The kinetic preference of mono-aqua cisplatin for nucleobase guanine has been verified from the higher transition state energy barrier (approximately 5.56 kcal/mol in water as a solvent) for the adduct formation between mono-aqua cisplatin and adenine compared to mono-aqua cisplatin and guanine.¹⁹ However, for the interaction of di-aqua complex of cisplatin with guanine the lowest transition state energy barrier is found to be 21.81 kcal/mol, where as for the interaction of di-aqua cisplatin and adenine it is 34.47 kcal/mol. These results argue a kinetically preferable guanine-di-aqua cisplatin interaction over that of adenine-di-aqua cisplatin one.

Although, the approach adopted in the present study is not that rigorous as that of Baik *et al.*,¹⁹ it is much simpler, easy to compute and yet reproduce the experimental trends¹⁷ qualitatively. The CDASE approach does not go through the computationally intensive transition state optimization because it is based on the electronic properties of the individual isolated cisplatin complexes and purine bases. In the following subsections reliability of different energy components (based on CDASE scheme) in establishing thermodynamic and kinetic preference of guanine over that of adenine in the adduct formation process with aqua-cisplatins will be tested.

2.3.1. Application of CDASE scheme to understand the relative stability of adducts formed by aqua-cisplatins and purine bases:

In the introduction chapter, we have briefly discussed the role of different reactivity parameters (based on CDASE scheme) in explaining various aspects of chemical interactions. These parameters are global electrophilicity value (w), positive energy component ($\Delta E_{B(A)}$), negative energy component ($\Delta E_{A(B)}$), amount of charge

transfer (ΔN) and overall stabilization energy ($\Delta E_{SE(AB)}$). In the following paragraphs we will try to establish how these reactivity parameters can be used to predict the most stable adducts between aqua-cisplatin and purine bases.

(i) *Justification for the relative rates of formation of adducts between aqua-cisplatin and purine bases according to the difference of global electrophilicity (Δw) values:*

Table 2.1 presents the difference of global electrophilicity (Δw) values between the acceptor A (aqua-cisplatin) and the donor B (purine bases). The values are generated as per the following Eqn,

$$\Delta w = w_A - w_B \quad 2.1$$

The higher are the differences between global electrophilicity values stronger the interaction between them will be. Thus, a positive value for Δw indicates an energetically favorable process, *i.e.*, flow of electrons from donor to acceptor. From the values of Δw we can determine the comparative rate of interaction between different systems. It is obvious from Table 2.1 that Δw values for mono-aqua complexes are much lower than the corresponding values of di-aqua complexes. This clearly indicates that interaction of di-aqua complex of cisplatin (with purine bases) is more favorable than that of mono-aqua complexes. Thus, in the absence of precise experimental knowledge on exact mechanism of interaction of cisplatin with DNA-bases, values of Δw can be very informative in understanding the reactivity of this anti-cancer drug with DNA-bases.

(ii) *Justification for the relative rates of formation of adducts between aqua-cisplatin and purine bases according to the positive energy component ($\Delta E_{B(A)}$) values:*

According to the theoretical interpretation from CDASE scheme, the energy component $\Delta E_{B(A)}$ is defined as a positive quantity. So, for a particular interaction $\Delta E_{B(A)}$ is an energy raising term. Simply, considering a chemical interaction between donor and acceptor system, $\Delta E_{B(A)}$ value can be correlated to the kinetic aspect of that particular interaction.⁴² The higher the value of $\Delta E_{B(A)}$, higher will be the rate of interaction between cisplatin complexes with DNA bases. From the values of $\Delta E_{B(A)}$ (Table 2.2) our interpretation is that, for both mono and di-aqua complexes of cisplatin,

the preferred active site for interaction in DNA is the guanine base (with solo exception in the MP2 method, where $\Delta E_{B(A)}$ value for the adduct between di-aqua cisplatin and adenine is 0.11 kcal/mol higher than that with the guanine one). This is what we expect from earlier experimental observations.¹⁷ Also, between the mono and di-aqua complex of cisplatin, $\Delta E_{B(A)}$ values of adducts formed by the second one are very high. This implies that di-aqua complex of cisplatin is the main active component during the platination process of DNA bases, and between the DNA bases it is guanine with which the adduct formation process is faster. Interestingly, the conclusion with Δw values was also.

(iii) *Justification for the relative stability of adducts formed by aqua-cisplatins and purine bases according to the negative energy component ($\Delta E_{A(B)}$) values:*

Taking the analogy from classical thermodynamics it is clear that in a spontaneous process (*i.e.*, when electrons flow from the donor to the acceptor) $\Delta E_{A(B)}$ should be a negative quantity. Also, as par our discussion, $\Delta E_{A(B)}$ can be written as, $|\Delta E_{A(B)}| = |\Delta E_{SE(AB)}| + |\Delta E_{B(A)}|$ in absolute terms. So, it can be directly correlated to both the kinetics (*i.e.*, the rate of adduct formation, because of the $\Delta E_{B(A)}$ component) as well as thermodynamics (*i.e.*, stability of the adduct formed, because of the $\Delta E_{SE(AB)}$ component) of the adduct formation process. The $\Delta E_{A(B)}$ values generated from CDASE scheme are produced in Table 2.3. In case of guanine-cisplatin adducts, $\Delta E_{A(B)}$ values are more negative than those generated for adenine-cisplatin adducts. Again, when di-aqua complex of cisplatin is involved in adduct formation with DNA-bases, $\Delta E_{A(B)}$ values became more negative in comparison to mono-aqua adducts. There is a sole exception and that is in the MP2 method the $\Delta E_{A(B)}$ value for adduct formed by di-aqua complex with adenine is 0.24 kcal/mol more negative than that formed with guanine. This gives a clear indication that adduct formation between di-aqua complex of cisplatin and purine bases is thermodynamically more favorable than that with mono-aqua complex.

(iv) *Justification for the relative stability of adducts formed by aqua-cisplatin and purine bases according to the amount of charge transfer (ΔN) values:*

As the charge transfer quantity (ΔN) is a multiplicative factor, so it is obvious that increase in charge transfer (ΔN) value will also increase the magnitude of both $\Delta E_{B(A)}$ and $\Delta E_{A(B)}$ (i.e., $\Delta E_{B(A)}$ will be more positive and $\Delta E_{A(B)}$ will be more negative). Hence, with the increase of the value of ΔN , both the rate of interaction as well as the stabilities of adducts should increase. Table 2.4 demonstrates the ΔN values for the process of adduct formation between cisplatin (both mono and di-aqua complexes) with DNA-bases. It is obvious from the ΔN values generated in the CDASE scheme that cisplatin-guanine interactions are both kinetically and thermodynamically more preferable to those of cisplatin-adenine, and also di-aqua complex of cisplatin is more effective (in both respects) than mono-aqua complex in the process of interaction with DNA.

(v) *Justification for the relative stability of adducts formed by aqua-cisplatin and purine bases according to the overall stabilization energy ($\Delta E_{SE(AB)}$) values:*

Finally, in Table 2.5 we have reported the overall stabilization energy ($\Delta E_{SE(AB)}$) values. The values of $\Delta E_{SE(AB)}$ also supports our observations on the basis of values of ΔN , and $\Delta E_{A(B)}$ and that is, between adenine and guanine the later one forms the most stable adduct with the di-aqua complex of cisplatin. Thus, overall it can be concluded that there is a possibility of forming two complexes during the hydrolysis of anti cancer agent cisplatin, namely the mono-aqua complex (when one chloride ligand is replaced by one water molecule) and the di-aqua complex (when both chloride ligands are replaced by two water molecules). However, it is the di-aqua complex which interacts more strongly with DNA-bases guanine and adenine. Also, the adduct of di-aqua cisplatin with guanine is the most stable one in the platination process.

2.3.2. Identification of the Donor and Acceptor on the Basis of CDASE Scheme:

Normally, in a chemical reaction it is not possible to predict rigorously the donor and acceptor species only by simple observation (although common wisdom about the

electronic properties of the two interacting species sometimes helps to guess the donor and the acceptor). To know precisely which one between cisplatin and the purine base (*i.e.*, guanine or adenine) acts as an acceptor (A) and which one as donor (B) we have summarized the values of ΔN , $\Delta E_{B(A)}$, $\Delta E_{A(B)}$ and $\Delta E_{SE(AB)}$ (already reported in Tables 2.4, 2.2, 2.3 and 2.5, respectively) in Table 2.6. The values are for mono-aqua cisplatin complex. We observe that when we consider cisplatin as model acceptor (A) and purine base as model donor (B) both ΔN and $\Delta E_{B(A)}$ values are positive and $\Delta E_{A(B)}$ values become negative. This observation (*i.e.*, the direction of electron flow) is justified as cisplatin, with an electron deficient center (presence of vacant d-orbitals in Pt metal), can act as an electron acceptor. On the other hand, the purine bases with lone pair of electrons (on nitrogen as well as on oxygen atoms), can act as an electron donor. However, when we consider cisplatin as donor (*i.e.*, B) and purine base (guanine or adenine) as acceptor (*i.e.*, A) sign of ΔN , $\Delta E_{B(A)}$ and $\Delta E_{A(B)}$ are changed (Table 2.6, lower part). This implies that the process cannot be a spontaneous one. Another interesting aspect is that $\Delta E_{SE(AB)}$ values, alone, cannot decide the donor and acceptor in the adduct formation process. This is because the same negative values are obtained for $\Delta E_{SE(AB)}$ even if we change the donor and acceptor systems (*i.e.*, taking cisplatin as donor and purine base as acceptor).

This is also justified from the equation for ΔN (*i.e.*, $\Delta N = \frac{\mu_B^0 - \mu_A^0}{(\eta_A + \eta_B)}$) where the

numerator is $(\mu_A^0 - \mu_B^0)^2$ and so the sign of $\Delta E_{SE(AB)}$ does not change if donor (B) and acceptor (A) species are interchanged.

2.4 Conclusions:

In this work, the preferred binding interaction of the two possible hydrolysis products of the well known chemotherapeutic drug cisplatin (*i.e.*, $cis\text{-}[\text{Pt}(\text{NH}_3)_2\text{Cl}(\text{H}_2\text{O})]^+$ and $cis\text{-}[\text{Pt}(\text{NH}_3)_2(\text{H}_2\text{O})_2]^{2+}$) to nucleobases adenine and guanine is investigated by density functional reactivity theory. Components of stabilization energy [$\Delta E_{SE(AB)}$] values (as generated by the CDASE scheme) are used to explain the interaction of cisplatin and

purine bases. These are, positive energy component [$\Delta E_{B(A)}$], negative energy component [$\Delta E_{A(B)}$], the overall stabilization energy [$\Delta E_{SE(AB)}$] and the amount of charge transfer [ΔN]. The generated trends by all these four parameters are as per experimental observations. More preferred reactivity for nucleobase guanine has been observed, when di-aqua complex of cisplatin (*i.e.*, $\text{cis-}[\text{Pt}(\text{NH}_3)_2(\text{H}_2\text{O})_2]^{2+}$) act as platination agent. Also, the di-aqua complex of cisplatin has been found to form more stable adducts (with both guanine and adenine) than the mono-aqua complex, supporting the former as a preferable precursor in the platination process. Thus, CDASE seems to be a reliable scheme to explain the reaction mechanism of cisplatin. This observation is also further supported by the difference of global electrophilicity values (*i.e.*, Δw) between the acceptor and the donor (Table 2.1).

The role of ΔN values in identifying the donor and acceptor systems in case of spontaneous electron flow is something new and interesting aspect of the present study. For a spontaneous process, the ΔN value will always be positive. This fact is very clearly demonstrated through our study when we consider aqua-cisplatin as acceptor (A) and adenine or guanine as donor (B) (Table 2.6). Charge transfer, ΔN , values generated from CDASE scheme, provide important clue for this purpose. Because in the CDASE scheme the charge transfer (ΔN) is evaluated using energy based parameters (*i.e.*, μ and η), it is very reliable (at least for qualitative prediction).

The mechanism of interaction of cisplatin drugs with genomic DNA is a very broad and extensive field of research. We are aiming further to extend our proposed theoretical approach (*i.e.*, CDASE scheme) to study the interaction of cisplatin on a relatively large system by considering three to five DNA base pair units. An explicit theoretical investigation on sequence-specific intrastrand cross-linking of cisplatin with DNA will shed some new light on the interesting problem of drug-DNA interaction. A clear concept of the action of cisplatin as an anti-cancer drug will help to design new cisplatin analogues, which are more effective and efficient. Also, reduction of the cisplatin-induced toxic side effects is a major concern in recent times. We are trying to gain some new insights into this problem along with improvement and modification of

the CDASE scheme (after inclusion of electrostatic and dispersion interactions) in our upcoming study.

References:

1. E. Wong, C. M. Giandomenic, *Chem. Rev.* 1999, **99**, 2451.
2. A. Dedieu, *Chem. Rev.* 2000, **100**, 543.
3. B. Rosenberg, L. Van Camp, T. Krigas, *Nature* 1965, **205**, 698.
4. S. E. Sherman, S. J. Lippard, *Chem. Rev.* 1987, **87**, 1153.
5. G. J. Bosl, D. F. Bajorin, J. Sheinfeld, R. Motzer, In *Cancer: Principles and Practice of Oncology*, 6th ed.; DeVita, V. T., Hellman, S., Rosenberg, S. A., Eds.; Lippincott, Williams & Wilkins: Philadelphia, PA, 2000.
6. H. M. Pinedo, J. H. Schornagel, *Platinum and Other Metal Coordination Compounds in Cancer Chemotherapy*; Plenum Press: New York, 1996.
7. D. Wang, S. J. Lippard, *Nat. Rev. Drug Discov.* 2005, **4**, 307.
8. R. S. Go, A. A. Adjei, *J. Clin. Oncol.* 1999, **17**, 409.
9. E. R. Jamieson, S. J. Lippard, *Chem. Rev.* 1999, **99**, 2467.
10. M. Gordon, S. Hollander, *J Med.* 1990, **24**, 209.
11. J. Reedijk, *Chem. Commun.* 1996, **7**, 801.
12. I. Judson, L. R. Kelland, *Drugs* 2000, **59**, 29.
13. (a) M. A. Fuertes, C. Alonso, J. M. Perez, *Chem. Rev.* 2003, **103**, 645. (b) D. V. Deubel, *J. Am. Chem. Soc.* 2002, **124**, 5834.
14. S. Akiyama, Z. S. Chen, T. Sumizawa, T.; Furukawa, *Anti-Cancer Drug Des.* **1999**, *14*, 143.
15. H. C. Harder, B. Rosenberg, *Int. J. Cancer* 1970, **6**, 207.
16. (a) J. A. Howle, G. R. Gale, *Biochem. Pharmacol.* 1970, **19**, 2757. (b) S. E. Sherman, D. Gibson, A. H. J. Wang, S. J. Lippard, *Science* 1985, **230**, 412.
17. (a) D. P. Bancroft, C. A. Lepre, S. J. Lippard, *J. Am. Chem. Soc.* 1990, **112**, 6860; (b) J. C. Dabrowiak, W. T. Bradner, *Prog. Med. Chem.* 1987, **24**, 129.
18. S. Khiati, D. Luvino, K. Oumzil, B. Chauffert, M. Camplo, P. Barthélémy, *ACS Nano* 2011, **5**, 8649.
19. M. H. Baik, R. A. Friesner, S. J. Lippard, *J. Am. Chem. Soc.* 2003, **125**, 14082.
20. S. S. G. E. Van Boom, S. J. Reedijk, *J. Chem. Soc. Chem. Commun.* 1993, 1397.
21. T. D. Tullius, H. M. Ushay, C. M. Merkel, J. P. Caradonna, S. J. Lippard, *ACS Symp. Ser.* 1983, **209**, 51.
22. (a) J. M. Malinge, A. Schwartz, M. Leng, *Nucleic Acids Res.* 1987, **15**, 1779. (b) A. Eastman, *Cancer Cell Mon. Rev.* 1990, **2**, 275. (c) A. Eastman, *Biochemistry* 1983, **22**, 3927. (d) A. M. J. Fichtinger-Schepman, J. L. van der Veer, J. H. L. den Hartog, P. H. M. Lohman, J. Reedijk, *Biochemistry* 1985, **24**, 707. (e) K. Inagaki and Y. Kidani, *Inorg. Chim. A: Bioinor.* 1983, **80**, 171. (f) B. Van Hemelryck, J. P. Girault, G. Chottard, P. Valadon, A. Laoui, J. C. Chottard, *Inorg. Chem.* 1987, **26**, 787.
23. (a) D. B. Zamble, D. Mu, J. T. Reardon, A. Sancar, S. J. Lippard, *Biochemistry* 1996, **35**, 10004. (b) D. B. Zamble, S. J. Lippard, *Trends Biochem. Sci.* 1995, **20**, 435. (c) J. L. Vanderveer, H. Vandanelst, J. H. J. Denhartog, A. M. J. Fichtinger-Schepman and J. Reedijk, *Inorg. Chem.* 1986, **25**, 4657. (d) J. C. Dewan, *J. Am. Chem. Soc.* 1984, **106**, 7239. (e) S. E. Sherman, D. Gibson, A. H. J. Wang, S. J. Lippard, *J. Am. Chem. Soc.* 1988, **110**, 7368. (f) B. E. Bowler, S. J. Lippard, *Biochemistry* 1986, **25**, 3031.

-
24. (a) Z. Chval, M. J. Sip, *Mol. Struct. THEOCHEM*, 2000, **532**, 59. (b) Y. Zhang, Z. Guo, X. Z. You, *J. Am. Chem. Soc.*, 2001, **123**, 9378. (c) L. A. S. Costa, W. R. Rocha, W. B. D. Almeida, H. F. Dos Santos, *J. Chem. Phys.* 2003, **118**, 10584. (d) P. Sarmah, R. C. Deka, *Int. J. Quantum. Chem.* 2008, **108**, 1400. (e) P. Sarmah, R. C. Deka *J. Comput. Aided. Mol. Des.* 2009, **23**, 343. (f) P. Carloni, M. Sprik, W. Andreoni, *J. Phys. Chem. B* 2000, **104**, 823.
25. (a) J. Raber, C. Zhu, L. A. Eriksson, *Mol. Phys.* 2004, **102**, 2537. (b) J. K. C. Lau, D. V. Deubel, *J. Chem. Theory. Comput.* 2006, **2**, 103.
26. (a) Y. Mantri, S. J. Lippard, M. H. Baik, *J. Am. Chem. Soc.* 2007, **129**, 5023. (b) J. Raber, C. Zhu, L. A. Eriksson, *J. Phys. Chem. B* 2005, **109**, 11006.
27. (a) M. Zeizinger, J. V. Burda, J. Leszczynski, *Phys. Chem. Chem. Phys.* 2004, **6**, 3585. (b) A. Robertazzi, J. A. Platts, *Chem. Eur. J.* 2006, **12**, 5747. (c) P. N. V. Pavankumar, P. Seetharamulu, S. Yao, J. D. Saxe, D. G. Reddy, F. H. Hausheer, *J. Comput. Chem.* 1999, **20**, 365.
28. (a) K. Spiegel, U. Rothlisberger, P. Carloni, *J. Phys. Chem. B* 2004, **104**, 2699. (b) T. Matsui, Y. Shigeta, K. Hirao, *Chem. Phys. Lett.* 2006, **423**, 331. (c) T. Matsui, Y. Shigeta, K. Hirao, *J. Phys. Chem. B* 2007, **111**, 1176.
29. R. Wysokinski, D. Michalska, *J. Comput. Chem.* 2001, **22**, 901.
30. (a) R. G. Parr, W. Yang, *Annu. Rev. Phys. Chem.* 1995, **46**, 701. (b) P. Geerlings, F. De Proft, W. Langenaeker, *Chem. Rev.* 2003, **103**, 1793. (c) P. W. Ayers, J. S. M. Anderson, L. Bartolotti, *J. Int. J. Quantum Chem.* 2005, **101**, 520.
31. (a) R. K. Roy, S. Saha, *Annu. Rep. Prog. Chem., Sect. C* 2010, **106**, 118. (b) R. K. Roy, S. Krishnamurti, P. Geerlings, S. Pal, *J. Phys. Chem. A.* 1998, **102**, 3746. (c) R. K. Roy, F. De. Proft, P. Geerlings, *J. Phys. Chem. A.* 1998, **102**, 7035.
32. (a) R. G. Parr, W. Yang, *Density—Functional Theory of Atoms and Molecules*; Oxford University Press; New York, 1989. (b) W. Koch and M. C. Holthausen, *A Chemist's Guide to Density Functional Theory*; Wiley-Vch Weinheim, 2000.
33. (a) P. Hohenberg, W. Kohn, *Phys. Rev.* 1964, **136**, B864. (b) R. M. Dreizler, E. K. U. Gross, *Density Functional Theory*, Springer-Verlag, Berlin, 1990 (c) R. G. Parr, W. Yang, *Annu. Rev. Phys. Chem.* 1995, **46**, 710. (d) W. Kohn, A. D. Becke, R. G. Parr, *J. Phys. Chem.* 1996, **100**, 978.
34. (a) R. G. Parr, R. G.; Pearson, *J. Am. Chem. Soc.* 1983, **105**, 7512. (b) R. G. Parr, W. Yang, *J. Am. Chem. Soc.* 1984, **106**, 4049. (c) R. G. Parr, R. A. Donnelly, M. Levy, W. E. Palke, *J. Chem. Phys.* 1978, **68**, 3801. (d) W. Yang, W. J. Mortier, *J. Am. Chem. Soc.* 1986, **108**, 5708.
35. A. T. Maynard, M. Huang, W. G. Rice, D. G. Covell, *Proc. Natl. Acad. Sci. U. S. A.* 1998, **95**, 11578.
36. R. G. Parr, L. V. Szentpaly, S. Liu, *J. Am. Chem. Soc.* 1999, **121**, 1922.
37. (a) P. W. Ayers, R. G. Parr, *J. Am. Chem. Soc.* 2001, **123**, 2007. (b) P. Jaramillo, P. Perez, R. Contreras, W. Tiznadoand, P. Fuentealba, *J. Phys. Chem. A* 2006, **110**, 8181. (c) A. Cedillo, R. Contreras, M. Galvan, A. Aizman, J. Andres, V. S. Safont, *J. Phys. Chem. A* 2007, **111**, 2442.
38. (a) P. W. Ayers, J. S. M. Anderson, J. I. Rodriguez, Z. Jawed, *Phys. Chem. Chem. Phys.* 2005, **7**, 1918. (b) P. R. Campodonico, C. Perez, M. Aliaga, M. Gazitua, R. Contreras, *Chem. Phys. Lett.* 2007, **447**, 375.
39. R. G. Parr, W. Yang, *Proc. Natl. Acad. Sci. U. S. A.* 1985, **82**, 6723.

-
40. (a) S. K. Ghosh, M. Berkowitz, *J. Chem. Phys.* 1985, **83**, 2976. (b) W. Langenaeker, F. De Proft, P. Geerlings, *J. Phys. Chem.* 1995, **99**, 6424. (c) P. K. Chattaraj, D. R. Roy, P. Geerlings, M. Torrent-Sucarrat, *Theor. Chem. Acc.* 2007, **18**, 923.
 41. (a) S. Saha, R. K. Roy, *J. Phys. Chem. B* 2007, **111**, 9664. (b) S. Saha, R. K. Roy, *J. Phys. Chem. B* 2008, **112**, 1884. (c) S. Saha, R. K. Roy, *Phys. Chem. Chem. Phys.* 2008, **10**, 5591.
 42. P. Bagaria, S. Saha, S. Murru, V. Kavala, B. K. Patel, R. K. Roy, *Phys. Chem. Chem. Phys.* 2009, **11**, 8306.
 43. A. Sarmah, S. Saha, P. Bagaria, R. K. Roy, *Chem. Phys.* 2011, **394**, 29.
 44. S. Saha, R. K. Roy, S. Pal, *Phys. Chem. Chem. Phys.* 2010, **12**, 9328.
 45. (a) R Dennington, T. Keith and J. Millam, GaussView, Version 5., *Semichem Inc.*, Shawnee Mission KS, 2009. (b) M. J. Frisch, et .al. GAUSSIAN 03, Revision E.01, Gaussian, Inc., 340 Quinnipiac St., Bldg. 40, Wallingford CT 06492.
 46. (a) C. C. Roothan, *Rev. Mod. Phys.* 1951, **23**, 69. (b) J. A. Pople, R. K. Nesbet, *J. Chem. Phys.* 1954, **22**, 571. (c) R. McWeeny, G. Dierksen, *J. Chem. Phys.* 1968, **49**, 4852.
 47. C. Møller, M. S. Plesset, *Phys. Rev.* 1934, **46**, 618.
 48. A. D. Becke, *J. Chem. Phys.* 1993, **98**, 5648.
 49. C. T. Lee, W. T. Yang, R. G. Parr, *Phys. Rev. B* 1988, **37**, 785.
 50. G. A. Peterson, M. A. Al-Laham, *J. Chem. Phys.* 1991, **94**, 6081.
 51. W. J. Hehre, R. F. Stewart, J. A. Pople, *J. Chem. Phys.* 1969, **68**, 2657.
 52. G. A. Peterson, A. Bennett, T. G. Tensfeldt, M. A. Al-Laham, W. A. Shirley, J. Mantzaris, *J. Chem. Phys.* 1988, **89**, 2193.
 53. R. Ditchfield, W. J. Hehre, J. A. Pople, *J. Chem. Phys.* 1971, **54**, 724.
 54. P. J. Hay, W. R. Wadt, *J. Chem. Phys.* 1985, **82**, 270.
 55. P. J. Hay, W. R. Wadt, *J. Chem. Phys.* 1985, **82**, 299.

Table 2.1: The difference between the global electrophilicity values (*i.e.*, Δw) (in kcal/mol) of the chosen aqua-cisplatins and nucleobases. Three different levels of theories (HF/LanL2DZ, MP2/LanL2DZ and B3LYP/LanL2DZ for the platinum complexes and HF/6-31G(d,p), MP2/6-31G(d,p) and B3LYP/6-31G(d,p) for nucleobases) are used to generate the w values. Here, the acceptor, A = aqua-cisplatin and the donor B = nucleobases. Larger the value of Δw , higher will be the reactivity of the corresponding aqua-cisplatin and nucleobase pair.

Method	Aqua-cisplatins (A)	Nucleobases (B)	Δw (in kcal/mol)
HF	Mono-aqua	Adenine	14.47
		Guanine	17.72
	Di-aqua	Adenine	38.94
		Guanine	42.19
MP2	Mono-aqua	Adenine	14.24
		Guanine	16.00
	Di-aqua	Adenine	30.89
		Guanine	32.64
B3LYP	Mono-aqua	Adenine	21.13
		Guanine	28.53
	Di-aqua	Adenine	28.19
		Guanine	32.59

Table 2.2: $\Delta E_{B(A)}$ values (in kcal/mol) corresponding to the adduct formation process between aqua-cisplatin and nucleobases. The required parameters are generated at three different levels of theories (HF/LanL2DZ, MP2/LanL2DZ and B3LYP/LanL2DZ for aqua-cisplatin and HF/6-31G(d,p), MP2/6-31G(d,p) and B3LYP/6-31G(d,p) for nucleobases). Here, the acceptor, A = aqua-cisplatin and the donor B = nucleobases. The larger the positive value of $\Delta E_{B(A)}$, the higher will be the reactivity between the corresponding aqua-cisplatin and nucleobase pair.

Method	Aqua-cisplatin (A)	Nucleobases (B)	$\Delta E_{B(A)}$ kcal/mol
HF	Mono-aqua	Adenine	25.56
		Guanine	26.88
	Di-aqua	Adenine	101.54
		Guanine	103.30
MP2	Mono-aqua	Adenine	24.50
		Guanine	24.58
	Di-aqua	Adenine	96.55
		Guanine	96.44
B3LYP	Mono-aqua	Adenine	10.60
		Guanine	12.45
	Di-aqua	Adenine	108.21
		Guanine	108.33

Table 2.3: $\Delta E_{A(B)}$ values (in kcal/mol) corresponding to the adduct formation process between aqua-cisplatin and nucleobases. The required parameters are generated at three different levels of theories (HF/LanL2DZ, MP2/LanL2DZ and B3LYP/LanL2DZ for aqua-cisplatin and HF/6-31G(d,p), MP2/6-31G(d,p) and B3LYP/6-31G(d,p) for nucleobases). Here, the acceptor, A = aqua-cisplatin and the donor B = nucleobases. The larger the negative value of $\Delta E_{A(B)}$, the stronger will be the interaction (both kinetically and thermodynamically) between the corresponding aqua-cisplatin and nucleobase pair.

Method	Aqua-cisplatin	Nucleobases (B)	$\Delta E_{A(B)}$ (in kcal/mol)
HF	Mono-aqua	Adenine	-37.10
		Guanine	-41.78
	Di-aqua	Adenine	-173.91
		Guanine	-185.38
MP2	Mono-aqua	Adenine	-34.01
		Guanine	-34.66
	Di-aqua	Adenine	-172.82
		Guanine	-172.58
B3LYP	Mono-aqua	Adenine	-12.40
		Guanine	-15.28
	Di-aqua	Adenine	-182.15
		Guanine	-188.73

Table 2.4: The amount of charge transferred (ΔN) in the process of adduct formation between aqua-cisplatin and nucleobases. Relevant parameters are generated at three different levels of theories (HF/LanL2DZ, MP2/LanL2DZ and B3LYP/LanL2DZ for aqua-cisplatin and HF/6-31G(d,p), MP2/6-31G(d,p) and B3LYP/6-31G(d,p) for nucleobases). The larger the value of ΔN , more preferable will be the interaction process (both kinetically and thermodynamically) between the corresponding pairs.

Method	Aqua-cisplatin (A)	Nucleobases (B)	ΔN Value
HF	Mono-aqua	Adenine	0.3538
		Guanine	0.4054
	Di-aqua	Adenine	0.9546
		Guanine	1.0267
MP2	Mono-aqua	Adenine	0.2859
		Guanine	0.2922
	Di-aqua	Adenine	0.8190
		Guanine	0.8176
B3LYP	Mono-aqua	Adenine	0.1317
		Guanine	0.1652
	Di-aqua	Adenine	0.8911
		Guanine	0.9302

Table 2.5: Stabilization energy values ($\Delta E_{SE(AB)}$) generated for different mode of interactions between aqua-cisplatin and nucleobases. The relevant parameters are generated at three different levels of theories (HF/LanL2DZ, MP2/LanL2DZ and B3LYP/LanL2DZ for the aqua-cisplatin and HF/6-31G(d,p), MP2/6-31G(d,p) and B3LYP/6-31G(d,p) for nucleobases). Larger negative value of stabilization energy signifies more stable adduct formation. Values are given in kcal/mol.

Method	Aqua-cisplatin (A)	Nucleobases (B)	$\Delta E_{SE(AB)}$ (in kcal/mol)
HF	Mono-aqua	Adenine	-11.54
		Guanine	-14.90
	Di-aqua	Adenine	-72.38
		Guanine	-82.08
MP2	Mono-aqua	Adenine	-9.51
		Guanine	-10.08
	Di-aqua	Adenine	-75.27
		Guanine	-76.14
B3LYP	Mono-aqua	Adenine	-1.80
		Guanine	-2.83
	Di-aqua	Adenine	-73.94
		Guanine	-80.41

Table 2.6: Prediction of the direction of charge (ΔN) transfer using CDASE scheme based parameters. The values in the upper part of the Table (*i.e.*, when nucleobases are considered to be donors B, and aqua-cisplatin as acceptors, A) are taken from Tables 4, 2, 3 and 5. The values in the lower part (*i.e.*, when nucleobases are considered to be acceptors A, and aqua-cisplatin as donors, B) are generated anew using the same methods. The energy parameters are in kcal/mol.

	B=Guanine : A=Cisplatin			(Mono-aqua)	B=Adenine : A=Cisplatin		
	HF	MP2	B3LYP	HF	MP2	B3LYP	
ΔN	0.4054	0.2922	0.1652	0.3538	0.2859	0.1317	
$\Delta E_{B(A)}$	26.88	24.58	12.45	25.56	24.50	10.60	
$\Delta E_{A(B)}$	-41.78	-34.66	-15.28	-37.10	-34.01	-12.40	
$\Delta E_{SE(AB)}$	-14.90	-10.08	-2.83	-11.54	-9.51	-1.80	

	A=Guanine : B=Cisplatin			(Mono-aqua)	A=Adenine : B=Cisplatin		
	HF	MP2	B3LYP	HF	MP2	B3LYP	
ΔN	-0.4054	-0.2922	-0.1652	-0.3538	-0.2859	-0.1317	
$\Delta E_{B(A)}$	-41.78	-34.66	-15.28	-37.10	-34.01	-12.40	
$\Delta E_{A(B)}$	26.88	24.58	12.45	25.56	24.50	10.60	
$\Delta E_{SE(AB)}$	-14.90	-10.08	-2.83	-11.54	-9.51	-1.80	

Chapter III

A Density Functional Reactivity Theory
Based Approach to Understand the Cisplatin
Analogues Interaction with Protecting
Agents

3.1 Introduction:

In the previous chapter, we have discussed the therapeutic utility of cisplatin along with the mechanistic pathways of its interaction with DNA. In this particular chapter we have addressed a major concern, that is the undesired toxic side-effects associated with cisplatin therapy and tried to develop a protocol for the application of protecting agents to inhibit the toxicity of cisplatin through computer aided molecular modeling technique.

Cis-diamminedichloroplatinum(II), cisplatin¹, along with its analogues have the decade long series of major accomplishment on different types of cancer cell lines. Although, it is well known that the primary target of cisplatin analogues is genomic DNA,²⁻⁸ an ultimate mechanism of this platination process is not fully understood. Despite the excellent cure rate of up to 90%,^{9,10} severe toxic side-effects of cisplatin¹¹⁻¹³ are major disadvantages, raising a big question on their therapeutic exertion for cancer treatment. Because of the competitive protein binding of cisplatin analogues, toxic side-effects such as nephrotoxicity, ototoxicity, hematological toxicity and seizures¹⁴⁻²⁰ are prevalent among the patients undergoing cisplatin treatment. Thus, reducing the toxic side-effects of cisplatin has become a major concern among the worldwide scientific community and researchers throughout the last four decades. Medical research to eradicate the toxic side-effects of cisplatin analogues is boosted by the introduction of Pearson's hard soft acid base (HSAB) principle.²¹⁻²³ Platinum (Pt), being a soft metal center, prefers to bind with soft nucleophilic center such as sulfur ligand based compounds. It is the underlying perception behind the introduction of sulfur based cisplatin modulators, which are termed rescue or protecting agents.²⁴⁻²⁸ There exist two customary protocols for the design and development of modulating agents. These are,

1. To protect the non-carcinogenic normal tissues from the effect of therapeutic agents.
2. Ameliorate (to make more satisfactory anticancer agent) the chemotherapeutic application of cisplatin analogues with the significant minimization of its toxic side-effect.

Keeping these two important aspects in mind, scientists proficiently venture the HSAB principle. They have successfully designed various sulfur ligand based rescue agents, which effectively diminished the toxic side-effects of cisplatin drug without

reducing antineoplastic efficacy (i.e., relative ability to damage dividing cells than to resting cells) of these drugs much.²⁹⁻³⁴

Interaction of cisplatin with genomic DNA has been the subject of extensive theoretical and computational investigation³⁵⁻⁴⁵ over the years. However, reported literatures on the interaction of cisplatin analogues with sulfur based rescue agents are limited in terms of theoretical aspects (i.e., how to define the best possible protecting agent against a particular cisplatin analogue). So, to the best of authors' knowledge the present one may be the first theoretical study in this direction and that is also through an approach based on density functional reactivity theory (DFRT).

In the context of density functional reactivity theory, (DFRT) several local and global reactivity descriptors⁴⁶⁻⁵⁹ have been developed in the last three decades. Reactivity descriptors such as Fukui functions $[f(r)]$,^{60, 61} local softness (s_k^+ , s_k^- and s_k^0),⁶² local hardness,⁶³⁻⁶⁶ relative electrophilicity (s_k^+/s_k^-) and relative nucleophilicity (s_k^-/s_k^+),^{67,68} local electrophilicity⁶⁹⁻⁷¹ etc. are booked under local reactivity descriptor. Global reactivity descriptors such as chemical potential⁷² (i.e., the negative of electronegativity⁷³), chemical hardness (η),⁴⁹ global electrophilicity index,^{74, 75} nucleophilicity,⁷⁶⁻⁷⁸ electrofugality and nucleofugality^{79, 80} etc. are mainly used for intermolecular reactivity study. Very recently Saha *et al.* have proposed two new local reactivity descriptors (known as variant of hardness potential) which have the potential to be used as intermolecular reactivity descriptors.⁸¹ In a subsequent investigation the relative contribution of combined kinetic and exchange energy terms vs electronic component of molecular electrostatic potential in hardness potential derivatives are explored by Bhattacharjee *et al.*⁸²

Utilizing the basic foundation of density functional reactivity theory (DFRT), Roy and collaborators recently formulated a new theoretical scheme⁸³ termed as "Comprehensive Decomposition Analysis of Stabilization Energy" (CDASE) to rationalize the kinetics and thermodynamics of chemical reactions. They have introduced an useful correlation between the energy components (of the stabilization energy⁴⁹) and the rate of a chemical reaction. The scheme is successfully used by Sarmah *et al.*⁸⁴ to explain the most stable binary non-covalently bonded complex formation between urea and *meta*-nitrobenzoic acid. The intrinsic complementary nature of CDASE scheme to

conventional supermolecular approach was also highlighted in this study. Preferential binding interaction of aqua-cisplatin with DNA base guanine over adenine could also be explained by CDASE scheme.⁸⁵ The advantage of CDASE scheme as an alternative low cost computational methodology to study large molecular systems is elaborated through a recent study by Sarmah *et al.*⁸⁶ Saha and co-workers⁸⁷ used this scheme to investigate the normal electron demand (NED) and inverse electron demand (IED) nature of Diels-Alder (DA) reaction between 108 pairs of dienes and dienophiles.

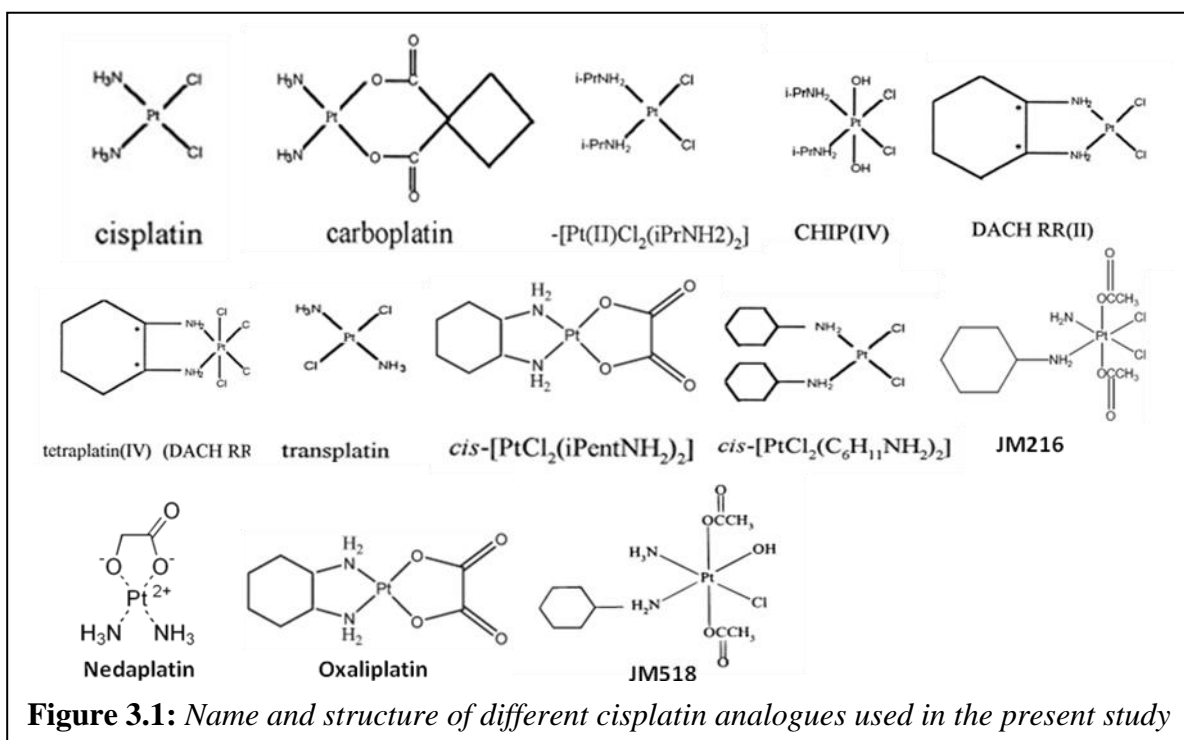
In the present study an effort is made to investigate the strength of interaction between different pairs comprising of cisplatin analogues and sulfur ligand based protecting agents. Also, the stability of the complexes formed by each pair will be evaluated using different energy components generated by CDASE scheme. These, together, will help to get an idea of the kinetics and thermodynamics of interaction between cisplatin analogues and rescue agents which can be extended further to develop a strategy of choosing a specific protecting agent against a particular type of cisplatin drug.

Normally, the major obstacles for theoretical studies in case of biological systems are the very high computational cost. However, use of the CDASE scheme has an advantage as the route which is taken here to reach the combined system (*i.e.*, the drug + nucleobases or drug + protecting agents) is from the corresponding isolated component which, to a significant extent, reduces the computational cost.

Adopted computational methodology is elaborated in section 3.2. In subsection 3 (A) the strategic protocol to be used to define the best possible combination of cisplatin analogues and rescue agents (that may reduce the toxic side effects) is explained. Subsection 3 (B) and 3 (C) contain discussion on the interaction of different cisplatin analogues with DNA and protecting agents, respectively. Discussion on the strength of interaction between protecting agents and DNA bases is also included in section 3 (C). In subsection 3 (D) use of the proposed strategy (section 3 (A)), by establishing a systematic correlation of the results obtained in the previous two subsections, are highlighted. Finally, in Section 3.4 we have summarized our entire work with a short note on some promising aspects of CDASE scheme and its advantages over other approaches where reactivity descriptors are mainly based on electron population.

3.2. Computational Methodology:

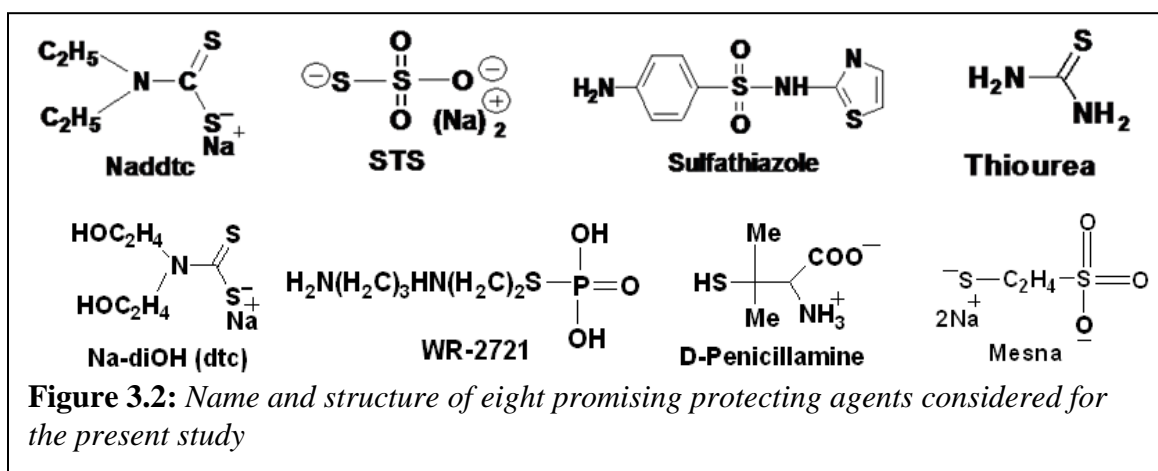
Altogether, twelve different cisplatin analogues (Fig.3.1) and eight promising cisplatin modulators (Fig. 3.2) have been included in the present study. Model cisplatin analogues consist of both Pt (II) and Pt (IV) metal centers. It is worth mentioning here that, in the treatment of cancer both the oxidation states of Pt play significant roles. The protecting agents which are chosen here are of moderate size, recently developed as well as known to be very effective. A study on the relative rate of interaction of cisplatin analogues with the DNA is also carried out.



Initial crude structures of cisplatin analogues, DNA bases as well as protecting agents are generated using Gauss View⁸⁹ visualization program. Full geometry optimization as well as relevant single point calculations of protecting agents and DNA bases are performed at B3LYP^[90-92]/6-31G(d,p)^[93-96] method. Subsequent frequency analysis has been performed for every structure to ensure no imaginary frequency is present (*i.e.*, minimum energy state has been achieved in potential energy surface).

Geometries of cisplatin analogues are also optimized at the same level of theory (*i.e.*, B3LYP) but the basis set used here is LanL2DZ (with effective core potential,

ECP).^[97-99] Vertical ionization potential (IP) and electron affinity (EA) values are considered in the present study to evaluate η , μ , ΔN etc. These quantities were generated after performing single point calculations for neutral, cationic and anionic systems using the geometry of the optimized neutral structures only. While restricted level of theory (RB3LYP) was used for the neutral systems, unrestricted level of the same theory (UB3LYP) was used for calculations of ionic systems. Gaussian 03¹⁰⁰ program suit has been used for the entire computational calculations.



level basis sets such as 6-311G(2d,2p), 6-311++G(d,p) (results are not shown here). The observation is that optimizations with these higher level basis sets hardly make any changes to the sequence of the values of the reactivity descriptors generated by CDASE scheme using 6-31G (d,p) basis sets for the protecting agents.

3.3. Results and Discussion:

3.3.1. Strategy for choosing the best possible protecting agent against a particular cisplatin analogue:

It is believed that the anticancer activity of the cisplatin drug originates from the intrastrand adduct formation with DNA base pairs.⁷ More specifically, attachment of cisplatin analogues to DNA takes place through the N-7 positions of purine bases.²⁰ It is apparent that stronger the interaction of cisplatin analogues with DNA bases, higher will be the anticancer activity. However, another important factor, which needs to be

considered here, is the binding ability of the drug with other biomolecules. If a drug interacts strongly with DNA then it is expected that the extent of interaction of the drug with other biomolecules, such as proteins and amino acids, will also be significantly high. This is because the basic inorganic chemistry knowledge refers Pt as a soft metal center and it is natural that it has higher affinity towards soft nucleophilic centers present in sulfur containing compounds. There is a significant abundance of sulfur containing biomolecules in the cytosol as well as the nucleus of human cell. Indeed, the most reasonable implication is the possibility of a strong interaction between the highly active platinum anticancer drugs and biomolecules present inside the cell. Therefore, it can be argued that the toxic side effects will be more for a strongly active drug.

Similarly, selection of an effective protecting agent against a particular cisplatin drug is decided by testing the interaction of that protecting agent with cisplatin analogues. The basic requisite of protecting agents is to restrain the higher activity of cisplatin analogues to such an extent that, without compromising the anti-cancer property of the drug the undesired binding affinity of the drug towards other biomolecules (like proteins) is restricted. However, for an explicit understanding of the activity of a protecting agent it is also important to take into account the interaction between protecting agents and other active biomolecules. An effective protecting agent must have the low reactive interaction with the active biomolecules so that it can restore its maximum ability to provide protection against the cisplatin drug.

The ongoing discussion on three types of possible interactions (*i.e.*, the interaction of a particular cisplatin drug with genomic DNA, the effect of protecting agents on that particular drug as well as on other active biomolecules) leads the way to develop a strategy of choosing suitable combination of cisplatin drugs and protecting agents that minimize toxic side effects. If the activity of a particular drug is low towards DNA bases, application of a strong protecting agent (distinction between weak and strong protecting agents can be made on the basis of the strength of interaction with drugs) reduce the activity of the drug to such an extent that the drug might lose its anti-cancer activity in the presence of that particular protecting agent. In another situation, may be the drug is highly active towards DNA bases. In such a case, it is obvious that the toxic side-effects of the drug will be more because of its higher binding ability with other biomolecules.

So, to diminish the toxic side effects of the highly active cisplatin analogue the required protecting agent should also have strong affinity for the drug (*i.e.*, a strong protecting agent). Also, if the strength of interaction of the protecting agent with biomolecules is much lower when compared to those between drugs and protecting agents as well as between drugs and biomolecules, then the first factor should play negligible role in the choice of protecting agents. However, if in a particular case the reactive interaction between a protecting agent and biomolecules are comparable to the other two types of interactions then it may also play a critical role in the choice of protecting agents. After a thorough analysis of the three types of interactions in different subsections of 3.3.2 and 3.3.3 the results are synchronized in subsection 3.3.4 to implement the adopted strategy.

3.3.2. Interaction of different cisplatin analogues with DNA

It is well accepted that N-7 position of the purine bases is the most active site for platination.^{7,10} It is also well established that the binding interaction of cisplatin with guanine is preferred to that with adenine.^{28,41,45,85} So, to make the observation broader, to the extent that it will help to apply the adopted strategy as discussed in the subsection 3.3.1 above, 12 different cisplatin analogues have been included in the present one. The strength of interaction is evaluated on the basis of different kinetic and thermodynamic parameters derived in the CDASE scheme. The values of these parameters are summarized in Table 3.1. Here, higher values for ΔW and $\Delta E_{B(A)}$ predict faster rate of interaction, whereas those of ΔN , $\Delta E_{A(B)}$ and $\Delta E_{SE(AB)}$ talk about the stability of adducts. It is worth observing here that all the 12 different cisplatin analogues show a greater affinity for the nucleobase guanine, both from kinetic and thermodynamic aspects.

As the anti-tumor activity of these platinum drugs mainly depends on their preferential binding ability to DNA bases, more effectively, they bind to DNA, more actively they will inhibit the process of DNA replication and thus the cell growth will stop. The DNA damaging activity of different cisplatin analogues have been systematically analyzed by Murray *et al.*¹⁰¹ They have studied the rate of interaction of a number of cisplatin drugs with DNA and based on their experimental results proposed an order of activity for a series of cisplatin analogues. Significantly, higher degrees of DNA

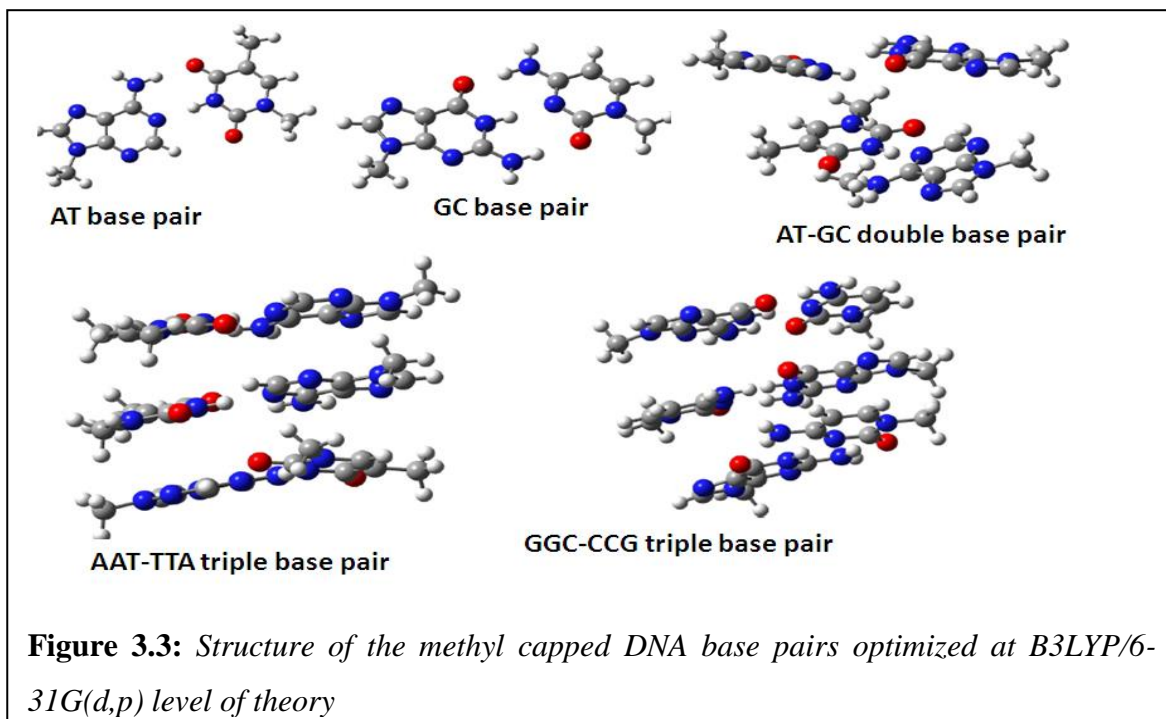
damaging activity have been reported for tetrachloro(1,2-diaminocyclohexane)platinum(IV), Tetraplatin (Fig.3 1).It is encouraging to notice here that CDASE scheme based theoretical results (in Table 3.1.a) also clearly reproduce the experimental evidence. The values generated for all the five parameters (*i.e.*, ΔW , $\Delta E_{B(A)}$, ΔN , $\Delta E_{A(B)}$, and $\Delta E_{SE(AB)}$) are significantly high for Tetraplatin . Therefore, it can be argued that among the series of chosen model cisplatin analogues Tetraplatin will be the most effective antineoplastic agent according to our observations.

Also, a comprehensive study on the anti-cancer activity of four of the chosen cisplatin analogues [e.g., Oxaliplatin (*trans*-L-Diaminocyclohexane)oxalatoplatinum(II), Tetraplatin, Carboplatin (*cis*-diammine (1,1-Cyclobutanedicarboxylato) platinum(II)) and Cisplatin] has been reported by Rixe *et al.*¹⁰² According to their observation, interaction of dichloro(1,2-diaminocyclohexane)platinum(IV), DACH group of compounds (such as Tetraplatin, etc.) with DNA is far more active than cisplatin group of compounds (like Carboplatin, etc.).

To obtain some more realistic features of the interaction between cisplatin analogues and DNA, our study have been extended to relatively large DNA clusters. In the present study, we have considered the single, double and triple base pair units of Watson-Crick DNA double helix as our model systems (optimized structures of the base pairs are provided in the Fig. 3.3). Model DNA structures are generated by trimming the reported crystal structure of DNA having PDB ID 2VAH¹⁰³ up to the specific base pair units (one, two or three base pair). For computational simplicity, the sugar and phosphate units are replaced with methyl groups in their respective positions. We have evaluated different CDASE scheme based parameters for the interaction between 12 cisplatin analogues and single base pair units A-T (Adenine- Thymine) and G-C (Guanine-cytosine) followed by double base pair unit AG-TC as well as the triple base pair units AAT-TTA and GCG-CGC and values are reported in Tables 3.1 (b), (c) and (d), respectively.

In case of single base pair units, all the 12 cisplatin analogues have shown kinetic as well as thermodynamic preference for GC pair over AT (Table 3.1.b). The higher activity of cisplatin analogues toward guanine is already justified from our reported CDASE scheme based calculations (Table 3.1.a). This seems to be logical as the presence

of nucleobase guanine enhances the interaction probability and that finally leads to the stronger interaction of GC pair with cisplatin analogues compared to that of the AT pair. The relative order of interaction for the 12 cisplatin analogues with single base pair unit is found to be consistent with that of the individual purine bases except JM 518, which shows lower activity in case of higher DNA cluster. Cisplatin analogue Nedaplatin shows lowest and Tetraplatin shows highest activity against W-C complementary base pair AT and GC.



In Table 3.1.c, we have reported the CDASE scheme based parameters values for the activity of cisplatin analogues against higher order DNA cluster having two base pair units (GA-CT). The 12 cisplatin analogues exhibit exactly similar interaction trend with double base pair unit to that of obtained for individual bases as well as the single base pair unit. Except the JM 518, there is no major discrepancy is observed in the CDASE scheme based calculations for the extended DNA sequence and the relative order is consistent with the former predictions on the DNA binding activity of cisplatin analogues.

To justify the preferential binding affinity of cisplatin analogues for GC base pair over AT, we have further calculated the CDASE scheme based parameters for the larger DNA clusters containing triple base pair units. The two model systems are containing the

standard W-C double helix sequence CGG-GCC and ATT-TAA, where letters represent the individual nucleobases. The incorporation of more base pair units in the model system enhances the reliability of theoretical calculation and approaching closer to the real situation. The comparative study for the interaction between extended AT and GC pairs and cisplatin analogues are reported in Table 3.1.d. The results are also convincing with greater affinity of cisplatin analogues toward extended GC pair in comparison to that of the extended AT pair. It is worth mentioning here that, the observed order of interaction for the 12 different cisplatin analogues is exactly similar and consistent throughout the calculations and does not have much impact of the size of the DNA clusters. The overall CDASE scheme based kinetic and thermodynamic predictions on the interaction of cisplatin analogues with DNA is well justified from the earlier experimental as well as theoretical evidences.⁴¹⁻⁴⁵

3.3.3. Relative strength of interaction of protecting agents with cisplatin analogues as well as active biomolecules:

In this section we have implemented the CDASE scheme to evaluate the reliability of different kinetic and thermodynamic parameters in explaining the interaction between platinum anticancer drugs and sulfur containing protecting agents. Table 3.2 includes some earlier experimental and theoretical reports on the sulfur based compounds (protecting agent), those behave as effective chemoprotector against different platinum anticancer drugs. It is to be seen whether the reactivity parameters, based on the CDASE scheme can reproduce the relative strength of interaction between cisplatin drugs and protecting agents (Tables 3.3 to 3.7 and Figs. 3.4 to 3.8), whichever are available in the literature (Table 3.2).

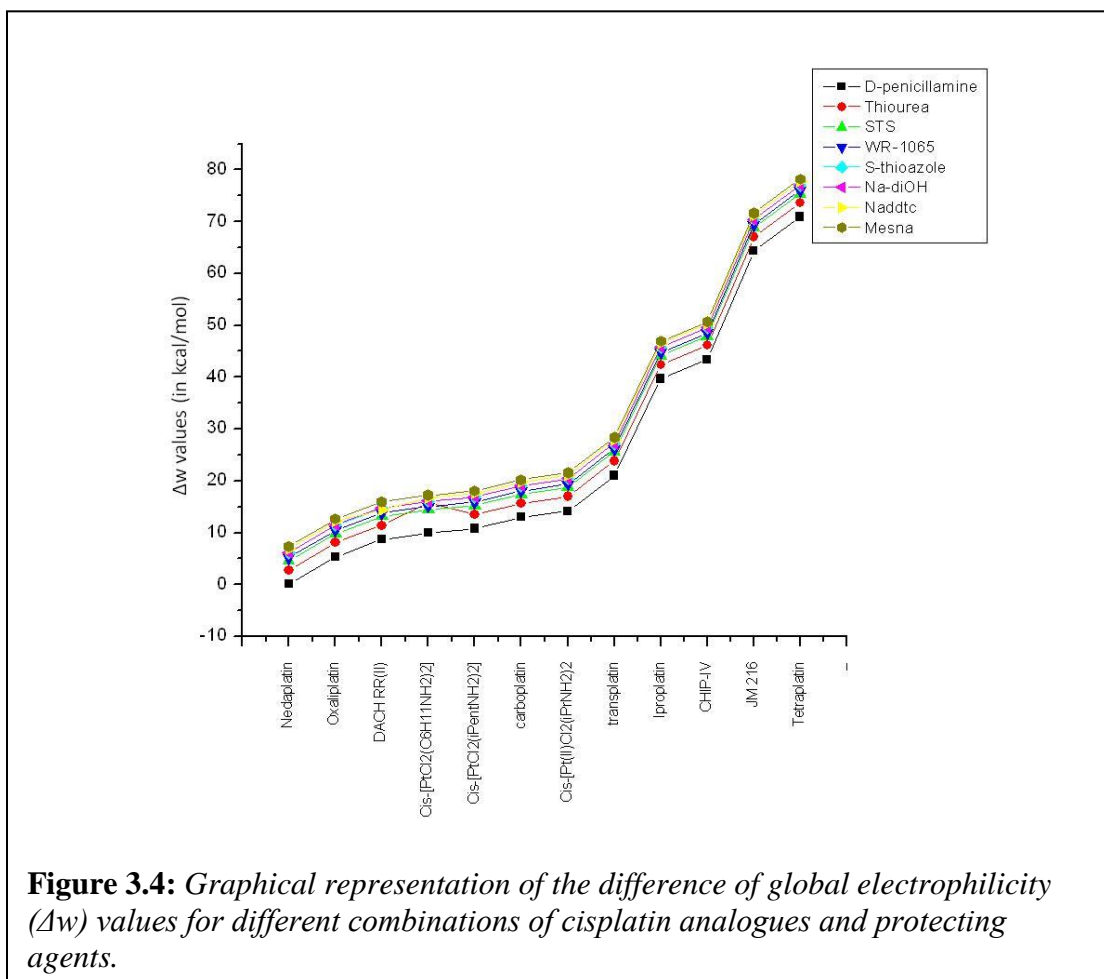
The last row in Tables 3.3-3.7 are the values for the five CDASE scheme based parameters corresponding to the interaction of protecting agents with the active biomolecule (we have considered guanine as the prototype of active biomolecule for the present study). Analysis of these values together with those demonstrated in Table 3.1 and use of the strategy as outlined in Section 3.2.1 will assist to predict the most preferable protecting agent against a specific drug.

(i) Relative strength of interaction between cisplatin analogues and protecting agents on the basis of the difference in global electrophilicity values i.e., Δw :

The numbers in each box in Table 3.3 demonstrate the difference in global electrophilicity values ($\Delta w = w_A - w_B$) between cisplatin analogues (behaving as an electron acceptor, $w_A = \frac{(\mu_A^0)^2}{2\eta}$) and protecting agents (behaving as an electron

donor, $w_B = \frac{(\mu_B^0)^2}{2\eta}$) (see also Fig. 3.4). Higher the difference between w_A and w_B (i.e.,

$\Delta w = w_A - w_B$) stronger is the interaction for that particular combination of cisplatin analogue and protecting agent. This is also demonstrated through the change in the color sequence of Table 3.3. As the Δw values increase downwards as well as rightwards, the color also shifts from lower to higher intensity indicating the increase in the strength of interaction between cisplatin analogues and protecting agents.



To predict the most suitable protecting agent for a cisplatin drug it is also necessary to focus on the extent of interaction between protecting agent and active biomolecules. The numbers in the last row of Table 3.3 represent the differences in global electrophilicity values (*i.e.*, Δw) between the corresponding protecting agent (behaving as an acceptor) and the nucleobase guanine (behaving as donor). An effective protecting agent should have low strength of interaction with biomolecules. Otherwise, higher degree of interaction between a protecting agent and biomolecules results in a significant decrease in the activity of that particular protecting agent. An ideal protecting agent should sustain its activity to inhibit the toxic side-effect of cisplatin analogues. Simply, we can argue that a protecting agent is said to be more capable of modulating the activity of drugs if the Δw values in each box of Table 3.3 is larger (and positive) than the ones in the corresponding boxes in the last row of Table 3.3.

The general observation from Table 3.3 and Fig.3.4 is that as we move towards right the values of Δw in each row go on increasing while the ones in the last row go on decreasing and thus indicating higher efficiency of the protecting agents in the same direction. Also, the most common observation about Δw values presented in Table 3.3 is that strong sulfur nucleophiles such as NaDDTC (sodium diethyldithiocarbamate) and Mesna (sodium 2-mercaptoethanesulfonate) show significantly higher rate of interaction with all the cisplatin analogues. Thus considering the Δw values generated from the interaction between cisplatin drugs and nucleobases (in Table 3.1) and the Δw values generated from interaction between cisplatin drugs and protecting agents as well as protecting agents and the biomolecule (here guanine) a prescription can be made for choosing a suitable protecting agent against a particular drug. As one moves down the Table 3.1 (or Table 3.3) to use a cisplatin drug he has to move towards the right of Table 3.3 to choose the suitable protecting agent. Some earlier reported studies (Table 3.2) also agree to the just proposed prescription. Boelrijk *et al.* extensively studied the action of Sodium diethyldithiocarbamate (NaDDTC), thiourea and sodium thiosulfate (STS) as promising protecting agents against cisplatin drug.³⁰ They have concluded that the protecting agents NaDDTC and thiourea are capable of breaking the Pt-methionine type binding, whereas, the protecting agent STS is able only to inhibit the nephrotoxicity by inactivating unbound Pt compounds in the cell. Thus, the study by Boelrijk *et al.* suggests

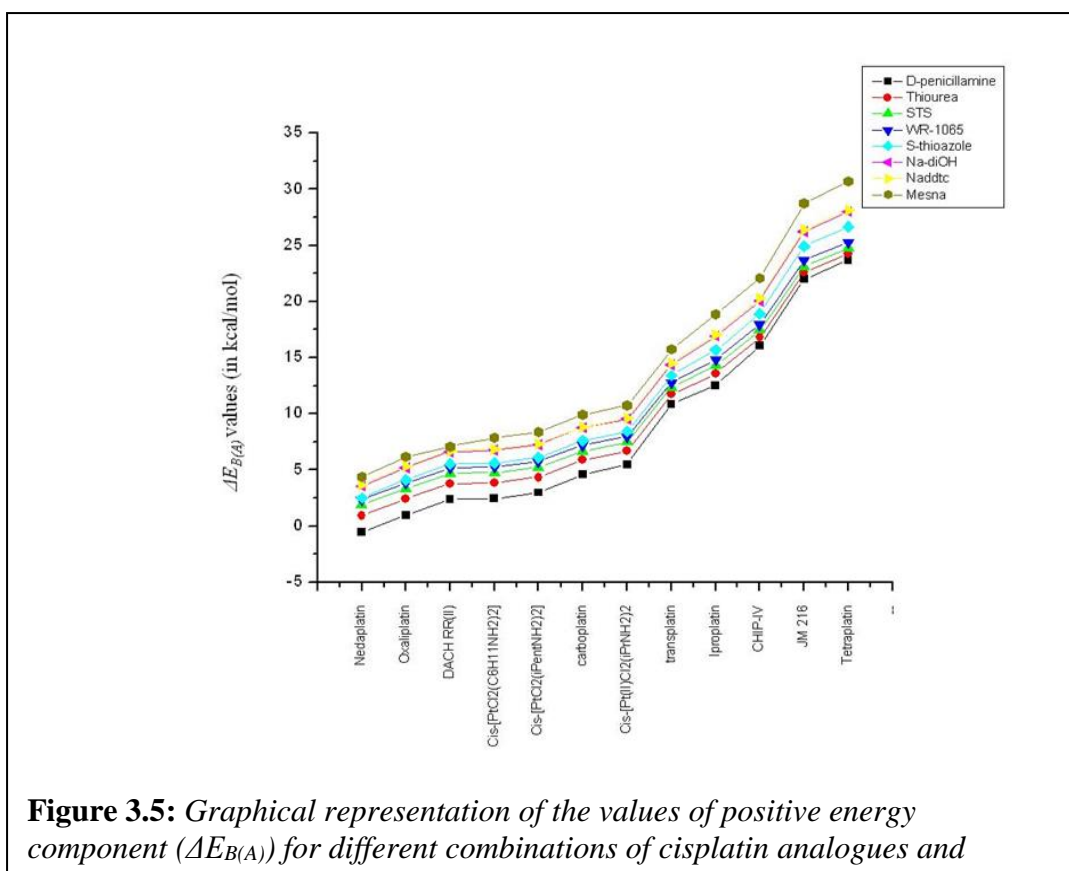
NaDDTC to be the most effective protecting agent against Pt-compounds. The mode of interaction of different sulfur-containing biologic and nonbiologic nucleophiles with cisplatin drugs was explored by Dedon *et al.*³² Their experimental study suggest a relatively more favorable interaction between cisplatin drugs and diethyldithiocarbamate (DDTC) compared to that of the cisplatin drugs and thiosulfate. The potential application of amifostine (Ethyol^R; WR 2721) and its main metabolites (WR 1065) as an effective chemoprotective agent was explored by Korst *et al.*²⁶ The experimental findings by Korst *et al.* reveals short initial half-life of WR-1065. A suitable explanation for this observation is the process of faster uptake of WR-1065 in cellular environment and the formation of disulphides. The relatively high affinity of moderately active protecting agent WR 1065 towards active biomolecules suggests that it will be a suitable protecting agent against moderately active cisplatin analogues (i.e., the ones near the midway of Table 3.3 while moving from top to bottom). It is encouraging to notice that the CDASE scheme based Δw values also predict the same.

(ii) *Relative strength of interaction between cisplatin analogues and protecting agents on the basis of positive energy components, i.e., $\Delta E_{B(A)}$:*

In the introduction we have already discussed that $\Delta E_{B(A)}$ is the positive energy component of the stabilization energy. Earlier $\Delta E_{B(A)}$ was correlated to the kinetic aspect (i.e., rate) of a reactive interaction.⁸³⁻⁸⁷ Thus, higher the value of $\Delta E_{B(A)}$ higher should be the rate of interaction between the cisplatin analogue and the protecting agent.

The $\Delta E_{B(A)}$ values for 96 pairs of cisplatin analogues and protecting agents (12 cisplatin analogues and 8 protecting agents) are presented in Table 3.4 and Fig.3.5. Each box in Table 3.4 carries the $\Delta E_{B(A)}$ value for the interaction between the corresponding cisplatin analogue and the protecting agent. Analysis of these values of $\Delta E_{B(A)}$ reveals a periodic variation in the trends of kinetically favorable interaction for different combinations of cisplatin analogues and protecting agents. As one moves along Table 3.4 (or Fig. 3.5) from left to right the interaction between cisplatin analogues and protecting agents seems to be more and more kinetically favorable and that is obvious from the gradual increase in the $\Delta E_{B(A)}$ values in each successive box. The similar trend of $\Delta E_{B(A)}$

values (for interaction between cisplatin analogues and protecting agents) has been observed if someone is moving from lower to higher ordinates in Fig. 3.5. On the other hand the $\Delta E_{B(A)}$ values in the boxes of the last row are decreasing as one moves from left to right. Thus, the interaction between protecting agents and the active biomolecule gradually decreases as we go from left to right along the Table 3.4. So, it is logical to define an effective protecting agent from the higher value of $\Delta E_{B(A)}$ for the interaction between a drug and a protecting agent with a much smaller value of $\Delta E_{B(A)}$ for the interaction between a protecting agent and a biomolecule (i.e., values in each box of the last row of Table 3.4).



An extensive study by Treskes *et al.*²⁴ provide worthy evidence regarding the change in reversibility of binding interaction between cisplatin drugs and proteins with the variation in applied protecting agents. Eventually, a reasonable correlation can be

obtained for the experimental observations made by Treskes *et al.*²⁴ and the calculated CDASE scheme based $\Delta E_{B(A)}$ values.

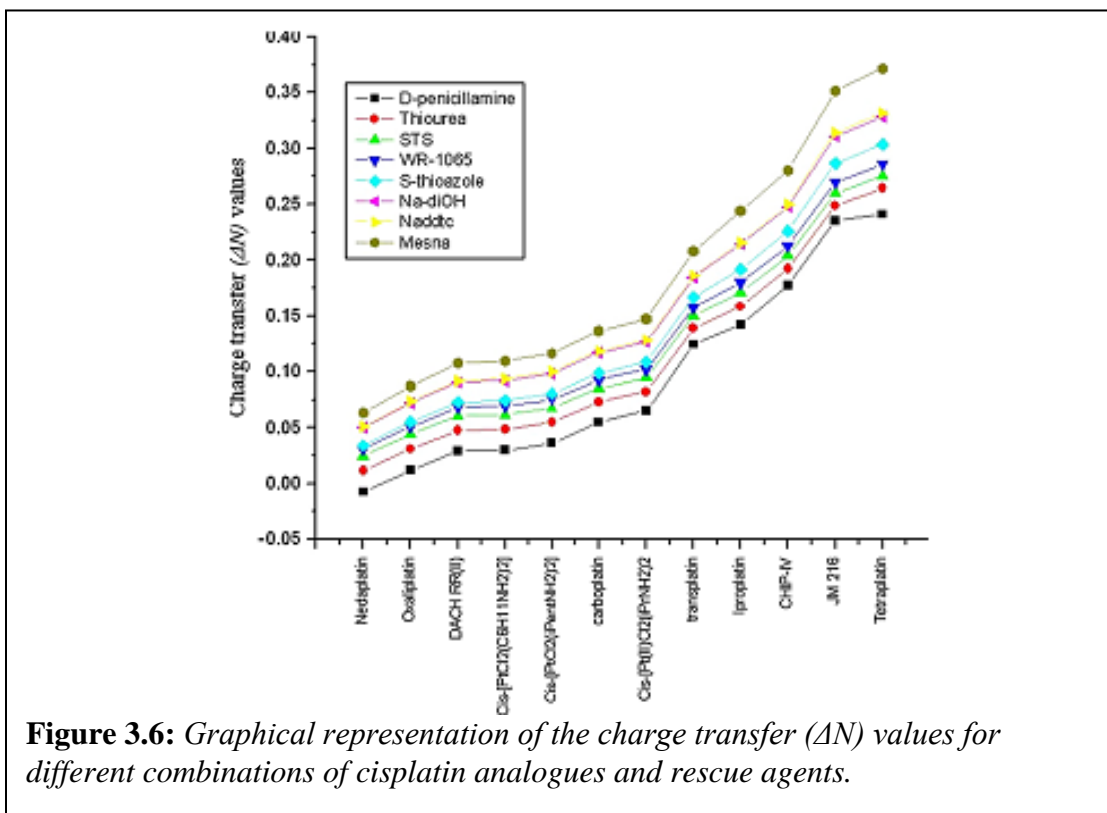
The outcome of the experimental study by Treskes *et al.*²⁴ establish a comparatively slow rate for the drug-protein reversal activity (Table 3.5) in presence of protecting agent WR-1065 [S-2-(3-(aminopropyl)amino)ethylphosphorothioic acid] (rate constant $k_2 = 0.142 \text{ M}^{-1} \text{ s}^{-1}$) in comparison to the reversal ability of the same reaction by DDTC (rate constant $k_2 = 3.66 \text{ M}^{-1} \text{ s}^{-1}$). It is possible to offer a logical explanation for the kinetic preference of DDTC over WR-1065 to revert the drug-protein interaction using the corresponding $\Delta E_{B(A)}$ values. Here, the calculated value of $\Delta E_{B(A)}$ for the combination of cisplatin analogue DACH RR (II) [dichloro(1,2-diaminocyclohexane)platinum(II) RR isomer] and protecting agent WR-1065 is found to be $5.17 \text{ kcal mol}^{-1}$. The $\Delta E_{B(A)}$ value for the interaction between WR-1065 and guanine is $1.69 \text{ kcal mol}^{-1}$. Similarly, for the combination of the protecting agent DDTC, cisplatin analogue DACH RR (II) and the biomolecule guanine the $\Delta E_{B(A)}$ values are $6.72 \text{ kcal mol}^{-1}$ and $0.28 \text{ kcal mol}^{-1}$, respectively. These results clearly indicate that the interaction of WR-1065 with guanine is stronger than that between DDTC and guanine and so the ability of WR-1065 to revert the drug-protein interaction to an effective drug-protecting agent interaction is lower than the same by DDTC. So, as argued earlier (Section 3.3.3 (i)) a significant amount of activity of DDTC is retained after interaction with biomolecules and it can more efficiently reverse the drug-protein interaction into an active drug-protecting agent interaction.

(iii) Relative stability of the adducts formed between cisplatin analogues and protecting agents on the basis of electron transfer values i.e., ΔN :

In the present study cisplatin analogues are considered as electron acceptors (i.e., A) and protecting agents as electron donors (i.e., B). The logic behind this consideration is that cisplatin analogues, having electropositive metal center (i.e., Pt metal with vacant d-orbitals), can better act as an electron acceptors and the protecting agents having the lone pair of electrons on the sulfur atom behave as electron donors. From the earlier discussion, charge transfer component ΔN will be positive when $\mu_B^0 \mu_A^0$ (or $\chi_A^o > \chi_B^o$). This also supports our consideration about donor and acceptor systems (i.e., chemical

potential values of protecting agents will be higher than those of cisplatin analogues). Thus, for a favorable interaction process, electrons will be transferred from donor to acceptor until an equilibrium has been established (*i.e.*, $\mu_B \approx \mu_A$ or $\chi_B \approx \chi_A$)

The process of electron transfer plays a vital role in chemical interactions. As discussed before, a larger amount of electron exchange between the interacting donor and acceptor system demonstrates a higher extent of stabilization of the resultant adduct. So, it can be argued that a higher value of ΔN is the indication of a thermodynamically favorable interaction between that particular pair of cisplatin analogue and protecting agent. Table 3.6 (and Fig. 3.6) represent the charge transfer (*i.e.*, ΔN) values for all the possible combinations of cisplatin analogues (considered as acceptor A) and protecting agents (considered as donor B) included in the present study. Each box in Table 3.6 contains charge transfer value for the interaction between cisplatin analogue and the protecting agent. The values in the last row are for interaction between the biomolecule (guanine) and the corresponding protecting agent.



The periodic changes in color intensity of Table 3.6 indicate the extent of charge transfer interaction between different cisplatin analogues and protecting agents. Thus, higher the color intensity greater will be the amount of charge transfer that results to a more thermodynamically favorable interaction between the drug and the protecting agent. The exceptional case of negative value of charge transfer (ΔN) in the combination of *cis*-diammine-glycolato- *O,O*-platinum(II), Nedaplatin and D-penicillamine only shows that electron transfer is taking place in the reverse direction. The qualitative interpretation for this kind of observation is that such interactions will be no longer a thermodynamically favorable process.

Here also the logic to choose a suitable protecting agent against a particular cisplatin analogue is similar to that outlined in Section 3.3.3 (i). It can be easily noticed that as one moves down the Table 3.6 to select a cisplatin analogue the suitable protecting agents will be more and more right side of the Table.

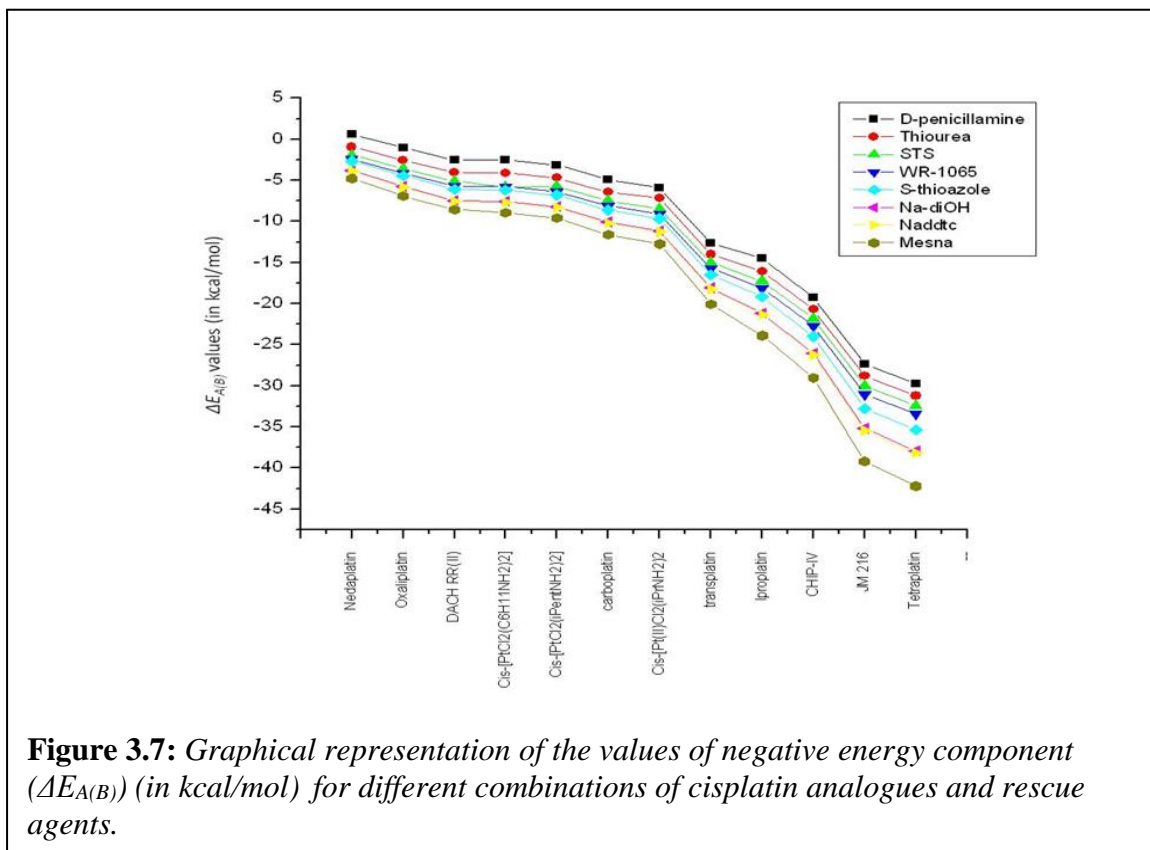
(iv) *Relative stability of the adducts formed between cisplatin analogues and protecting agents on the basis of negative energy components, i.e., $\Delta E_{A(B)}$:*

Values of $\Delta E_{A(B)}$ generated from CDASE scheme are presented in Table 3.7 and the relative trends of these values are shown graphically in Fig. 3.7. In the earlier discussion about theoretical background of CDASE scheme, we have explained that $\Delta E_{A(B)}$ is the negative energy component of the overall stabilization energy. As it is an energy lowering term it can be correlated to the thermodynamic stability of the adduct formed. Mathematically $\Delta E_{A(B)}$ can be expressed as,

$$|\Delta E_{A(B)}| = |\Delta E_{B(A)}| + |\Delta E_{SE(AB)}| \quad 3.1$$

Thus, it can be argued that larger the negative value of $\Delta E_{A(B)}$ higher will be the interaction between that particular pair of cisplatin analogue and protecting agent, causing higher stability of the resultant adduct. The gradual change in the color intensity from light to a highly intense one represents the increasing stability of adducts formed between the cisplatin analogues and protecting agents. Interestingly, the observed trend for $\Delta E_{A(B)}$ values on the basis of the color code of Table 3.7 appeared to be exactly

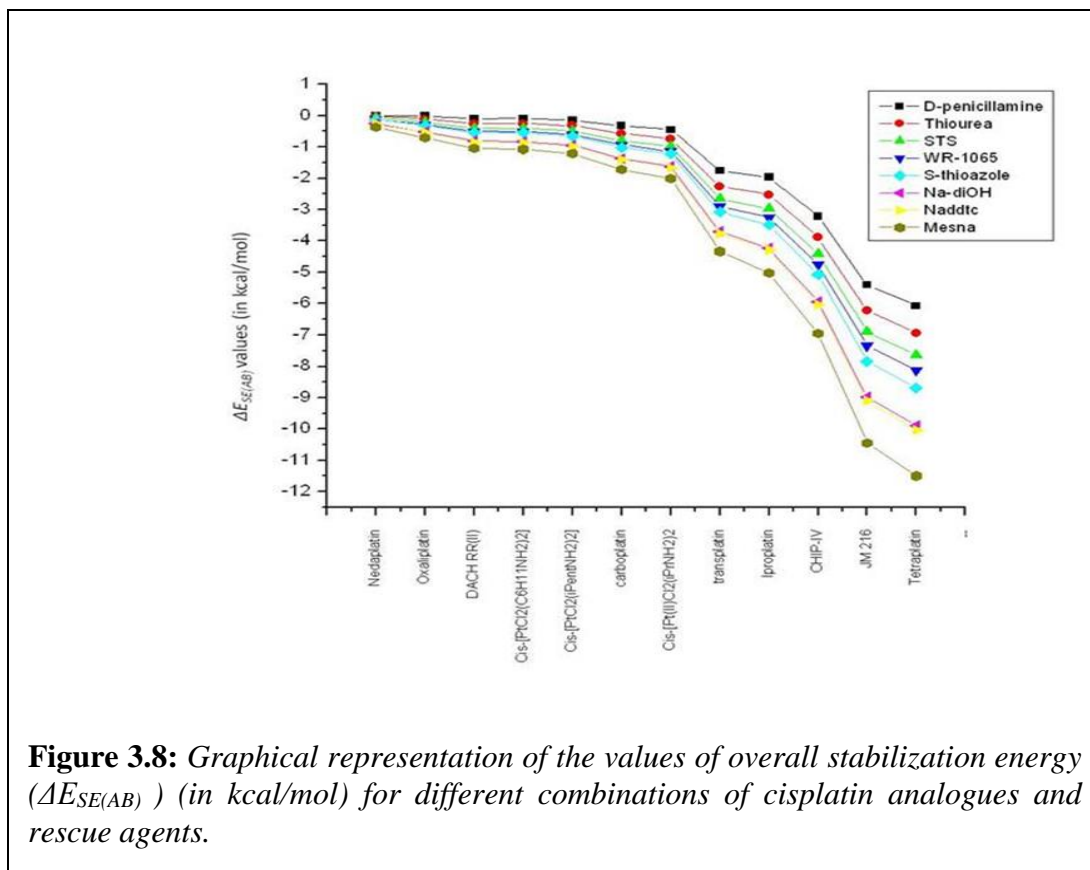
similar to that of $\Delta E_{B(A)}$ values presented in Table 3.4, indicating identical trend of interaction from both kinetic and thermodynamic point of view.



$\Delta E_{A(B)}$ values are reported for two different types of interactions. All the $\Delta E_{A(B)}$ values (except the last row) of these tables represent the interaction between cisplatin analogue and protecting agent. The last row represents the $\Delta E_{A(B)}$ values for the interaction between the protecting agent and the active biomolecule (i.e., guanine).

The observed values of $\Delta E_{A(B)}$ for the drug Tetraplatin are significantly high against all protecting agents chosen in the present study. This means that interaction of all the protecting agents with Tetraplatin is highly favorable thermodynamically when compared to other cisplatin analogues. An ideal protecting agent must have highly negative $\Delta E_{A(B)}$ value for interaction with the drug along with relatively lower negative value of $\Delta E_{A(B)}$ for the interaction with the bio-molecule. Then only the protecting agent can form a more stable adduct (i.e., thermodynamically favorable) with the cisplatin analogues than that with active biomolecules. It is to be noted here that when it comes to

the choice of protecting agents prescription here will also be similar to those made on the basis of Tables 3.3, 3.4 and 3.6.



(v) Relative stability of the adducts formed between cisplatin analogues and protecting agents on the basis of the overall stabilization energy, (i.e., $\Delta E_{SE(AB)}$) values:

The overall stabilization energy, $\Delta E_{SE(AB)}$, is an indicator of the overall stability of the adduct formed in a particular interaction. The more negative is the value of $\Delta E_{SE(AB)}$ higher will be the stability of the adduct formed in the course of an interaction. The $\Delta E_{SE(AB)}$ values are shown in Table 3.8 and the relative trends are demonstrated in Fig. 3.8.

In Table 3.8 the interaction energies between the drugs and the protecting agents are presented in different rows, whereas the stabilities of the adducts formed between the protecting agents and the biomolecule are presented in the last row. A trend of increasing relative stability for the adducts formed between cisplatin drugs and protecting agents is

observed as one moves along the Table 3.8 from left to right as well as from top to bottom. This is more obvious from Fig. 3.8. The color intensity changes (from a lighter zone to a more intense one) according to the variation of adduct stability.

One important outcome of the analysis of the stabilization energy values is that none of the protecting agents is able to produce reasonably large amount of $\Delta E_{SE(AB)}$. Most of the values are in between the range of $-0.5 \text{ kcal mol}^{-1}$ to $-10 \text{ kcal mol}^{-1}$. The physical interpretation is that these types of interactions are not stable enough to sustain for a long period. This is what it should be if these chemical systems qualify as rescue agents because they are used only to eliminate the higher probability of interaction of cisplatin analogues with sulfur donors in protein chain. This undesired interaction leading toward the toxic side effects of cisplatin drugs. The data in the present study also support the argument that these rescue agents produce some weak interactions with the drugs so that the activity of drugs reduces to a certain extent. Consequently, a protecting agent does not hinder the antitumor activity of a cisplatin drug. The relevance of the $\Delta E_{SE(AB)}$ values generated by CDASE scheme is also supported by the experimental observations.¹⁰⁴⁻¹⁰⁸

3.3.4 Synchronization of the data generated by different reactivity parameters and use of the strategy proposed in Sec. 3.3.1:

The ongoing discussion in the last three sub-sections helps to understand the action of different protecting agents to minimize the toxic side effects of cisplatin analogues. Here, one needs to focus on three types of possible interactions. These are interaction

- (i) of a particular cisplatin drug with genomic DNA.
- (ii) between rescue agent and that particular drug.
- (iii) of rescue agent with active biomolecules.

To determine the most suitable protecting agent against a particular cisplatin analogue a systematic correlation among the above three interactions is warranted for.

The study on the strength of relative interaction between cisplatin analogues and nucleobases ascertain the difference in their ability to interact. We can justify our terminology for ‘strong’ and ‘weak’ cisplatin drugs based on the data presented in Table

3.1. The relevance of the interpretation of this information in defining a specific protecting agent for a particular cisplatin analogue will be clear if it is explained with examples. In Table 3.1 the values of both kinetic [$\Delta W, \Delta E_{B(A)}$] and thermodynamic [$\Delta N, \Delta E_{A(B)}, \Delta E_{SE(AB)}$] descriptors predict that interaction of Carboplatin with adenine and guanine is moderate (as these values are in the middle of Table 3.1 and the strength of interaction increases as someone moves towards bottom from top). Thus, the theoretical calculation predicts moderate tumor inhibition activity of Carboplatin. So, if a highly active rescue agent (ranking of the rescue agents in terms of strength of their interaction with cisplatin analogues is discussed in different sub-sections of Section 3.3.3), such as NaDDTC, is selected in cancer therapy with Carboplatin as anti-cancer drug it will probably reduce the anti-tumor activity of Carboplatin to a large extent. As a result, Carboplatin might lose its activity toward cancer cells in the presence of protecting agent NaDDTC. To avoid this, chemotherapeutic application of Carboplatin should be accompanied by a moderately active protecting agent such as D-penicillamine or WR-1065, which will result in a minor decrease of the activity of Carboplatin. Again, as per the values of the reactivity descriptors, aminodiacetatochloro (cyclohexylamine)platinum(IV), JM-216 shows significantly high interaction with nucleobases (Table 3.1). So, in case of a treatment with JM-216 we can go for a rescue agent with higher activity so that it can effectively modulate the undesirable protein binding affinity of the drug. Some earlier reported experimental and theoretical studies, as summarized in Table 3.2 and described in different subsections of 3.3.3, also support the above claim.

3.4 Conclusions:

Basically, selection of a protecting agent that could be the potential modulator for a specific cisplatin analogue depends on three critical factors. The first one is how strongly a particular drug interacts with nucleobases (guanine N-7 position is the most active site) of DNA. The second one is the activity of that particular drug towards that protecting agent. The third factor is how strongly the protecting agent interacts with other biomolecules. All these three factors complement each other in the process of deciding the most effective combination of drugs and protecting agents in cancer therapy. The

present study uses the density functional theory based reactivity descriptors in framing up a qualitative strategy to aid such a selection process.

It is encouraging to note that the trend of Δw values (i.e., difference of global electrophilicity values between cisplatin analogues and rescue agents, Table 3.3) generated by this scheme is quite similar to the experimental trend of activity observed by Boelrijk *et al.*³⁰ Also, the findings by Elferink *et al.*³¹ on the rate of interaction of cisplatin analogues with the protecting agent STS is also correlated well with our CDASE scheme based results. The stronger interaction between cisplatin drugs with protecting agent diethyldithiocarbamate (DDTC) as compared to that with thiosulfate compound was experimentally explored by Dedon *et al.*³² This experimental observation is correlated well with our reported CDASE scheme based theoretical findings in the present study [Sec. 3.3.3 (i)]. An extensive experimental study by Korst *et al.*²⁶ strongly supports the CDASE scheme based prediction on WR-1065 as a moderately active chemoprotective agent. Relatively higher degree of interactions between WR-1065 with active biomolecules, to some extent, inhibits the chemoprotective activity of WR-1065. Treskes *et al.*²⁴ experimentally analyzed the reversal of drug-protein binding interaction to an effective drug-DNA interaction in presence of two different protecting agents WR-1065 and DDTC. The CDASE scheme based positive energy component ($\Delta E_{B(A)}$) values are able to provide a logical explanation for the kinetic aspect (experimentally obtained rate constant values) of these interactions (as discussed in Section 3.3.3 (ii)). Analysis of different reactivity descriptor values from Table 3.3-3.7 prescribes that as one moves down these Tables to select a drug he has to move more and more right in these tables to select the corresponding protecting agent.

Understanding of the interaction behavior of cisplatin analogues with protecting agents using density functional reactivity theory (DFRT) based descriptors through the CDASE scheme is an ongoing initiative in the research group of the authors to develop an alternative and computationally cost-effective approach to explore interesting biological phenomena. To the best of author's knowledge, the present one may be the very first theoretical attempt in this direction as there is no such study reported in the literature to understand the interaction of cisplatin analogues with various protecting agents using DFRT based descriptors. The explicit interaction protocol for cisplatin

analogues and protecting agents will hopefully lay the foundation for an extensive theoretical as well as experimental research work to verify all the emerging aspects of the present study.

The authors are more hopeful because the qualitative prediction made here are based on the direction of electron transfer which is generated from different energy based parameters (i.e., $\Delta E_{A(B)}$ and $\Delta E_{B(A)}$). High sensitivity of reactivity descriptors generated from electronic population is well documented in the literature.

Finally, there is increasing evidence that systematic analysis of the data generated from ab-initio quantum chemistry based simulation is an important tool in the field of discovery and development of new anti-cancer drugs.¹⁰⁴ Rapid advancement in the computational power along with some sophisticated software programs makes it possible to outplay the primary limitations in the accuracy of theoretical chemistry based approaches. Multidisciplinary research applications like the combination of quantum chemistry, computer programming and clever modeling techniques constantly endeavor to reduce the possibility of unsuccessful attempts in different phases of clinical trials for a newly developed drug. The present study may be perceived as an attempt to develop a computationally cost-effective and reliable theoretical technique in this direction.

References:

1. B. Rosenberg, L Van Camp, Krigas, *Nature* 1965, **205**, 698.
2. E. R. Jamieson, S. J. Lippard, *Chem. Rev.* 1999, **99**, 2467.
3. H. C. Harder, B. Rosenber, *Int J Cancer* 1970, **6**, 207.
4. J. A. Howle, G. R. Gale, *Biochem Pharmacol*, 1970, **19**, 2757.
5. M.A. Fuertes, C. Alonso, J. M. Perez *Chem Rev*, 2003, **103**, 645.
6. D. P. Bancroft, C. A. Lepre, S. J. Lippard, *J Am Chem Soc*, 1990, **112**, 6860.
7. S. E. Sherman, S. J. Lippard *Chem Rev* 1987, **87**, 1153.
8. J. A. Mello, S. J. Lippard, J. M. Essigmann, *Biochemistry* 1995, **34**, 14783.
9. R. S. Go, A. A. Adjei *J Clin Oncol* 1999, **17**, 409.
10. Y. Jung, S. J. Lippard, *Chem Rev* 2007, **107**, 1387.
11. V. Sresht, J. R. Bellare, S. K. Gupta, *Ind Eng Chem Res*, 2011, **50**, 12872.
12. M. Yoshida, A. R. Khokhar, Y. Kido, F. Ali-Osman, Z. H. Siddik, *Biochem Pharmacol* 1994, **48**, 793.
13. M. E. Palm-Esplin, P. Wittung-Stafshede, *Biochem Pharmacol*, 2012, **83**, 874.
14. R. A. Alderden, D. M. Hall, T. W. Hambley, *J Chem Edu*, 2006, **83**, 728.
15. Y. Kasherman, S. Sturup, D. Gibson, *J Med Chem*, 2009, **52**, 4319.
16. M. Marty, P. Pouillart, S. J. P. Scholl Droz, M. Azab, M. Brion, E. Pujade-Lauraine B. Paule, D. Paes, J. Bon, *New Engl J Med*, 1993, **322**, 816.
17. L. Z. Cubeddu, I. S. Horrmann, T. N. Fuenmayor, A. L. Finn, *New Engl J Med*, 1990, **322**, 810.
18. R. B. Weiss, M. C. Christian, *Drugs*, 1993, **46**, 360.
19. G. Laurell, C. Beskow, B. Frankendal, E. Borg, *Cancer* 1996, **78**, 1798.
20. R. F. Ozols, B. J. Corden, J. Collins, R. C. Young, *Platinum Coordination Complexes in Cancer Chemotherapy* Eds. Martinus Nijhoff Boston 1984 p 321.
21. R. G. Pearson, *J. Am. Chem. Soc.* 1963, **85**, 3533.
22. R. G. Pearson, *J. Chem. Educ.* 1965, **45**, 581.
23. R. G. Pearson, *J. Chem. Educ.*, 1968, **45**:643.
24. M. Treskes, J. F. W. van der Vijgh, *Cancer Chemother. Pharmacol.* 1993, **33**:93.
25. J. S. Berners-Price, P. W. Kuchel, *J Inorg Biochem.* 1990, **38**, 327.
26. A. E. C. Korst, C. M. Eeltink, J B Vermorken, W. J. F. van der Vijgh, *Eur. J. Cancer* 1990 **33**, 1425.
27. J. C. Dabrowiak, J. Goodisman, A. K. Souid, *Drug Metab Dispos* 2002, **30**, 1378.
28. J. Reedijk, *Chem. Rev.* 1999, **99**, 2499.
29. S. B. Howell, C. L. Pfeifle, W. E. Wung, R. A. Olshen, *Cancer Res.* 1983, **43**, 1426.
30. A. E. M. Boelrijk, P. J. Boogaard, E. L. M. Lempers, J. Reedijk, *J Inorg Biochem* 1991, **41**, 17.
31. F. Elferink, W. J. F. van der Vijgh, I. Klein, *Clin Chem* 1986, **32**, 641.
32. P. C. Dedon, R. F. Borch, *Biochem. Pharmacol.* 1987, **36**, 1955.
33. D. L. Bodenner, P. C. Dendon, P. C. Keng, J. C. Katz, R. F. Borch, *Cancer Res* 1986, **46**, 2751.
34. D. L. Bodenner, P. C. Dendon, P. C. Keng, R. F. Borch, *Cancer Res* 1986, **46**, 2745.
35. Z. Chval, M. Sip, *J. Mol. Struct. THEOCHEM* 2000, **532**, 59.

-
36. Y. Zhang, Z. Guo, X. Z. You, *J. Am. Chem. Soc.* 2001, **123**, 9378;
 37. P. Sarmah, R. C. Deka, *Int. J. Quantum. Chem.* 2008, **108**, 1400
 38. P. Sarmah, R. C. Deka, *J. Comput. Aided. Mol. Des.* 2009, **23**, 343
 39. J. Raber, C. Zhu, L. A. Eriksson, *Mol. Phys.* 2004, **102**, 2537
 40. J. K. C. Lau, D. V. Deubel, *J. Chem. Theory. Comput.* 2006, **2**, 103.
 41. Y. Mantri, S. J. Lippard, M. H. Baik, *J. Am. Chem. Soc.* 2007, **129**, 5023
 42. J. Raber, C. Zhu, L. A. Eriksson, *J. Phys. Chem. B* 2005, **109**, 11006.
 43. M. Zeizinger, J. V. Burda, J. Leszczynski, *Phys. Chem. Chem. Phys.* 2004, **6**, 3585
 44. K. Spiegel, U. Rothlisberger, P. Carloni, *J. Phys. Chem. B* 2004, **104**, 2699.
 45. T. Matsui, Y. Shigeta, K. Hirao, *J. Phys. Chem. B* 2007, **111**, 1176.
 46. R. G. Parr, W. Yang, *Density—Functional Theory of Atoms and Molecules*; Oxford University Press; New York, 1989.
 47. W. Koch, M. A. Holthausen, *Chemist's Guide to Density Functional Theory*; VCH, Weinheim, 2000.
 48. P. Geerlings, F. De Proft, W. Langenaeker, *Chem. Rev.* 2003, **103**, 1793.
 49. R. G. Parr, R. G. Pearson, *J. Am. Chem. Soc.* 1983, **105**, 7512
 50. R. G. Parr, W. Yang, *Proc. Natl. Acad. Sci. U. S. A.* 1985, **82**, 6723.
 51. P.K. Chattaraj, B. Maiti, U. Sarkar, *J. Phys. Chem. A* 2003, **107**, 4973
 52. P.K.Chattaraj, D.R. Roy, *Chem. Rev.* 2007, **107**, PR46.
 53. S. Krishnamurty, S. Pal, *J. Phys. Chem. A*, 2000, **104**, 7639.
 54. R. K. Roy, *J. Phys. Chem. A* 2004, **108**, 4934.
 55. R. K. Roy, V. Usha, J. Paulovic, K. Hirao, *J. Phys. Chem. A* 2006, **109**, 4601.
 56. R. K. Roy, V. Usha, B. K. Patel, K. Hirao, *J. Comput. Chem.* 2006, **27**, 773.
 57. R. K. Roy, P. Bagaria, S. Naik, V. Kavala, B. K. Patel, *J. Phys. Chem. A* 2006, **110**, 2181.
 58. P. Bagaria, R. K. Roy, *J. Phys. Chem. A* 2008, **112**, 97.
 59. C. Cárdenas, N. Rabi, P. W. Ayers, C. Morell, P. Jaramillo, P. Fuentealba, *J Phys Chem A* 2009, **113**:8660.
 60. R. G. Parr, W. Yang, *J. Am. Chem. Soc.* 1984, **106**, 4049.
 61. W. Yang, W. J. Mortier, *J. Am. Chem. Soc.* 1986, **108**, 5708..
 62. W. Yang, R. G. Parr, *Proc. Natl. Acad. Sci. U. S. A.* 1985, **82**, 6723.
 63. R. G. Parr, J. L. Gazquez, *J. Phys. Chem.*, 1993, **97**, 3939.
 64. S. Saha, R. K. Roy, *J. Phys. Chem. B.* 2007, **111**, 9664.
 65. S. Saha, R. K. Roy, *J. Phys. Chem. B (Addition/Correction)* 2008, **112**, 1884.
 66. S. Saha, R. K. Roy, *Phys. Chem. Chem. Phys.* 2008, **10**, 5591.
 67. R. K. Roy, S. Krishnamurti, P. Geerlings, S. Pal, *J. Phys. Chem. A.* 1998, **102**, 3746.
 68. R. K. Roy, F. De Proft, P. Geerlings, *J. Phys. Chem. A.* 1998, **102**, 7035.
 69. P. Perez, A. Toro-Labbe, A. Aizman, R. Contreras, *J. Org. Chem.* 2002, **67**, 4747.
 70. A. M. Lamsabhi, C. A., Escobar, P. Perez, *J Phys Org Chem* 2000, **18**, 1161.
 71. L. R. Domingo, P. Perez, R. Contreras, *J. Org. Chem.*, 2003, **68**,6060.
 72. R. G. Parr, R. A. Donnelly, M. Levy, W. E. Palke, *J. Chem. Phys.* 1978, **68**, 3801.
 73. R. S. Mulliken, *J. Chem. Phys.*, 1934, **2**,782.
 74. A. T. Maynard, M. Huang, W. G. Rice, D. G.; Covell, *Proc. Natl. Acad. Sci. USA* 1998, **95**, 11578.

-
75. R. G. Parr, L. V. Szentpaly, S. Liu, *J. Am. Chem. Soc.* 1999, **121**, 1922.
 76. P. W. Ayers, R. G. Parr *J. Am. Chem. Soc.* 2001, **123**, 2007.
 77. P. Jaramillo, P. Perez, R. Contreras, W. Tiznado and, P. Fuentealba, *J Phys Chem A* 2007, **110**, 2221.
 78. P. Jaramillo, P. Perez, R. Contreras, W. Tiznado, P. Fuentealba, *J. Phys. Chem. A* 2006, **110**, 8181.
 79. P. W. Ayers, J. S. M. Anderson, J. I. Rodriguez, Z. Jawed, *Phys. Chem. Chem. Phys.* 2005, **7**, 1918.
 80. P. Pe´ rez, L. R. Domingo, M. Duque-Nore˜ na, E. Chamorro, *THEOCHEM* 2009, **895**, 86.
 81. S. Saha, R. Bhattacharjee, R. K. Roy, *J. Comp. Chem.* 2013, **34**, 662.
 82. R. Bhattacharjee, R. K. Roy, *J. Phys. Chem. A* 2014, **117**, 11528.
 83. P. Bagaria, S. Saha, S. Murru, V. Kavala, B. K. Patel, R. K. Roy, *Phys. Chem. Chem. Phys.* 2009, **11**, 8306.
 84. A. Sarmah, S. Saha, P. Bagaria, R. K. Roy, *Chem. Phys.* 2012, **394**, 29.
 85. A. Sarmah, R. K. Roy, *RSC Adv.* 2013, **3**, 2822.
 86. A. Sarmah, R. K. Roy, *J. Phys. Chem. C* 2013, **117**, 21539.
 87. S. Saha, R. K. Roy, S. Pal, *Phys. Chem. Chem. Phys.* 2010, **12**, 9328
 88. A. Cedillo, R. Contreras, M. Galvan, A. Aizman, J. Andres, V. S. Safont, *J. Phys. Chem. A* 2007, **111**, 2442.
 89. R. Dennington, T. Keith, J. Millam, .GaussView, Version 5. Semichem Inc., Shawnee Mission KS, **2009**.
 90. A. D. Becke, *Phys. Rev. A* 1988, **38**, 3098.
 91. A. D. Becke, *J. Chem. Phys.* 1993, **98**, 5648.
 92. C. T. Lee, W. T. Yang, R. G. Parr, *Phys. Rev. B* 1988, **37**, 785.
 93. G. A. Peterson, M. A. Al-Laham, *J. Chem. Phys.* 1991, **94**, 6081.
 94. Hehre W J, Stewart R F, Pople J A (1969) *J Chem Phys* 51:2657-2665.
 95. W. J. Hehre, R. F. Stewart, J. A. Pople, *J. Chem. Phys.* 1969, **51**, 2657.
 96. R. Ditchfield, W. J. Hehre, J. A. Pople, *J. Chem. Phys.* 1971, **54**, 724.
 97. P. J. Hay, W. R. Wadt, *J. Chem. Phys.* **1985**, 82,270.
 98. P. J. Hay, W. R. Wadt, *J. Chem. Phys.* **1985**, 82, 284.
 99. P. J. Hay, W. R. Wadt, *J. Chem. Phys.* **1985**, 82, 284.
 100. M. J. Frisch *et al.* GAUSSIAN 03, Revision E.01, Gaussian, Inc., 340 Quinnipiac St., Bldg. 40, Wallingford CT 06492..
 101. V. Murray, J. Whittaker, D. M. Temple, W. D. J. F. McFadyne, *Biochim. et Biophys. Acta* 1997, **1534**, 261.
 102. O. Rixe, W. Ortuzar, M. Alvarez, R. Parker, E. Reed, K. Paull, *Biochem. Pharmacol.* 1996, **52**, 1855.
 103. D. J. Wilton, M. Ghosh, K. V. A. Chary, K. Akasaka, M. J. Williamson, *Nucleic Acids Res.* 2008, **36**, 4032.
 104. P. D. Dans, E. L. Coitin˜ o, *J. Chem. Inf. Model*, 2009, **49**, 1407.
 105. B. H. Stephen, E. P. Craigoh, W. E. Wung, R. A. Olshen, *Cancer Res* 2009, **43**, 1426.
 106. H. H. Frederick *et al.* *Cancer Chemother Pharmacol* 2003, **52**, S3.
 107. B. C. Millar, Z. H. Siddik, J. I. Millar, S. Jinks, *Cancer Chemother Pharmacol*, 1985, **15**, 307.
 108. J. L. Aull, A. C. Rice, L. A. Tebbetts, *Biochemistry*, 1977, **16**, 672.

Table 3.1: Five CDASE scheme based parameters namely, ΔW , $\Delta E_{B(A)}$, ΔN , $\Delta E_{A(B)}$, and $\Delta E_{SE(AB)}$ calculated for the interaction of 12 different cisplatin analogues with DNA. Method used for cisplatin analogues is B3LYP/LanL2DZ, whereas for nucleobases it is B3LYP/6-31 G(d,p).

(a) Computed CDASE scheme based parameters for the interaction between cisplatin analogues and individual purine bases adenine (A) and guanine (G)

A = Cisplatin Analogue: B = Adenine (A)/ Guanine (G)					
Combinations	Δw kcal/mol)	$\Delta E_{B(A)}$ (kcal/mol)	ΔN	$\Delta E_{A(B)}$ (kcal/mol)	$\Delta E_{SE(AB)}$ (kcal/mol)
Nedaplatin: Adenine	4.66	1.98	0.0265	-2.05	-0.07
Nedaplatin: Guanine	9.06	4.10	0.0589	-4.47	-0.37
Oxaliplatin: Adenine	9.99	3.55	0.0468	-3.78	-0.23
Oxaliplatin: Guanine	14.39	5.69	0.0804	-6.35	-0.67
DACH RR II: Adenine	13.26	4.95	0.0644	-5.38	-0.43
DACH RR II: Guanine	17.65	7.04	0.0981	-8.03	-0.99
Cis-[PtCl ₂ (C ₆ H ₁₁ NH ₂) ₂]: Adenine	14.57	5.04	0.0656	-5.48	-0.44
Cis-[PtCl ₂ (C ₆ H ₁₁ NH ₂) ₂]: Guanine	18.97	7.17	0.0998	-8.18	-1.00
Cis- [PtCl ₂ (iPentNH ₂) ₂]: Adenine	15.37	5.55	0.0718	-6.07	-0.53
Cis-[PtCl ₂ (iPentNH ₂) ₂]: Guanine	19.76	7.64	0.1059	-8.78	-1.14
Carboplatin: Adenine	17.53	7.05	0.0901	-7.90	-0.85
Carboplatin: Guanine	21.92	9.04	0.1236	-10.63	-1.59
Cis-[Pt(II)Cl ₂ (iPrNH ₂) ₂]: Adenine	18.88	7.86	0.0998	-8.91	-1.04
Cis-[Pt(II)Cl ₂ (iPrNH ₂) ₂]: Guanine	23.28	9.80	0.1331	-11.65	-1.85
Transplatin: Adenine	25.65	12.90	0.1576	-15.69	-2.79
Transplatin: Guanine	30.05	14.45	0.1886	-18.44	-3.99
CHIP-IV: Adenine	48.03	18.29	0.2153	-22.95	-4.66
CHIP-IV: Guanine	52.42	19.98	0.2501	-26.26	-6.28
JM 518: Adenine	65.04	19.38	0.2265	-24.01	-4.63

[Table 3.1 (a). Continued]

JM 518: Guanine	69.43	21.42	0.2654	-27.76	-6.34
JM216: Adenine	68.96	24.25	0.2745	-31.54	-7.29
JM216: Guanine	73.35	25.90	0.3114	-35.24	-9.34
Tetraplatin: Adenine	75.50	25.96	0.2914	-34.06	-8.10
Tetraplatin: Guanine	79.88	27.62	0.3284	-37.87	-10.26

(b) Computed CDASE scheme based parameters for the interaction between cisplatin analogues and W-C single base pair unit

Combinations	A= Cisplatin Analogue: B = A-T/ G-C Base pair				
	ΔW (kcal/mol)	$\Delta E_{B(A)}$ (kcal/mol)	ΔN	$\Delta E_{A(B)}$ (kcal/mol)	$\Delta E_{SE(AB)}$ (kcal/mol)
Nedaplatin: AT	0.32	1.66	0.022	-1.71	-0.05
Nedaplatin: GC	11.39	3.78	0.0534	-4.05	-0.27
Oxaliplatin: AT	22.64	3.33	0.0436	-3.52	-0.18
Oxaliplatin: GC	33.71	5.52	0.0768	-6.07	-0.55
DACH RR II: AT	36.30	4.83	0.0625	-5.21	-0.38
DACH RR II: GC	47.37	7.01	0.0965	-7.88	-0.86
<i>Cis</i> -[PtCl ₂ (C ₆ H ₁₁ NH ₂) ₂]: AT	41.80	4.93	0.0637	-5.21	-0.39
<i>Cis</i> -[PtCl ₂ (C ₆ H ₁₁ NH ₂) ₂]: GC	52.86	7.16	0.0983	-8.04	-0.88
<i>Cis</i> - [PtCl ₂ (iPentNH ₂) ₂]: AT	45.13	5.47	0.0704	-5.94	-0.47
<i>Cis</i> - [PtCl ₂ (iPentNH ₂) ₂]: GC	56.20	7.68	0.1050	-8.69	-1.01
Carboplatin: AT	54.17	7.08	0.0906	-7.87	-0.79
Carboplatin: GC	65.24	9.22	0.1247	-10.67	-1.46
<i>Cis</i> -[Pt(II)Cl ₂ (iPrNH ₂) ₂]: AT	59.84	7.95	0.1005	-8.93	-0.98
<i>Cis</i> -[Pt(II)Cl ₂ (iPrNH ₂) ₂]: GC	70.91	10.05	0.1352	-11.78	-1.72
Transplatin: AT	88.20	13.27	0.1619	-16.03	-2.76
Transplatin: GC	99.26	15.09	0.1959	-19.00	-3.92
CHIP-IV: AT	181.83	19.04	0.2243	-23.74	-4.70
CHIP-IV: GC	192.90	21.22	0.2650	-27.55	-6.34
JM 518: AT	94.74	9.66	0.1207	-11.00	-1.34
JM 518: GC	105.81	11.94	0.2265	-14.16	-2.22

[Table 3.1 (b). Continued]

JM216: AT	269.44	25.40	0.2889	-32.87	-7.46
JM216: AT	280.51	27.74	0.3339	-37.35	-9.61
Tetraplatin: AT	296.78	27.24	0.3068	-35.55	-8.31
Tetraplatin: GC	307.85	29.64	0.3532	-40.25	-10.60

(c) Computed CDASE scheme based parameters for the interaction between cisplatin analogues and double base pair unit

Combinations $\Delta E_{SE(AB)}$ (kcal/mol)	A= Cisplatin Analogue: B = GA-CT Base pairs				
	Δw (kcal/mol)	$\Delta E_{B(A)}$ (kcal/mol)	ΔN	$\Delta E_{A(B)}$ (kcal/mol)	
Nedaplatin: GA-CT	10.37	3.65	0.0511	-3.89	-0.24
Oxaliplatin: GA-CT	11.95	5.51	0.0762	-6.02	-0.51
DACH RR II: GA-CT	25.61	7.12	0.0971	-7.93	-0.82
<i>Cis</i> -[PtCl ₂ (C ₆ H ₁₁ NH ₂) ₂]: GA-CT	31.10	7.26	0.0991	-8.10	-0.84
<i>Cis</i> - [PtCl ₂ (iPentNH ₂) ₂]: GA-CT	34.44	7.82	0.1063	-8.79	-0.97
Carboplatin: GA-AT	43.48	9.46	0.1273	-10.88	-1.42
<i>Cis</i> -[Pt(II)Cl ₂ (iPrNH ₂) ₂]: GA-CT	49.15	10.35	0.1384	-12.04	-1.69
Transplatin: GA-CT	77.50	15.64	0.2026	-19.58	-3.95
CHIP-IV: GA-CT	171.14	22.21	0.2776	-28.70	-6.49
JM 518: GA-CT	84.40	12.38	0.1635	-14.59	-2.21
JM216: GA-CT	258.75	31.22	0.3523	-39.14	-9.96
Tetraplatin: GA-CT	286.09	29.18	0.3733	-42.23	-11.02

(d) Computed CDASE scheme based parameters for the interaction between cisplatin analogues and triple base pair unit

A = Cisplatin Analogue: B = GCG-CGC/ATT-TAA Base pairs					
Combinations	Δw (kcal/mol)	$\Delta E_{B(A)}$ (kcal/mol)	ΔN	$\Delta E_{A(B)}$ (kcal/mol)	$\Delta E_{SE(AB)}$ (kcal/mol)
Nedaplatin: (AT) ^t	0.38	1.99	0.0266	-2.06	-0.07
Nedaplatin: (GC) ^t	5.45	4.76	0.0689	-5.18	-0.42
Oxaliplatin: (AT) ^t	0.96	3.79	0.0500	-4.02	-0.22
Oxaliplatin: (GC) ^t	16.87	6.66	0.0952	-7.43	-0.77
DACH RR II: (AT) ^t	4.22	5.39	0.0704	-5.84	-0.44
DACH RR II: (GC) ^t	30.53	8.25	0.1167	-9.41	-1.16
<i>Cis</i> -[PtCl ₂ (C ₆ H ₁₁ NH ₂) ₂]: (AT) ^t	5.53	5.51	0.0718	-5.96	-0.45
<i>Cis</i> -[PtCl ₂ (C ₆ H ₁₁ NH ₂) ₂]: (GC) ^t	36.02	8.44	0.1191	-9.61	-1.19
<i>Cis</i> - [PtCl ₂ (iPentNH ₂) ₂]: (AT) ^t	6.33	6.08	0.0790	-6.63	-0.55
<i>Cis</i> - [PtCl ₂ (iPentNH ₂) ₂]: (GC) ^t	39.06	8.97	0.1063	-10.32	-1.34
Carboplatin: (AT) ^t	8.49	7.78	0.0999	-8.68	-0.90
Carboplatin: (GC) ^t	48.43	10.58	0.1473	-12.44	-1.86
<i>Cis</i> -[Pt(II)Cl ₂ (iPrNH ₂) ₂]: (AT) ^t	9.84	8.69	0.1110	-9.81	-1.12
<i>Cis</i> -[Pt(II)Cl ₂ (iPrNH ₂) ₂]: (GC) ^t	54.07	11.45	0.1585	-13.62	-2.17
Transplatin: (AT) ^t	16.62	14.22	0.1758	-17.26	-3.04
Transplatin: (GC) ^t	82.42	16.57	0.2223	-21.23	-4.66
CHIP-IV: (AT) ^t	38.99	20.50	0.2450	-25.70	-5.20
CHIP-IV: (GC) ^t	176.06	23.35	0.3017	-30.86	-7.50
JM 518: (AT) ^t	8.18	10.57	0.1335	-12.09	-1.52
JM 518: (GC) ^t	88.97	13.59	0.1856	-16.37	-2.78
JM216: (AT) ^t	59.92	27.33	0.3159	-35.58	-8.25
JM216: (GC) ^t	263.67	30.43	0.3794	-41.71	-11.28

[Table 3.1 (d). Continued]

Tetraplatin: (AT) ^t	66.45	29.32	0.3357	-38.50	-9.18
Tetraplatin: (GC) ^t	291.00	32.50	0.3733	-44.94	-12.44

* (AT)^t = ATT-TAA, and (GC)^t = CGC-GCG

Table 3.2: Earlier reported experimental as well as theoretical studies, which are relevant to understand the mode of interaction of some promising protecting agents (chosen in the present study) against platinum based anticancer drugs

Protecting agent	Method	Ref.
Penicillamine	Experimental	32,107
Thiourea	Experimental	30,32
DDTC	Experimental	32,33, 34
STS	Exp. + Theoretical	29, 30, 31, 104
Mesna	Exp + Theoretical	105, 106
WR-2721	Experimental	24, 26, 28

Table 3.3: The difference between global electrophilicity (Δw) values (in kcal mol⁻¹) for different combinations of cisplatin analogues (acceptor, A) and protecting agents (donor, B). While in a particular row the number in a box represents the Δw value for the interaction between the corresponding cisplatin analogue and the protecting agent the values in the last row are for interaction between guanine (i.e., the biomolecule here) and the corresponding protecting agent.

Protecting agents Cisplatin analogues	D-							
	penicill amine	Thiourea	STS	WR-1065	S-thioazole	Na-diOH	NaDDTC	Mesna
Nedaplatin	0.09	2.78	4.55	5.16	6.16	6.19	6.86	7.35
Oxaliplatin	5.34	8.11	9.88	10.49	11.49	11.52	12.19	12.69
DACH RR(II)	8.69	11.37	13.15	13.75	14.76	14.78	14.46	15.95
<i>Cis</i> -[PtCl ₂ (C ₆ H ₁₁ NH ₂) ₂]	10.00	15.69	14.46	15.07	16.07	16.09	16.76	17.26
<i>Cis</i> -[PtCl ₂ (iPentNH ₂) ₂]	10.80	13.48	15.25	15.86	16.86	16.89	17.57	18.06
Carboplatin	12.96	15.64	17.41	18.02	19.03	19.05	19.73	20.21
<i>Cis</i> -[Pt(II)Cl ₂ (iPrNH ₂) ₂]	14.13	17.00	18.76	19.37	20.38	20.41	21.08	21.57
Transplatin	21.03	23.77	25.54	26.15	27.15	27.18	27.85	28.34
CHIP-IV	43.46	46.14	47.91	48.52	49.52	49.55	50.23	50.71
JM 518	60.47	63.15	64.92	65.53	66.53	66.56	67.24	67.73
JM 216	64.39	67.07	68.84	69.45	70.45	70.48	71.16	71.64
Tetraplatin	70.92	73.61	75.37	75.98	76.99	77.01	77.68	78.18
Guanine	8.97	6.28	4.51	3.90	2.90	2.87	2.20	1.70

Table 3.4: The values of the positive energy component, $\Delta E_{B(A)}$, (in kcal/mol) for different combinations of cisplatin analogues (considered as A) and protecting agents (considered as B). While in a particular row the number in a box represents the $\Delta E_{B(A)}$ value for the interaction between the corresponding cisplatin analogue and the protecting agent the values in the last row are for interaction between guanine (i.e., the biomolecule here) and the corresponding protecting agent.

Protecting agents Cisplatin analogues	Protecting agents							
	D- penicilla mine	Thiourea	STS	WR- 1065	S- thioazole	Na- diOH	NaDDTC	Mesna
Nedaplatin	-0.57	0.92	1.86	2.33	2.52	3.56	3.66	4.40
Oxaliplatin	0.96	2.42	3.35	3.83	4.11	5.21	5.31	6.19
DACH RR(II)	2.41	3.79	4.69	5.17	5.52	6.62	6.72	7.07
<i>Cis</i> -[PtCl ₂ (C ₆ H ₁₁ NH ₂) ₂]	2.46	3.87	4.77	5.27	5.62	6.75	6.85	7.86
<i>Cis</i> -[PtCl ₂ (iPentNH ₂) ₂]	2.98	4.36	5.25	5.75	6.12	7.24	7.34	8.38
Carboplatin	4.60	5.87	6.67	7.18	7.62	8.78	8.81	9.92
<i>Cis</i> -[Pt(II)Cl ₂ (iPrNH ₂) ₂]	5.4	6.67	7.48	7.96	8.43	9.51	9.61	10.76
Transplatin	10.88	11.74	12.35	12.79	13.41	14.38	14.48	15.75
CHIP-IV	16.05	16.87	17.45	18.00	18.90	20.08	20.28	22.07
JM 518	16.59	17.67	18.31	18.97	20.12	21.55	21.71	24.05
JM 216	21.99	22.57	23.11	23.67	24.93	26.22	26.37	28.75
Tetraplatin	23.68	24.22	24.73	25.31	26.66	28.00	28.15	30.69
Guanine	4.19	2.94	2.13	1.69	1.36	0.37	0.28	0.61

Table 3.5: A qualitative comparison between the experimental rate constant (k) with the computed $\Delta E_{B(A)}$ values.

Experimental Observation		Theoretical $\Delta E_{B(A)}$ values (in kcal/mol)	
Protecting agent	Drug-Protein reversal activity (experimental Rate constant)	For interaction between Drug and Protecting agent	For interaction between Protecting agent and Biomolecule
WR1065	k ₂ = 0.142 M-1s-1 (slow)	5.17	1.69
DDTC	k ₂ = 3.66 M-1s-1 (fast)	6.72	0.28

Table 3.6: The charge transfer (ΔN) values for different combinations of chosen cisplatin analogues (considered as A) and protecting agents (considered as B). While in a particular row the number in a box represents the ΔN value for the interaction between the corresponding cisplatin analogue and the protecting agent the values in the last row are for interaction between guanine (i.e., the biomolecule here) and the corresponding protecting agent.

Protecting agents Cisplatin analogues	D- penicilla mine	Thiourea	STS	WR- 1065	S- thioazole	Na-diOH	NaDDTC	Mesna
Nedaplatin	-0.0072	0.0119	0.0248	0.0315	0.0343	0.0503	0.0516	0.0632
Oxaliplatin	0.0119	0.0310	0.0441	0.0511	0.0551	0.0721	0.0736	0.0875
DACH RR(II)	0.0293	0.0479	0.0608	0.0681	0.0729	0.0905	0.0920	0.1076
<i>Cis</i> - [PtCl ₂ (C ₆ H ₁₁ NH ₂) ₂]	0.0299	0.0488	0.0619	0.0693	0.0743	0.0921	0.0937	0.1097
<i>Cis</i> -[PtCl ₂ (iPentNH ₂) ₂]	0.0362	0.0549	0.0678	0.0752	0.0805	0.0984	0.1000	0.1165
Carboplatin	0.0550	0.0728	0.0853	0.0928	0.0989	0.1169	0.1186	0.1364
<i>Cis</i> -[Pt(II)Cl ₂ (iPrNH ₂) ₂]	0.0649	0.0822	0.0946	0.1021	0.1087	0.1267	0.1285	0.1470
Transplatin	0.1245	0.1390	0.1500	0.1575	0.1665	0.1845	0.1863	0.2079
CHIP-IV	0.1777	0.1923	0.2039	0.2128	0.2259	0.2476	0.2499	0.2802
JM518	0.1846	0.2005	0.2133	0.2232	0.2386	0.2631	0.2658	0.3018
JM216	0.2352	0.2485	0.2600	0.2698	0.2868	0.3109	0.3137	0.3515
Tetraplatin	0.2410	0.2640	0.2755	0.2855	0.3037	0.3286	0.3314	0.3715
Guanine	0.0637	0.0465	0.0346	0.0279	0.0232	0.0071	0.0056	0.0088

Table 3.7: The values of the negative energy component, $\Delta E_{A(B)}$ (in kcal/mol), for different combinations of cisplatin analogues (considered as A) and protecting agents (considered as B). While in a particular row the number in a box represents the $\Delta E_{A(B)}$ value for the interaction between the corresponding cisplatin analogue and the protecting agent the values in the last row are for interaction between guanine (i.e., the biomolecule here) and the corresponding protecting agent.

Protecting agents Cisplatin analogues	D- penicilla mine	Thiourea	STS	WR- 1065	S- thioazole	Na-diOH	NaDDTC	Mesna
Nedaplatin	0.58	-0.94	-1.93	-2.44	-2.65	-3.84	-3.93	-4.78
Oxaliplatin	-0.99	-2.53	-3.56	-4.12	-4.42	-5.73	-5.84	-6.89
DACH RR(II)	-2.50	-4.04	-5.09	-5.67	-6.06	-7.43	-7.56	-8.56
<i>Cis</i> -[PtCl ₂ (C ₆ H ₁₁ NH ₂) ₂]	-2.55	-4.12	-5.81	-5.78	-6.18	-7.57	-7.70	-8.94
<i>Cis</i> -[PtCl ₂ (iPentNH ₂) ₂]	-3.12	-4.68	-5.75	-6.35	-6.78	-8.19	-8.32	-9.60
Carboplatin	-4.92	-6.44	-7.49	-8.11	-8.63	-10.08	-10.22	-11.63
<i>Cis</i> -[Pt(II)Cl ₂ (iPrNH ₂) ₂]	-5.90	-7.14	-8.46	-9.09	-9.65	-11.13	-11.27	-12.76
Transplatin	-12.64	-14.00	-15.0	-15.70	-16.49	-18.08	-18.24	-20.09
CHIP-IV	-19.26	-20.65	-21.9	-22.70	-23.98	-26.03	-26.24	-29.03
JM518	-19.85	-21.44	-22.7	-23.69	-25.18	-27.55	-27.80	-31.17
JM216	-27.38	-28.80	-30.0	-31.00	-32.76	-35.20	-35.47	-39.18
Tetraplatin	-29.76	-31.20	-32.4	-33.40	-35.34	-37.90	-38.18	-42.19
Guanine	-5.14	-3.71	-3.50	-2.19	-1.82	-0.55	-0.43	-0.67

Table 3.8: The values of the overall stabilization energy, $\Delta E_{SE(AB)}$ (in kcal/mol) for different combinations of cisplatin analogues (considered as A) and the protecting agents (considered as B). While in a particular row the number in a box represents the $\Delta E_{SE(AB)}$ value for the interaction between the corresponding cisplatin analogue and the protecting agent the values in the last row are for interaction between guanine (i.e., the biomolecule here) and the corresponding protecting agent.

Protecting agents Cisplatin analogues	D- penicilla mine	Thiourea	STS	WR- 1065	S- thioazole	Na-diOH	NaDDTC	Mesna
Nedaplatin	-0.09	-2.78	-4.55	-5.16	-6.16	-6.19	-6.86	-7.35
Oxaliplatin	-5.34	-8.11	-9.88	-10.49	-11.49	-11.52	-12.19	-12.69
DACH RR(II)	-8.69	-11.37	-13.15	-13.75	-14.76	-14.78	-14.46	-15.95
<i>Cis</i> -[PtCl ₂ (C ₆ H ₁₁ NH ₂) ₂]	-10.00	-15.69	-14.46	-15.07	-16.07	-16.09	-16.76	-17.26
<i>Cis</i> -[PtCl ₂ (iPentNH ₂) ₂]	-10.80	-13.48	-15.25	-15.86	-16.86	-16.89	-17.57	-18.06
Carboplatin	-12.96	-15.64	-17.41	-18.02	-19.03	-19.05	-19.73	-20.21
<i>Cis</i> -[Pt(II)Cl ₂ (iPrNH ₂) ₂]	-14.13	-17.00	-18.76	-19.37	-20.38	-20.41	-21.08	-21.57
Transplatin	-21.03	-23.77	-25.54	-26.15	-27.15	-27.18	-27.85	-28.34
CHIP-IV	-43.46	-46.14	-47.91	-48.52	-49.52	-49.55	-50.23	-50.71
JM 518	-60.47	-63.15	-64.92	-65.53	-66.53	-66.56	-67.24	-67.73
JM 216	-64.39	-67.07	-68.84	-69.45	-70.45	-70.48	-71.16	-71.64
Tetraplatin	-70.92	-73.61	-75.37	-75.98	-76.99	-77.01	-77.68	-78.18
Guanine	-8.97	-6.28	-4.51	-3.90	-2.90	-2.87	-2.20	-1.70

Chapter IV

Understanding the Interaction of
Nucleobases with Chiral Semi-conducting
Single-Walled Carbon Nanotubes
(SWCNTs): An Alternative Theoretical
Approach Based on Density Functional
Reactivity Theory (DFRT)

4.1 Introduction:

In the previous two chapters, we have addressed the application of molecular modeling techniques to understand a couple of interesting problems related to biological systems. There our motivation is to pinpoint the emerging aspects of CDASE scheme as a cost-effective computational tool to understand different chemical interactions. In this particular chapter, we have tried to extend the application of CDASE scheme through some high level computations on carbon nanosystems. Due to the quantum confinement effect, carbon based nanostructures exhibit some extraordinary electronic properties and it is one of the most extensively explored research area for the last two decades. However, the huge molecular structures of nanosystems are always a challenging task to perform quantum chemical calculations. In the upcoming chapters we have projected, our CDASE scheme based theoretical formalism as a possible solution to encounter this problem for a considerable extent.

One of the most exciting allotropes of carbon discovered recently is the carbon nanotube (CNT).^{1,2} These are cylindrical tube-shaped materials consists of a long series of sp^2 hybridized carbon atoms³ and typically have the diameter ranging from less than 1 to 50 nanometers⁴. Conceptually, CNTs are considered as hollow graphene sheets designed in rolled-up fashion. When only one layer of graphene sheet is present, it is called as single-walled carbon nanotube (SWCNT) and multilayer structures are known as multi-walled carbon nanotube (MWCNT).¹ Extraordinary mechanical, optoelectronic and thermal properties of CNT uncorked its application in biosensors,^{5,6} biocompatible agents,⁷ DNA and protein transporter⁸ and many more. However, chemical inertness of SWCNT constricts its application to a major extent. Thus, to enhance the chemical reactivity of CNT some chemical modifications need to be done on the surface of the SWCNT and this whole procedure is termed ‘functionalization of SWCNT’.⁹⁻¹³ One of the most promising techniques to carry out the SWCNT functionalization is to exploit the non-covalent interaction of SWCNTs with DNA or protein.¹⁰ Recently, studies on DNA/CNT combination has become an emerging area in the field of nanotechnology as it finds some potential applications in the electrochemical detection of DNA,¹⁴ DNA sensor,¹⁵ DNA encapsulation,¹⁶ transformations of DNA conformation,¹⁷ etc. The

DNA/CNT adducts showed promising activity in anti-tumor drug delivery system and enzyme immobilization.¹⁸

To offer a detailed insight into the interaction of semi-conducting SWCNTs with DNA, considerable increase in the experimental as well as the theoretical studies has been observed in the last few years. The isolation of SWCNTs from synthetic aggregates is a major technical concern. Zheng *et al.* reported the formation of stable DNA/CNT complex, which can efficiently disperse CNTs in the aqueous solution.^{19,20} A thorough study on the adsorption of nucleobases adenine and thymine and their radicals on SWCNT surface has been performed by Shtogun *et al.*²¹ The interaction between the π -orbitals of nucleobases and SWCNTs play a crucial role during the physisorption process of nucleobases on SWCNTs. Wang has reported²² that the cross-stacking gas phase binding energy of nucleobases with both (10,0) and (5,5) SWCNTs follow the order $G > A > C > T$. However, in aqueous phase the order of binding energies changes to $A > G > T > C$ for the isomer (10,0).²² In a combined theoretical and experimental study Das *et al.*²³ have observed that the binding energy variation in the gas phase for four nucleobases A, T, G and C with the isomer (5,5) follows the order $G > A > T > C$. In an experimental study Sowerby *et al.*²⁴ reported the adsorption isotherm for purine and pyrimidine bases in a solid-liquid interface. The observed trend in the variation of adsorption behavior of nucleobases on crystalline graphite surface was following the order $G > A > Hypoxanthine > T > C > U$.

In the last three decades a substantial growth of computational chemistry has been observed with the development of various local and global reactivity descriptors²⁵⁻⁴⁰ in the context of Density Functional Reactivity Theory (DFRT).⁴¹⁻⁴⁷ In recent years, newly proposed reactivity descriptors are widely used to explain the mechanisms of different types of chemical reactions.⁴⁸⁻⁶⁰ Local reactivity indices include Fukui function $[f(r)]$,^{26,31} local softness $(s_k^+, s_k^-$ and $s_k^0)$,³⁰ local hardness $[\eta(r)]$,^{32,38-40} relative electrophilicity (s_k^+/s_k^-) and relative nucleophilicity (s_k^-/s_k^+) ,³³⁻³⁴ local electrophilicity⁵⁸⁻⁶⁰ etc. Global reactivity descriptors such as chemical potential⁶¹ (*i.e.*, the negative of electronegativity⁶²), chemical hardness²⁵(η), global electrophilicity index,^{63,64} nucleophilicity,⁶⁵⁻⁶⁷ electrofugality and nucleofugality,^{68,69} etc. are mainly used for intermolecular reactivity study.

Recently, Roy and collaborators proposed a new energy decomposition scheme,⁷⁰ termed CDASE (Comprehensive Decomposition Analysis of Stabilization Energy). This scheme has been effectively used to explore different types of chemically as well as biologically important reactive interactions.⁷⁰⁻⁷³ They have also argued that the global electrophilicity descriptor (w),⁶⁴ proposed by Parr *et al.*, can be conceptually correlated to the expression of stabilization energy²⁵ when the donor is a perfect one. Considering certain approximations (i.e., the chemical potential and the chemical hardness of the perfect donor to be zero) Roy and collaborators proposed a new reactivity descriptor, ‘internal assistance’⁷⁰ as it depends solely on the structural and electronic properties of the two isolated chemical species. More appropriately, it can be called the ‘kinetic assistance’ as it can play a key role in determining the rate of a chemical reaction.

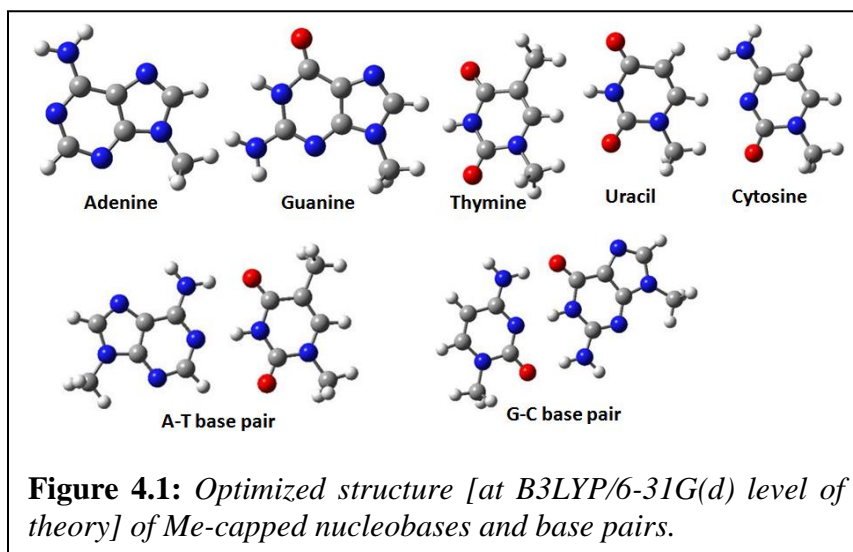
The study as described in the present article will be centered on the theoretical investigation of the kinetic and thermodynamic factors associated with the interaction between the nucleobases and the semi-conducting SWCNTs. The strategy as described here can be considered as an alternative methodology to perform comprehensive investigations on relatively large systems without explicitly going through computationally intensive transition state or thermochemistry calculations. Still it is possible to obtain relevant kinetic and thermodynamic information in the process of complex formation between the two interacting systems. Traditional binding energy calculation on some selected systems are also carried out (using ONIOM QM:MM approach) to justify the qualitative trend obtained from the five CDASE scheme based parameters.

The chapter is organized in the following way: Adopted computational methodology is described in Section 4.2. Section 4.3 contains the results and discussion. Here, the values of different kinetic and thermodynamic reactivity parameters generated from CDASE scheme are analyzed in sub-section 4.3 (a). The analysis carried out in a systematic way, critically acclaiming their roles in explaining the interaction of nucleobases with semiconducting chiral SWCNTs. The calculation of binding energy for four different SWCNTs with five nucleobases is discussed in sub-section 4.3 (b). Finally, in Section 4.4 we have summarized our entire study on the interaction of nucleobases with SWCNTs.

4.2 Adopted Models and Computational Methodology:

To carry out the investigation eight different types of semi-conducting chiral SWCNTs are chosen as prototype electron acceptors, whereas five nucleobases, A, T, G, C and U along with two Watson-Crick (W-C) base pairs, A-T and G-C, are chosen as electron donors. Selected SWCNTs, consisting of lattice vector (10,2), (8,3), (9,2), (6,5), (9,5), (7,6), (7,5) and (9,7), belong to the chiral SWCNT conformation. For convenience, nucleobases are modeled after capping N_1 (pyrimidines) and N_9 (purines) nitrogen atoms with a methyl group. Although the absence of phosphate and sugar moieties, which connect the nucleobases, changes the environment of the systems significantly, it is a well-accepted modeling technique⁷⁴⁻⁷⁸ and provides valuable information for qualitative understanding of interactions related to DNA. The methyl-capped DNA bases and base pairs are shown in Figure 4.1.

The numerical values are generated by using hybrid B3LYP functional (Becke 3-Parameter exchange functional⁷⁹⁻⁸² along with correlation functional as proposed by Lee, Yang, and Parr⁸³) as implemented in Gaussian 09, Revision C.01 software package.⁸⁴



Particularly, the kinetic aspects are studied using the difference of global electrophilicity descriptor between the acceptor and the donor (i.e., $\Delta w = w_A - w_B$) and the energy raising component, $\Delta E_{B(A)}$. The thermodynamic aspects are investigated using $\Delta E_{A(B)}$ and $\Delta E_{SE(AB)}$. The charge transfer values ΔN can be used to study both kinetic and thermodynamic aspects because it is formally linked to $\Delta E_{B(A)}$, $\Delta E_{A(B)}$, and $\Delta E_{SE(AB)}$.

That is ΔN can be considered both as a kinetic and thermodynamic descriptor of reactivity.

The geometries of eight SWCNTs, nucleobases as well as base pairs have been optimized (without imposing any constraint) at B3LYP/6-31G(d)⁸⁵⁻⁸⁸ level of theory. Subsequent single-point calculations are carried out at the same level of theory. Vertical ionization potential (IP) and electron affinity (EA) values are considered in the present study (i.e., calculations of cationic and anionic systems are performed using the geometries of the neutral systems only). While the restricted level of theory (RB3LYP/6-31G(d)) is used for the neutral systems, the unrestricted level of the same theory (UB3LYP/6-31G(d)) is chosen for calculations of the corresponding ionic systems. The details of binding energy calculations on some of the chosen SWCNT's with DNA bases are given in Section 4.3 (b).

4.3 Results and Discussion:

Normally, genetic DNA consists of four bases, Adenine (A), Guanine (G), Cytosine (C) and Thymine (T). However, another component Uracil (U), which is a constituent of RNA, is also considered as a mutagenic base in DNA sequence. Both A and G are purine bases, containing one six membered pyrimidine ring fused with a five membered imidazole ring. Adenine has the functional group $-\text{NH}_2$ and guanine contains both $-\text{NH}_2$ and $-\text{C}=\text{O}$ as functional groups. On the other hand, T and C are known as pyrimidine bases consisting of a single six membered pyrimidine ring. These four bases are arranged in stable complementary base pair sequence as A-T and G-C by strong H-bonding interaction between them in double-helical DNA structure. In a number of reported literatures⁷⁴⁻⁷⁸ DNA bases are taken as the prototype of DNA sequence to understand the interaction of DNA with different surfaces (semi conducting or metallic).

Semi-conducting SWCNTs are constituted as networks formed by a series of sp^2 -hybridized carbon atoms. The delocalized π -orbitals of this network structure of carbon atoms are perpendicular to the plane of carbon atoms. At this insistence, the paradigm of interaction between SWCNTs and nucleobases can be considered as the interplay between the carbon π systems of SWCNTs and nitrogenous π systems of DNA bases.

(a). Critical evaluation of the five CDASE scheme based parameters in explaining interaction between nucleobases and SWCNTs:

The said interaction can be investigated under two aspects. The first one is the kinetic aspect i.e., comparison of the rate of interaction between different pairs of SWCNTs and DNA bases. The second one is the thermodynamic aspect i.e., comparison of the stability of the complexes formed due to this interaction. In the next few subsections the generated values of different kinetic and thermodynamic parameters will be analyzed to have a general idea of the trend of interaction between different pairs of SWCNTs and DNA bases (as well as base pairs).

(i) Understanding the rate of interaction between SWCNTs and nucleobases on the basis of difference in their global electrophilicity values (i.e., Δw):

The values of Δw , calculated for different combinations of SWCNTs (i.e., the acceptors, A) and nucleobases (i.e., the donors, B) are reported in Table 4.1. A positive value of Δw indicates that the choice of the donor and the acceptor is justified. Also, higher is the value of Δw , kinetically more favorable the interaction is.

It is obvious from Table 4.1 that the choice of donors and acceptors are physically justified (functionalized SWCNT usually behaves as an electron acceptor, and this fact is widely exploited in the photoinduced electron transfer systems in combination with nitrogen donor such as phthalocyanines)⁸⁹ and that the interactions of purine bases (guanine and adenine) with semi-conducting SWCNTs are kinetically more favorable than the pyrimidine bases cytosine and thymine. However, earlier study also suggest relatively easier immobilization of purine bases rather a pyrimidine one, on the surface of SWCNT.²¹ Moreover, according to Δw values the interaction between G-C base pair and SWCNTs is faster when compared to that between A-T base pair and SWCNTs. The observations made on the basis of the Δw values correlate well with the recently reported extensive MD simulation study, combined with thermodynamic analysis, by Xiao *et al.*⁹⁰ The lowest reactivity is observed for Uracil with all SWCNTs.¹⁶

(ii) Understanding the rate of interaction between SWCNTs and nucleobases on the basis of the positive energy component (i.e., $\Delta E_{B(A)}$):

As $\Delta E_{B(A)}$ is an energy raising term (*i.e.*, positive quantity) and generated from the electronic parameters (e.g., IP and EA, indirectly) of the interacting species it assists to overcome the activation barrier (hence it is called the ‘internal assistance’ or more appropriately be called the ‘kinetic assistance’). So, higher the positive value of $\Delta E_{B(A)}$ higher will be the rate of interaction between a particular pair of interacting SWCNT and nucleobase. Table 4.2 contains the $\Delta E_{B(A)}$ values calculated on the basis of CDASE scheme for various combinations of SWCNTs and nucleobases.

The generated $\Delta E_{B(A)}$ values clearly show that the fastest interaction is between DNA bases with chiral SWCNT (8,3). The rate of interaction of nucleobases with semi-conducting SWCNTs, as per data in Table II, follow the sequence, $G \rangle A \rangle T \rangle C \rangle U$. It is encouraging to note that the above trend closely resembles with those reported recently by some experimental as well as theoretical studies²¹⁻²⁴ For example, Shtogun *et al.*²¹ reported a DFT based study on the adsorption behavior of purine and pyrimidine bases (considering adenine and thymine as the model systems) along with their radicals on the surface of SWCNT. Observations in that study attribute higher value of adsorption energy for purine/SWCNT combination (*i.e.*, Adenine/SWCNT) compared to that between pyrimidine and SWCNT (*i.e.*, Thymine/SWCNT). They also concluded that the DNA-CNT interaction is mainly controlled by the nucleobases and the rest part of the composite DNA system play secondary role.²¹ It is gratifying to note that the results generated from CDASE scheme based calculations also provide the similar variation in the rate of interaction, showing higher value of $\Delta E_{B(A)}$ for purine/SWCNT combination and a lower value for that between pyrimidine and SWCNT.

Some interesting observations are made on the rate of interaction of mutagenic base uracil with SWCNTs. In case of interaction of SWCNTs (6,5) and (9,7) with uracil the $\Delta E_{B(A)}$ values are found to be negative. The physical interpretation of these observations is that the interaction between uracil and these two SWCNTs might not be kinetically feasible or probably occurs due to the reversal of charge transfer that was initially assumed to be (*i.e.*, from Uracil to SWCNTs). However, positive Δw values for the interaction of Uracil with these two SWCNTs (Table 4.1) strengthen the argument that the direction of charge transfer is from Uracil to SWCNTs only and negative values

of $\Delta E_{B(A)}$ might have been generated due to some theoretical artifact. This last argument seems to be more justified as these two values becomes positive (hence as expected) when a higher level of basis sets [6-31G (d,p)] is used. For SWCNT (9,7) the value of $\Delta E_{B(A)}$ is 0.42 kcal/mol, whereas for the one having lattice vector (6,5) the value is 0.44 kcal/mol.

(iii) *Understanding the interaction between SWCNTs and nucleobases on the basis of the charge transfer value (i.e., ΔN):*

It is already established from the discussion on theoretical background of CDASE scheme that in case of a favorable interaction (both kinetically and thermodynamically) ΔN value should be positive and this is possible when $\mu_B^0 > \mu_A^0$ or $(\chi_A^0 > \chi_B^0)$. Thus, it can be argued that a higher value of ΔN for a particular pair of SWCNT and nucleobase implies a greater extent of interaction between the pair. The charge transfer (ΔN) values for different combination of SWCNTs and nucleobases, calculated on the basis of CDASE scheme, are presented in Table 4.3.

The generated ΔN values clearly show that the nucleobase guanine exhibits significantly higher value of charge transfer against all SWCNTs chosen in the present study. This important observation justifies that among the nucleobases guanine interacts fastest with SWCNTs as well as forms the most stable complex followed by adenine, thymine, cytosine and uracil, respectively (i.e., $G > A > T > C > U$). Also, SWCNT (8,3) exhibits highest ΔN values against all the nucleobases. Hence, it can be argued that SWCNT (8,3) interacts fastest as well as forms the most stable complex with all the nucleobases compared to other chiral SWCNTs chosen here. Another important observation from the generated ΔN values is that the base pair G-C forms more stable complexes with all SWCNTs than the A-T pair. It is worth mentioning here that similar trends of interaction was also observed by Xiao *et al.*⁹⁰ Unexpected negative values of ΔN for SWCNT (9,7) and SWCNT (6,5) with uracil are corrected by performing the calculations at a higher order basis sets (i.e., 6-31 G(d,p) level) and the corresponding values are 0.0048 and 0.0050, respectively.

(iv) *Stabilities of the complexes formed between SWCNTs and nucleobases on the basis of the negative energy component ($\Delta E_{A(B)}$):*

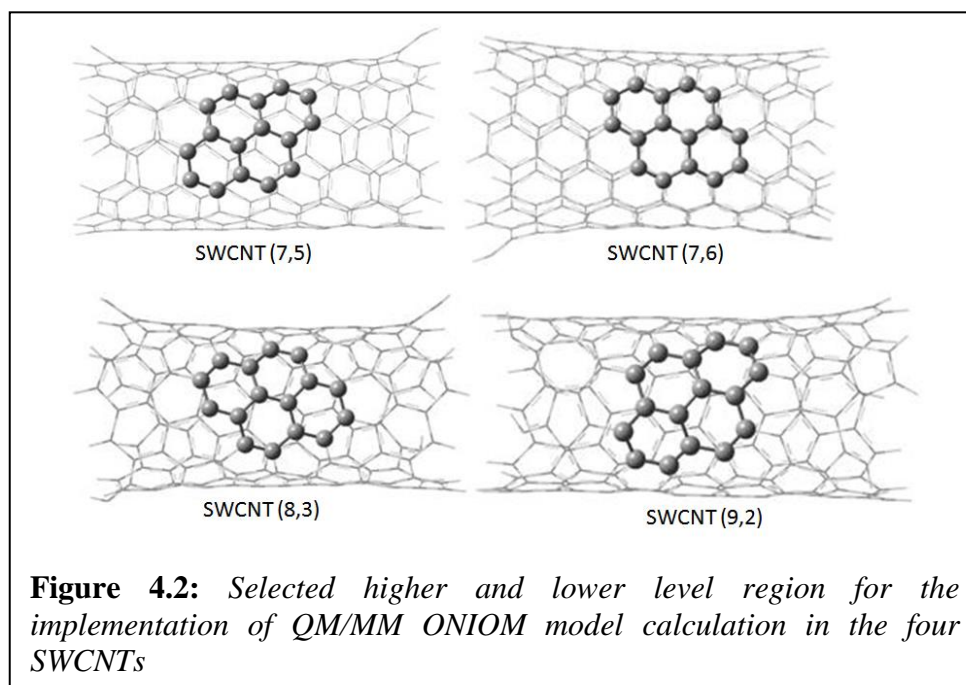
From the CDASE scheme based interpretation, $\Delta E_{A(B)}$ is an energy lowering term i.e., the values are negative. This is because $\Delta E_{B(A)}$ is a positive quantity. Whereas, the overall process of interaction should be an energy lowering one (i.e., the net energy change, $\Delta E_{SE(AB)}$, should be a negative quantity). A large negative value of $\Delta E_{A(B)}$ indicates higher thermodynamic stability of the resultant complex. The calculated $\Delta E_{A(B)}$ values for different combinations of SWCNTs and nucleobases are reported in Table 4.4. As per the data in Table 4, the complexes formed by the G-C base pair with SWCNTs are more stable than those formed between the A-T base pair and SWCNTs. Also, the stabilities of the complexes formed by the individual DNA bases with SWCNTs follow the order, $G > A > T > C > U$. It is worth mentioning here that Sowerby *et al.*²⁴ had the similar observation in one of their experimental studies. Based on the adsorption of nucleobases on the crystalline graphite-water interface they observed highest surface adsorption for nucleobase guanine, followed by adenine, thymine, cytosine and the mutagenic base uracil showing the lowest one. Phenomenologically, a particular adsorption on the solid-liquid interface can be viewed as a thermodynamically controlled one. Thus, it can be argued that the CDASE scheme based energy component $\Delta E_{A(B)}$ can be used as a thermodynamic parameter to predict the stability of complexes formed during chemical interaction. The unexpected positive $\Delta E_{A(B)}$ values generated by the interaction of SWCNTs (9,7) and (6,5) with the mutagenic base uracil come out to be negative when calculations are performed at 6-31G (d,p) level of basis sets and the values are -0.4241 kcal/mol and -0.442 kcal/mol, respectively.

(v) *The stabilities of the complexes formed between SWCNTs and nucleobases on the basis of stabilization energy [i.e., $\Delta E_{SE(AB)}$]:*

The overall stabilization energy values (i.e., $\Delta E_{SE(AB)}$) are generated through CDASE scheme based computation and demonstrated in Table 4.5. For a favourable interaction (i.e., a spontaneous charge transfer process) $\Delta E_{SE(AB)}$ will be a negative quantity and in this way a stable complex will be formed. If the $\Delta E_{SE(AB)}$ value is high (i.e., more negative) for a particular interacting pair (of SWCNT and nucleobase) the stability of the corresponding complex formed will be more. From the observation of

$\Delta E_{SE(AB)}$ values in Table V it is obvious that the order of stabilities of the corresponding complexes follow the trend as $G > A > T > C > U$ i.e., the most and the least stable adducts are formed with nucleobases guanine and uracil, respectively. Very recently, Das *et al.*²³ performed an extensive theoretical and experimental investigation on the binding interaction of nucleobases with SWCNT (5,5). They have observed that the variation in binding energy in gas phase for the four nucleobases with the SWCNT follows the order $G > A > T > C$.²³ The values of the stabilization energy for the interaction between nucleobases and semi-conducting chiral SWCNTs calculated using the CDASE scheme (Table 4.5) also generate the same trend as observed by Das *et al.* and Sowerby *et al.*²⁴

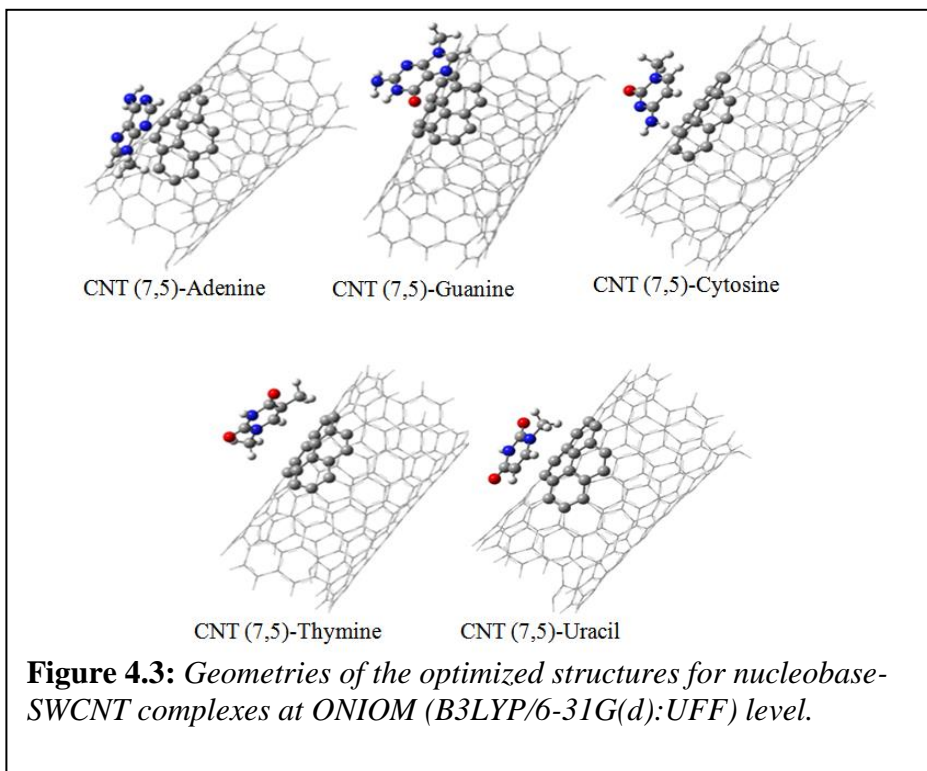
It is also observed that the SWCNT (8,3) produces highest values of $\Delta E_{SE(AB)}$ for all the nucleobases as well as for A-T and G-C base pairs. This indicates SWCNT (8,3) is capable of forming thermodynamically more stable complexes with nucleobases compared to other



SWCNTs chosen in the present study. Similar is the observation with ΔN and $\Delta E_{A(B)}$ values also and as far as the rate of interaction is concerned the $\Delta E_{B(A)}$ values also predict the same trend.

(b). A brief discussion on the ONIOM (QM:MM) calculation for the interaction between SWCNT and nucleobases:

It is evident from the earlier studies that ONIOM QM:MM^{91,92} type of calculation is the best possible approach to explore the noncovalent interaction in large systems like nucleobases and SWCNT.⁹³⁻⁹⁵ We have performed an explicit QM/MM ONIOM model calculation (implemented in Gaussian09)⁸⁴ on the interaction between four different types SWCNTs with five nucleobases. To account the order of preferential binding interaction of the five nucleobases with SWCNTs, we have considered SWCNT (7,5), SWCNT (7,6), SWCNT (8,3) and SWCNT (9,2) as our model systems.

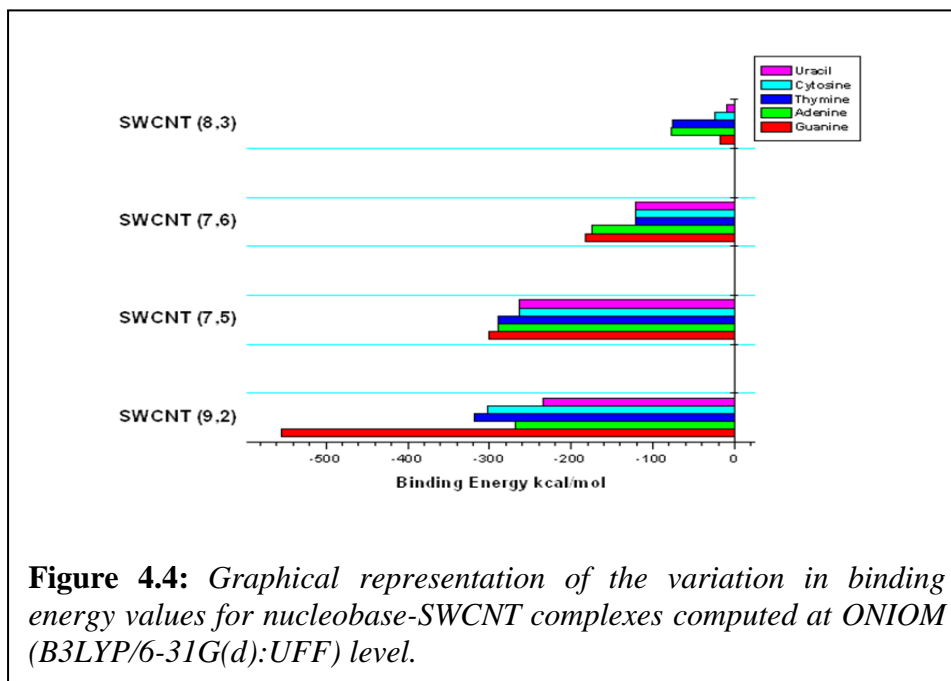


In a conventional ONIOM model calculation it is possible to implement two or three different levels of theory in two or three different regions of the particular system for the calculation. The flexibility of assembling a high-level *Ab-initio* calculation for a particular domain (area of highest importance) of the system with a relatively lower level of computation to the rest part provides more emancipation to perform theoretical study on large systems with greater efficiency at a lower computational cost. In the present calculation, we have defined two ONIOM regions for the combined SWCNT-nucleobases system. The high and low layers of the SWCNTs, according to the standard practice of ONIOM model computation, are represented in Fig. 4.2. The high-level zone of the calculation includes the nucleobase and extends up to four hexagonal rings of

SWCNT, whereas the rest part of the SWCNT is considered in the low-level zone. Density functional theory based B3LYP method is being used with 6-31G(d) basis set for the high-level zone along with universal force field (UFF) molecular mechanics has been adopted for the low-level zone of the system. It is worth mentioning here that an earlier study suggests an improvement of the result obtained from ONIOM B3LYP:UFF method in comparison to that of ONIOM B3LYP:AM1 alternative.⁹⁴

The optimized structures of the SWCNTs with different nucleobases represent a parallel orientation of the nucleobase over the SWCNT surface in a slight wrap-around fashion (Fig. 4.3). Table 4.6 represent the binding energy (ΔE) values calculated for the interaction between nucleobases with four SWCNTs. The graphical representation of the variation in binding energy between the four SWCNTs with nucleobase is also included in Fig.4.4. The observed variation of binding energy of the five nucleobases with SWCNT (9,2) follows the trend $G \rangle T \rangle C \rangle A \rangle U$. This order of binding energy variation is very close to that of the earlier reported theoretical observations of Stepanian *et al.*⁹⁶ and Shukla *et al.*⁹⁷ According to the study of Stepanian *et al.* the relative interaction of nucleobase cytosine and thymine with SWCNT (10,0) appeared to be almost equal.⁹⁶ The equivalent interaction strength of the two nucleobases cytosine and thymine with SWCNT (7,0) is also evident from another comprehensive study by Shukla *et al.*⁹⁷ The binding energy data computed for both SWCNT (7,5) and SWCNT (7,6) with five different nucleobases produce a good agreement to the trend obtained from CDASE scheme based calculations. In these two types of SWCNTs, we have got the highest negative value of binding energy for the interaction with nucleobase guanine succeeded by adenine, thymine cytosine, and uracil (i.e., $G \rangle A \rangle T \rangle C \rangle U$). However, the trend of interaction obtained for SWCNT (8,3) with five nucleobases is marginally away from the anticipation. Here, we have found that nucleobase adenine has the highest affinity for SWCNT (8,3) and followed by thymine, cytosine, guanine and uracil. A more extensive study on the anomalies of SWCNT (8,3) might lead to some interesting theoretical findings, and that can be exploited to understand the exceptional behavior of the other armchair SWCNTs in this category. Perhaps, the interaction of SWCNT (8,3) with different nucleobases could be inexplicitly justified from the reported study of Varghese *et al.*⁹⁸ Without considering the existence of guanine, computed data for adenine, thymine

and cytosine in our present ONIOM QM:MM calculation reproduce the same trend obtained by Varghese *et al.*⁹⁶ in case of carbon nano system. It is worthy of mentioning here that the trend of interaction of SWCNT (9,2) and SWCNT (8,3) with nucleobases, when evaluated by CDASE scheme, reproduce the experimental trends correctly. This only emphasizes that a perfect combination of higher level of theory along with intelligent modeling technique for ONIOM QM:MM approach will reproduce the experimental trends.



4.4 Conclusions:

The results obtained from the CDASE scheme based calculations provide some useful insights to understand the binding interaction of nucleobases with semi-conducting chiral SWCNTs. The interaction is explained on the basis of five reactivity descriptors (*i.e.*, ΔW , ΔN , $\Delta E_{B(A)}$, $\Delta E_{A(B)}$, and $\Delta E_{SE(AB)}$) derived from CDASE scheme. It is worth mentioning here that the data generated from both the kinetic (*i.e.*, Δw and $\Delta E_{B(A)}$) and thermodynamic (*i.e.*, $\Delta E_{A(B)}$ and $\Delta E_{SE(AB)}$) descriptors as well as charge transfer values (*i.e.*, ΔN , which plays the role of both kinetic and thermodynamic descriptor) produce the similar trend of the rate of interaction and complex stability when nucleobases interact with chiral SWCNTs. As far as nucleobases are concerned the trend is as, $G > A > T > C > U$, which is observed experimentally. However, the rate of complex

formation of different SWCNTs with a particular nucleobase differs when different kinetic parameters (i.e., Δw and $\Delta E_{B(A)}$) are used. As observed from the generated data in Table 4.1 (i.e., Δw values) the rate of adduct formation of SWCNTs with a particular nucleobase vary as, (7,5) > (10,2) > (8,3) > (7,6) > (9,2) > (9,5) > (9,7) > (6,5). However, the trend changes to (8,3) > (9,2) > (9,5) > (10,2) > (7,5) > (7,6) > (6,5) > (9,7) when the corresponding $\Delta E_{B(A)}$ values are compared. In absence of any earlier reported results (either experimental or theoretical), it is difficult to conclude which one is more appropriate trend.

The functionalization of carbon nanotube (CNT) with active biomolecules is an emerging area of research both from experimental and theoretical point of view. A theoretical study on large systems like carbon nanotubes is a challenging task. Minimization of computational cost without compromising the reliability of the obtained results is a highly demanding aspect of theoretical research in recent times. In the present study we have focused on the effective application of the CDASE scheme as a computationally cost-effective (as it avoids computationally intensive transition state optimizations or thermochemistry calculations), simple and alternative approach to study the interaction between nucleobases and chiral SWCNTs. Worthiness of the study is evident from the fact that the observed trend of interaction, both kinetic and thermodynamic (obtained from the systematic analysis of the CDASE scheme based reactivity parameters), between the chosen semi-conducting chiral SWCNTs and nucleobases, matches satisfactorily with earlier reported experimental as well as theoretical results.

The study also highlights the fact that the CDASE scheme based charge transfer value is an essential parameter to judge the direction of spontaneous electron flow. This is because for a particular interaction numerical value of ΔN helps to determine the donor and the acceptor systems involved in the process of interaction.

The binding energy values (calculated by ONIOM QM:MM approach) for four SWCNTs with five nucleobases generate mixed trends. We have found that for SWCNT (7,5) and SWCNT (7,6) the trends are similar to those observed experimentally as well as by CDASE scheme. But the resultant trends of interaction for SWCNT (9,2) and SWCNT

(8,3) with five nucleobases generated on the basis of ONIOM QM:MM approach is not consistent with the experimental observations. This inconsistency of theoretical result from experimental finding substantiates that care should be taken in defining the high and low level zones as well as the optimized combination of theories (QM/MM or QM/semi-empirical) while adopting ONIOM approach if generated values are to be reliable. Also in such a situation, the most reliable benchmark should be the experimental trends.

Finally, the following points can summarize the overall theoretical findings from the present study:

- (1) The calculated values of reactivity parameters establish the fact that SWCNTs interact more effectively with purine bases (*i.e.*, guanine and adenine) than with pyrimidines (*i.e.*, cytosine, thymine) of DNA. The mutagenic base uracil shows the least interaction.
- (2) Interaction of SWCNTs with Watson-Crick complementary base pair G-C is both kinetically and thermodynamically more favorable than that with A-T pair.
- (3) Some unusual interaction behavior is exhibited by the mutagenic base uracil with few of the semi-conducting SWCNTs [e.g., (6,5) and (9,7)]. The generated values of the descriptors ($\Delta E_{B(A)}$, ΔN , and $\Delta E_{A(B)}$) claim that during interaction with these two SWCNTs uracil behaves as an electron acceptor whereas those two SWCNTs as electron donors. However, with the ΔW values this unusual trend is not observed and unusual observation by CDASE scheme based parameters is attributed to the theoretical artifact incurred during generation of these values. This argument seems to be justified because use of higher level of basis sets [6-31 G(d,p)] corrects the trend.
- (4) The calculated values of all the five parameters justify the experimentally verified trend of interaction of nucleobases with semi-conducting SWCNTs (*i.e.*, $G > A > T > C > U$).

References:

-
1. S. Iijima, *Nature* 1991, **354**, 56.
 2. M. S. Dresselhaus, G. Dresselhaus, P. Avouris, *Carbon Nanotubes: Synthesis, Structure, Properties and Applications*, Springer, Berlin, Germany 2001.
 3. P. M. Ajayan, *Chem. Rev.* 1999, **99**, 1787.
 4. M. Panhuis, A. Maiti, I. N. Coleman, A. B. Dalton, B. McCarthy, W. I. Blau, in: H. Kuzmany, (Ed.), *Electronic Properties of Molecular Nanostructures*, 591, American Institute of Physics, Woodbury–Melville–New York, 2001.
 5. R. Satio, G. Dresselhaus, M. Dresselhaus, *Physical Properties of Carbon Nanotubes*; Imperial College Press: London, UK, 2003.
 6. Y. Lin, S. Taylor, H. P. Li, K. A. S. Fernando, L. W. Qu, W. Wang, L. R. Gu, B. Zhou, Y. P. Sun, *J. Mater. Chem.* 2004, **14**, 527.
 7. N. W. S. Kam, M. O'Connell, J. A. Wisdom, H. Dai, *Proc. Natl. Acad. Sci. U.S.A.* 2005, **102**, 11600.
 8. A. Bianco, K. Kostarelos, C. D. Partidos, M. Prato, *Chem. Commun.* 2005, **5** 571.
 9. P. Singh, S. Campidelli, S. Giordani, D. Bonifazi, A. Bianco, M. Prato, *Chem. Soc. Rev.*, 2009, **38**, 2214.
 10. R. J. Chen, Y. G. Zhang, D. W. Wang, H. J. Dai, *J. Am. Chem. Soc.* 2001, **123**, 3838.
 11. T. C. Dinadayalane, J. Leszczynski, *Handbook of Computational Chemistry*; J. Leszczynski, Ed.; Springer Netherlands: 2012, pp 793.
 12. S. Saha, T. C. Dinadayalane, J. S. Murray, D. Leszczynska, J. Leszczynski, *J. Phys. Chem. C* 2012, **116**, 22399.
 13. T. C. Dinadayalane, J. Leszczynski, *Toward Nanomaterials: Structural, Energetic and Reactivity Aspects of Single-Walled Carbon Nanotubes*. In *Nanomaterials: Design and Simulation* ; Balbuena, P. B.; Seminario, J. M., Eds.; Elsevier: Amsterdam, 2006; pp 167.
 14. J. Li, H. Tee Ng, A. Cassell, W. Fan, H. Chen, Q. Ye, J. Koehne, J.; Han, M. Meyyappan. *Nano Lett.* 2003, **3**, 597.
 15. A. Bianco, M. Prato, *Adv. Mater.* 2003, **15**, 1765.
 16. E. Y. Lau, F. C. Lightstone, M. E. Colvin, *Chem. Phys. Lett.* 2005, **412**, 82.
 17. C. R. Martin, P. Kohli, *Nat. Rev. Drug Discov.* 2003, **2**, 29.
 18. Y. Lin, L. F. Allard, Y. P. Sun, *J. Phys. Chem. B* 2004, **108**, 3760.
 19. Zheng *et al.* *Nature Mater.* 2003, **2**, 338.
 20. Zheng *et al.* *Science* 2003, **302**, 1545.
 21. Y. V. Shtogun, L. M. Woods, G. I. Dovbeshko *J. Phys. Chem. C* 2007, **111**, 18174.
 22. Y. Wang, *J. Phys. Chem. C* 2008, **112**, 14297.
 23. A. Das, A. K. Sood, P. K. Maiti, M. Das, R. Varadarajan, C. N. R. Rao, *Chem. Phys. Lett.* 2008, **453**, 266.
 24. Sowerby, S. J.; Cohn, C. A.; Heckl, M. W.; Holm, N. G. *Proc. Natl. Acad. Sci. USA* **2001**, **98**, 820-822.
 25. R. G. Parr, R. G. Pearson, *J. Am. Chem. Soc.* 1983, **105**, 7512.
 26. R. G. Parr, W. Yang, *J. Am. Chem. Soc.* 1984, **106**, 4049.
 27. S. K. Ghosh, M. Berkowitz, *J. Chem. Phys.* 1985, **83**, 2976.
 28. W. Langenaeker, F. De Proft, P. Geerlings, *J. Phys. Chem.* 1995, **99**, 6424.
 29. P. K. Chattaraj, B. Maiti, U. Sarkar, *Chem. Rev.* 2006, **106**, 2065.

-
30. W. Yang, R. G. Parr, *Proc. Natl. Acad. Sci. U. S. A.* 1985, **82**, 6723.
 31. W. Yang, W. J. Mortier, *J. Am. Chem. Soc.* 1986, **108**, 5708.
 32. R. G. Parr, J. L. Gazquez, *J. Phys. Chem.*, 1993, **97**, 3939.
 33. R. K. Roy, S. Krishnamurti, P. Geerlings, S. Pal, *J. Phys. Chem. A* 1998, **102**, 3746.
 34. R. K. Roy, F. De Proft, P. Geerlings, *J. Phys. Chem. A* 1998, **102**, 7035.
 35. N. Russo, M. Toscano, A. Grand, T. Mineva, *J. Phys. Chem. A*, 2000, **104**, 4017.
 36. S. Krishnamurty, S. Pal, *J. Phys. Chem. A*, 2000, **104**, 7639.
 37. T. Mineva, V. Parvanov, I. Petrov, N. Neshev, N. Russo, *J. Phys. Chem. A*, 2001, **105**, 1959.
 38. S. Saha, R. K. Roy, *J. Phys. Chem. B* 2007, **111**, 9664.
 39. S. Saha, R. K. Roy, *J. Phys. Chem. B* 2008, **112**, 1884.
 40. S. Saha, R. K. Roy, *Phys. Chem. Chem. Phys.* 2008, **10**, 5591.
 41. R. G. Parr, W. Yang, *Density—Functional Theory of Atoms and Molecules*; Oxford University Press: New York, 1989.
 42. R. G. Parr, W. Yang, *Annu. Rev. Phys. Chem.* 1995, **46**, 701.
 43. W. Kohn, A. D. Becke, R. G. Parr, *J. Phys. Chem.* 1996, **100**, 12974.
 44. W. Koch, M. Holthausen, *A Chemist's Guide to Density Functional Theory*, Wiley-Vch Weinheim, 2000.
 45. P. Geerlings, F. De Proft, W. Langenaeker, *Chem. Rev.* 2003, **103**, 1793.
 46. P. A. Johnson, L. J. Bartolotti, P. W. Ayers, T. Fievez, P. Geerlings, Charge Density and Chemical Reactions: A Unified View from Conceptual DFT. *Modern Charge-Density Analysis*. Ed C. Gatti, P. Macchi, Springer 2012, pp 715.
 47. R. K. Roy, S. Saha, *Annu. Rep. Prog. Chem., Sect. C* 2010, **106**, 118.
 48. S. Pal, K. R. S. Chandrakumar, *J. Am. Chem. Soc.* 2000, **122**, 4145.
 49. K. R. S. Chandrakumar, S. Pal, *J. Phys. Chem. A* 2002, **106**, 5737.
 50. A. Tanwar, B. Bagchi, S. Pal, *J. Chem. Phys.* 2006, **125**, 214304.
 51. R. Kar, K. R. S. Chandrakumar, S. Pal, *J. Phys. Chem. A* 2007, **111**, 375.
 52. R. Kar, S. Pal, *Chemical Reactivity Theory: A Density Functional View*, ed. P. K. Chattaraj, CRC Press, 2009.
 53. R. K. Roy, *J. Phys. Chem. A* 2004, **108**, 4934.
 54. R. K. Roy, V. Usha, J. Paulovic, K. Hirao, *J. Phys. Chem. A* 2005, **109**, 4601.
 55. R. K. Roy, V. Usha, B. K. Patel, K. Hirao, *J. Comput. Chem.* 2006, **27**, 773.
 56. R. K. Roy, P. Bagaria, S. Naik, V. Kavala, B. K. Patel, *J. Phys. Chem. A* 2006, **110**, 2181.
 57. P. Bagaria, R. K. Roy, *J. Phys. Chem. A* 2008, **112**, 97.
 58. P. Perez, A. Toro-Labbe, A. Aizman, R. Contreras, *J. Org. Chem.*, 2002, **67**, 4747.
 59. A. M. Lamsabhi, C. A. Escobar, P. Perez, *J. Phys. Org. Chem.* 2005, **18**, 1161.
 60. L. R. Domingo, P. Perez, R. Contreras, *J. Org. Chem.* 2003, **68**, 6060.
 61. R. G. Parr, R. A. Donnelly, M. Levy, W. E. Palke, *J. Chem. Phys.* 1978, **68**, 3801.
 62. R. S. Mulliken, *J. Chem. Phys.*, 1934, **2**, 782.
 63. A. T. Maynard, M. Huang, W. G. Rice, D. G. Covell, *Proc. Natl. Acad. Sci. U. S. A.* 1998, **95**, 11578.
 64. R. G. Parr, von. L. Szentpaly, S. Liu, *J. Am. Chem. Soc.* 1999, **121**, 1922.
 65. P. W. Ayers, R. G. Parr, *J. Am. Chem. Soc.* 2001, **123**, 2007.

-
- 66 P. Jaramillo, P. Perez, R. Contreras, *J. Phys. Chem. A* 2006, **110**, 8181.
 67. P. Jaramillo, P. Fuentealba, P. Perez, *Chem. Phys. Lett.* 2006, **427**, 421.
 68. P. W. Ayers, J. S. M. Anderson, J. I. Rodriguez, Z. Jawed, *Phys. Chem. Chem. Phys.* 2005, **7**, 1918.
 69. P. Pérez, R. Contreras, R. Aizman, *THEOCHEM* 1999, **493**, 267.
 70. P. Bagaria, S. Saha, S. Murru, V. Kavala, B. Patel, R. K. Roy, *Phys. Chem. Chem. Phys.* 2009, **11**, 8306.
 71. S. Saha, R. K. Roy, S. Pal, *Phys. Chem. Chem. Phys.* 2010, **12**, 9328.
 72. A. Sarmah, S. Saha, P. Bagaria, R. K. Roy, *Chem. Phys.* 2012, **394**, 29.
 73. A. Sarmah, R. K. Roy, *RSC Adv.* 2013, **3**, 2822.
 74. J. Sponer, P. Jurecka, I. Marchan, F. J. Luque, M. Orozco, P. Hobza, *Chem. Eur. J.* 2006, **12**, 2854.
 75. Y. Zhao, D. G. Truhlar, *Phys. Chem. Chem. Phys.* 2005, **7**, 2701.
 76. G. Gossens, I. Tavernelli, U. Rothlisberger, *J. Chem. Theory Comput.* 2007, **3**, 1212.
 77. M. E. Alberto, B. Butera, N. Russo, *Inorg. Chem.* 2011, **50**, 6965.
 78. F. Moroni, A. Famulari, M. Raimondi, M. Sabat, *J. Phys. Chem. B* 2003, **107**, 4196.
 79. A. D. Becke, *Phys. Rev. A* 1988, **38**, 3098.
 80. A. D. Becke, *J. Chem. Phys.* 1993, **98**, 5648.
 81. J. P. Perdew, *Phys. Rev. B* 1986, **33**, 8822.
 82. P. M. W. Gill, *Mol. Phys.* 1996, **89**, 433.
 83. C. T. Lee, W. T. Yang, R. G. Parr, *Phys. Rev. B* 1988, **37**, 785.
 84. GAUSSIAN 09, Revision C.01, M. J. Frisch, *et .al.* Gaussian, Inc., Wallingford CT, **2009**.
 85. G. A. Peterson, M. A. Al-Laham, *J. Chem. Phys.* 1991, **94**, 6081.
 86. W. J. Hehre, R. F. Stewart, J. A. Pople, *J. Chem. Phys.* 1969, **51**, 2657.
 87. G. A. Peterson, A. Bennett, T. G. Tensfeldt, M. A. Al-Laham, W. A. Shirley, J. Mantzaris, *J. Chem. Phys.* 1988, **89**, 2193.
 88. R. Ditchfield, W. J. Hehre, J. A. Pople, *J. Chem. Phys.* 1971, **54**, 724.
 89. V. Sgobba, D. M. Guldi, *Chem. Soc. Rev.*, 2009, **38**, 165.
 90. Z. Xiao, X. Wang, X. Xu, H. Zhang, Y. Li, Y. Wang, *J. Phys. Chem. C* 2011, **115**, 21546.
 91. F. Maseras, K. Morokuma, *J. Comput. Chem.* 1995, **16**, 1170.
 92. T. Vreven, K. S. Byun, I. Koma'romi, S. Dapprich, J. A., Jr. Montgomery, K. Morokuma, M. J. Frisch, *J. Chem. Theory Comput.* 2006, **2**, 815.
 93. D. Umadevi, G. N. Sastry, *J. Phys. Chem. Lett.* **2011**, **2**, 1572.
 94. V. A. Basiuk, *J. Phys. Chem. B* 2003, **107**, 8890.
 95. Y.-J. Xu, J.-Q. Li, *Chem. Phys. Lett.* 2005, **412**, 439.
 96. S. G. Stepanian, M. V. Karachevtsev, A. Y. Glamazda, V. A. Karachevtsev,; L. Adamowicz, *J. Phys. Chem. A* 2009, **113**, 3621.
 97. M. K. Shukla, M. Dubey, E. Zakar, R. Namburu, Z. Czyznikowska, J. Leszczynski, *Chem. Phys. Lett.* 2009, **480**, 269.
 98. N. Varghese, U. Mogera, A. Govindaraj, A. Das, P. K. Maiti, A. K. Sood, C. N. R. Rao, *ChemPhysChem* 2009, **10**, 206.



Table 4.1: The values of the global electrophilicity difference, Δw (in kcal mol⁻¹) for different combination of chosen SWCNTs (considered as acceptor, A) and nucleobases (considered as donor, B). The values are generated at B3LYP/6-31G(d) level of theory.

<i>DNA Bases</i> <i>SWCNT</i>	Guanine	Adenine	Thymine	Cytosine	Uracil	A-T	G-C
m:n							
6, 5	114.58	111.82	108.85	104.46	101.71	106.06	108.87
m:n							
9, 7	134.13	131.36	128.39	124.00	121.26	125.61	128.42
m:n							
9, 5	142.03	141.75	141.45	141.01	140.74	141.17	141.45
m:n							
9, 2	158.30	155.55	151.16	148.20	145.43	151.14	153.95
m:n							
7, 6	165.65	162.88	159.92	155.52	152.78	157.13	159.94
m:n							
8, 3	174.91	172.16	167.77	164.80	162.03	167.75	170.55
m:n							
10,2	217.66	214.89	211.92	207.53	204.78	209.12	211.94
m:n							
7, 5	231.87	229.10	226.13	221.74	218.99	223.35	226.15

Table 4.2: The values of positive energy component, $\Delta E_{B(A)}$ (in kcal mol⁻¹) for different combination of chosen SWCNTs (considered as acceptor, A) and nucleobases (considered as donor, B). The values are generated at B3LYP/6-31G(d) level of theory.

<i>DNA Bases</i> <i>SWCNT</i>	Guanine	Adenine	Thymine	Cytosine	Uracil	A-T	G-C
m:n 9, 7	10.42	7.94	5.13	1.54	-1.61	7.187	11.40
m:n 6, 5	10.89	8.51	5.79	2.34	-0.73	7.85	11.92
m:n 7, 6	13.94	11.42	8.55	4.50	1.72	11.08	15.54
m:n 7, 5	14.91	12.24	9.20	5.44	2.04	11.98	16.78
m:n 10,2	15.41	12.78	9.77	6.06	2.69	12.58	17.35
m:n 9, 5	18.00	14.88	11.36	7.10	3.23	14.93	20.83
m:n 9, 2	27.15	21.70	15.84	9.16	3.32	23.19	35.61
m:n 8, 3	29.67	24.32	18.53	12.00	6.14	26.37	38.71

Table 4.3: CDASE scheme based charge transfer, ΔN values for different combination of chosen SWCNTs (considered as acceptor, A) and nucleobases (considered as donor, B). The values are generated at B3LYP/6-31G(d) level of theory.

DNA Bases SWCNT	Guanine	Adenine	Thymine	Cytosine	Uracil	A-T	G-C
m:n							
9, 7	0.140	0.103	0.064	0.018	-0.019	0.091	0.152
m:n							
6, 5	0.146	0.110	0.072	0.028	-0.008	0.099	0.159
m:n							
7, 6	0.182	0.144	0.104	0.058	0.019	0.137	0.202
m:n							
7, 5	0.193	0.153	0.111	0.063	0.023	0.147	0.216
m:n							
10,2	0.199	0.159	0.118	0.070	0.030	0.154	0.223
m:n							
9, 5	0.228	0.183	0.135	0.081	0.036	0.180	0.262
m:n							
9, 2	0.323	0.254	0.183	0.104	0.037	0.267	0.413
m:n							
8, 3	0.348	0.281	0.210	0.133	0.067	0.298	0.442

Table 4.4: The values of the negative energy component, $\Delta E_{A(B)}$ (in kcal mol⁻¹) for different combination of chosen SWCNTs (considered as acceptor, A) and nucleobases (considered as donor, B). The values are generated at B3LYP/6-31G(d) level of theory.

DNA Bases SWCNT	Guanine	Adenine	Thymine	Cytosine	Uracil	A-T	G-C
m:n 9, 7	-11.70	-8.63	-5.39	-1.56	1.59	-7.67	-12.69
m:n 6, 5	-12.32	-9.33	-6.14	-2.39	0.72	-8.45	-13.36
m:n 7, 6	-16.07	-12.77	-9.26	-5.18	-1.74	-12.17	-17.77
m:n 7, 5	-17.21	-13.70	-9.99	-5.69	-2.08	-13.17	-19.20
m:n 10, 2	-17.87	-14.37	-10.66	-6.37	-2.75	-13.91	-19.95
m:n 9, 5	-20.86	-16.74	-12.40	-7.47	-3.31	-16.50	-23.92
m:n 9, 2	-30.99	-24.13	-17.12	-9.58	-3.37	-25.361	-40.23
m:n 8, 3	-34.25	-27.35	-20.28	-12.70	-6.32	-29.17	-44.24

Table 4.5: The values of overall stabilization energy, $\Delta E_{SE(AB)}$ (in kcal mol⁻¹) for different combination of chosen SWCNTs (considered as acceptor, A) and nucleobases (considered as donor, B). The values are generated at B3LYP/6-31G(d) level of theory.

DNA Bases	Guanine	Adenine	Thymine	Cytosine	Uracil	A-T	G-C
-----------	---------	---------	---------	----------	--------	-----	-----

SWCNT							
m:n							
9, 7	-1.28	-0.67	-0.27	-0.02	-0.02	-0.49	-1.28
m:n							
6, 5	-1.43	-0.82	-0.36	-0.05	-0.01	-0.60	-1.45
m:n							
7, 6	-2.13	-1.35	-0.71	-0.22	-0.03	-1.09	-2.22
m:n							
7, 5	-2.30	-1.46	-0.78	-0.25	-0.03	-1.20	-2.42
m:n							
10, 2	-2.46	-1.60	-0.88	-0.31	-0.06	-1.33	-2.60
m:n							
9, 5	-2.85	-1.85	-1.03	-0.37	-0.08	-1.57	-3.10
m:n							
9, 2	-3.84	-2.42	-1.28	-0.41	-0.06	-2.17	-4.62
m:n							
8, 3	-4.58	-3.03	-1.75	-0.70	-0.19	-2.81	-5.52

Table 4.6: Binding Energies (kilocalories per mole) of SWCNT-Nucleobase Complexes

at ONIOM (B3LYP/6-31G(d):UFF) Level of Theory.

	Guanine	Adenine	Thymine	Cytosine	Uracil
SWCNT (9,2) 235.18	-553.61	-268.34	-318.75	-301.47	-
SWCNT (7,5) 262.84	-300.80	-289.54	-288.82	-262.97	-
SWCNT (7,6) 121.41	-182..89	-175.18	-121.86	-121.85	-
SWCNT (8,3)	-17.38	-78.55	-76.20	-24.52	-9.16

*Binding energy, $\Delta E = E_{Nucleobase+SWCNT} - (E_{SWCNT} + E_{Nucleobase})$

Chapter V

A DFT Based Approach to Understand the
Effect of Fullerene Symmetry on the
Kinetic, Thermodynamic and Structural
Properties of Carbon NanoBuds

5.1 Introduction:

Taking analogy from the previous chapter, we have introduced the newly proposed methodology (i.e., CDASE scheme) to some rigorous and exciting applications in nanotechnology. This includes the implementation of theoretical findings to design and fabrication of some hybrid nanomaterials. This particular study directs more toward computational aspect of chemistry and considerable amount of conventional approaches have also been applied to justify the CDASE scheme based results.

The discovery of two highly symmetric allotropes of carbon, Buckminsterfullerene (C_{60}) and carbon nanotube (CNT), consolidate the expeditious progress of nanotechnology in the last three decades.¹⁻⁶ The structures of fullerene can best be described by a specific number of sp^2 hybridized carbon atoms containing both pentagonal and hexagonal rings arranged in spherical fashion. Within the structure of fullerene, each carbon atom participates in the formation of one double bond and two single bonds. Iijima and co-workers have reported the existence of another new allotrope of carbon, i.e., carbon nanotube (CNT) in 1991.³ A single-walled carbon nanotube (SWCNT) is an one atom thick graphite sheet (called ‘graphene’) rolled up into a seamless cylinder with diameter in the order of nanometer scale. Depending on the chiral vectors and helix angle, SWCNTs can be grouped as either ‘metallic’ or ‘semi-conducting’. Due to quantum confinement effect, these two allotropes of carbon exhibit some extraordinary electronic properties. In a recent study, Feng *et al.*⁷ showed that under certain conditions it is possible to maximize the conductivity of C_{60} fullerene up to the level of metals. The promising electronic, magnetic and optical properties of both fullerene and CNT generate immense interest to explore their adequate applications to the technological advancement.⁸⁻¹⁴ It is anticipated that in coming decades the components made-up of carbon nanotube (CNT) and other carbon nanostructures will become the building blocks for the future electronic devices.

Fabrication of sustainable hybrid nano materials by combining fullerene with SWCNT or graphene in a single framework is an emerging area of research. Smith and co-workers,¹⁵ reported the synthesis of a novel hybrid nano material called ‘Nanopeapod’ by encapsulating C_{60} fullerene within SWCNT. Basically, van der Waals interaction is the driving force for their structural stability.¹⁵ In 2007, Nasibulin *et al.*^{16,17} reported the laboratory synthesis of another hybrid nano material, so called NanoBud, where the

fullerene is covalently bonded to the outer surface of a SWCNT. It is worth mentioning here that the covalent interaction between fullerene and SWCNT incorporate some modulation in the electronic environment of the hybrid carbon nano-structure and that is different from the electronic environment of the individual interacting species. The extent of modulation in the electronic environment of hybrid NanoBuds can be accounted for its exceptional electronic properties such as high electron density and high field-emission, etc.¹⁸ On the other hand NanoBud has significant structural advantages as well. Higher chemical reactivity of fullerene can be exploited to functionalize carbon NanoBud. Also, fullerenes attached to the graphene surface can act as the linkers that provide specific gap (i.e., definite distance) between two particular layers of graphene sheets in the composite system.¹⁹ Most importantly, these hybrid nano materials have significant importance in the next generation electronic as well mechanical devices.²¹⁻²²

Li *et al.*²⁰ reported a simple mechanochemical approach to functionalize single walled carbon nanotube (SWCNT) with fullerenes. Nasibulin and co-workers¹⁷ first reported the laboratory synthesis of carbon NanoBud by the chemical vapor deposition (CVD) method using ferrocene vapor in the atmosphere of carbon monoxide. Wu *et al.*^{18,19} used density functional theory (DFT) to explore different electronic, structural and field emission properties of carbon NanoBud. He and co-workers²¹ have performed an extensive DFT based study to investigate the Raman features associated with the hybrid carbon NanoBud structure. In a combined study Raula *et al.*²² used experimental techniques along with DFT based theoretical approach to explore the relative reactivity of the two components of carbon NanoBud (i.e., SWCNT and fullerene) towards amine nucleophile. Tian and co-workers²³ performed a spectroscopic study to validate the simultaneous presence of both SWCNT and fullerene in a single molecular framework. The interesting magnetic behavior of hybrid NanoBud system has been explored by Zhu *et al.*²⁴ In another contemporary study, Seif *et al.* explored chemical, physical, and energetic aspects of hybrid carbon NanoBud system in details.²⁵

In the last three decades a series of conceptual Density Functional Theory (DFT)²⁶⁻³⁰ based reactivity descriptors.³¹⁻³⁷ have been developed to understand a wide verity of chemical interactions.³⁸⁻⁴⁴ A reliable intramolecular interaction trend can better be evaluated through the application of local reactivity descriptors such as Fukui function

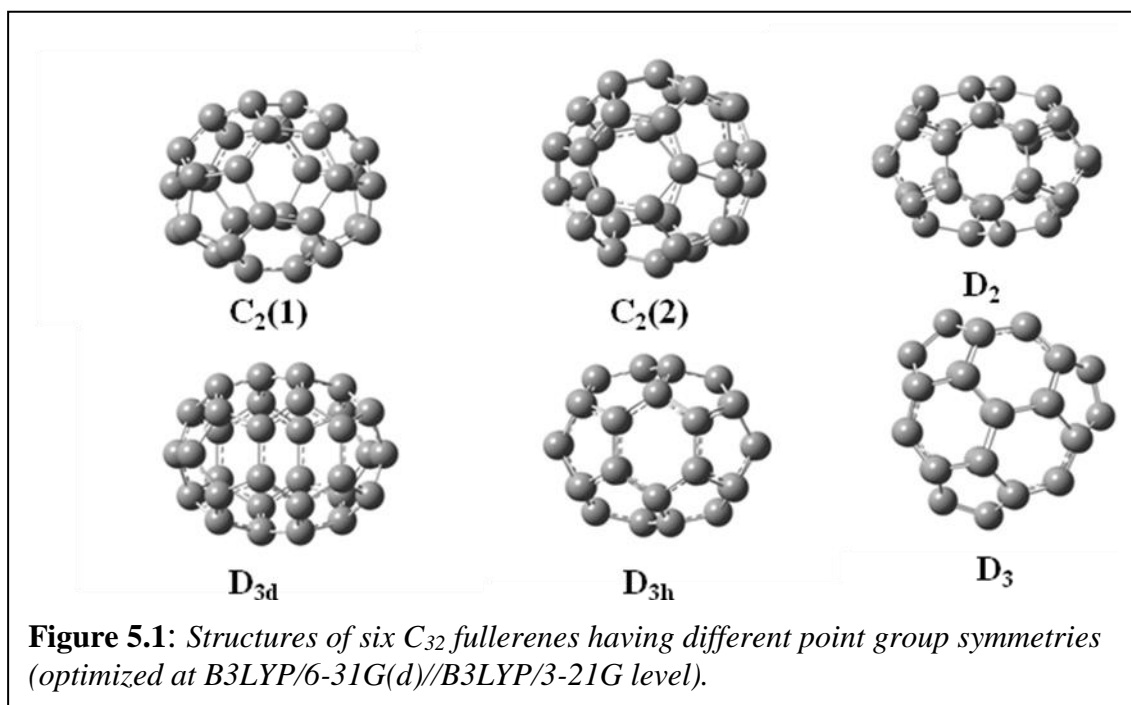
$[f(r)]$,^{45,46} local softness (s_k^+, s_k^- and s_k^0),⁴⁷ local hardness $\eta(r)$,⁴⁸⁻⁵¹ relative electrophilicity (s_k^+/s_k^-) and relative nucleophilicity (s_k^-/s_k^+),^{35,36} local electrophilicity,^{43,44} etc. The global reactivity descriptors such as chemical potential⁵² (*i.e.* the negative of electronegativity⁵³), chemical hardness (η)³¹, global electrophilicity index,^{54,55} nucleophilicity,⁵⁶⁻⁵⁸ electrofugality and nucleofugality^{59,60} etc. are primarily used to understand the intermolecular interactions.

Proposed Comprehensive Decomposition Analysis of Stabilization Energy (CDASE) scheme⁶¹ is a theoretical model of Roy and collaborators to understand the kinetic and thermodynamic aspects of a particular interaction. The formalism of CDASE scheme fundamentally originates from the concept of stabilization energy introduced by Parr and Pearson way back in 1983.³¹ Conceptually, CDASE is an energy decomposition scheme assuming the interaction between a donor (electron rich species) and an acceptor (electron deficient species) systems of comparable sizes. Some recently reported studies⁶²⁻⁶⁵ substantiate the reliability of CDASE scheme to understand the kinetic and thermodynamic factors associated with different interactions.

The present study correlates the changes in point group symmetry of smaller size fullerene (C_{32}) with the growth and stability of hybrid nano materials.⁶⁶ Although, C_{60} fullerene is a subject of extensive research for more than three decades, the same is not true for smaller fullerenes (between C_{20} - C_{40}). At the same time to design some efficient hybrid nano materials it is essential to understand the thermodynamics and kinetics of the nanosystems containing smaller fullerenes. The aspect of symmetry-stability correlation in smaller fullerene system has been explored recently.⁶⁵⁻⁷¹ So, investigation of symmetry-stability correlation in hybrid nanostructures containing fullerene and SWCNT (*i.e.*, NanoBuds) seems to be quite contextual. More so because the methodology adopted here is an unconventional one.

The chapter is structured in the following way: Implemented theoretical methodologies to accomplish the study have been discussed in Section 5.2. The results and discussion part in Section 5.3 is divided into divided into three sub-sections. Sub-section 5.3 (A) contains elaborate discussion on the kinetic and thermodynamic aspects of the interaction between fullerenes and SWCNTs, evaluated on the basis of five parameters derived from the CDASE scheme. To support the thermodynamic stability of

the hybrid nano-structures formed as well as kinetic aspects of their formation, as observed by CDASE scheme based parameters, conventional binding energy calculations and ‘synchronous transit-guided quasi-Newton’ (STQN) transition state (TS) studies are performed on some of the selected systems and the results are analyzed in Section 5.3 (B). The results of ADMP (Atom Centered Density Matrix Propagation) molecular dynamics simulation study, performed on six different hybrid NanoBuds, are analyzed in Section 5.3 (C). Finally, in the concluding remarks (Section 5.4) we have summarized the outcomes of our entire study.



5.2 Computational Details:

To accomplish the theme of our proposed study i.e., to understand the interaction between smaller size fullerenes with semi-conducting SWCNTs, we have considered six different types of fullerene systems along with eight different forms of SWCNTs. Required library of fullerene has been taken from the freely available webpage of M. Yoshida.⁷⁴ Chem3D⁷⁵ software is used to visualize the fullerene library as well as to generate the Gaussian input files for the fullerenes. The fullerenes chosen here are of 32 carbon atoms (i.e., C_{32} fullerene) with different point group symmetry (two C_2 conformers, D_2 , D_3 , D_{3h} and D_{3d})⁷⁶ (Figure 5.1). For computational convenience we will refer the two different C_2 conformers as $C_2(1)$ and $C_2(2)$ and these nomenclature will be

followed throughout the manuscript. Eight semi-conducting SWCNTs belong to three different groups (on the basis of conformational aspect). SWCNTs consisting of lattice vector, (n,m) (10,2), (6,5), (7,5) and (7,6) belong to the chiral group; the two having lattice vectors (6,0) and (5,0) are in the zigzag conformation; and the two with lattice vectors (6,6) and (5,5) can be grouped in the armchair category. The initial Gaussian input coordinates of the SWCNTs have been created using web accessible Nanotube structure generator TubeGen 3.4 online version.⁷⁷ The visual graphics forms of the nano structures were obtained using GaussView⁷⁸ visualization program. Geometries of the fullerenes as well as the SWCNT structures were optimized at DFT based B3LYP⁷⁹⁻⁸¹ level of theory using 3-21G basis set.⁸²⁻⁸⁵ For large chemical systems geometry optimization with 3-21G basis sets has been found to be reliable from the earlier studies.⁸⁶⁻⁸⁸ Subsequent energy refinement (with single point energy calculation) of the optimized structures have been done at B3LYP/6-31G(d) level of theory.

It is obvious from the discussion in Section 1.5 in the Introduction that CDASE scheme is developed on the basis of two isolated chemical systems (one is electron donor and the other is an electron acceptor). Unlike supermolecular approach, which considers both the interacting species together. So, in principle, the effect of weak forces such as van der waals interaction, hydrogen bonding, dispersion interaction, etc. need not be considered to compute kinetic and thermodynamic parameters in CDASE scheme. Also, earlier studies,⁶²⁻⁶⁵ reveals that B3LYP method exhibits significant level of accuracy for the qualitative interpretation of experimental findings. However, when conventional approaches are adopted to evaluate different thermodynamic and kinetic parameters for hybrid NanoBud systems, M06 level⁸⁹ of computations are performed in addition to B3LYP. As dispersion interaction is an important parameter in determining certain specific properties of nanosystems, it is expected that M06 functional will ensure improvement in the quality of present study.

As per requirement of the CDASE scheme the vertical ionization potential (IP) and the vertical electron affinity (EA) values are calculated by performing additional single point calculations of the cationic, neutral and anionic systems at the geometry of the neutral systems only and using B3LYP/6-31G(d) level of theory. Thus Δ SCF method is used here (not the Koopmanns' approximation) to evaluate the ionization potential and

electron affinity of the system. Restricted level of theory (i.e., RB3LYP/6-31G(d)) has been used for neutral systems whereas the ionic systems were treated with unrestricted (i.e., UB3LYP/6-31G(d)) level of theory. The entire DFT based calculations have been performed by using Gaussian 09⁹⁰ program suite.

5.3 (A) Kinetics and thermodynamics of NanoBud formation:

The covalent binding between fullerenes and SWCNTs induces structural stability to hybrid NanoBuds. The kinetics and thermodynamics of the covalent bond formation process are investigated here using five parameters based on the CDASE scheme. To augment the observations of CDASE scheme, conventional binding energy (BE) calculations as well as transition state (TS) optimization are also performed. Atom Centered Density Matrix Propagation (ADMP)⁹¹ MD simulation study [at semi-empirical molecular mechanics corrected PM3 level (PM3MM)⁹²] on the hybrid NanoBuds are also carried out to make the conclusions further convincing. The reliability of PM3MM based MD simulation in understanding various aspects of interactions between relatively large systems is evident from earlier reported studies⁹³⁻⁹⁶ and discussed in details in Section 5.3 (C).

(a): Kinetics of NanoBud formation using CDASE based parameters:

(i) *On the basis of (Δw) values:*

The difference in global electrophilicity (i.e., Δw) values calculated for various combinations of SWCNTs and fullerenes are reported in Table 5.1. The higher ease of interaction (i.e., higher reactivity) between a particular pair of SWCNT and fullerene system is indicated from the larger value of Δw . The working equation for the calculation of Δw value is given by,

$$\Delta w = w_A - w_B \quad (5.1)$$

Where, w_A and w_B are the global electrophilicity values of the acceptor A (i.e.,

$w_A = \frac{(\mu_A^0)^2}{2\eta_A}$) and the donor B (i.e., $w_B = \frac{(\mu_B^0)^2}{2\eta_B}$), respectively. In the present study we

have considered SWCNTs as electron donors (i.e., B) and the fullerenes as electron acceptors (i.e., A). The positive Δw values in Table I confirms the fact that above consideration is indeed justified.

It is evident from Table 5.1 that out of four chiral CNTs, CNT (7,5) and CNT (10,2) show higher degree of interactions with all the fullerene species. Moderate and very low values of Δw have been observed for CNT (7,6) and CNT (6,5), respectively. With a higher value of Δw , interactions of CNT (6,0) with different C₃₂ fullerenes are preferable to the other member of the zigzag category, the CNT (5,0). Between the two armchair conformations of SWCNT, the extent of interaction of CNT (6,6) with all C₃₂ fullerenes are kinetically more favorable compared to the other member, i.e., CNT (5,5).

The results obtained from Table 5.1 infer that the NanoBud formation between SWCNTs and C₃₂ fullerenes is more favorable when the fullerenes have D-type symmetry point groups (i.e., D₂, D₃, D_{3h} and D_{3d}) than those having C-type symmetry point groups (i.e., C₂(1) or C₂(2)). Also, on the basis of the computed Δw values it is possible to propose a general trend of interaction between C₃₂ fullerenes of different point group symmetries and SWCNTs. The trend is as follows:

$$C_2(1) \langle C_2(2) \rangle \langle D_{3d} \approx D_{3h} \rangle \langle D_2 \rangle \langle D_3.$$

(ii) *Using the positive energy component (i.e., $\Delta E_{B(A)}$):*

As argued initially, the positive energy component (i.e., $\Delta E_{B(A)}$) is an energy raising quantity and expected to have a positive value. In our earlier studies $\Delta E_{B(A)}$ was qualitatively correlated to the kinetic aspect (i.e., the rate) of a reactive interaction.⁶²⁻⁶⁶ This is because of the fact that $\Delta E_{B(A)}$ helps to cross the activation barrier. Higher the value of $\Delta E_{B(A)}$ faster should be the rate of interaction between the SWCNTs and the fullerenes.

The generated values of $\Delta E_{B(A)}$ for different pairs of SWCNTs and fullerenes are reported in Table 5.2. It is obvious from the $\Delta E_{B(A)}$ values that the interaction between SWCNTs and fullerenes is a kinetically favorable process because the $\Delta E_{B(A)}$ values for all the combinations of SWCNTs and fullerenes are appeared to be positive and within a consistent range of 25-45 kcal/mol. The thermodynamic parameters of CDASE scheme (which will be discussed in the next few sub-sections) also predict a stable interaction between C₃₂ fullerenes and SWCNTs. Out of four chiral SWCNTs, CNT (7,5) seems to produce slightly more kinetically favorable interaction with all the chosen C₃₂ fullerenes

(Table 5.2) (although the difference between the generated $\Delta E_{B(A)}$ values are quite close to each other. A moderately active interaction for the two zigzag SWCNTs, [i.e., CNT (6,0) and CNT (5,0)] with fullerenes is estimated from their range of $\Delta E_{B(A)}$ values. The CNT (6,6), which belongs to armchair conformation, produces highest value of $\Delta E_{B(A)}$ for the all possible combinations with C₃₂ fullerenes. It is worth mentioning here that the prediction of the relative trend of interaction between C₃₂ fullerenes of different point group symmetry with SWCNTs, on the basis of $\Delta E_{B(A)}$ values, is almost similar to that generated from the ΔW values, i.e., $C_2(1) \langle C_2(2) \langle D_{3h} \langle D_{3d} \langle D_2 \langle D_3$.

(b) Thermodynamics of NanoBud formation using CDASE based parameters:

(i) On the basis of charge transfer (ΔN) values:

The computed values of the charge transfer component, ΔN for the various combinations of fullerenes and SWCNTs are presented in Table 5.3. Charge transfer component is an important parameter to compare relative stability of the adducts (i.e., NanoBuds) formed. In the present study ΔN values are generated by considering different SWCNTs, behave as electron donors (i.e., B) and corresponding C₃₂ fullerenes as electron acceptors (i.e., A). The consideration of SWCNTs as electron donors and fullerenes as electron acceptors, respectively, is validated from the positive ΔN values generated in all cases (Table 5.3). In a recent study, Wu *et al.*¹⁸ showed that the electron transfer takes place from SWCNTs to fullerenes in case of stable NanoBud formation.

For a favorable interaction process (both kinetically and thermodynamically) ΔN value should be positive and this is possible when $\mu_B^0 > \mu_A^0$ (or $\chi_A^0 > \chi_B^0$). Thus, we can argue that a higher value of ΔN for a particular pair of SWCNT and fullerene implies a greater extent of interaction between the pair. On the basis of ΔN values presented in Table 5.3 it is clear that among the eight different SWCNTs, CNT (6,6) of armchair configuration is able to produce the most stable interactions with different forms of C₃₂ fullerenes. In case of fullerenes with D- point group symmetries the interactions with SWCNTs are found to form more stable adducts than the ones formed between fullerenes having C point group symmetry. C₃₂ fullerene having the D₃ point group symmetry is found to have the highest charge transfer values with all the three different configurations

of SWCNTs considered in the present study. Thus, thermodynamically more favorable interaction is anticipated between three different conformations of SWCNTs with C₃₂ fullerene of D₃ point group symmetry. So, in a qualitative approach ΔN can be used as a simple theoretical tool to determine the donor and acceptor nature of the interacting systems as well as the stability of the adduct formed.

(ii) *On the basis of negative energy component, (i.e., $\Delta E_{A(B)}$):*

In the relevant section included in introduction it was argued why $\Delta E_{A(B)}$ is the energy lowering (i.e., the negative energy) component of the overall stabilization energy. As it is the energy lowering term it can be correlated, in principle, to the thermodynamic stability of the adduct formed. Mathematically $\Delta E_{A(B)}$ can be expressed as,

$$|\Delta E_{A(B)}| = |\Delta E_{B(A)}| + |\Delta E_{SE(AB)}| \quad (5.2)$$

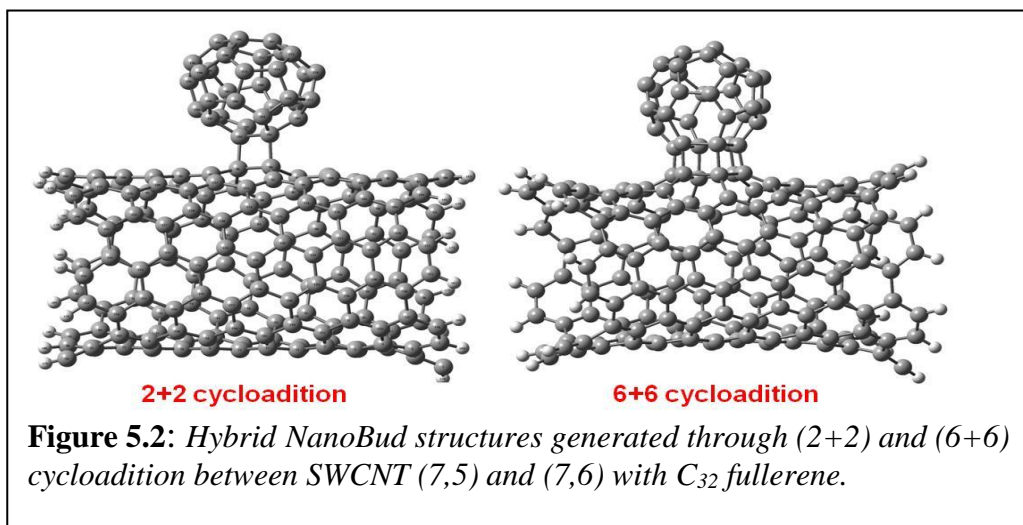
Thus, from the theoretical definition of negative energy component, it seem to be an acceptable interpretation that larger the negative value of $\Delta E_{A(B)}$, thermodynamically more favorable the interaction will be for a particular pair of SWCNT and fullerene, providing higher stability to the resultant hybrid adduct.

In Table 5.4 the $\Delta E_{A(B)}$ values for various combinations of SWCNTs and fullerenes are presented. Low thermodynamic preference for the interaction between all three types of SWCNTs and fullerenes having C type (i.e., C₂(1) and C₂(2)) symmetry is evident from relatively smaller $|\Delta E_{A(B)}|$ values for those combinations. Among the four chiral SWCNTs, CNT (7,5) produces higher values of $|\Delta E_{A(B)}|$, followed by CNT (10,2), CNT (7,6) and CNT (6,5), in decreasing order (except with C₂(1), C₂(2) and D_{3h} fullerenes, where CNT(6,5) produces higher values). For SWCNTs of zigzag conformation, the one with lattice vector (5,0) undergoes thermodynamically more favorable interaction with fullerenes than the one with lattice vector (6,0). The observed differences between the $\Delta E_{A(B)}$ values generated by two SWCNTs of armchair conformation with fullerenes are relatively high. CNT (6,6) appeared to have generated the highest value of $|\Delta E_{A(B)}|$ among all considered in the present study. High $|\Delta E_{A(B)}|$ values for CNT (6,6) predict higher thermodynamic stability for the hybrid NanoBud

structures generated as a result of interactions between CNT (6,6) and different C₃₂ fullerenes.

(iii) *On the basis of overall stabilization energy, (i.e., $\Delta E_{SE(AB)}$):*

An idea about stability of an adduct formed can be obtained from the value of stabilization energy, $\Delta E_{SE(AB)}$. The higher stability of the adduct formed in the course of an interaction is justified from the higher negative value of $\Delta E_{SE(AB)}$. The $\Delta E_{SE(AB)}$ values computed for all the possible pairs of SWCNTs and fullerenes are given in Table 5.5. As one moves down the Table 5.5, an increasing order of stability for the NanoBud structures become more obvious (as $|\Delta E_{SE(AB)}|$ values go on increasing). The increasing stability of the NanoBud structures with the increase in the order of symmetry from C to D is also reflected from stabilization energy values. The impact of fullerene symmetry on the stability of hybrid NanoBud framework found to follow the order, C₂(1) < C₂(2) < D_{3d} < D_{3h} < D₂ < D₃ [except with CNT(6,5), CNT(7,5) and CNT(6,6), in which case C₂(2) > C₂(1)]. The generated $|\Delta E_{SE(AB)}|$ values also suggest (like ΔN and $\Delta E_{A(B)}$ values) highest stability for the hybrid NanoBuds generated from the interaction between armchair conformation of CNT (6,6) and fullerenes.



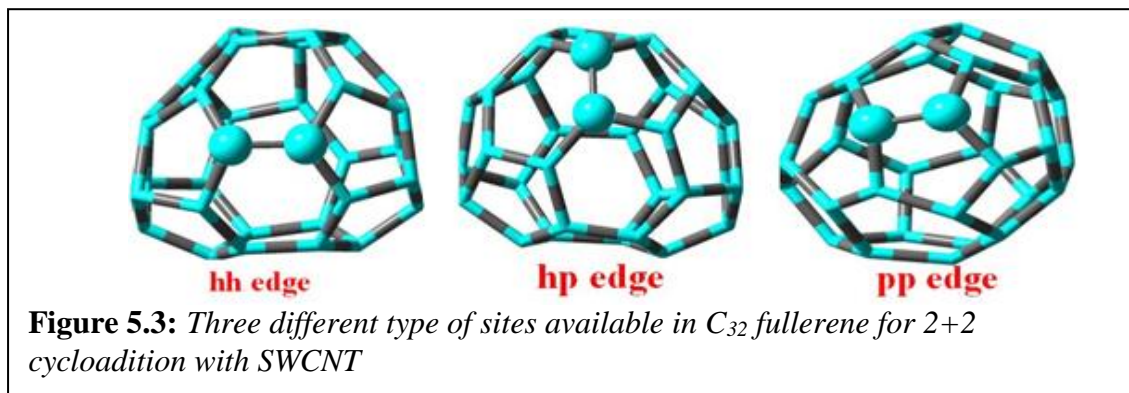
Indeed, CDASE scheme based different kinetic and thermodynamic parameters, altogether, predicted similar trend of reactivity and stability of NanoBuds generated from the interaction between C₃₂ fullerenes having different point group symmetries and SWCNTs. Also, as per the trend of the generated data it can be argued that fullerenes

with D-point group symmetry exhibits kinetically and thermodynamically more favorable interaction with all the SWCNTs.

(B) (i) *Comparison of conventional binding energy (BE) values and geometrical parameters to assess the relative stabilities of NanoBuds:*

SWCNT (7,5) and C_{32} fullerenes having $C_2(1)$ and D_2 point group symmetries are used as model systems for the binding energy calculation. Structural parameters and binding energy (BE) values associated with the interactions of these systems are analyzed in two different levels (B3LYP and M06) to compare the relative stabilities of the corresponding adducts.

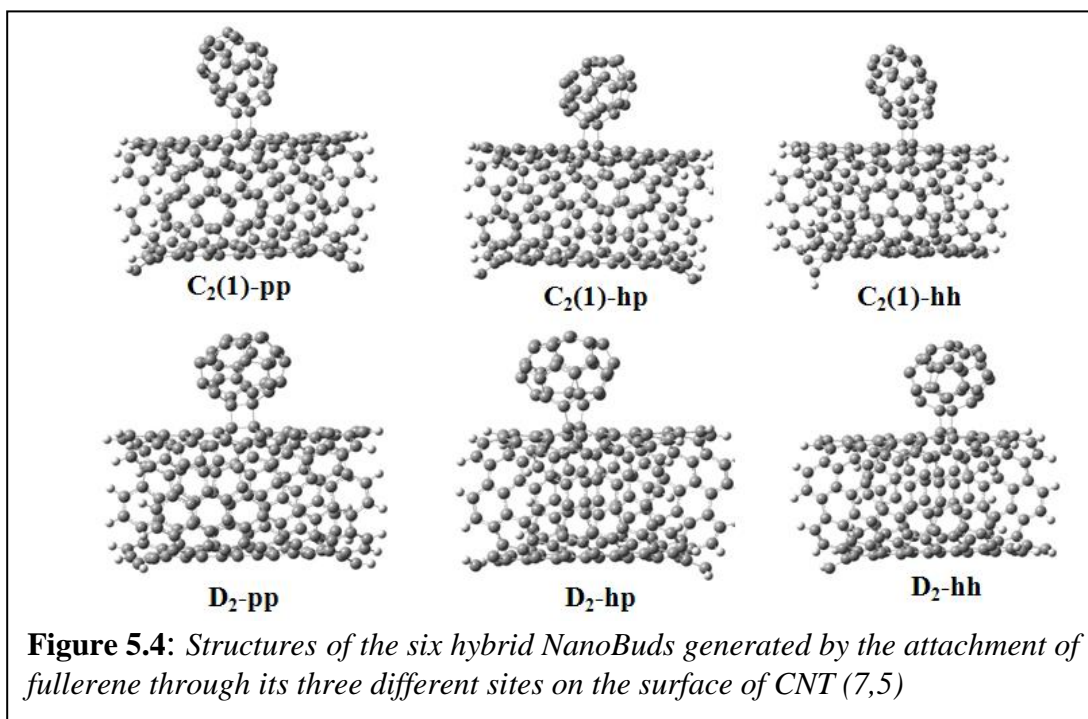
Primarily two different modes of covalent binding interactions are possible in the process of NanoBud formation between C_{32} fullerene and chiral SWCNT. One type of probable binding is through (2+2) and another is through (6+6) cycloaddition reaction between the π -electrons of fullerene and SWCNT (Figure 5.2). Some of the published theoretical studies^{18,19} claim energetically unfavorable (6+6) type of cycloaddition between fullerene and SWCNT. Fundamentally, large number of bond formation (6 bonds) imposes a robust strain in the structural orientation of the hybrid framework and this cannot be compensated through the enthalpy of formation for six new C-C bonds. That is why the mode of covalent binding considered here is energetically favorable (2+2) cycloaddition reaction between fullerene and SWCNT.



In a particular fullerene molecule existence of three different types of C-C sites are possible for the 2+2 cycloaddition reaction with SWCNTs (Figure 5.3). First, one is the common edge between two hexagons (hh-bond). Another type of C-C bond is the

common edge between a hexagon and a pentagon (hp-bond). Finally, third possibility is the common edge between two pentagons (pp-bond).

Full geometry optimizations (i.e., without imposing any constraint) at B3LYP and M06 level using 3-21G basis sets followed by single point calculation at B3LYP (and M06)/6-31G(d) level have been performed for all the six hybrid structures (Figure. 5.4). It is observed that the two C-atoms (on the surface of SWCNT), which are involved in the covalent bond formation, are pulled-up towards the fullerene causing some deformation on the SWCNT structures. The change in the hybridization from sp^2 to sp^3 for the two carbon atoms is the best possible explanation for this kind of structural reorientation.



Binding energy values computed at B3LYP level for six hybrid structures (considering the three possible orientations) are presented in Table 5.6 (a). Calculated binding energy value for the hybrid NanoBud structure resulting from the interaction between $C_{32}(C_2(1))$ and $CNT(7,5)$ through (pp) common edges is -5.37 kcal/mol. Similarly, reasonably higher binding energy value (-11.10 kcal/mol) is observed for the NanoBud structure formed through $C_{32}(C_2(1))-CNT(7,5)$ (hp) mode of covalent binding. In case of $C_2(1)$ symmetry fullerene, the calculated binding energy value is highest (i.e.,

the most negative, 22.44 kcal/mol) for its interaction with CNT(7,5) through (hh) site. It is interesting to note that some similar kind of observation was made by Wu and Zeng.¹⁸ They predicted higher stability for the NanoBud structures resulted from the 2+2 cycloaddition between zigzag and armchair CNTs with C₆₀ fullerene through covalent binding interaction at the common edge of two hexagonal rings. (i.e., hh site)

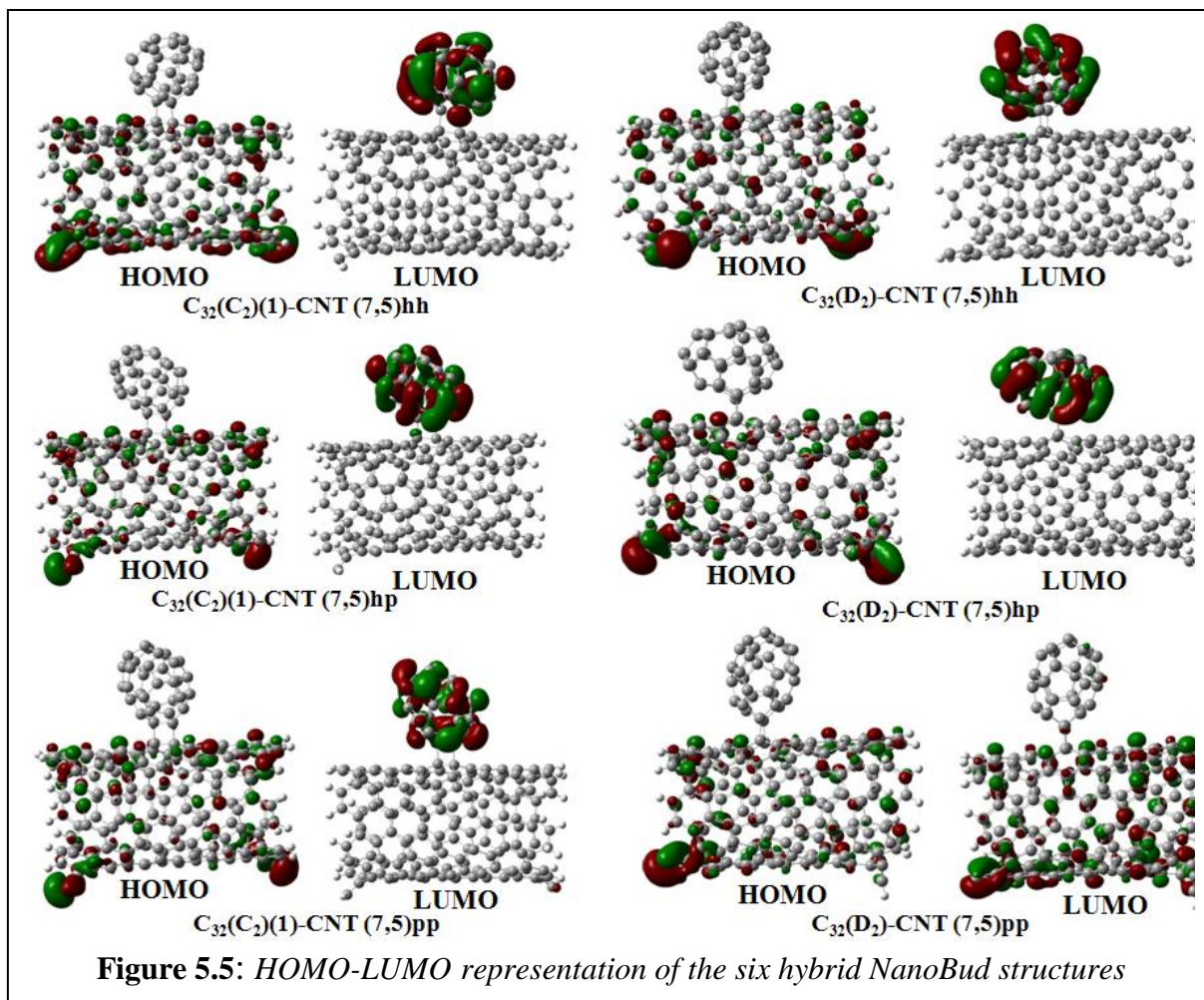
The hybrid NanoBuds formed by the interaction of fullerenes having D₂ symmetry with CNT (7,5) are generally found to be more stable than those formed with fullerenes having C₂(1) symmetry. However, in this case the most stable NanoBud is formed when the mode of interaction is of ‘hp’ type.

Because the two constituents of hybrid NanoBuds are chemically identical (i.e., one is C₃₂ fullerene and the other is SWCNT) but differ only in the symmetry of fullerenes, it is logical to compare the corresponding optimized energy values for the six different NanoBud systems. The optimized energy values for individual NanoBud structures are also reported in Table 5.6 (a) and (b). It is gratifying to note that observed trend of stability for the hybrid NanoBuds on the basis of optimized energy values is exactly similar to that obtained from the calculated BE values.

The average bond length values computed for six NanoBud structures at B3LYP as well as M06 level are also included in Table 5.6 (a) and (b). These values support the observed binding energy trend within a particular symmetry type of C₃₂ fullerene. It is noteworthy that the average bond length values calculated for the different NanoBud systems are close to the earlier reported values of average bond length for carbon NanoBud systems by Wu *et al.*^{18,19} Conceptually, a shorter bond length is associated with higher negative binding energy that implies greater stabilization for the hybrid nanosystem.

The BE values for the above-mentioned hybrid structures generated at M06 level are reported in Table 5.6 (b). It is worth noting that with M06 level also the order of stability for the hybrid system remains similar to that predicted from the B3LYP calculation. However, some variations are observed for the calculated BE values for NanoBud structures having fullerenes of D₂ symmetry. The computation at B3LYP method seems to have underestimated the BE values for these NanoBuds. The BE calculation at M06 level produced lowest value (-17.71 kcal/mol) for the hybrid system

containing D_2 symmetry fullerene attached to the surface of SWCNT through pentagon-pentagon (pp) common edge, followed by through hexagon-hexagon (hh) (-23.04 kcal/mol) and hexagon-pentagon (hp) (-31.17 kcal/mol) common edges. It is to be noted here that the average C-C distance is decreased to some extent for hp and pp mode of binding [Table 5.6 (b)] when the level of computations is M06/3-21G.



Among the three selected carbon atoms (here the C-atoms numbering is as per the default optimized structures) the first and the second ones belong to the surface of SWCNT and the third one belongs to the attached C_{32} fullerene. It is observed that the bond angles are slightly deviated from the perfect perpendicular orientation. The best possible explanation for this kind of deformation is the minimization of structural constraint induced during the formation of covalent bonding through 2+2 cycloaddition reaction between C_{32} fullerene and SWCNT. A significant amount of angular strain is

generated due to the conversion of these two individual nano materials into a single framework hybrid nanostructure. Perhaps, in the context of structural stability, a minor change in the contact angle plays a critical role. The stability of NanoBud structure is enhanced to some extent with the relaxation of structural strain that originates from the attachment of fullerene to the outer surface of SWCNT through the minimum deformation of contact angles. The larger deviation of contact angle from the perfect perpendicular orientation leads to a greater stability of the resulting NanoBud structures (comparing the binding energy and corresponding bond angle values from Tables 5.6 (a) and 5.6 (b)).

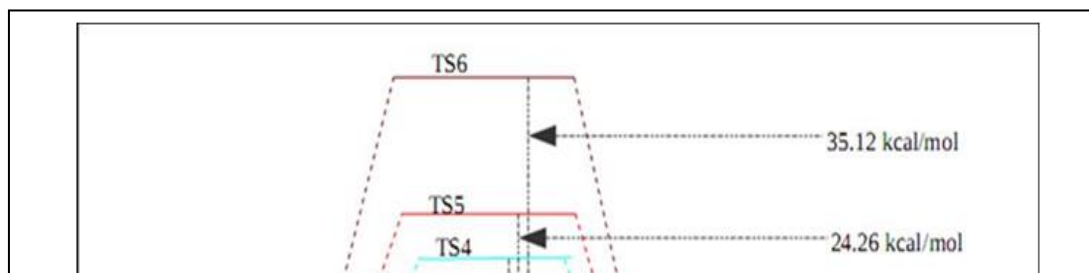
To address the ground state electron behavior, we have computed the charge density plot for the hybrid NanoBud structures. The representations of Frontier Molecular Orbital (FMO) (generated at M06 level) for the six different hybrid NanoBud systems are given in Figure 5.5. It is observed that in the combined structures, the HOMOs are primarily contributed by the SWCNT and LUMOs are from the attached C₃₂ fullerenes. Thus the pictorial representations of computed FMOs clearly show that the electron density is transferred from the SWCNT to fullerene in the process of NanoBud formation. This justifies the fact that SWCNTs behave as electron donor (i.e., B) and fullerenes behave as electron acceptor (i.e., A) when they interact to form hybrid NanoBuds.

(ii) Synchronous transit-guided quasi-Newton (STQN) Transition State (TS) optimization of the NanoBud structures to evaluate activation energy involved in the hybrid nano-structure formation:

An adequate approach to locate the transition state of a particular reactive interaction is the dual-end method. In this theoretical approach search for the possible transition state (TS) structure is performed by combining the information from both the reactants and the product structures. Synchronous transit-guided quasi-Newton (STQN) method, proposed by Peng and Schlegel,⁹⁷ is used to locate the TS structure for the NanoBud systems with QST3 keyword as implemented in Gaussian09.⁹⁰ With the use of QST3 keyword a reactant, a product and an initial guess for the TS structure are defined in the input. The STQN method is believed to be a better option for the TS search in case of large molecular systems as it performs the calculations by using updated approximations without considering analytical Hessians.

The STQN calculations for the six NanoBud structures are performed at B3LYP as well as M06 level using 3-21G basis sets. The calculated values of the energy barriers are reported in Table 5.7 and the corresponding pictorial representation is in Figure 5.6. It is obvious that the energy barriers for the hybrid NanoBud structures formed between CNT (7,5) with fullerene having C_2 symmetry are relatively higher than the ones formed between CNT (7,5) and fullerenes with D_2 symmetry. As the transition state energy barrier is lower for the interaction between D_2 symmetry fullerene with CNT (7,5), a kinetically favorable process of NanoBud generation for this particular interaction is expected. It is worth mentioning here that thermodynamically more favorable NanoBud formation between D_2 symmetry fullerenes and CNT (7,5) over those formed between C_2 symmetry fullerenes and CNT (7,5) is already established from the CDASE scheme based parameters (Tables 5.3, 5.4 and 5.5) as well as conventional binding energy values (Tables 5.6). Kinetically favorable NanoBud formation from fullerenes having D_2 symmetry than those having C_2 symmetry is also predicted from the CDASE scheme based reactivity parameters (Tables 5.1 and 5.2).

A significant variation in the kinetic preference of NanoBud formation with change in the point of attachment of the fullerene moiety can be observed from the STQN TS search results. A very low TS energy value is observed for the NanoBud structure where a D_2 fullerene is covalently bonded to CNT (7,5) through a common hexagon-hexagon (hh) edge. However, for the same hybrid structure when the D_2 fullerene is bonded to SWCNT through two other equivalent positions [i.e., hexagon-hexagon (hh) and pentagon-pentagon (pp) edges], calculated TS energy barriers are found to be relatively high. At the same instance, TS energy barrier for the interaction between C_2 fullerene with SWCNT (7,5) is found to be 20.22, 24.26 and 35.12 kcal/mol at different points of attachment for C_{32} fullerene namely, hexagon-hexagon (hh), hexagon-pentagon (hp) and pentagon-pentagon (pp) edges, respectively. It is worth mentioning here that the observed energy barriers computed in both the method (i.e., B3LYP and M06) for six different NanoBud systems are consistent and correlate well with the expected trend generated from the different CDASE scheme based kinetic parameters [(i.e., Δw and $\Delta E_{B(A)}$).

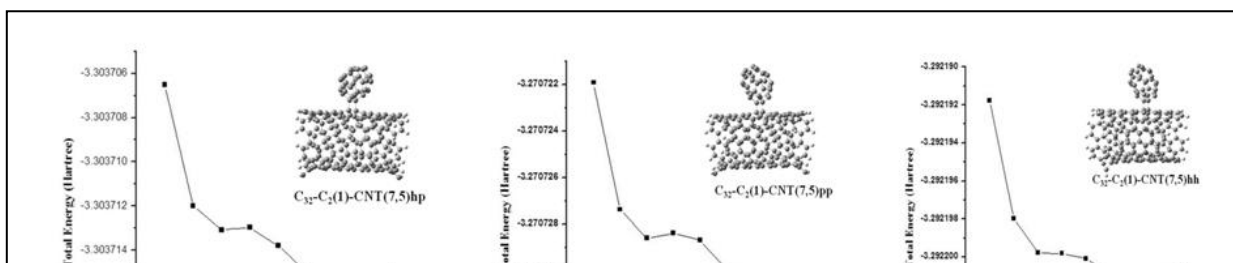


(C) Atom Centered Density Matrix Propagation (ADMP) molecular dynamics simulation study on hybrid NanoBud structures:

In addition to static DFRT as well as DFT based studies we have performed molecular dynamics simulation on the six hybrid NanoBud (Figure 5.4) structures. Projected Atom Centered Density Matrix Propagation (ADMP)⁹¹ MD simulation study measures the continuous change in energy of the system with respect to the variation in structural orientation of the hybrid structure throughout the fabrication of two nano materials within a specific time frame. The ADMP-MD simulation has been performed at semi-empirical molecular mechanics corrected PM3 (PM3MM)⁹² level to reduce the cost of rigorous *Ab initio* computations accounted for massive size of the hybrid structures (218 atoms in the NanoBud framework). Although, the PM3 level of computation seems to have poor performance for the computation of structural (C-C bond distance) and energetic (relative energy values of different isomers with respect to the most stable one) parameters of smaller fullerenes,⁹⁸ recently, Hsu *et al.*⁹⁹ reported some interesting results of ADMP based MD simulation at PM3MM level. They have performed ADMP-MD simulation using PM3MM method to understand the functioning of molecular machinery

(e.g., single-molecule electric revolving door) that responds to the variation of conductance with the change in molecular conformation. Also, here the input geometries for dynamics simulation were taken from the optimized transition state structures generated by STQN method at M06/3-21G level). The calculated relative energy values of the isomers of the C₃₂ fullerene at both B3LYP and M06/3-31G levels follow the same trend as shown by Zheng et al.⁹⁸ (Table 5.8). It is worthy of pointing out here that both DFRT based CDASE scheme and conventional DFT calculations have established the NanoBud formation to be a kinetically and thermodynamically favorable process. Which means the transition state is the highest energy (i.e., the least stable) point on the interaction energy profile. The purpose of this ADMP-MD study is just to show the same for individual NanoBud formation process. Fullerene constitutes only a small portion of the overall NanoBud structure. The major portion is contributed by the SWCNT having hexagonal rings. Zheng et al.⁹⁸ have shown that AM1 and PM3 methods work reasonably well for higher fullerenes because number of adjacent pentagon rings decreases, thus lowering the ring strain. Almost similar may be the situation here. It will be interesting to see whether ADMP-MD simulation using PM3MM method can really show that NanoBud formation process is a thermodynamically favorable one.

The simulation temperature is set at 300 K and the time frame is restricted to 5000 femtosecond. Within specified time limit the paths depicting continuous energy minimization for the six hybrid NanoBud systems have been tracked and the graphical representations of the simulation results at some particular points are presented in Fig. 5.8. The energetically favorable fabrication of D₂ symmetry fullerene with CNT (7,5) is also evident from the ADMP molecular dynamics study. These plots suggest that NanoBud formation is a thermodynamically favorable process (as the total energy continuously goes down within the chosen time frame) and generates relatively stable hybrid nanomaterials. Also, between the C₂(1) and D₂ isomers, the later one seems to have formed more stable NanoBud as the total energy goes to the lowest when the mode of binding is hp. It is encouraging to observe that conventional BE calculation [Table 5.6 (a) and (b)] and CDASE scheme based parameters [Table 5.4 and 5.5] also show the same trend.



5.4: Conclusion:

In the present study, some interesting findings on the kinetic, thermodynamic and structural properties of hybrid NanoBuds obtained from both DFRT based CDASE scheme as well as the conventional approaches are reported. To the best of knowledge of the authors, it is one of the very first attempts to understand the effect of symmetry of the attached fullerenes on the stability and structural properties of hybrid NanoBuds. In that sense this particular study is focused on the importance of computer aided molecular modeling techniques in designing some novel nano materials.

In the first part of the chapter kinetic and thermodynamic aspects of hybrid NanoBuds are explored with the recently devised density functional reactivity theory based CDASE scheme. The kinetic and thermodynamic preference for the interaction between higher symmetry fullerenes (i.e., D_2 point group symmetry) over the lower symmetry one (i.e., C_2 point group symmetry) with all the three conformations of SWCNTs are well established using different reactivity parameters based on the CDASE

scheme. Thus, CDASE-scheme can be considered as a computationally cost-effective alternative approach to handle large systems like hybrid NanoBuds.

In the later part of the study different conventional approaches [e.g., binding energy (BE) calculation, transition state optimization and molecular dynamics simulations] are adopted to investigate the fabrication of fullerenes having point group symmetries C_{2v} and D_{2d} on the surface of chiral SWCNT.(7,5). There are three possible binding sites available in C_{32} fullerene through which it can be covalently attached to the surface of SWCNTs. Conventional binding energy (BE) calculations are performed to understand the impact of these three possible binding orientations to the overall thermodynamic stability of the hybrid NanoBuds. The influence of fullerene symmetry on the structural properties of the hybrid NanoBuds is also addressed using the optimized geometries of NanoBuds. The kinetic aspects of NanoBud formation has also been explored by computing activation energy through Synchronous Transit-guided Quasi-Newton (STQN) method. Both BE and activation energy values correlate well with the predictions made on the basis of CDASE scheme based parameters. To gain some insights into the structural flexibility of the hybrid structures generated from the interaction between fullerenes and SWCNTs within a particular time frame, Atom Centered Density Matrix Propagation (ADMP) molecular dynamics simulation is also performed on the same NanoBud structures. The MD simulation study also agrees well with CDASE-scheme based parameters, BE values and activation energy values.

Presently, design and development of hybrid nano material is an emerging area of research. In material science, the QM based computational modeling techniques are an integral part of the material design and fabrication. Advanced computer aided theoretical techniques provide a unique platform to simulate and verify different properties of a new material, without going for expensive laboratory experiments. Applications of cost-effective and at the same time reliable molecular modeling techniques will assist experimental set-up to explore different hybrid nano materials. The present study may be considered as a small initiative to use theory and computational modeling techniques to help experimental material chemists in designing future electronic devices.

References:

-
1. M. S. Dresselhaus, G. Dresselhaus, P. C. Eklund, *Science of Fullerenes and Carbon Nanotubes*; Academic Press: New York, 1996.
 2. H. W. Kroto, J. R. O. Heath, S. C. O'Brien, R. F. Curl, R. E. Smalley, *Nature* 1985, **318**, 162.
 3. S. Iijima, *Nature* 1991, **354**, 56.
 4. D. S. Beghune, C. H. Kiang, M. S. de Vries, G. Gorman, R. Savoy, J. Vazquez, R. Beyers, *Nature* 1993, **363**, 605.
 5. S. G. Louie, *Top. Appl. Phys.* 2001, **80**, 113.
 6. R. H. Baughman, A. A. Zakhidov, W. A. de Heer, *Science* 2002, **297**, 787.
 7. M. Feng, J. Zhao, H. Petek, *Science* 2008, **320**, 359.
 8. M. Wu, J. Tse, J. Jiang, *J. Phys. Chem. Lett.*, 2010, **1**, 1394.
 9. K. S. Novoselov, A. K. Geim, S. V. Morozov, D. Jiang, M. I. Katsnelson, I. V. Grigorieva, S. V. Dubonos, A. A. Firsov, *Nature* 2005, **438**, 197.
 10. Y. B. Zhang, Y. W. Tan, H. L. Stormer, P. Kim, *Nature* 2005, **438**, 201.
 11. A. K. Geim, K. S. Novoselov, *Nat. Mater.* 2007, **6**, 183.
 12. K. S. Novoselov, E. McCann, S. V. Morozov, V. I. Fal'ko, M. I. Katsnelson, U. Zeitler, D. Jiang, F. Schedin, A. K. Geim, *Nat. Phys.* 2006, **2**, 177.
 13. K. S. Novoselov; Z. Jiang, Y. Zhang, S. V. Morozov, H. L. Stormer, U. Zeitler, J. C. Maan, G. S. Boebinger, P. Kim, A. K. Geim, *Science* 2007, **315**, 1379.
 14. A. F. Hebard, M. J.; Rosseinsky, R. C. Haddon, D. W. Murphy, S. H. Glarum, A. P. Ramirez, A. R. Kortan, *Nature* 1991, **350**, 600.
 15. B. W. Smith, M. Monthieux, D. E. Luzzi, *Nature* 1998, **396**, 323.
 16. A. G. Nasibulin *et al.* *Nat. Nanotechnol.* 2007, **2**, 156.
 17. A. G. Nasibulin, A. S. Anisimov, P. V. Pikhitsa, H. Jiang, D. P. Brown, M. Choi, E. I. Kauppinen, *Chem. Phys. Lett.* 2007, **446**, 109.
 18. X. J. Wu, X. C. Zeng, *ACS Nano* 2008, **2**, 1459.
 19. X. Wu, X. C. Zeng, *Nano Lett.*, 2009, **9**, 250.
 20. X. Li, L. Liu, Y. Qin, W. Wu, Z. X. Guo, L. Dai, D. Zhu, *Chem. Phys. Lett.* 2003, **377**, 32.
 21. H. Y. He, B. C. Pan, *J. Phys. Chem. C* 2009, **113**, 20822.
 22. Raula *et al.* *Chem. Mater.* 2010, **22**, 4347.
 23. Y. Tian, D. Chassaing, A. G. Nasibulin, P. Ayala, H. Jiang, A. S. Anisimov, E. I. Kauppinen, *J. Am. Chem. Soc.* 2008, **130**, 7188.
 24. X. Zhu, H. Su, *Phys. Rev. B* 2009, **79**, 165401.
 25. A. Seif, E. Zahedi, T. S. Ahmadi, *Eur. Phys. J. B* 2011, **82**, 147.
 26. P. Hohenberg, W. Kohn, *Phys. Rev. B* 1964, **86**, 1463.
 27. W. Kohn, L. J. Sham, *J. Phys. Rev. A* 1965, **140**, 1133.
 28. R. G. Parr, W. Yang, *Density—Functional Theory of Atoms and Molecules*; Oxford University Press; New York, 1989.
 29. W. Koch, M. Holthausen, *A Chemist's Guide to Density Functional Theory*; Wiley-Vch Weinheim, 2000.
 30. W. Kohn, A. D. Becke, R. G. Parr, *J. Phys. Chem.* 1996, **100**, 12974.
 31. R. G. Parr, R. G. Pearson, *J. Am. Chem. Soc.* 1983, **105**, 7512.
 32. P. Geerlings, F. De Proft, W. Langenaeker, *Chem. Rev.* 2003, **103**, 1793.
 33. R. K. Roy, S. Saha, *Annu. Rep. Prog. Chem., Sect. C* 2010, **106**, 118.
 34. P. K. Chattaraj, B. Maiti, U. Sarkar, *Chem. Rev.* 2006, **106**, 2065.

-
35. R. K. Roy, S. Krishnamurti, P. Geerlings, S. Pal, *J. Phys. Chem. A*. 1998, **102**, 3746.
 36. R. K. Roy, F. De Proft, P. Geerlings, *J. Phys. Chem. A*. 1998, **102**, 7035.
 37. P. A. Johnson, L. J. Bartolotti, P. W. Ayers, T. Fievez, P. Geerlings, *Modern Charge-Density Analysis*. Ed Gatti, C.; Macchi, P. Springer 2012, pp 715.
 38. S. Krishnamurty, S. Pal, *J. Phys. Chem. A*, 2000, **104**, 7639.
 39. S. Saha, R. K. Roy, *J. Phys. Chem. B*. 2007, **111**, 9664.
 40. S. Pal, K R. S. Chandrakumar, *J. Am. Chem. Soc.* 2000, **122**, 4145.
 41. R. K. Roy, V. Usha, B. K. Patel, K. Hirao, *J. Comput. Chem.* 2006, **27**, 773.
 42. R. K. Roy, P. Bagaria, S. Naik, V. Kavala, B. K. Patel, *J. Phys. Chem. A* 2006, **110**, 2181.
 43. A. M. Lamsabhi, C. A. Escobar, P. Perez, *J. Phys. Org. Chem.* 2005, **18**, 1161.
 44. L. R. Domingo, P. Perez, R. Contreras, *J. Org. Chem.* 2003, **68**, 6060.
 45. R. G. Parr, W. Yang, *J. Am. Chem. Soc.* 1984, **106**, 4049.
 46. Yang, W.; Mortier, W. J. *J. Am. Chem. Soc.* **1986**, *108*, 5708-5711.
 47. W. Yang, R. G. Parr, *Proc. Natl. Acad. Sci. U. S. A.* 1985, **82**, 6723.
 48. R. G. Parr, J. L. Gazquez, *J. Phys. Chem.*, 1993, **97**, 3939.
 49. S. Saha, R. K. Roy, *J. Phys. Chem. B*. 2007, **111**, 9664.
 50. S. Saha, R. K. Roy, *J. Phys. Chem. B (Addition/Correction)* 2008, **112**, 1884.
 51. S. Saha, R. K. Roy, *Phys. Chem. Chem. Phys.* 2008, **10**, 5591.
 52. R. G. Parr, R. A. Donnelly, M. Levy, W. E. Palke, *J. Chem. Phys.* 1978, **68**, 3801.
 53. L. Pauling, *J. Am. Chem. Soc.*, 1932, **54**, 3570.
 54. A. T. Maynard, M. Huang, W. G. Rice, D. G. Covell, *Proc. Natl. Acad. Sci. U. S. A.* 1998, **95**, 11578.
 55. R. G. Parr, L. von Szentpaly, S. Liu, *J. Am. Chem. Soc.* 1999, **121**, 1922.
 56. P. W. Ayers, R. G. Parr, *J. Am. Chem. Soc.* 2001, **123**, 2007.
 57. P. Jaramillo, P. Perez, R. Contreras, W. Tiznadoand, P. Fuentealba, *J. Phys. Chem. A* 2006, **110**, 8181.
 58. P. Jaramillo, P. Fuentealba, P. Perez, *P. Chem. Phys. Lett.* 2006, **427**, 421.
 59. P. W. Ayers, J. S. M. Anderson, J. I. Rodriguez, Z. Jawed, *Phys. Chem. Chem. Phys.* 2005, **7**, 1918.
 60. P. Pérez, R. Contreras, A. Aizman, *THEOCHEM* 1999, **493**, 267.
 61. P. Bagaria, S. Saha, S. Murru, V. Kavala, B. K. Patel, R. K. Roy, *Phys. Chem. Chem. Phys.* 2009, **11**, 8306.
 62. S. Saha, R. K. Roy, S. Pal, *Phys. Chem. Chem. Phys.* 2010, **12**, 9328.
 63. Sarmah, A.; Saha, S.; Bagaria, P.; Roy, R. K. *Chem. Phys.* **2012**, *394*, 29.
 64. A. Sarmah, R. K. Roy, *RSC Adv.* 2013, **3**, 2822.
 65. A. Sarmah, R. K. Roy, *J. Phys. Chem. C* 2013, **117**, 21539.
 66. Q. C. Sun, *Prog. in Solid State Chem.* 2007, **35**, 1.
 67. D. Manna, A. Sirohiwal, T. K. Ghanty, *J. Phys. Chem. C* 2014, **118**, 7211.
 68. D. Manna, T. K. Ghanty, *J. Phys. Chem. C*, 2012, **116**, 25630.
 69. D. Manna, T. K. Ghanty, *J. Phys. Chem. C*, 2012, **116**, 16716.
 70. D. Manna, T. K. Ghanty, *J. Phys. Chem. C*, 2013, **117**, 17859.
 71. D. Manna, A. Sirohiwal, T. K. Ghanty, *J. Phys. Chem. C*, 2013, **117**, 18777.
 72. K. Kitaura, K. Morokuma, *Int. J. Quantum Chem.* 1976, **10**, 325.
 73. K. Morokuma, *J. Chem. Phys.* 1971, **53**, 1236.

-
74. Yoshida, M. <http://www.cochem2.tutkie.tut.ac.jp/Fuller/Fuller.html>.
 75. CS Chem3D Pro, CambridgeSoft Corporation, 100 Cambridge Park Dr., Cambridge MA 02140-2317.
 76. P. W. Fowler, D. E. Manolopoulos, *An atlas of fullerenes*. Volume 30 of International series of monographs on chemistry, Clarendon Press, 1995.
 77. J. T. Frey, D. J. Doren, TubeGen 3.4 (web-interface, <http://turin.nss.udel.edu/research/tubegenonline.html>), University of Delaware, Newark DE, 2011.
 78. R.; Keith, T.; Millam, GaussView, Version 5, Dennington, J. Semichem. Inc., Shawnee Mission KS, 2009.
 79. A. D. Becke, *Phys. Rev. A* 1988, **38**, 3098.
 80. A. D. Becke, *J. Chem. Phys.* 1993, **98**, 5648.
 81. C. T. Lee, W. T. Yang, R. G. Parr, *Phys. Rev. B* 1988, **37**, 785.
 82. G. A. Peterson, M. A. Al-Laham, *J. Chem. Phys.* 1991, **94**, 6081.
 83. W. J. Hehre, R. F. Stewart, J. A. Pople, *J. Chem. Phys.* 1969, **51**, 2657.
 84. G. A. Peterson, A. Bennett, T. G. Tensfeldt, M. A. Al-Laham, W. A. Shirley, J. A. Mantzaris, *J. Chem. Phys.* 1988, **89**, 2193.
 85. R. Ditchfield, W. J. Hehre, J. A. Pople, *J. Chem. Phys.* 1971, **54**, 724.
 86. A. Gupta, B. K. Shaw, S. K. Saha, *J. Phys. Chem. C* 2014, **118**, 6972.
 87. K. Terakura, H. Akai, "Interatomic Potential and Structural Stability", Proceedings of the 15th Taniguchi Symposium," Kashikojima, Japan, Springer Series, 1993.
 88. H. Rafii-Tabar, G. A. Mansoori, "Interatomic Potential Models for Nanostructures" Encyclopedia Nanoscience & Nanotechnology, American Scientific Publishers, 2004.
 89. Y. Zhao, D. G. Truhlar, *Theor. Chem. Account* 2006, **120**, 215.
 90. GAUSSIAN 09, Revision C.01, Frisch, M. J. *et al.* Gaussian, Inc., Wallingford CT, **2009**.
 91. H. B. Schlegel, J. M. Millam, S. S. Iyengar, G. A. Voth, A. D. Daniels, G. E.; Scuseria, M. J. Frisch, *J. Chem. Phys.* 2001, **114**, 9758.
 92. E. Anders, R. Koch, P. Freunshcht, *J. Comp. Chem.*, 1993, **14**, 1301.
 93. B. Abdelaziz, N. Leila, H. Sakinn, D. Imen, M. Fatiha, K. DjamelEddine, *J. Incl. Phenom. Macrocycl. Chem.* 2013, **77**, 455.
 94. G. V. Papamokos, I. N. Demetropoulos, *J. Phys. Chem. A*, 2004, **108**, 8160.
 95. G. L. Borosky, S. J. Lin, *Chem. Inf. Model.*, 2011, **51**, 2538.
 96. V. Svetlov, E. Nudler, *Biochimica. biophysica. acta.* 2013, **1829**, 20.
 97. C. Peng, H. B. Schlegel, *Isr. J. Chem.*, 1994, **33**, 449.
 98. G. Zheng, S. Irle, K. Morokuma, *Chem. Phys. Lett.* 2005, **412**, 210.
 99. L. Y. Hsu, E. Y. Li, H. Rabitz, *Nano Lett.*, 2013, **13**, 5020.
 100. W. Q. Tian, Y. A. Wang, *J. Chem. Theory Comput.*, 2005, **1**, 353.

Table 5.1: Difference in global electrophilicity (Δw) values (in kcal/mol) of interacting fullerenes (considered as acceptor, A) and SWCNTs (considered as donor, B). The values are calculated at the B3LYP/6-31G(d)//B3LYP/3-21G level.

SWCNT Fullerene	CNT	CNT	CNT	CNT	CNT	CNT	CNT	CNT
	10,2	6,5	7,5	7,6	5,0	6,0	6,6	5,5
C ₃₂ -C ₂ (1)	97.73	1.81	111.94	49.26	8.25	13.78	115.66	13.61
C ₃₂ -C ₂ (2)	101.26	5.35	115.47	45.72	21.66	10.25	119.20	27.01
C ₃₂ -D _{3h}	111.54	8.44	125.72	59.51	21.66	24.03	129.44	27.02
C ₃₂ -D _{3d}	111.54	8.47	125.75	59.53	21.68	24.06	129.47	27.04
C ₃₂ -D ₂	111.55	8.48	125.77	59.53	31.93	24.06	129.47	37.29
C ₃₂ -D ₃	124.95	21.88	139.16	72.94	35.47	37.47	142.88	40.83

Table 5.2: Positive energy component ($\Delta E_{B(A)}$) values (in kcal/mol) for different combinations of fullerenes (considered as acceptor, A) and SWCNTs (considered as donor, B). The values are calculated at the B3LYP/6-31G(d)//B3LYP/3-21G level.

SWCNT Fullerene	CNT	CNT	CNT	CNT	CNT	CNT	CNT	CNT
	10,2	6,5	7,5	7,6	5,0	6,0	6,6	5,5
C ₃₂ -C ₂ (1)	32.26	33.09	33.79	31.89	31.18	26.84	40.89	29.61
C ₃₂ -C ₂ (2)	32.29	33.14	33.84	31.91	31.20	26.96	42.45	29.63
C ₃₂ -D _{3h}	32.46	33.16	33.86	32.09	31.35	27.81	42.47	29.98
C ₃₂ -D _{3d}	37.13	37.42	38.85	36.46	35.05	31.00	47.94	33.33
C ₃₂ -D ₂	38.65	38.67	40.27	37.92	36.32	32.66	48.68	34.65
C ₃₂ -D ₃	40.51	40.18	41.89	39.75	38.0	35.13	48.73	36.52

Table 5.3: Charge transfer (ΔN) values for different combinations of fullerenes (considered as acceptor, A) and SWCNTs (considered as donor, B). The values are calculated at the B3LYP/6-31G(d)//B3LYP/3-21G level.

SWCNT Fullerene	CNT	CNT	CNT	CNT	CNT	CNT	CNT	CNT
	10,2	6,5	7,5	7,6	5,0	6,0	6,6	5,5
C ₃₂ -C ₂ (1)	0.3411	0.3618	0.3611	0.3393	0.3400	0.2779	0.4742	0.3193
C ₃₂ -C ₂ (2)	0.3414	0.3623	0.3617	0.3396	0.3402	0.2782	0.4916	0.3195
C ₃₂ -D _{3h}	0.3431	0.3625	0.3619	0.3414	0.3417	0.2865	0.4919	0.3231
C ₃₂ -D _{3d}	0.3908	0.4064	0.4134	0.3859	0.3793	0.3179	0.5526	0.3567
C ₃₂ -D ₂	0.4061	0.4192	0.4280	0.4006	0.3921	0.3341	0.5608	0.3699
C ₃₂ -D ₃	0.4249	0.4346	0.4445	0.4191	0.4090	0.3581	0.5613	0.3884

Table 5.4: Negative energy component ($\Delta E_{A(B)}$) values (in kcal/mol) for different combinations of fullerenes (considered as acceptor, A) and SWCNTs (considered as donor, B). The values are calculated at the B3LYP/6-31G(d)//B3LYP/3-21G level.

SWCNT Fullerene	CNT	CNT	CNT	CNT	CNT	CNT	CNT	CNT
	10,2	6,5	7,5	7,6	5,0	6,0	6,6	5,5
C ₃₂ -C ₂ (1)	-36.35	-38.41	-38.35	-36.18	-36.25	-30.09	-50.45	-34.22
C ₃₂ -C ₂ (2)	-36.38	-38.44	-38.38	-36.21	-36.27	-30.11	-50.48	-34.24
C ₃₂ -D _{3h}	-37.18	-38.99	-38.93	-37.01	-37.04	-31.55	-49.44	-35.01
C ₃₂ -D _{3d}	-42.25	-43.78	-44.46	-41.77	-41.23	-34.94	-57.54	-38.86
C ₃₂ -D ₂	-44.44	-45.73	-46.59	-43.90	-43.06	-37.20	-59.08	-40.84
C ₃₂ -D ₃	-47.71	-48.66	-49.63	-47.13	-46.12	-40.95	-60.64	-44.04

Table 5.5: Overall stabilization energy ($\Delta E_{SEA(B)}$) values (in kcal/mol) for different combinations of fullerenes (considered as acceptor, A) and SWCNTs (considered as donor, B). The values are calculated at the B3LYP/6-31G(d)//B3LYP/3-21G level.

SWCNT Fullerene	CNT	CNT	CNT	CNT	CNT	CNT	CNT	CNT
	10,2	6,5	7,5	7,6	5,0	6,0	6,6	5,5
C ₃₂ -C ₂ (1)	-4.09	-5.32	-4.56	-4.29	-3.25	-3.14	-9.56	-4.61
C ₃₂ -C ₂ (2)	-4.10	-5.28	-4.54	-4.30	-5.07	-3.15	-8.03	-4.61
C ₃₂ -D _{3h}	-4.72	-5.83	-5.07	-4.92	-5.70	-3.74	-6.97	-5.03
C ₃₂ -D _{3d}	-5.11	-6.36	-5.61	-5.31	-6.18	-3.94	-9.59	-5.54
C ₃₂ -D ₂	-5.80	-7.06	-6.32	-5.99	-6.74	-4.54	-10.40	-6.18
C ₃₂ -D ₃	-7.2	-8.48	-7.75	-7.38	-8.12	-5.82	-11.91	-7.53

Table 5.6 (a): Calculated binding energies (in kcal/mol), average bond lengths and bond angles values at the common attached site for six hybrid NanoBuds. The values are calculated through optimization at B3LYP/ 3-21G level with addition to an energy correction at B3LYP/ 6-31G (d) level.

NanoBuds	BE (kcal/mol)	Average bond length (\AA)	Optimized energy values (Hartree)	Bond angles
$C_{32}(C_2)$ -CNT (7,5)pp	-5.37	1.62	-7365.8080	$C_{187}C_{96}C_{98}=89.41$ $C_{189}C_{98}C_{96}= 89.34$
$C_{32}(C_2)$ -CNT (7,5)hp	-11.10	1.60	-7365.8298	$C_{197}C_{96}C_{98}= 90.09$ $C_{194}C_{98}C_{96}= 90.87$
$C_{32}(C_2)$ -CNT (7,5)hh	-22.44	1.55	-7365.8628	$C_{202}C_{96}C_{98}= 89.81$ $C_{201}C_{98}C_{96}= 90.04$
$C_{32}(D_2)$ -CNT (7,5)pp	-17.46	1.59	-7365.8528	$C_{127}C_6C_5 = 89.74$ $C_{144}C_5C_6 = 89.27$
$C_{32}(D_2)$ -CNT (7,5)hp	-29.87	1.57	-7365.8834	$C_{30}C_{127}C_{144}=105.8$ $C_3C_{144}C_{127}= 107.4$
$C_{32}(D_2)$ -CNT (7,5)hh	-26.83	1.58	-7365.8791	$C_{13}C_{127}C_{144}= 92.2$ $C_{12}C_{144}C_{127}= 93.0$

*Binding energy, $\Delta E = E_{SWCNT+Fullerene} - (E_{SWCNT} + E_{fullerene})$

[§] Here pp = pentagon-pentagon, hp = hexagon-pentagon and hh = hexagon-hexagon edge shearing

[#] Numberings of atoms are according to the optimized structure.

Table 5.6(b): Calculated binding energies (in kcal/mol), average bond lengths and bond angles values at the common attached site for six hybrid NanoBuds. The values are calculated through optimization at M06/ 3-21G level with addition to an energy correction at M06/ 6-31G (d) level.

NanoBuds	BE (kcal/mol)	Average bond length (Å^0)	Optimized energy values (Hartree)	Bond angles
$C_{32}(C_2)$ -CNT (7,5)pp	-4.67	1.59	-7362.9645	$C_{187}C_{96}C_{98}=89.49$ $C_{189}C_{98}C_{96}= 89.55$
$C_{32}(C_2)$ -CNT (7,5)hp	-20.16	1.57	-7362.9778	$C_{197}C_{96}C_{98}= 90.36$ $C_{194}C_{98}C_{96}= 90.60$
$C_{32}(C_2)$ -CNT (7,5)hh	-28.50	1.56	-7363.0025	$C_{202}C_{96}C_{98}= 89.74$ $C_{201}C_{98}C_{96}= 89.99$
$C_{32}(D_2)$ -CNT (7,5)pp	-7.71	1.57	-7362.9338	$C_{127}C_6C_5 = 87.60$ $C_{144}C_5C_6 = 86.89$
$C_{32}(D_2)$ -CNT (7,5)hp	-23.04	1.56	-7363.0201	$C_{30}C_{127}C_{144}=105.9$ $C_3C_{144}C_{127}= 107.71$
$C_{32}(D_2)$ -CNT (7,5)hh	-41.17	1.58	-7362.9423	$C_{13}C_{127}C_{144} = 88.32$ $C_{12}C_{144}C_{127}= 88.15$

*Binding energy, $\Delta E = E_{SWCNT+Fullerene} - (E_{SWCNT} + E_{fullerene})$

[§] Here pp = pentagon-pentagon, hp = hexagon-pentagon and hh = hexagon-hexagon edge shearing

[#] Numberings of atoms are according to the optimized structure.

Table 5.7: Calculated STQN TS energy barrier values (in kcal/mol) for six hybrid NanoBuds generated at B3LYP and M06 level.

Hybrid NanoBuds	TS energy barrier (in kcal/mol)	
	B3LYP	M06
C ₃₂ (C ₂)-CNT (7,5)hh	20.22	20.00
C ₃₂ (C ₂)-CNT (7,5)hp	24.26	23.66
C ₃₂ (C ₂)-CNT (7,5)pp	35.12	36.12
C ₃₂ (D ₂)-CNT (7,5)hh	10.80	8.96
C ₃₂ (D ₂)-CNT (7,5)hp	1.84	2.44
C ₃₂ (D ₂)-CNT (7,5)pp	6.91	7.11

Table 5.8: Calculated relative energy values (in kcal/mol) for six isomers of C₃₂ fullerenes generated at B3LYP/3-21G and M06/3-21G level.

Isomers	Relative Energy values (in kcal/mol)	
	B3LYP	M06
D ₃	0	0.0005
D _{3h}	52.22	146.57
D _{3d}	23.65	0
C ₂ (1)	12.73	120.43
D ₂	4.36	111.84
C ₂ (2)	3.10	100.65

Chapter VI

Interaction between Small Atomic Gold
Clusters and Nucleobases: A Density
Functional Reactivity Theory Based Study

6.1 Introduction:

The tuneable electronic properties of the gold nano particles and DNA composite system finds some sophisticated applications for the development of instrumentation in the contemporary progress of nanobiotechnology. This attributes promising scope for the biochip technology, which is the core building block for programmable nanobiodevices. DNA-based nanoscale devices offer adaptability in synchronization through variation in the particular DNA base sequence.^{1,2} Gold nanoparticles coated with DNA is an integral part of the machineries of diagnostic devices like surface plasmon resonance spectroscopy (SPRS), surface enhanced Raman spectroscopy (SERS), colorimetric, electrochemical and scanometric detection of DNA, etc.³⁻⁶ Assembly of gold nanoparticles and DNA within a single framework structure exhibit suitable properties for design and fabrication of sensors, drug delivery, biochip technology, imaging etc.⁷⁻⁹ The possibility of synthesizing three dimensional metalized nanomaterial by incorporating metal atoms to the interior of DNA stimulates the concept of bioelectronics.¹⁰⁻¹² Eventually, the four nucleobases contain unique electronic transport phenomena on account of the intrinsic difference in their chemical structure and electronic environment. The interaction of DNA with transition metal surface is highly probed due to its importance in the development of different experimental techniques targeting DNA sequence and imaging.¹³⁻²⁰

The combined system of gold nanoparticle and DNA has extremely promising technological aspects. A better understanding of the interaction between individual nucleobases with gold surface at electronic level will accelerate the recent progress on design and fabrication of component for bioelectronics devices. It is believed that the dispersion plays key role in the interaction between gold surface and DNA. Ostblom *et al.* experimentally determined highest thermodynamic heat of desorption value for guanine followed by adenine, cytosine and thymine on gold surface.²¹ In another major breakthrough Kryachko *et al.* explained the stability of Au-DNA complex through the formation of nonconventional hydrogen bonding interaction between small Au cluster and nucleobases.²² According to their study a unique N-H---Au type of hydrogen bonding interaction is possible between Au₃ and Au₄ clusters and DNA bases. In a combined spectroscopic and DFT based study Cao *at el.* provided a strong experimental evidence to

support the nonconventional hydrogen bonding interaction between gold cluster and nucleobases.²³ Jena and co-workers present an innovative idea by projecting the Au-DNA composite system as a possible catalytic source for the carbon monoxide oxidation reaction.²⁴ Kimura-Suda *et al.* used X-ray photoelectron spectroscopy along with FTIR technique to determine the adsorption affinity of the individual nucleobases on Au-surface.²⁵ They have found relatively higher adsorption affinity for A and followed by C, G and T, respectively on Au-surface.

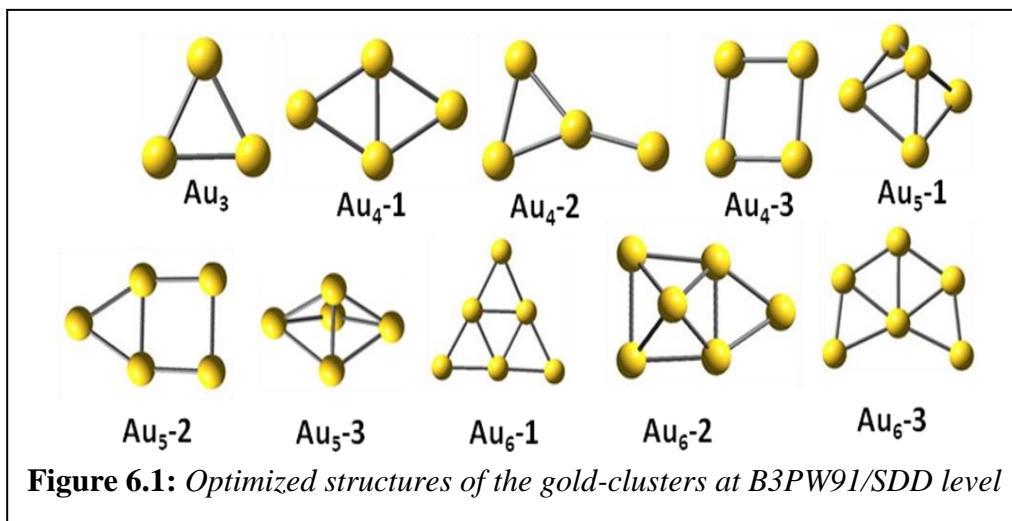
In the conceptual frame work of density functional theory (DFT),²⁶⁻³⁰ a group of reactivity descriptors has been drafted in the last three decades.³¹⁻³⁸ These reactivity descriptors are mainly divided into two categories local and global ones. Normally local reactivity descriptors e.g., Fukui function $[f(r)]$,^{32,39} local softness (S_k^+ , S_k^- and S_k^0),³⁴ local hardness $[\eta(r)]$,^{37,38,40,41} relative electrophilicity (S_k^+/S_k^-) and relative nucleophilicity (S_k^-/S_k^+),^{42,43} etc. are useful to evaluate intramolecular reactivity sequence. Similarly, the global reactivity descriptors such as chemical potential⁴² (i.e. the negative of electronegativity),⁴⁵ chemical hardness³¹(η), global electrophilicity index,^{46,47} nucleophilicity,⁴⁸⁻⁵⁰ are proposed to study intermolecular reactivity trend. In a recent study, Bhattacharjee *et al.*⁵¹ investigated the relative contribution of combined kinetic and exchange energy terms vs electronic component of molecular electrostatic potential in hardness potential derivatives.

Roy and collaborators developed the formalism of CDASE (comprehensive decomposition analysis of stabilization energy)⁵² scheme. Based on the components of stabilization energy (due to the charge transfer interaction between two chemical species), initially proposed by Parr and co-workers,³¹ Roy *et al.* systematically devised the CDASE as a compact energy decomposition scheme by considering the mutual effect of the interacting species. Different parameters of CDASE scheme were shown to carry qualitative information about the kinetics and thermodynamics of a reactive interaction and the theoretical findings are correlated well with the experimental evidence.⁵³⁻⁵⁶

Inspired by the promising futuristic applications of Au-DNA composite nanosystem in nanobiotechnology, this particular study attempts to understand the kinetic and thermodynamic aspects of the interaction between gold clusters with DNA bases as well as electronic properties of the corresponding complexes. In addition to this,

influence of structural features (like coordination sites, orientation of Au_n cluster with respect to the nucleobases, H-bonding interaction, etc.) on the stability of resultant complex is also analyzed.

The chapter is organized in the following way: The computational techniques used to accomplish the study are discussed in Section 6.2. The results and related inferences evaluated on the basis of parameters generated by CDASE scheme are reported in Section 6.3 (a). Section 6.3 (b) carries an elaborate discussion on the findings of conventional binding energy calculations along with different structural and electronic properties of some selected Au_n -Nucleobase composite systems. The kinetic aspects of CDASE scheme based findings are also tested against a more general Synchronous transit-guided quasi-Newton (STQN) calculation for some of the Au_n -Nucleobase complexes (Section 6.3 (c)). The results generated by TDDFT based calculations on the complex formed by Au_4 and Au_6 clusters with nucleobases are discussed on Section 6.3 (d). Finally, in Section 6.4, we have summarized our entire study on the interaction of small gold clusters with DNA bases and the prospect of promising application of the proposed CDASE scheme as an alternative theoretical tool to study nanosystems.

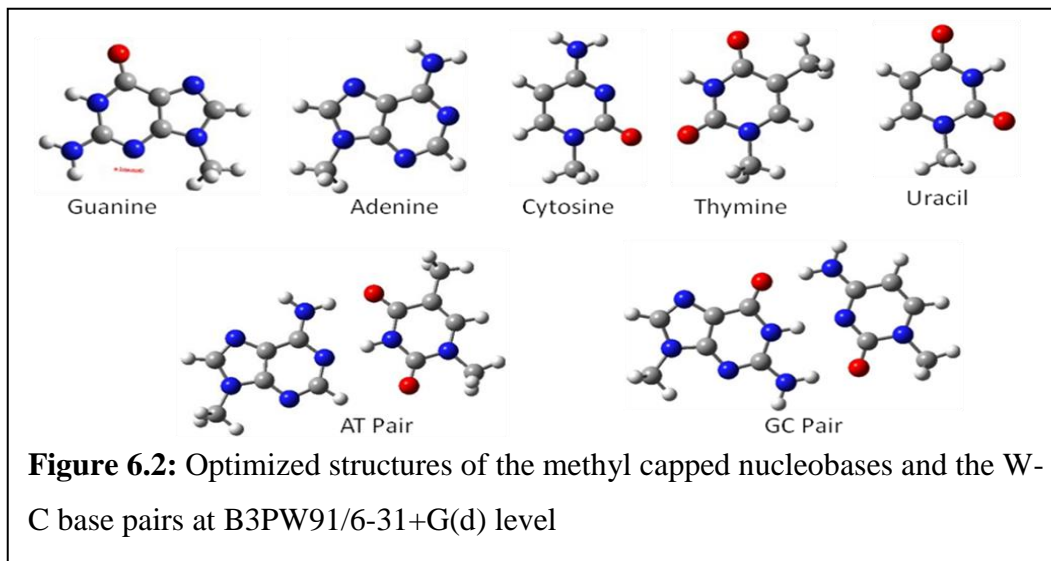


6.2: Computational Techniques:

In the present study, calculations for understanding the interaction between nucleobases and Au_n ($n = 3-6$) clusters are performed using Gaussian09 software package.⁵⁷ For the adequate modeling purpose, we have tried different orientations for Au_n cluster reviewed through earlier reported literatures.^{22,24} The optimized structures of

gold clusters (in different orientation and shape) are given in Figure 6.1. The most stable geometry of the five nucleobases along with the W-C base pairs are provided in Figure 6.2. To reduce computational cost of the calculation phosphate linkage sites of the individual nucleobases are capped with methyl groups. The two Watson-Crick base pair combinations (A-T and G-C) are generated by trimming the reported PDB crystal structure 2VAH up to a single base pair unit. The phosphate linkage sites of the base pairs are also capped with methyl groups.

All the geometries of the Au_n clusters and nucleobases are optimized, without imposing any restrictions, using hybrid Becke three-parameter exchange density functional combined with the gradient-corrected Perdew-Wang 91 correlation functional (B3PW91)⁵⁸. Selection of specific method (i.e., B3PW91) is based on the reliability of results reviewed through earlier reported literatures on small gold-clusters.⁵⁹⁻⁶¹ To provide additional support to the DFT based calculations, the CDASE scheme based parameters are also evaluated at MP2 level.⁶² Here, for gold atoms scalar relativistic effective core potential Stuttgart/Dresden (SDD) basis set⁶³ is used (as implemented in the Gaussian09 (G09) package⁵⁷). Application of small-core ECPs (19-electron ECP) can minimize errors in the treatment of electron correlation.⁶⁴ The geometries of nucleobases are optimized at the same level of theory using all-electron 6-31+G(d) basis sets. Similarly, calculations for the Gold-DNA combined system are carried out at B3PW91 level of theory using mixed basis sets (i.e., GenECP/SDD for the Au and 6-31+G(d) basis



sets are used for light atoms). Subsequent frequency analysis is also performed on every structure to ensure that no imaginary frequency is present (*i.e.*, minimum energy state has been achieved in potential energy surface).

Vertical ionization potential (IP) and electron affinity (EA) values are considered in the present study to evaluate η , μ , ΔN etc. These quantities were calculated by running single point calculations for cationic and anionic systems using the optimized geometry of the corresponding neutral structures. While restricted level of theory (RB3PW91) was used for the neutral systems, unrestricted level of the same theory (UB3PW91) was used for calculations of ionic systems.

6.3: Results and Discussions:

The interaction of gold nanoclusters with DNA has enormous potential to become integral part of the future nanobiotechnology and core building block for many sophisticated detection and sensor devices.⁶⁵ Basically, a covalent bonding between gold-clusters and nucleobases reinforce stability to the overall complex. The anchored covalent bond is formed between oxygen or nitrogen atom of the nucleobase and the Au atom of the clusters. Thus the lone pairs on oxygen or nitrogen atom are in action to share the 5d and 6s orbitals of Au atom. The relative stability of the Au-DNA composite system with the variation in shape and size of the gold-clusters is one of the prime concerns for the present study. Although, the number of gold atoms for a particular cluster is fixed but a slightly different structural orientation of the cluster has significant impact on the stability of the composite system. It is expected that the precise understanding of the charge transfer process between DNA and gold clusters is a critical factor to tune the electronic properties of the composite system as per the requirement. Various important aspects of the structural stability, charge transfer process and the rate of the interaction between Au-clusters and DNA bases will be addressed in the following sub-sections.

6.3.1: Understanding the interaction between gold-clusters and DNA bases using CDASE scheme based parameters:

In the introduction (Chapter I), we have extensively discussed the role of different parameters of CDASE scheme. Application of these parameters substantially reduces the computational cost to analyze the kinetic and thermodynamic aspects of a particular

interaction. The two components of the stabilization energy (i.e., $\Delta E_{B(A)}$, and $\Delta E_{A(B)}$), difference in global electrophilicity (Δw), along with the charge transfer (ΔN) values are known to exhibit reliable outcome of the kinetics and thermodynamics a reactive interaction.⁵³⁻⁵⁶ To be more specific, the positive energy component ($\Delta E_{B(A)}$), difference of global electrophilicity (Δw) can be correlated to the kinetics of interaction between the two the systems, whereas, the negative energy component ($\Delta E_{A(B)}$) and stabilization energy ($\Delta E_{SE(AB)}$) can provide information regarding the thermodynamic stability of the adduct formed. The charge transfer component (ΔN) can be correlated to both.

(i) *Evaluation of the kinetics of interaction between gold-cluster and nucleobases:*

(a) On the basis of their difference in global electrophilicity (Δw) values:

The trend of interaction between gold-clusters and DNA bases can be determined from the difference of global electrophilicity values (i.e., $\Delta w = w_A - w_B$). Where A denotes the acceptor and B denotes the donor species. According to consideration here gold-clusters are the acceptors (with global electrophilicity w_A) and the nucleobases are the donors (having global electrophilicity w_B). Table 6.1 (a) and 6.1 (b) contain the Δw values (in kcal/mol) evaluated at B3PW91 and MP2 levels, respectively.

The positive Δw values in all cases clearly justify the choice of gold clusters as acceptors and nucleobases as donors. As per the proposed CDASE scheme the global electrophilicity difference (i.e., Δw) is a kinetic parameter and can be correlated to the rate of interaction between gold-clusters and nucleobases. Higher the value of Δw , faster will be the interaction. The interactions of four-atom gold-clusters with nucleobases are found to be highly favourable from the computed Δw values. More specifically, the Au₄-2 (Figure 6.1) is the most active gold-clusters against all the nucleobases. A significant variation in the activity of gold-clusters is observed with the change in their sizes and shapes. As the number of Au atoms increase from three (in Au₃) to six (in Au₆) the Δw values does not increase as per expectation. Interestingly, clusters containing equal number of Au atoms show variation in their activity providing a different structural orientation.

The purine bases, adenine and guanine, are more active towards gold-clusters in comparison to the pyrimidine counterparts cytosine and thymine. It is worth mentioning here that the mutagenic base uracil is the least reactive one against all types of Au_n

clusters. As per the generated Δw values, the Watson-Crick base pair GC interacts faster with gold-clusters than the AT pair. In a recent study, Jena *et al.* also reported a slightly more favourable interaction between GC and small gold-clusters over AT base pair.²⁴ It is also noteworthy that the Δw values computed at DFT (B3PW91) and MP2 level theories produce similar trends. As in the B3LYP methods interaction of five nucleobases with Au_n -clusters follows the order $G > A > C > T > U$, but in MP2 method, few cases we have observed minor variation in the expected interaction trend of the nucleobases with Au_n -clusters.

(b) On the basis of the values of positive energy component ($\Delta E_{B(A)}$):

In the proposed CDASE scheme, $\Delta E_{B(A)}$ is identified as the energy raising part of an interaction between a donor and an acceptor system. Thus, it is a reasonable assumption that this energy helps to cross the barrier height of the transition state. So, this parameter ($\Delta E_{B(A)}$) can logically be correlated to the kinetic aspects of a particular reactive interaction and hence called the ‘internal assistance’.

This essentially means that higher value of $\Delta E_{B(A)}$ predicts a kinetically more favorable interaction between gold-clusters and nucleobases. In Table 6.2 (a) and 6.2 (b) the $\Delta E_{B(A)}$ values for 70 pairs of gold-clusters and nucleobases (calculated at B3PW91 and MP2 level of theories).

As per the computed $\Delta E_{B(A)}$ values, GC pair seems to interact with gold cluster more favorably than the AT pair. This holds true for all the chosen gold clusters. If we look into the individual nucleobases, purine (guanine and adenine) bases show relatively faster interaction with Au_n clusters (higher values of $\Delta E_{B(A)}$) than the pyrimidine (cytosine, thymine and uracil) ones. Nucleobase guanine has the highest and uracil has the lowest values of $\Delta E_{B(A)}$ against all the Au_n clusters. The observed trend for the relative rate of interaction of gold-clusters with five nucleobases can be represented as $G > A > C > T > U$. Rapino and co-workers reported a similar trend through their molecular dynamics study.⁶⁶ They have performed MD simulation to investigate the stability and dynamics of DNA bases on gold surface and observed relatively higher rate of interaction for purine bases with gold surface, whereas for pyrimidine base the activity was moderate.

(c). On the basis of charge transfer (ΔN) values:

The formation of covalent bond that anchored nucleobases with the gold nanoparticles is the origin of stability for the composite system.²² The nucleobases are well known for their labile lone-pair electrons located over N and O atoms. Charge transfer (ΔN) values calculated for the different combinations of gold-clusters and nucleobases at B3PW91 and MP2 level are presented in Tables 6.3 (a) and 6.3 (b), respectively.

The positive value for ΔN accounts favourable interaction between a particular pair of gold-cluster and nucleobase. A numerically higher value of charge transfer ascertains relatively faster Au_n -nucleobase interaction. The calculated charge transfer values indicate the interaction between guanine and Au_n clusters to be the most preferable ones, followed by adenine, cytosine, thymine, and uracil, in decreasing order. Based on ΔN values, it is clear that among the small gold-clusters Au_4 is the one, which is most active towards DNA. Also, according to the calculated charge transfer values GC base pair exhibit higher reactivity with small gold-clusters than when compared to the AT base pair. The overall trend of interaction of the five individual nucleobases with gold-clusters appeared to be $G > A > C > T > U$, which is identical to the trend generated by $\Delta E_{B(A)}$ values.

The ΔN values generated at the MP2 level show minor vibration in the trend of reactivity. These variations are mainly observed between cytosine and thymine [Table 6.3 (b)]. The trends with other nucleobases as well as base pairs are more or less similar to those obtained by the DFT methods.

(ii) Evaluation of thermodynamics of interaction between gold-cluster and nucleobases:

(a) On the basis of the values of the negative energy component ($\Delta E_{A(B)}$):

$\Delta E_{A(B)}$ is the energy lowering part of the overall stabilization energy and typically a negative quantity. Hence, $\Delta E_{A(B)}$ value is a specific parameter to determine the thermodynamic stability of the adduct formed by the interaction of gold-clusters and nucleobases. The $\Delta E_{A(B)}$ values for different combinations of gold-clusters and nucleobases computed at B3PW91 and MP2 levels are provided in Table 6.4 (a) and 6.4 (b), respectively.

Observed $\Delta E_{A(B)}$ values for the interaction between Au_4 -clusters and nucleobases are found to be most negative ones. This infers that Au-clusters form most stable

complexes with nucleobases. The effect of structural orientation of the clusters (having equal number of gold atoms) on the stability of cluster-nucleobase composite systems is apparent from the calculated $\Delta E_{A(B)}$ values. Three different structural orientations for each of the Au₄, Au₅, and Au₆ clusters show significant variation in the thermodynamic stability of the corresponding Au_n- nucleobase composite systems. The general trend of thermodynamic stability for the composite systems with the type of gold-clusters follows the order Au₄ > Au₆ > Au₅ > Au₃, although some minor variations are there.

As far as nucleobase is concerned guanine produce the most stable adduct within gold clusters followed by adenine, cytosine, thymine, and uracil. Some of the already reported experimental and theoretical studies validate the observed trend of interaction generated from the $\Delta E_{A(B)}$ values.^{21,66} Ostblom *et al.* investigated the desorption dynamics of nucleobases adsorbed on gold surface through temperature programmed technique.²¹ This study was focused on the complex adsorption behaviour of the purine bases adenine and guanine on gold surface. The conclusion was that apparent binding energy of the substrate is controlled by the adhesive (adenine) and cohesive (guanine) interactions.²¹ The trend of the experimentally observed desorption peak energy for the interaction of nucleobases with gold clusters follows the order of G > A > C > T.²¹ A qualitative measure of the $\Delta E_{A(B)}$ values with respect to the experimentally observed desorption peak energy is presented below,

Nucleobases	desorption peak energy (in kJ/mol) ⁶⁷	CDASE scheme based $\Delta E_{A(B)}$ values (in kcal/mol) (Au ₄ -3) at B3PW91 method
Guanine	139 ±2	-36.295
Adenine	136 ±2	-32.658
Cytosine	122 ±2	-29.164
Thymine	104 ±2	-24.891

It is obvious that the interaction of guanine with the gold clusters is thermodynamically the most favorable one. From the point of thermodynamic stability Watson-Crick base

pair GC forms moststable adduct with gold-clusters than AT and this is true in both the methods.

(b) On the basis of overall stabilization energy ($\Delta E_{SE(AB)}$) values:

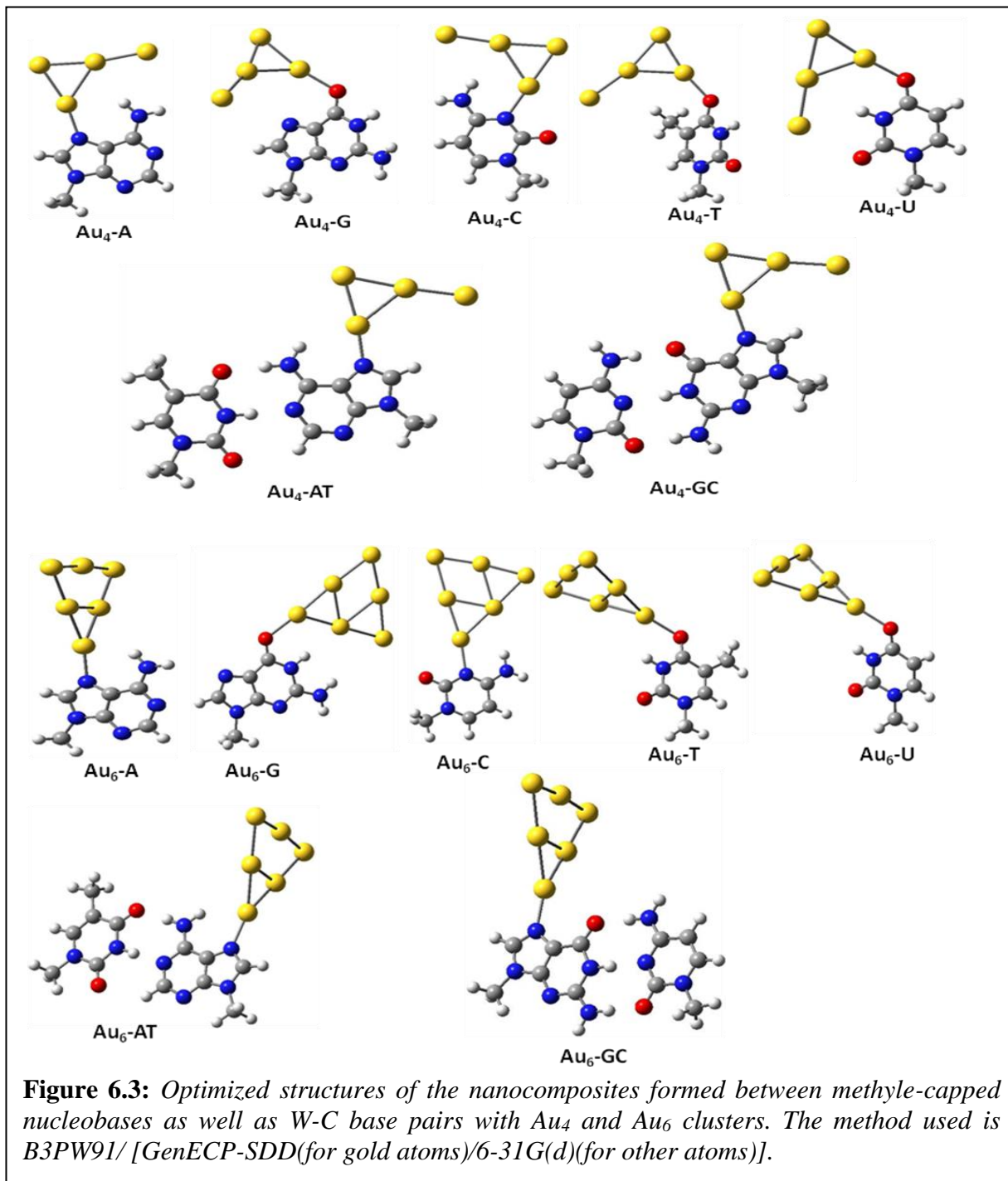
The overall stabilization energy, $\Delta E_{SE(AB)}$, is the sum of the positive ($\Delta E_{B(A)}$) and negative ($\Delta E_{A(B)}$) energy components. Overall stabilization energy is a negative quantity and provides valuable information regarding the stability of the composite system formed between gold cluster and nucleobase (or base pair). Higher the value of $|\Delta E_{SE(AB)}|$ greater will be the stability of the Au_n -DNA complex. Calculated $\Delta E_{SE(AB)}$ values (for different Au_n -DNA composite systems) at B3PW91 and MP2 level of theories are given in Table 6.5 (a) and (b), respectively.

As per $\Delta E_{SE(AB)}$ values the stability Au_n -nucleobase composite system vary with the nucleobase as follows $U < T < C < A < G$. The binding interactions of the purine bases with gold-clusters are thermodynamically more favourable when compared to that with the pyrimidine bases. It is encouraging to note that Demers *et al.*⁸, through their reflection absorption FT-IR and temperature programmed desorption (TPD) studies, also obtained similar kind of results. In another experimental study, Storhoff and co-workers investigated the binding affinity of deoxynucleosides (dA, dG, dC, and dT) for gold nanoparticles⁶⁷ and found lowest binding affinity for binding between dT and gold nanoparticles. The experimental study by Kimura-Suda *et al.* (using FTIR and XPS techniques) also provides reasonable justification for the lowest binding affinity of the nucleobase thymine with gold-clusters.²⁵ Barring the sole expectation of guanine the trend of binding affinity observed by Kimura-Suda *et al.* matches exactly with the ones obtained from CDASE scheme based $\Delta E_{SE(AB)}$ values. In Table 6.6, we have reported a qualitative comparison between the experimental results and CDASE scheme based stabilization energy values for the interaction between gold clusters and individual nucleobases.

As far as stability of Au_n -nucleobase (Au_n -nb) complex is concerned, the trend is as follows: Au_4 -nb $>$ Au_6 -nb $>$ Au_5 -nb $>$ Au_3 -nb. Also, the stability of the complex Au_4 -GC is found to be higher than the complex formed between Au_4 and AT. Kryachko and Remacle have attributed the higher stability of the Au_4 -GC complex over that of Au_4 -AT complex to the more favourable unconventional hydrogen bonding in the former one⁶⁸

6.3.2: Conventional binding energy calculation for selected gold-clusters and nucleobase composite systems:

It is obvious from the above discussion that proposed CDASE scheme based formalism is a reliable, alternative, and most importantly, computationally cost effective approach to explore the interaction between gold-clusters and nucleobases. To test the



reliability of the CDASE scheme based parameters in this particular section we have reported the findings of the conventional binding energy calculations for the adduct formation between Au₄ and Au₆ with the five chosen nucleobases as well as the two Watson-Crick base pairs. Density Functional Theory based calculations are found to be reliable to explore the molecular dissociation, energetics of interaction processes, electronic rearrangements during complex formation, surface phenomena, etc.⁶⁹⁻⁷¹ Basically, the ability to treat d-electrons with reasonable accuracy significantly improve the scope of DFT based approach to study different interactions involving d-block elements.

Optimized structures (at B3PW91/ genECP-SDD(gold)U6-31+G(d) (DNA bases) level of theory) of the combined Au_n-nucleobase systems are given in Figure 6.3 and corresponding B.E. values are reported in Table 6.7.

The binding energy value for a particular interaction is the measure of thermodynamic stability for the resultant composite system. Calculated BE values (Table 6.7) indicate greater thermodynamic stabilities for the Au₄-nucleobase composites and than the Au₆-nucleobase ones. A probable explanation of the higher stability of the former composite systems can be attributed to the presence of more number of nonconventional H-bonding interactions as suggested by Kryachko *et al.*^{22,68} They assumed that the favorable structural orientations of Au₄-clusters help to generate more H-bonding interactions with nucleobases than Au₆-clusters.⁶⁸

The two purine bases guanine and adenine form more stable complexes with the than the corresponding pyrimidines with Au₄-clusters. Calculated BE values for guanine and adenine with Au₄-cluster is -36.67 and -30.32 kcal/mol, respectively. This observation can be correlated to the anchored Au-O bond distance in the complex. In the optimized structures the Au-O anchoring bond is found to be slightly shorter (2.04 Å⁰) in Au₄-guanine complex compared to the anchored Au-N bond length in Au₄-adenine (2.1 Å⁰). Also, a planar structural orientation is observed for the Au₄-adenine complex. But a significant deviation from the planarity is appeared for the Au₄-guanine complex as the guanine is moving out of the clusters plane (Figure 6.3). The computed binding energy values for pyrimidine bases decrease in the following order C > T > U. The BE value for Au₄- cytosine complex is -18.6 kcal/mol followed by -17.11 and -16.47 kcal/mol for

complexes with thymine and mutagenic base uracil, respectively. Here, the Au-DNA anchoring bond lengths for cytosine, thymine and uracil are found to be 2.13 Å, 2.17 Å and 2.19 Å, respectively. All the three pyrimidine bases prefer the planar orientation with the gold-clusters in the complex form. The two W-C base pairs AT and GC have shown moderate binding stability with the Au₄ clusters. A higher degree of stability is observed for the Au₄-GC complex (binding energy value -27.91 kcal/mol) compared to that of Au₄-AT, having BE value -23.41 kcal/mol. The anchored Au-N bond in Au₄-GC is 0.05 Å shorter than the corresponding Au-N bond in Au₄-AT complex. It is interesting to note that in the individual guanine molecule the clusters prefer to bind with O₇ atom, but after pairing with cytosine (i.e., in the GC base pair) the N₄ atom is the most preferable site for the covalent binding interaction. As the N₂ site of the guanine is capped with methyl group for computational simplification the neighboring N₁₁ is not a preferable site for the interaction with Au clusters (probably, due to the steric hindrance from the methyl group). Kumar *et al.* also reported the preferential binding interaction of Au₄ clusters through the N₄ atom of the guanine.⁷²

A significant decrease in the stability of the complexes formed between Au₆ and nucleobases from those formed between Au₄ and nucleobases is observed. However, the qualitative trend of stabilities is exactly similar in both the cases and that is Au_n-G > Au_n-A > Au_n-C > Au_n-T > Au_n-U. Also, the trend of the stabilities of the complexes formed between Au_n clusters (n=4,6) with base pairs are similar and that is Au_n-GC > Au_n-AT.

The structural aspects of the combined gold nanoparticle-DNA system exhibit significant deviation from planarity for the Au₆-clusters. However, this is unlikely from the Au₄-clusters where most of the geometries for the composite system display a perfectly planar structural orientation after the attachment of gold-clusters with the nucleobases. During the interaction, Au₆-clusters is observed to be moving away from the plane containing the nucleobase and prefers to stay almost perpendicular to it. Although, the steric hindrance, arises from the relatively large size of Au₆-clusters, is minimized by preventing the combined system attaining a planar structural orientation the H-bonding interaction with nucleobases become unfavorable.²² Thus in the present study we can correlate the lower stability of the complexes of Au₆ clusters with nucleobases to the non-

planner structural orientations which constraint the possibility of nonconventional H-bonding interactions.

6.3.3: Synchronous transit-guided quasi-Newton (STQN) Transition State (TS) calculation for some selected composite systems formed by gold-clusters and nucleobase:

Conventionally the rate of an interaction is understood from the transition state calculation. So, to crosscheck the findings of CDASE scheme based kinetic parameters energy values of the transition state is computed here.

The STQN⁷³ method is used to optimize the transition state structures of the composite formed by Au₄ and Au₆ clusters with nucleobases and base pairs. The level of computation is B3PW91/ genECP-SDD(gold)U6-31G+(d)(DNA base). The option used is QST3 where a guess transition state geometry is incorporated in between the initial and the final optimized geometries of the complex to speed-up the convergence process. Additional frequency calculation is performed on the transition state structures and the presence of a single imaginary frequency ensures the proper transition state geometry for Au_n-nucleobase composite systems.

Calculated transition state energy barrier for different composite systems are reported in Table 6.8. The TS energy barriers for the Au₄-nucleobase composite systems are found to be lower than the Au₆-nucleobase composites. This justifies the claim by CDASE scheme on the kinetic preference of Au₄ clusters over Au₆ clusters while forming the composite systems with nucleobases.

The two purine bases guanine and adenine exhibit very low TS energy barriers while interacting with Au₄ clusters. The barrier heights are 1.14 kcal/mol and 1.76 kcal/mol for guanine and adenine, respectively. Among the pyrimidine bases, uracil shows highest energy barrier for the complex formation with Au₄-clusters with the barrier height of 10.81 kcal/mol. This is followed by 6.23 kcal/mol and 1.89 kcal/mol for thymine and cytosine, respectively. Calculated TS energy barriers are relatively higher for the interaction between Au₄ clusters and the two W-C base pairs. These values are 11.89 kcal/mol and 11.06 kcal/mol, respectively.

The values of the barrier heights computed through STQN calculation for the interaction of Au₆ clusters with nucleobases are higher than the corresponding values

generated from the interaction with Au₄ clusters. This indicates that the complex formation between Au₆ clusters and nucleobases is relatively slower. The predicted trend of interaction, based on the values of the TS energy barrier for the five nucleobases with Au₆ clusters is U < T < C < A < G. Also, the calculated barrier heights show that the interaction between Au₆ clusters and GC base pair is much faster (TS energy barrier is 6.64 kcal/mol) than the interaction with the AT pair (TS energy barrier is 19.15 kcal/mol).

6.3.4: TDDFT analysis to determine the nature of electronic excitations in gold cluster-DNA composite systems:

As the gold-DNA composite nanomaterials are the potential building blocks for nanobiodevices, it is highly demanding to figure out the nature of associated electronic transitions in the hybrid systems to manipulate electronic properties according to the mechanical requirement. Keeping this particular aspect in mind TDDFT computation⁷⁴ is carried out on the two specific orientations when Au₄ and Au₆ clusters interact with nucleobases. Water is taken as the solvent medium and the solvent effect is incorporated in the calculation through Integral Equation Formalism-Polarizable Continuum Model (IEF-PCM)⁷⁵ as implemented in Gaussian09.⁵⁶

The TDDFT results are given in Table 6.9 and 6.10 for Au₄-Nucleobase and Au₆-nucleobase composite systems, respectively. Excitation of the singlet state for the Au-DNA complexes is mainly considered here. In case of Au₄-nucleobase, composite system the range of the excitation energy is observed to be in between 3.10 eV to 3.50 eV, which correspond to the wavelength values from 350 to 400 nm. This indicates that the absorption occurs at UV-VIS region of the electromagnetic radiation, which is also reported earlier.⁷⁶⁻⁷⁹ However, a significant amount of red shifted absorption wavelength is observed for the Au₆-nucleobase composite systems. For these systems the computed wavelengths vary from 400 to 470 nm (variation in excitation energy values is from 2.60 to 3.00 eV). The % transition probabilities for various electronic excitations between different frontier molecular orbitals (FMO) for the first three singlet-excited states are also reported in Table 6.9 and 6.10. Relatively higher possibility for simple HOMO → LUMO type of electronic transitions in case of all the Au₄-nucleobase composite systems is observed except thymine, where HOMO-1 to LUMO seems to have higher transition

probabilities. Although, we have emphasized on $S_0 \rightarrow S_1$ type of transitions, the other two associative absorptions (due to $S_0 \rightarrow S_2$ and $S_0 \rightarrow S_3$) are also important to determine the photophysical properties of Au₄-nucleobase nanocomposites. On the other hand, probable electronic excitations associated with Au₆-nucleobase composites do not follow any regular trend (Table 6.10). It is clear that the HOMO-1 \rightarrow LUMO and HOMO \rightarrow LUMO+1 type of electronic transitions have profound impact on the photophysical properties of the Au₆-DNA complex. It is worth mentioning here that the FMOs of both types of complexes are located on the gold atoms of the complex and the AOs of corresponding nucleobases do not have much contributory effect on FMOs. To have more clear understanding on FMOs, we have plotted the orbital representations and the corresponding major AO contributions for all the gold cluster- DNA composites in Table 6.11. Indeed, solo contribution of s, p and d atomic orbitals of the individual gold atoms in the formation of frontier molecular orbitals is evident from the TDDFT calculations.

6.4: Conclusions:

In the present study, kinetic and thermodynamic aspects of the interaction of small gold-clusters and nucleobases along and the Watson-Crick base pairs are analyzed using an unconventional approach based on Density Functional Reactivity Theory (DFRT). Observations made by the DFRT based CDASE scheme are also augmented by the conventional binding energy (BE) and STQN-transition state (TS) calculations. Time-dependent DFT (TDDFT) calculations are also incorporated to understand the probable electronic transitions, which may occur in the corresponding nanobiocomposites.

CDASE scheme based thermodynamic parameters claim that the purine bases form relatively more stable nanocomposites with gold-clusters than the pyrimidine bases. Interaction of guanine with Au_n (n=4, 6) clusters are found to be the most favorable ones both kinetically and thermodynamically. Mutagenic base uracil exhibits very low tendency to interact with the gold-clusters. On the basis of CDASE scheme based parameters the overall trend of interaction of the five nucleobases with gold-clusters (Au₄ and Au₆) follow the order $G > A > C > T > U$ and it is exactly matching with the earlier reports.^{21,22,25,68} CDASE scheme based study, along with the conventional theoretical

approach (B.E. and TS calculations) predict greater activity for GC base pair than AT pair against Au_n (n=4, 6) clusters.

The effect of size and orientation of the clusters play crucial role in determining the stability of the composite systems. It is observed that the rate of interaction of Au₄ clusters with nucleobases are higher and the corresponding nanocomposites are also stabler than the ones formed by Au₆-clusters. This is, probably, due to the favorable structural orientations of the Au₄-clusters which enable them to form more number of nonconventional H- bonds with nucleobases.²² The above findings are also supported by the conventional BE and TS calculations. However, clusters containing equal number of atoms but having different structural orientations exhibit significant variation in stability as well. Thus, it is the favorable structural orientation of the clusters that induce maximum stability to the nanocomposite.

Calculated CDASE scheme based parameters justify the impact of structural orientation on the stability of adduct formation between Au_n-cluster and nucleobases. We have considered three different orientations for each four-atoms, five-atoms and six-atoms gold clusters and accordingly, a definite variation in the kinetic and thermodynamic stabilities is observed for the final adducts. Although, the number of gold atoms are same for a particular group of clusters (e.g., Au₄), depending on their structural orientation it exhibits significant variation in the stability of complex formation with nucleobases.

The photophysical properties of the nanocomposites are analyzed through TDDFT calculations. The high sensitivity of electronic properties (electronic transition, in particular) nanoscale level could be understood from the TDDFT study. Even for a minor increment in the cluster size from 4 to 6 gold atoms, there is a significant variation in the electronic excitations as well as the band gap of the composites. These are evident from the results given in the Table 10 and 11 and thus supports the difference in their kinetic and thermodynamic aspects as shown by CDASE scheme based parameters as well as conventional binding energy (BE) and STQN-TS calculations.

This particular study is a part of our continuing effort to test the reliability of CDASE scheme in studying some interesting chemical and biological interactions.⁵³⁻⁵⁶ This formalism is computationally cost effective for intensive quantum mechanical calculations as it considers the two interacting species in isolation rather than taking them

together (e.g., in conventional supermolecular approach, BE calculations, transition state optimization, etc.). It is possible to evaluate three types of parameters, kinetic, thermodynamic as well as charge transfer for a particular interaction from a single CDASE scheme based computation. This significantly reduces the computation time that is involved in the conventional approaches. Comprehensive decomposition analysis of stabilization energy (CDASE) is simple DFRT based approach and has the potential to become an alternative theoretical tool, albeit qualitative, to explore different reactive interactions.

References:

1. H. Yan, X. Zhang, Z. Shen, N. C. Seeman, *Nature* 2002, **415**, 62.
2. C. Mao, W. Sun, Z. Shen, N. C. Seeman, *Nature* 1999, **397**, 144.
3. K. A. Peterlinz, M. R. Georgiadis, T. M. Herne, M. J. Tarlov, *J. Am. Chem. Soc.* 1997, **119**, 3401.
4. L. He, M. D. Musick, S. R. Nicewarner, F. G. Salinas, S. J. Benkovic, M. J. Natan, C. D. Keating, *J. Am. Chem. Soc.* 2000, **122**, 9071.
5. A. B. Steel, T. M. Herne, J. M. Tarlov, *Anal. Chem.* 1998, **70**, 4670.
6. J. J. Storhoff, R. Elghanian, R. C. Mucic, C. A. Mirkin, R. L. Letsinger, *J. Am. Chem. Soc.* 1998, **120**, 1959.
7. D. Y. Petrovykh, H. Kimura-Suda, L. J. Whitman, M. J. Tarlov, *J. Am. Chem. Soc.* 2003, **125**, 5219.
8. L. M. Demers, M. Ostblom, H. Zhang, N. H. Jang, B. Liedberg, C. A. Mirkin. *J. Am. Chem. Soc.* 2002, **124**, 11248.
9. J. J. Storhoff, R. Elghanian, C. A. Mirkin, R. L. Letsinger, *Langmuir* 2002, **18**, 6666.
10. S. H. Park, R. Barish, H. Li, J. H. Reif, G. Finkelstein, H. Yan, T. LaBean, *Nano Lett.* 2005, **5**, 693.
11. K. Keren, M. Krueger, R. Gilad, G. Ben-Yoseph, U. Sivan, E. Braun, *Science* 2002, **297**, 72.
12. H. J. Kim, Y. Roh, B. Hong, *Langmuir* 2010, **26**, 18315.
13. E. Braun, Y. Eichen, U. Sivan, G. Ben-Yoseph, *Nature* 1998, **391**, 775.
14. Ch. Adessi, S. Walch, M. P. Anantram, *Phys. Rev. B* 2003, **67**, 081405.
15. F. Moreno-Herrero, P. Herrero, F. Moreno, J. Colchero, C. Gomez-Navarro, J. Gomez-Herrero, A. M. Baro, *Nanotechnology* 2003, **14**, 128.
16. J. Shendure, R. Mitra, C. Varma, G. Church, *Nat. Rev. Genet.* 2004, **5**, 335
17. D. Fologea, M. Gershow, B. Ledden, D. S. McNabb, J. A. Golovchenko, J. L. Li, *Nano Lett.* 2005, **5**, 1905.
18. R. Schreiber, S. Kempter, S. Holler, V. Schüller, D. Schiffels, S. S. Simmel, P. C. Nickels, T. Liedl, *Small* 2011, **7**, 1795.
19. J. Richter, M. Mertig, W. Pompe, I. Monch, H. K. Schackert, *Appl. Phys. Lett.* 2001, **78**, 536.
20. X. Li, Z. Cai, M. D. Sevilla, *J. Phys. Chem. A* **2002**, *106*, 1596.
21. M. Ostblom, B. Liedberg, L. M. Demers, C. A. Mirkin, *J. Phys. Chem. B* 2005, **109**, 15150.
22. E. S. Kryachko, F. Remacle, *Nano Lett.* 2005, **5**, 735.
23. G. J. Cao, H. G. Xu, R. Z. Li, W. Zheng, *J. Chem. Phys.* 2012, **136**, 014305.
24. N. K. Jena, K. R. S. Chandrakumar, S. K. Ghosh, *J. Phys. Chem. C* 2012, **116**, 17063.
25. H. Kimura-Suda, D. Y. Petrovykh, M. J. Tarlov, L. J. Whitman, *J. Am. Chem. Soc.* 2003, **125**, 9014.
26. Density—Functional Theory of Atoms and Molecules; R. G. Parr, W. Yang, Oxford University Press: New York, 1989.
27. R. G. Parr, W. Yang, *Annu. Rev. Phys. Chem.* 1995, **46**, 701.

-
28. W. Kohn, A. D. Becke, R. G. Parr, *J. Phys. Chem.* 1996, **100**, 12974.
 29. A Chemist's Guide to Density Functional Theory; W. Koch, M. Holthausen, Wiley-Vch Weinheim, 2000.
 30. P. Geerlings, F. De Proft, W. Langenaeker, *Chem. Rev.* 2003, **103**, 1793-1874.
 31. R. G. Parr, R. G. Pearson, *J. Am. Chem. Soc.* 1983, **105**, 7512-7516.
 32. R. G. Parr, W. Yang, *J. Am. Chem. Soc.* 1984, **106**, 4049.
 33. W. Langenaeker, F. De Proft, P. Geerlings, *J. Phys. Chem.* 1995, **99**, 6424.
 34. W. Yang, R. G. Parr, *Proc. Natl. Acad. Sci. U. S. A.* 1985, **82**, 6723.
 35. R. K. Roy, S. Krishnamurti, P. Geerlings, S. Pal, *J. Phys. Chem. A.* 1998, **102**, 3746.
 36. R. K. Roy, F. De Proft, P. Geerlings, *J. Phys. Chem. A.* 1998, **102**, 7035.
 37. S. Saha, R. K. Roy, *J. Phys. Chem. B.* 2007, **111**, 9664.
 38. S. Saha, R. K. Roy, *J. Phys. Chem. B.* 2008, **112**, 1884.
 39. W. Yang, W. J. Mortier, *J. Am. Chem. Soc.* 1986, **108**, 5708.
 40. S. K. Ghosh, M. A. Berkowitz, *J. Chem. Phys.* 1985, **83**, 2976.
 41. M. K. Harbola, P. K. Chattaraj, R. G. Parr, *Isr. J. Chem.* 1991, **31**, 395.
 42. N. Russo, M. Toscano, A. Grand, T. Mineva, *J. Phys. Chem. A*, 2000, **104**, 4017.
 43. S. Krishnamurty, S. Pal, *J. Phys. Chem. A*, 2000, **104**, 7639.
 44. R. G. Parr, R. A. Donnelly, M. Levy, W. E. Palke, *J. Chem. Phys.* 1978, **68**, 3801.
 45. R. S. Mulliken, *J. Chem. Phys.*, 1934, **2**, 782.
 46. A. T. Maynard, M. Huang, W. G. Rice, D. G. Covell, *Proc. Natl. Acad. Sci. U. S. A.* 1998, **95**, 11578.
 47. R. G. Parr, *J. Am. Chem. Soc.* 1999, **121**, 1922.
 48. P. W. Ayers, R. G. Parr, *J. Am. Chem. Soc.* 2001, **123**, 2007.
 49. A. Cedillo, R. Contreras, M. Galvan, A. Aizman, J. Andres, V. S. Safont, *J. Phys. Chem. A* 2007, **111**, 2442.
 50. P. Perez, L. R. Domingo, M. Duque-Norena, E. A. Chamorro, *THEOCHEM* 2009, **895**, 86.
 51. R. Bhattacharjee, R. K. Roy, *J. Phys. Chem. A* 2014, **117**, 11528.
 52. P. Bagaria, S. Saha, S. Murru, V Kavala, B. Patel, R. K Roy, *Phys. Chem. Chem. Phys.* 2009, **11**, 8306.
 53. S. Saha, R. K. Roy, S. Pal, *Phys. Chem. Chem. Phys.* 2010, **12**, 9328.
 54. A. Sarmah, S. Saha, P. Bagaria, R. K. Roy, *Chem. Phys.* 2012, **394**, 29.
 55. A. Sarmah, R. K. Roy, *RSC Adv.* 2013, **3**, 2822.
 56. A. Sarmah, R. K. Roy, *J. Phys. Chem. C* 2013, **117**, 21539.
 57. GAUSSIAN 09, Revision C.01, Frisch, M. J. *et al.* Gaussian, Inc., Wallingford CT, 2009.
 58. K. Burke, J. P. Perdew, Y. Wang, In *Electronic Density Functional Theory: Recent Progress and New Directions*; J. F. Dobson, G. Vignale, M. P. Das, Eds.; Plenum: New York, 1998.
 59. E. A. Carter, W. A.; Goddard III, *J. Chem. Phys.* 1988, **88**, 3132.
 60. K. P. Huber, G. Herzberg, *Molecular Spectra and Molecular Structure*; Van Nostrand Reinhold: New York, 1979.

-
61. A. Lyalin, T. Taketsugu, *J. Phys. Chem. C*, 2009 **113**, 12930.
 62. C. Møller, M. S. Plesset, *Phys. Rev.* 1934, **46**, 618.
 63. M. Dolg, U. Wedig, H. Stoll, H. Preuss, *J. Chem. Phys.* 1987, **86**, 866.
 64. S. Hou, R. Li, Z. Qian, J. Zhang, Z. Shen, X. Zhao, Z. Xue, *J. Phys. Chem. A*, 2005, **109**, 8356.
 65. S. S. Mallajosyula, S. K. Pati, *J. Phys. Chem. Lett.* 2010, **1**, 1881.
 66. S. Rapino, F. Zerbetto, *Langmuir* 2005, **21**, 2512.
 67. J. J. Storhoff, R. Elghanian, C. A. Mirkin, R. L. Letsinger, *Langmuir* 2002, **18**, 6666.
 68. E. S. Kryachko, F. Remacle, *J. Phys. Chem. B* 2005, **109**, 22746.
 69. A. S. Barnard, L. A. Curtiss, *Nano Lett.* 2005, **5**, 1261.
 70. S. Chretine, M. Gordon, H. Matiu, *J. Chem. Phys.* 2004, **121**, 9925.
 71. A. Puzdder, A. J. Williamson, N. Zaitseva, G. Galli, L. Manna, A. P. Alivisatos, *Nano Lett.* 2004, **4**, 2361.
 72. A. Kumar, P. C. Mishra, S. Suhai, *J. Phys. Chem. A* 2006, **110**, 7719.
 73. C. Peng, H. B. Schlegel, *Isr. J. Chem.*, 1994, **33**, 449.
 74. M. E. Casida, C. Jamorski, K. C. Casida, D. R. Salahub, *J. Chem. Phys.* 1998, **108**, 4439.
 75. E. Cancès, B. Mennucci, J. Tomasi, *J. Chem. Phys.* 1997, **107**, 3032.
 76. K. Kelly, E. Coronado, L. Zhao, G. Schatz, *J. Phys. Chem. B* 2003, **107**, 668.
 77. A. Moores, F. Goettmann, *New J. Chem.* 2006, **30**, 1121.
 78. A. P. Alivisatos, *Science* 1996, **271**, 933.
 79. H. Pan, D. Li, J. Liu, J. Li, W. Zhu, Y. Zhao, *J. Phys. Chem. C* 2011, **115**, 14461.

Table 6.1 (a). Calculated values of the global electrophilicity difference (Δw) (in kcal mol⁻¹) for different combination of Au_n clusters (considered as acceptor, A) and nucleobases (considered as donor, B). The values are calculated using SDD basis sets for gold atoms and 6-31G(d,p) for other atoms. Method used are B3PW91 [Table 6.1 (a)] and MP2 [Table 6.1 (b)]

(a)

	Au₃	Au₄-1	Au₄-2	Au₄-3	Au₅-1	Au₅-2	Au₅-3	Au₆-1	Au₆-2	Au₆-3
Guanine	68.16	89.11	94.75	114.35	74.24	68.21	94.08	73.96	74.04	74.07
Adenine	64.92	85.87	91.52	111.11	71.01	64.97	90.84	70.72	70.80	70.84
Cytosine	61.94	82.89	88.53	108.13	68.02	61.99	87.86	67.74	67.81	67.85
Thymine	56.40	77.35	82.99	82.32	62.48	56.45	82.32	62.20	62.28	62.31
Uracil	54.68	75.63	81.27	100.86	60.76	54.73	80.60	60.48	60.55	60.59
AT pair	58.98	79.93	85.57	105.16	65.06	59.02	84.90	64.78	64.85	64.89
GC Pair	61.62	82.56	88.21	107.80	67.70	61.66	87.53	67.42	67.49	67.53

(b)

	Au₃	Au₄-1	Au₄-2	Au₄-3	Au₅-1	Au₅-2	Au₅-3	Au₆-1	Au₆-2	Au₆-3
Guanine	56.35	80.84	84.28	80.82	77.74	59.41	70.68	56.52	56.55	56.49
Adenine	48.07	72.56	76.00	72.53	76.31	51.12	69.25	41.89	41.93	41.86
Cytosine	46.10	70.59	74.03	66.31	73.37	49.15	66.31	48.23	48.26	48.20
Thymine	43.15	67.64	71.08	67.62	71.40	46.21	64.34	46.26	46.30	46.24
Uracil	41.73	66.22	69.66	66.20	63.11	44.78	56.05	43.32	43.35	43.29
AT pair	44.15	68.64	72.08	68.62	75.31	47.21	68.25	44.32	44.35	44.29
GC Pair	48.27	72.76	76.20	72.74	71.20	51.32	64.14	48.43	48.47	48.40

Table 6.2 (a). Values of the positive energy component, $\Delta E_{B(A)}$, (in kcal/mol) calculated for different combination of Au_n clusters (considered as acceptor, A) and nucleobases (considered as donor, B). The values are calculated using SDD basis sets for gold atoms and 6-31G(d,p) for other atoms. Methods used are B3PW91 [Table 6.2 (a) and MP2 [Table 6.2 (b)].

(a)

	Au₃	Au₄-1	Au₄-2	Au₄-3	Au₅-1	Au₅-2	Au₅-3	Au₆-1	Au₆-2	Au₆-3
Guanine	16.81	24.18	26.38	27.82	16.65	20.22	23.98	23.07	23.08	23.08
Adenine	14.85	22.36	24.61	25.86	14.58	18.49	22.08	21.44	21.45	21.45
Cytosine	12.80	20.42	22.71	23.77	12.43	16.65	20.05	19.68	19.69	19.69
Thymine	9.90	17.83	20.22	21.07	9.41	14.12	17.35	17.32	17.33	17.33
Uracil	7.64	15.50	17.89	18.53	7.07	11.97	14.95	15.19	15.20	15.20
AT pair	14.98	23.16	25.61	27.02	14.68	18.95	22.87	22.13	22.14	22.14
GC Pair	18.09	26.30	28.73	30.53	17.95	21.79	26.15	24.90	24.92	24.92

(b)

	Au₃	Au₄-1	Au₄-2	Au₄-3	Au₅-1	Au₅-2	Au₅-3	Au₆-1	Au₆-2	Au₆-3
Guanine	9.75	18.72	19.72	18.71	14.58	16.45	16.79	16.61	16.61	16.60
Adenine	4.48	14.22	15.28	14.25	12.43	14.72	14.78	12.73	12.73	12.71
Cytosine	3.03	13.81	14.97	13.81	9.41	12.90	12.70	12.28	12.28	12.26
Thymine	3.69	13.69	14.78	13.69	7.07	10.32	9.76	12.25	12.25	12.23
Uracil	1.01	11.11	12.20	11.11	3.07	8.27	7.47	10.00	10.00	9.98
AT pair	5.87	15.83	16.92	15.83	14.68	14.86	14.91	14.08	14.09	14.07
GC Pair	9.88	21.25	22.50	21.24	17.95	17.57	18.10	18.40	18.40	18.38

Table 6.3 (a). Charge transfer (ΔN) values calculated for different combination of Au_n clusters (considered as acceptor, A) and nucleobases (considered as donor, B). The values are calculated using SDD basis sets for gold atoms and 6-31G(d,p) for other atoms. Method used are B3PW91 [Table 6.3 (a)] and MP2 [Table 6.3 (b)]

(a)

	Au₃	Au₄-1	Au₄-2	Au₄-3	Au₅-1	Au₅-2	Au₅-3	Au₆-1	Au₆-2	Au₆-3
Guanine	0.2115	0.2890	0.3110	0.3250	0.2097	0.2482	0.2870	0.2777	0.2779	0.2779
Adenine	0.1786	0.2560	0.2781	0.2900	0.1757	0.2170	0.2532	0.2469	0.2470	0.2470
Cytosine	0.1479	0.2250	0.2470	0.2570	0.1441	0.1877	0.2214	0.2179	0.2180	0.2180
Thymine	0.1087	0.1870	0.2095	0.2173	0.1036	0.1512	0.1825	0.1822	0.1823	0.1823
Uracil	0.0813	0.1577	0.1797	0.1855	0.0755	0.1241	0.1525	0.1547	0.1548	0.1548
AT pair	0.1772	0.2617	0.2856	0.2992	0.1740	0.2190	0.2587	0.2514	0.2515	0.2515
GC Pair	0.2257	0.3133	0.3379	0.3558	0.2242	0.2661	0.3117	0.2989	0.2991	0.2991

(b).

	Au₃	Au₄-1	Au₄-2	Au₄-3	Au₅-1	Au₅-2	Au₅-3	Au₆-1	Au₆-2	Au₆-3
Guanine	0.1338	0.2358	0.2463	0.2357	0.1757	0.2075	0.2111	0.2131	0.2132	0.2130
Adenine	0.0545	0.1598	0.1704	0.1598	0.1441	0.1772	0.1779	0.1446	0.1446	0.1444
Cytosine	0.0357	0.1514	0.1630	0.1513	0.1036	0.1490	0.1469	0.1358	0.1359	0.1357
Thymine	0.0441	0.1517	0.1625	0.1517	0.0755	0.1130	0.1072	0.1371	0.1371	0.1369
Uracil	0.0115	0.1180	0.1286	0.1180	0.0435	0.0876	0.0795	0.1070	0.1070	0.1068
AT pair	0.0730	0.1822	0.1932	0.1822	0.1740	0.1758	0.1764	0.1641	0.1641	0.1639
GC Pair	0.1301	0.2603	0.2737	0.2602	0.2242	0.2199	0.2256	0.2292	0.2292	0.2290

Table 6.4 (a). Values of the negative energy component, $\Delta E_{A(B)}$, (in kcal/mol) calculated for different combination of Au_n clusters (considered as acceptor, A) and nucleobases (considered as donor, B). Values are calculated using SDD basis sets for gold atoms and 6-31G(d,p) for other atoms. The methods used are B3PW91 [Table 6.4 (a)] and MP2 [Table 6.4 (b)].

(a)

	Au₃	Au₄-1	Au₄-2	Au₄-3	Au₅-1	Au₅-2	Au₅-3	Au₆-1	Au₆-2	Au₆-3
Guanine	-20.54	-31.24	-34.61	-36.30	-20.20	-25.68	-30.78	-30.03	-30.05	-30.04
Adenine	-17.52	-27.94	-31.24	-32.66	-17.09	-22.69	-27.40	-26.97	-26.99	-26.98
Cytosine	-14.65	-24.77	-27.99	-29.16	-14.14	-19.82	-24.16	-24.03	-24.05	-24.04
Thymine	-10.90	-20.81	-23.99	-24.89	-10.28	-16.16	-20.12	-20.34	-20.35	-20.35
Uracil	-8.21	-17.69	-20.74	-21.40	-7.55	-13.38	-16.95	-17.43	-17.44	-17.43
AT pair	-17.39	-28.51	-32.02	-33.62	-16.93	-22.88	-27.95	-27.42	-27.44	-27.43
GC Pair	-21.83	-33.63	-37.32	-39.44	-21.51	-27.37	-33.20	-32.08	-32.11	-32.10

(b)

	Au₃	Au₄-1	Au₄-2	Au₄-3	Au₅-1	Au₅-2	Au₅-3	Au₆-1	Au₆-2	Au₆-3
Guanine	-11.38	-23.99	-25.48	-23.99	-17.09	-20.36	-20.46	-21.39	-21.40	-21.37
Adenine	-4.75	-16.63	-18.02	-16.63	-14.14	-17.59	-17.41	-14.92	-14.92	-14.90
Cytosine	-3.13	-15.80	-17.27	-15.79	-10.28	-14.95	-14.50	-14.07	-14.07	-14.05
Thymine	-3.86	-15.83	-17.23	-15.83	-7.55	-11.49	-10.71	-14.19	-14.19	-14.17
Uracil	-1.02	-12.44	-13.77	-12.43	-3.22	-8.99	-8.01	-11.21	-11.21	-11.19
AT pair	-6.33	-18.84	-20.30	-18.83	-16.93	-17.46	-17.27	-16.80	-16.81	-16.78
GC Pair	-11.08	-26.29	-28.08	-26.28	-21.51	-21.48	-21.76	-22.85	-22.86	-22.83

Table 5 (a). Values of the overall stabilization energy, $\Delta E_{SE(AB)}$, (in kcal/mol) calculated for different combination of Au_n clusters (considered as acceptor, A) and nucleobases (considered as donor, B). The values are calculated using SDD basis sets for gold atoms and 6-31G(d,p) for other atoms. The methods used are B3PW91 [Table 6.5 (a)] and MP2 [Table 6.5 (b)].

(a)

	Au₃	Au₄-1	Au₄-2	Au₄-3	Au₅-1	Au₅-2	Au₅-3	Au₆-1	Au₆-2	Au₆-3
Guanine	-3.73	-7.06	-8.23	-8.48	-3.55	-5.46	-6.79	-6.96	-6.96	-6.96
Adenine	-2.68	-5.58	-6.63	-6.80	-2.51	-4.20	-5.32	-5.53	-5.54	-5.54
Cytosine	-1.86	-4.35	-5.28	-5.40	-1.71	-3.18	-4.11	-4.35	-4.35	-4.35
Thymine	-0.99	-2.98	-3.77	-3.82	-0.87	-2.04	-2.77	-3.02	-3.02	-3.019
Uracil	-0.57	-2.18	-2.85	-2.87	-0.48	-1.42	-1.99	-2.24	-2.24	-2.24
AT pair	-2.41	-5.34	-6.41	-6.60	-2.25	-3.94	-5.08	-5.29	-5.29	-5.29
GC Pair	-3.75	-7.33	-8.60	-8.91	-3.56	-5.58	-7.05	-7.18	-7.19	-7.18

(b)

	Au₃	Au₄-1	Au₄-2	Au₄-3	Au₅-1	Au₅-2	Au₅-3	Au₆-1	Au₆-2	Au₆-3
Guanine	-1.64	-5.28	-5.76	-5.28	-2.51	-3.91	-3.68	-4.78	-4.79	-4.78
Adenine	-0.27	-2.41	-2.75	-2.41	-1.71	-2.87	-2.63	-2.19	-2.19	-2.19
Cytosine	-0.11	-1.98	-2.30	-1.98	-0.88	-2.05	-1.81	-1.80	-1.79	-1.79
Thymine	-0.17	-2.14	-2.45	-2.14	-0.48	-1.17	-0.96	-1.94	-1.94	-1.94
Uracil	-0.01	-1.32	-1.57	-1.32	-0.15	-0.72	-0.54	-1.21	-1.21	-1.20
AT pair	-0.46	-3.01	-3.38	-3.01	-2.25	-2.60	-2.36	-2.72	-2.72	-2.71
GC Pair	-1.20	-5.04	-5.58	-5.04	-3.56	-3.91	-3.69	-4.45	-4.46	-4.45

Table 6.6. Comparison of the CDASE scheme based stabilization energy ($\Delta E_{SE(AB)}$) values at B3PW91 method (using SDD basis sets for Au₄ clusters and 6-31G(d) for other atoms) with the desorption energies obtained TPD and RAIR spectroscopic techniques.

Nucleobase	ΔH_{des} (kJ/mol) calculated by TPD*	ΔH_{des} (kJ/mol) calculated by RAIR*	CDASE scheme based $\Delta E_{SE(AB)}$ values (kj/mol)
Thymine	111±2	110±2	-16.00
Cytosine	128±4	130±5	-22.63
Adenine	131±3	129±4	-28.49
Guanine	131±3	144±2	-35.53

*Experimental [Reflection absorption infrared spectroscopy (RAIR) and Temperature-programmed desorption (TPD)] values are taken from reference 8.

Table 6.7. Computed binding energy values at B3PW91/GenECP-SDD (gold) U 6-31G (d) (DNA bases) level. The values are for the nanocomposites formed between Au₄ and Au₆ clusters and five nucleobases along with the two W-C base pairs.

System	BE values (in kcal/mol)	System	BE values (in kcal/mol)
Au ₄ -G	-36.67	Au ₆ -G	-19.15
Au ₄ -A	-30.32	Au ₆ -A	-15.34
Au ₄ -C	-18.6	Au ₆ -C	-11.47
Au ₄ -T	-17.11	Au ₆ -T	-8.81
Au ₄ -U	-16.47	Au ₆ -U	-8.2
Au ₄ -AT	-23.41	Au ₆ -AT	-10.16
Au ₄ -GC	-27.91	Au ₆ -GC	-13.64

$$^{\$} BE = E_{cluster + nucleobase} - (E_{cluster} + E_{nucleobase})$$

Table 6.8. Computed STQN TS energy values at B3PW91/GenECP-SDD (gold) U 6-31G+(d) (DNA bases) level. The values are for the transition states formed between Au₄ and Au₆ clusters with five nucleobases and also two W-C base pairs.

System	TS energy values (in kcal/mol)	System	TS energy values (in kcal/mol)
Au ₄ -G	1.14	Au ₆ -G	3.76
Au ₄ -A	1.76	Au ₆ -A	4.39
Au ₄ -C	1.89	Au ₆ -C	5.42
Au ₄ -T	6.23	Au ₆ -T	7.64
Au ₄ -U	10.81	Au ₆ -U	10.55
Au ₄ -AT	11.89	Au ₆ -AT	19.15
Au ₄ -GC	11.06	Au ₆ -GC	6.64

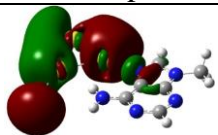
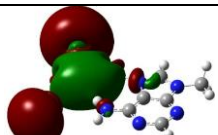
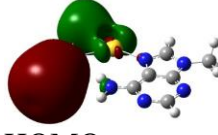
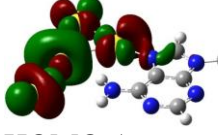
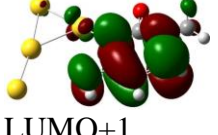

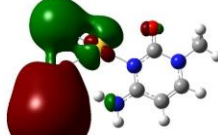
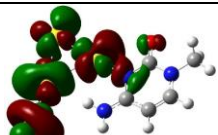
Table 6.9: Vertical excitation energies calculated for lowest singlet states of Au₄-nucleobase complex at B3PW91/GenECP-SDD (gold) U 6-31G+(d) (DNA bases) level.

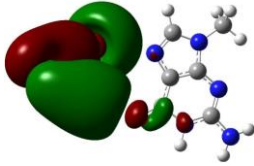
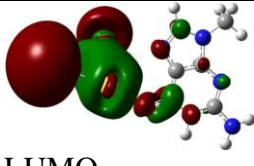
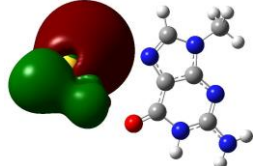
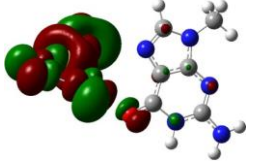
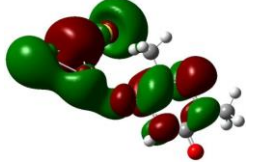
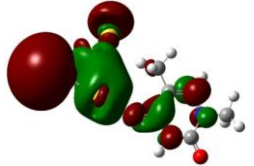
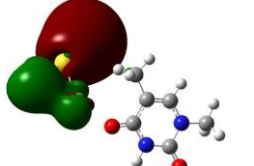
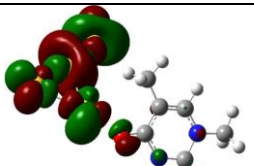
System	State	ΔE (eV) (nm)	Osc. Str.	Assign
Au ₄ -A	S ₁	3.20 (388)	0.1078	HOMO→LUMO (91%)
	S ₂	3.30 (376)	0.0091	HOMO-2→LUMO (93%)
	S ₃	3.52 (350)	0.0009	HOMO-3→LUMO (52%) HOMO-1→LUMO (44%)
Au ₄ -C	S ₁	3.17 (391)	0.1524	HOMO-1→LUMO (39%) HOMO→LUMO (53%)
	S ₂	3.28 (378)	0.3069	HOMO-1→LUMO (56%) HOMO→LUMO (35%)
Au ₄ -G	S ₃	3.55 (349)	0.0077	HOMO→LUMO+1 (78%)
	S ₁	3.12 (397)	0.1153	HOMO-2→LUMO (11%) HOMO-1→LUMO (10%) HOMO→LUMO (66%)
	S ₂	3.21 (386)	0.1600	HOMO-3→LUMO (29%) HOMO-1→LUMO (42%) HOMO→LUMO (22%)
Au ₄ -T	S ₃	3.40 (371)	0.0755	HOMO-2→LUMO+1 (12%) HOMO-1→LUMO+1 (10%) HOMO→LUMO+1 (66%)
	S ₁	3.14 (395)	0.051	HOMO-1→LUMO (86%) HOMO→LUMO (7%)
	S ₂	3.25 (381)	0.3842	HOMO-1→LUMO (7%) HOMO→LUMO (83%)
Au ₄ -U	S ₃	3.54 (350)	0.0629	HOMO-1→LUMO+1 (66%) HOMO→LUMO+1 (41%)
	S ₁	3.13 (396)	0.0987	HOMO-1→LUMO (10%) HOMO→LUMO (46%) HOMO-1→LUMO+1 (39%)
	S ₂	3.16(392)	0.1769	HOMO-1→LUMO+1 (8%) HOMO→LUMO (33%) HOMO→LUMO+1 (52%)
	S ₃	3.33(371)	0.1500	HOMO-1→LUMO (76%) HOMO-1→LUMO+1 (6%) HOMO→LUMO (11%)

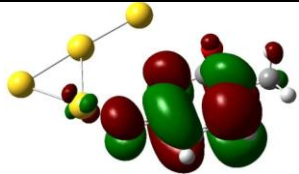
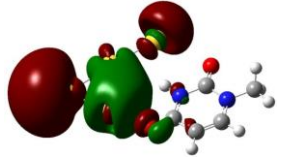
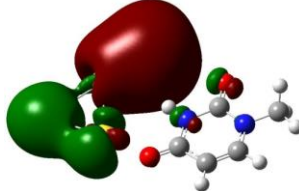
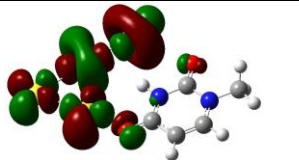
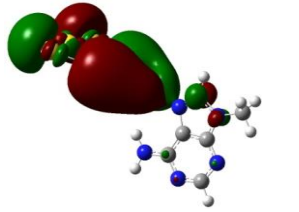
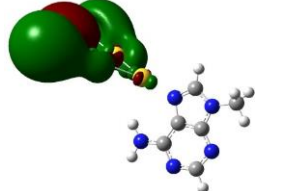

Table 6.10: Vertical excitation energies calculated for lowest singlet states in Au₆-DNA complex at B3PW91/GenECP-SDD (gold) U 6-31G+(d) (DNA bases) level

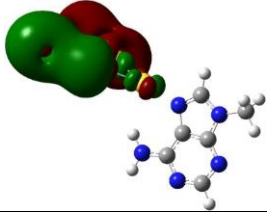
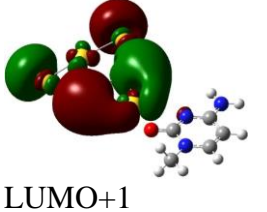
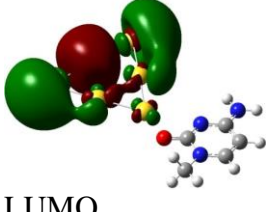
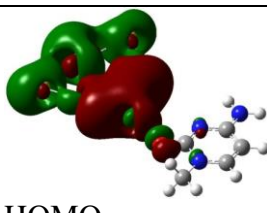
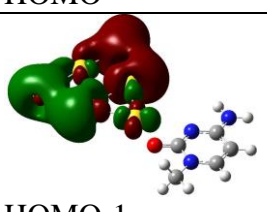
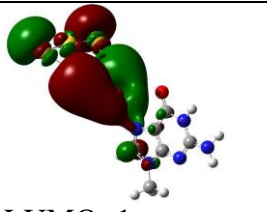
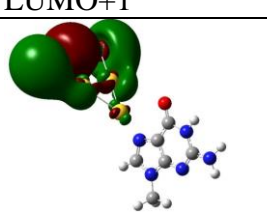
System	State	ΔE (eV) (nm)	Osc. Str.	Assign
Au ₆ -A	S1	2.66 (465)	0.0171	HOMO-1→LUMO (6%) HOMO→LUMO+1 (62%)
	S2	2.71 (456)	0.0001	HOMO-1→LUMO+1 (5%) HOMO→LUMO (93%)
	S3	2.98 (416)	0.2108	HOMO-1→LUMO (83%) HOMO→LUMO+1 (5%)
Au ₆ -C	S1	2.75 (450)	0.0105	HOMO-1→LUMO (8%) HOMO→LUMO (4%) HOMO→LUMO+1 (85%)
	S2	2.77 (448)	0.0025	HOMO-1→LUMO+1 (4%) HOMO→LUMO (61%) HOMO→LUMO+1 (3%)
	S3	2.99 (415)	0.1943	HOMO-1→LUMO (80%) HOMO→LUMO+1 (7%)
Au ₆ -G	S1	2.66 (466)	0.0179	HOMO-1→LUMO (4%) HOMO→LUMO+1 (91%)
	S2	2.70 (459)	0.00	HOMO-1→LUMO+1 (4%) HOMO→LUMO (94%)
	S3	2.97 (417)	0.2079	HOMO-1→LUMO (82%) HOMO→LUMO+1 (5%)
Au ₆ -T	S1	2.75 (450)	0.0117	HOMO-1→LUMO (8%) HOMO→LUMO+1 (89%)
	S2	2.80 (442)	0.0009	HOMO-1→LUMO+1 (9%) HOMO→LUMO (89%)
	S3	2.99 (414)	0.1992	HOMO-1→LUMO (90%) HOMO→LUMO+1 (6%)
Au ₆ -U	S1	2.75 (450)	0.0116	HOMO-1→LUMO (8%) HOMO→LUMO+1 (82%)
	S2	2.80 (442)	0.0010	HOMO-1→LUMO+1 (9%) HOMO→LUMO (88%)
	S3	2.99 (414)	0.2001	HOMO-1→LUMO (80%) HOMO-1→LUMO+2 (2%) HOMO→LUMO

Table 6.11: Pictorial representation of FMOs for the Au₄ cluster-nucleobase and Au₆ cluster-nucleobase complexes along with the major individual atomic orbital contributions to it.

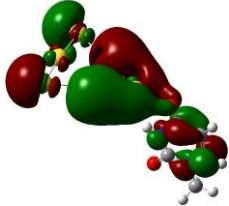
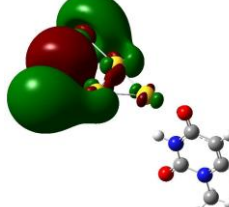
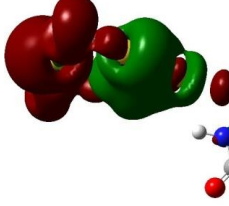
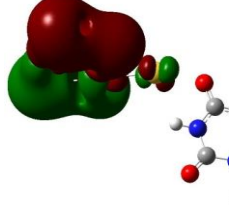
System	Orbital representation	AO contribution (Major)
Au ₄ -Adenine	 LUMO+1	Au ₁ -p=25% Au ₃ -s=20% Au ₂ -s=11% Au ₄ -p=10%
	 LUMO	Au ₁ -p=26% Au ₁ -s=20% Au ₄ -s=13%
	 HOMO	Au ₄ -s=54% Au ₂ -p=11%
	 HOMO-1	Au ₂ -d=37% Au ₄ -d=30% Au ₃ -d=14% Au ₁ -d=11%
Au ₄ -Cytosine	 LUMO+1	C7-p=36% C11-p=20%
	 LUMO	Au ₁ -p=24% Au ₁ -s=18% Au ₄ -s=14% Au ₂ -s=11% Au ₄ -p=11%
	 HOMO	Au ₄ -s=54% Au ₂ -p=11%
	 HOMO-1	Au ₂ -d=32% Au ₄ -d=22% Au ₃ -d=20% Au ₁ -d=13%

Au ₄ -Guanine	 <p>LUMO+1</p>	Au ₁ -p=20% Au ₃ -s=19% Au ₄ -p=16% Au ₂ -s=13% Au ₄ -s=13%
	 <p>LUMO</p>	Au ₁ -p=29% Au ₁ -s=22% Au ₃ -s=11%
	 <p>HOMO</p>	Au ₄ -s=56% Au ₂ -p=12%
	 <p>HOMO-1</p>	Au ₂ -d=35% Au ₄ -d=29% Au ₃ -d=17% Au ₁ -d=12%
Au ₄ -Thymine	 <p>LUMO+1</p>	C ₆ -p=21% C ₁₃ -p=16%
	 <p>LUMO</p>	Au ₃ -p=26% Au ₃ -s=20% Au ₁ -s=12%
	 <p>HOMO</p>	Au ₄ -s=55% Au ₂ -p=12%
	 <p>HOMO-1</p>	Au ₂ -d=35% Au ₄ -d=31% Au ₁ -d=16% Au ₃ -d=12%

Au ₄ -Uracil	 <p>LUMO+1</p>	C8-p=37% C12-p=22%
	 <p>LUMO</p>	Au ₁ -p=31% Au ₁ -s=21% Au ₃ -s=13%
	 <p>HOMO</p>	Au ₄ -s=52%
	 <p>HOMO-1</p>	Au ₂ -d=34% Au ₄ -d=31% Au ₃ -d=16% Au ₁ -d=11%
Au ₆ -Adenine		Au ₃ -s=14% Au ₄ -s=13% Au ₂ -p=11% Au ₆ -p=11% Au ₅ -p=11%
		Au ₂ -p=20% Au ₅ -p=19% Au ₁ -s=17% Au ₂ -s=10%
		Au ₁ -d=16%

		Au ₅ -s=18% Au ₂ -s=17% Au ₃ -d=17% Au ₄ -d=16%
Au ₆ -Cytosine	 LUMO+1	Au ₂₀ -s=15% Au ₁₇ -p=13% Au ₂₁ -s=12% Au ₂₂ -p=12% Au ₁₉ -p=11%
	 LUMO	Au ₁₉ -p=19% Au ₁₇ -p=19% Au ₁₈ -s=16% Au ₁₇ -s=11%
	 HOMO	Au ₁₈ -d=15% Au ₂₂ -s=14%
	 HOMO-1	Au ₂₀ -d=20% Au ₂₁ -d=18% Au ₁₉ -s=16% Au ₁₇ -s=13%
Au ₆ -Guanine	 LUMO+1	Au ₂₄ -s=14% Au ₂₃ -s=14% Au ₂₂ -p=11% Au ₂₀ -p=11%
	 LUMO	Au ₂₂ -p=20% Au ₂₀ -p=20% Au ₂₁ -s=17%

	<p>HOMO</p>	Au ₂₁ -d=15%
	<p>HOMO-1</p>	Au ₂₄ -d=18% Au ₂₃ -d=18% Au ₂₀ -s=17% Au ₂₂ -s=17%
Au ₆ -Thymine	<p>LUMO+1</p>	Au ₆ -p=13% Au ₃ -s=13% Au ₄ -s=13%
	<p>LUMO</p>	Au ₂ -p=19% Au ₅ -p=19% Au ₁ -s=16% Au ₂ -s=10% Au ₅ -s=10%
	<p>HOMO</p>	Au ₁ -d=17% Au ₆ -s=13%
	<p>HOMO-1</p>	Au ₅ -s=17% Au ₃ -d=17% Au ₄ -d=17% Au ₂ -s=17%

Au ₆ -Uracil	 <p>LUMO+1</p>	Au ₄ -s=13% Au ₃ -s=12%
	 <p>LUMO</p>	Au ₅ -p=19% Au ₂ -p=19% Au ₁ -s=16% Au ₅ -s=11%
	 <p>HOMO</p>	Au ₁ -d=17% Au ₆ -s=13%
	 <p>HOMO-1</p>	Au ₂ -s=17% Au ₄ -d=17% Au ₃ d=17% Au ₅ -s=17%

Chapter VII

On the Complementarity of CDASE Scheme and Supramolecular Approach

7.1 Introduction:

In this particular chapter, we are presenting a detail discussion on the effective application of proposed energy decomposition scheme to analyze the stability of adduct formed due to the non-bonding interaction. We have extensively studied the different aspects of kinetic and thermodynamic stability of H-bonded UNBA crystal structure (form due to the interaction between urea and *meta*-nitrobenzoic acid) using Density Functional Reactivity Theory based CDASE scheme.

A new class of reactivity descriptors, based on the conceptual frame work of density functional theory (DFT),¹⁻⁸ have been developed in last three decades⁹⁻²⁰ which have helped to understand a wide variety of chemical phenomena and explain different types of chemical reactions.^{21,22} These reactivity descriptors are mainly categorized as local and global ones. Intramolecular reactivity sequence (i.e., site selectivity) is normally studied by local reactivity descriptors e.g., Fukui function $[f(r)]$,^{10,13} local softness (S_k^+ , S_k^- and S_k^0),¹² local hardness $[\eta(r)]$,^{11,14,19} relative electrophilicity (S_k^+/S_k^-) and relative nucleophilicity (S_k^-/S_k^+),¹⁵ local electrophilicity,¹⁷ philicity¹⁸ etc. Similarly, to explain intermolecular reactivity sequence several global reactivity descriptors are proposed e.g., chemical potential²³ (i.e. the negative of electronegativity),²⁴ chemical hardness⁹(η), global electrophilicity index,^{25,26} nucleophilicity,²⁷⁻³¹ electrofugality and nucleofugality^{32,33} etc.

Components of stabilization energy, ΔE_{SE} (due to interaction of two chemical species) values, derived from the conceptual DFT based reactivity descriptors⁹ were shown to carry lot of information about the kinetics and thermodynamics of a reaction. Roy and collaborators have developed a scheme, known as CDASE (comprehensive decomposition analysis of stabilization energy), through which it was demonstrated how these components of stabilization energy value can be exploited to explain the rate of a chemical reaction and locate the rate determining step of a multistep chemical reaction.³⁴ A new reactivity descriptor is proposed (defined as ‘internal assistance’) which solely depends on the electronic and structural properties of the two interacting species. This newly defined reactivity parameter is believed to be one of the key factors to determine the reaction rate. Subsequently, this CDASE scheme is used to explain the reactivity sequence of quite a large number of Diels-Alder pairs clearly indicating whether the

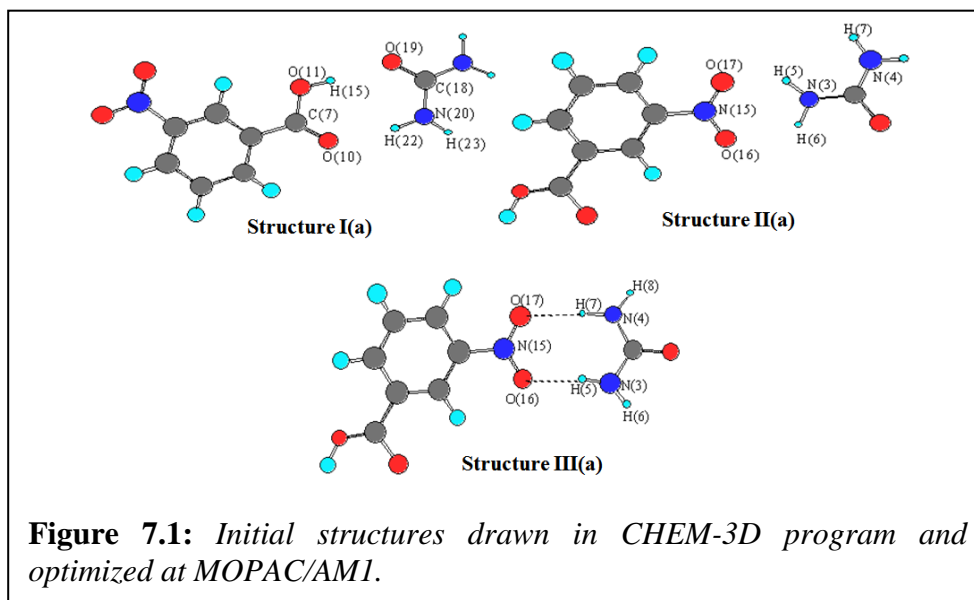
reaction between a pair is normal electron demand (NED) or inverse electron demand (IED).³⁵

In the present study, however, CDASE scheme is used to find out the most stable H-bonded structures between urea (U) and m-nitrobenzoic acid (m-NBA). Traditionally, this type of study is carried out through supermolecular approach in which the overall geometry of the non-covalently bonded systems is optimized. Basis set superposition error (BSSE) is taken care by performing counterpoise correction.^{36,37} Of several possible supermolecular structures, the one having minimum energy (supported by non-existence of any imaginary frequency), is considered to be the most preferable one. As the CDASE scheme also provides ΔE_{SE} of the combined species (due to electron transfer from one to the other) this scheme can also be used to evaluate the ΔE_{SE} values of individual supermolecular structures. Comparing the ΔE_{SE} values of the probable structures, the most stable one can, in principle, be predicted.

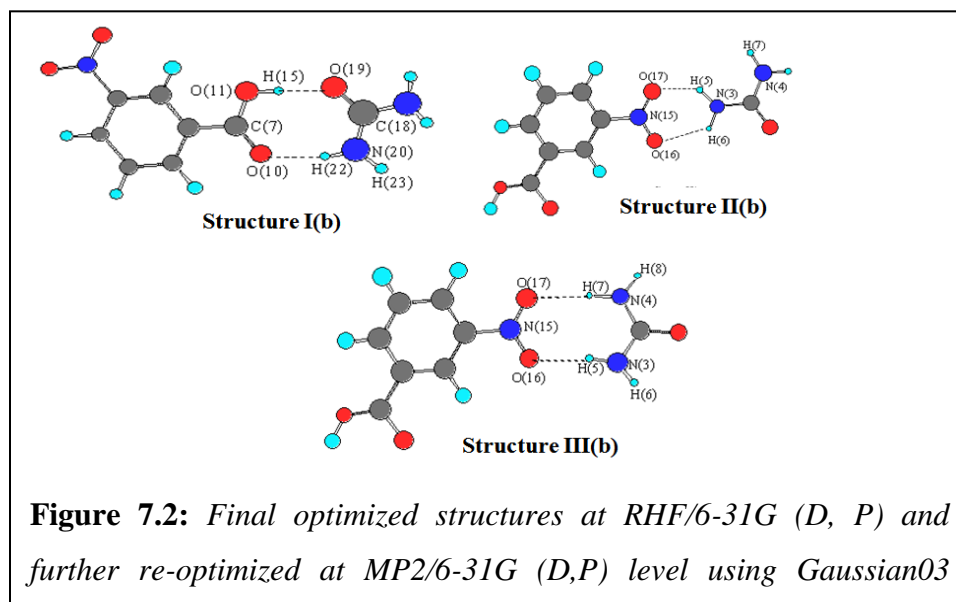
The article is structured as follows. Section 7.2 deals with computational details, which also include the probable H-bonded structures between Urea and m-NBA. Complimentarity of the two approaches will be highlighted at the end of this section. The interaction energy values of the probable H-bonded binary complexes (generated by supermolecular approach) are analyzed critically in section 7.3 (A). The corresponding geometrical and electronic parameters are also compared to explain the most stable binary structure. Stabilization energy values ΔE_{SE} as well as electronic parameters are elaborated in section 7.3 (B). In section 7.3 (C) individual energy components generated by the CDASE-scheme from the most stable binary (1:1) structure of UNBA (i.e., structure Ib) are discussed thoroughly, which also provides the direction of electron transfer in such complexes. Finally, in the conclusion (Section 6.4) we have summarized the overall study and discussed the appropriateness of such kind of study in explaining favorable binary (1:1) or ternary complexes. Probable way of making the DFT based stabilization energy value more reliable is also discussed.

6.2 Computational Details and Complementarity of CDASE Scheme and Supermolecular Approach:

As obvious from the individual structures of urea (U) and m-nitrobenzoic acid (m-NBA), three probable H-bonded stable binary (1:1) complexes are possible. These three structures differ from each other on the basis of O and H atoms involved in H-bonding. The initial rough structures were drawn using the Chem-3D software⁴⁰ and then optimized at the molecular mechanics and semi-empirical levels using the same program (given in Figs. 7.1). These structures were further re-optimized through the RHF⁴¹ and MP2⁴² method and 6-31G (d,p) basis set⁴³⁻⁴⁶ using Gaussian program suite⁴⁷ (with relevant frequency check). The re-optimized structures are represented by Figs. 7.2. Interaction energy values (Table 7.1) of these three structures are generated after taking care of basis set superposition error (BSSE) through counterpoise correction^{36,37} method (this is as implemented in Gaussian). The relevant geometrical and electronic parameters required to rationalize the observed interaction energy values are given in Table 7.2. It is worth mentioning here that as the crystallization of binary (1:1) complex is normally performed in presence of solvents⁴⁸ e.g., methanol, ethanol and acetone, the energy values of the optimized structures of supermolecules (i.e., I(b), II(b) and III(b)) are also repeated in these solvents (Table 7.3). These energy values provide some clues to predict the most stable binary (1:1) complex in these solvents. The charge transfer values (ΔN) generated by the supermolecular approach (calculated from the individual atomic populations of the two components in the supermolecule) are reported in Table 7.4.



The complementarity of CDASE scheme and supermolecular approach arises when DFT based stabilization energy (ΔE_{SE}), its different components ($\Delta E_{B(A)}$, and $\Delta E_{A(B)}$) and electron transfer (ΔN) values are evaluated. Because in the CDASE scheme only the individual (i.e. infinitely separated) structures of the donor (B) and the acceptor (A) is considered it is not possible to distinguish directly the three structures (Ib, IIb and IIIb) on the basis of this scheme. However, if the individual structures (i.e., co-ordinates) of urea and m-NBA are taken from the optimized structures of Ib, IIb, and IIIb and then CDASE scheme is implemented then three different sets of ΔE_{SE} , $\Delta E_{B(A)}$, $\Delta E_{A(B)}$ and ΔN values will be generated. On the basis of these three sets of values not only the most stable binary complex structure can be found, the direction of electron transfer (i.e. whether it is from U \rightarrow m-NBA or m-NBA \rightarrow U) will also be known.



The modeling and computational technique as discussed above will help to calculate the ΔE_{SE} values of the three structures using μ and η . Here, E_{HOMO} and E_{LUMO} were taken from the single point Gaussian job output of the individual neutral components (i.e. U and m-NBA, coordinates were taken from Ib, IIb, and IIIb). The values of ΔE_{SE} (both in gas phase as well as in solvents) are reported in Table 5.6 and the corresponding charge transfer (ΔN) values are shown in Table 6.5. The values of ΔE_{SE} and ΔN generated by the CDASE scheme are generated in the solvent medium also.

6.3. Results and Discussion:

A. Most Stable Structure from Supermolecular Approach:-

In Table 7.1 we have presented the interaction energy values (i.e., ΔE_{SE}) of the three H-bonded structures (i.e., Ib, Iib and IIb). The extra stability of Structure Ib is obvious as for this structure the value is -13.546 kcal/mol, whereas, for Structures Iib and IIb these values are -4.691 kcal/mol and -4.828 kcal/mol, respectively. Interestingly, single crystal X-ray diffraction study of Rai and Lan⁴⁸ also suggests Structure Ib to be the most stable binary (1:1) complex present in UNBA crystal. Thus, the simple ab-initio energetic study of the binary complex can explain satisfactorily a rigorous experimental observation.

Different geometrical and electronic parameters extracted from the three probable optimized structures of the binary complex provide us important clues why Structure Ib is the most stable one. In Table 7.2 we have presented the corresponding distances of the H-bonds (shown by dashed lines in the structures) and also the corresponding charges of the atoms involved in the H-bonding. The arguments adopted in explaining structure-stability relationship are, (i) shorter the H-bond stronger it is, which will lead to more stable binary (1:1) complex and (ii) higher are the opposite charge values on the atoms involved in H-bonding the stronger is the electrostatic attraction between them forming a more stable binary complex. Based on above arguments we can justify the higher stability of the Structure Ib (Table 7.2). In this structure the opposite charges on the H-bonded atoms are higher than those in Structures Iib and IIb. As a result the electrostatic force of attraction between the H-bonded O and H atoms is higher causing shorter H-bond distances and higher stability to the binary complex. Very close interaction energy values of Structures Iib and IIb (Table 6.1) can also be explained from the corresponding charge values of the H-bonded O and H atoms (and so from the O---H distances). Although, the O₁₆---H₅ bond distance in Structure IIb (2.355 Å) is higher than the corresponding distance in Structure Iib (2.315 Å) (which means that Structure IIb will be stabilized less than Structure Iib due to this H-bond), the other H-bond (i.e., O₁₇---H₇ bond) is stronger in Structure IIb than in Structure Iib). So, Structure IIb has little more overall structural stability than Structure Iib. However, the most stable binary complex among the three is the one represented by Structure-Ib.

The energy values of supermolecules (Ib, IIb and IIIb) in presence of three solvents are shown in Table 3. From the energy values (i.e., E_{UNBA} values) in Table 7.3 we can argue that the structures are more stable when formed in methanol, followed by ethanol and acetone. This trend is as expected because the stability of the complex formed depends on the polarity of the solvent. Methanol, being the most polar solvent here, provides maximum stability to the structures. Here again we notice that the stability of the structure Ib is more than those of IIb and IIIb in all the three solvents and in both the methods.

B. The Most Stable Structure from DFT Based Stabilization Energy:-

The stabilization energy values (ΔE_{SE}), are given in Table 7.6. Here again the extra stability of Structure Ib to those of IIb and IIIb is clearly demonstrated by the numerical values of ΔE_{SE} . This trend is maintained in both the methods and in all the solvents as well as in gas phase.

However, when we compare the interaction energy values (i.e., ΔE_{int}) from Table 7.1 with the stabilization energy values (i.e., ΔE_{SE}) from Table 7.6 we found that the numerical values of ΔE_{SE} are smaller than those of ΔE_{int} . In particular, for Structure Ib this difference is significant. Although, we can ascribe it to the different theoretical basis of evaluation of ΔE_{int} and ΔE_{SE} , there might be some other factors causing this numerical difference. The ΔE_{int} values are evaluated by supermolecular approach, which takes care of all kinds of effects e.g., charge transfer, electrostatic, polarization etc. But the method used here to calculate ΔE_{SE} values takes care of only charge transfer effect. Although, an elaborate analytical expression of DFT based ΔE_{SE} is proposed,⁴⁹ working equation for the same is yet to be implemented in CDASE scheme. This limitation of evaluating ΔE_{SE} values might be the major reason for their lower numerical values when compared to those of ΔE_{int} , although the amount of charge transfer are higher in the CDASE scheme (Table 7.5) than in the supermolecular approach (Table 7.4).

Another interesting observation regarding the charge transfer values (from both Table 7.4 and Table 7.5) might justify the extra stability of Structure Ib when compared

to those of Structure IIb and IIIb. Here, according to the chosen convention in the present work, the positive ΔN values indicate that the charge is transferred from urea (U) to m-nitrobenzoic acid (m-NBA) and the negative ΔN values indicate the opposite flow. (i.e. m-NBA to U). Normally m-NBA, because of the presence of highly electron-withdrawing $-NO_2$ group, should behave as electron acceptor here showing positive charge transfer values. However, this is observed only for Structure Ib in both the approaches [i.e., while evaluating ΔE_{int} (corresponding ΔN values are in Table 7.4) and ΔE_{SE} (corresponding charge transfer values are in Table 7.5)]. The unphysical charge transfer in Structure IIb and Structure IIIb might be the reason of overall lower ΔE_{int} and ΔE_{SE} values. (i.e., lower stability of these two structures when compared to Structure Ib).

C. CDASE – Scheme Based Energy Components and Prediction of Donors and Acceptors:-

The energy components as well as the charge transfer values generated by the CDASE scheme are reported in Table 7.7 (for HF/6-31G(D,P) method) and Table 7.8 (for MP2/6-31G(D,P) method). Here, to test which one of Urea and m-NBA behaves as electron donor (B) and acceptor (A) the geometries of the systems are optimized independently instead of taking from Ib (or IIb or IIIb). Thus, as expected, the values of ΔE_{SE} generated here are different from those reported in Table 7.6. Also, the values of ΔN and $\Delta E_{B(A)}$ are positive ($\Delta E_{A(B)}$ values are negative) when Urea (U) is considered as donor and m-nitrobenzoic acid (m-NBA) as an acceptor. This is what we expect as m-NBA, having a strong electron withdrawing group (i.e. $-NO_2$) as a substitution, should behave as an electron acceptor here. However, the sign of ΔN , $\Delta E_{B(A)}$ and $\Delta E_{A(B)}$ changes when U is considered as acceptor and m-NBA as donor in the CDASE scheme, justifying that this is not the real situation. Thus, CDASE scheme compliments supermolecular approach in deciding donor and acceptor in the complex formation process. This is more so because the parameters in the CDASE scheme, on the basis of which the direction of electron flow is decided (i.e., ΔN , $\Delta E_{B(A)}$ and $\Delta E_{A(B)}$) are based on different types of energy terms and so are more reliable than in supermolecular approach, in which the direction is decided solely on individual atomic populations of the

two interacting species. Dependence of electronic populations of individual atoms on the chosen basis sets and methods are well known and sometimes not very reliable.

It is seen from the previous discussion that ΔE_{SE} values alone cannot predict the donor and acceptor in the complex. That is why the same negative values of ΔE_{SE} (which indicates that the complex is more stable than the individual interacting species) are obtained when U is donor (B) and m-NBA is acceptor (A) and vice versa (Table 7.7 and 7.8). This observation holds true in both the methods.

7.4 Conclusion:-

In the present study it is shown how the conventional supermolecular approach and the recently proposed CDASE scheme³⁴ compliments each other in predicting the most stable structure of the binary (1:1) complex as well as identifying the donor and acceptor in it. When there are possibilities of more than one stable structures of the binary complex, having very close energy values (i.e., within few kcal/mol), initial structures of the two complexing species (i.e. donor and acceptor) to be used in the CDASE-scheme are taken from the optimized supermolecular structures. As the geometries of the donor and acceptor are different in different optimized supermolecules, choosing these geometries help to mimic the actual complex formation process and in this way supermolecular approach compliments the CDASE-scheme. The trend of the interaction energy (ΔE_{int}) values generated by supermolecular approach and the DFT based stabilization energy (ΔE_{int}) values are found to be exactly similar when applied to the binary (1:1) complex formation process between Urea (U) and m-nitrobenzoic acid (m-NBA). Both the methods could correctly predict the most stable structure of the binary complex in gas phase as well as in three different solvents (e.g., methanol, ethanol and acetone) at two different levels of theories (HF/6-31G (D,P) and MP2/6-31G (D,P)).

However, the direction of electron flow (i.e., deciding the electron donor and acceptor) in the complex formation process can be predicted more reliably by the CDASE scheme. This is because the electron transfer (ΔN) in this scheme is evaluated by different energy parameters. Also, the components of ΔE_{SE} generated by CDASE scheme (i.e., $\Delta E_{B(A)}$ and $\Delta E_{A(B)}$) depend on different types of energy parameters and

hence are more reliable than the atomic electronic populations on the basis of which charge transfer (i.e., ΔN) in supermolecular approach is decided. In this way, CDASE-scheme may compliment supermolecular approach to judge the donor and acceptor in the complex formation process.

At present, the CDASE-scheme is limited to the complex formation involving two species only. The authors are actively engaged in applying this idea to situations where more than two species are involved simultaneously and that is also to interesting biological processes. Also, there is a scope to improve the CDASE-scheme by inclusion of electrostatic, polarizability and dispersion interactions.

References

1. R. G. Parr, W. Yang, *Density—Functional Theory of Atoms and Molecules*; Oxford University Press; New York, 1989.
2. R. G. Parr, W. Yang, *Annu. Rev. Phys. Chem.* 1995, **46**, 701
3. W. Kohn, A. D. Becke, R. G. Parr, *J. Phys. Chem.* 1996, **100**, 978.
4. H. J. Chermette, *J. Comput. Chem.* 1999, **20**, 129.
5. *A Chemist's Guide to Density Functional Theory*; W. Koch, M. Holthausen, Wiley-Vch Weinheim, 2000.
6. P. Geerlings, F. De Proft, W. Langenaeker, *Chem. Rev.* 2003, **103**, 1793
7. P. W. Ayers, J. S. M. Anderson, L. Bartolotti, *J. Int. J. Quantum Chem.* 2005, **101**, 520.
8. R. K. Roy, S. Saha, *Annu. Rep. Prog. Chem., Sect. C* 2010, **106**, 118.
9. R. G. Parr, R. G.; Pearson, *J. Am. Chem. Soc.* 1983, **105**, 7512
10. R. G. Parr, W. Yang, *J. Am. Chem. Soc.* 1984, **106**, 4049
11. (a) S. K. Ghosh, M. Berkowitz, *J. Chem. Phys.* 1985, **83**, 2976 (b) W. Langenaeker, F. De Proft, P. Geerlings, *J. Phys. Chem.* 1995, **99**, 6424.. (c) P. K. Chattaraj, D. R. Roy, P. Geerlings, M. Torrent-Sucarrat, *Theor. Chem. Acc.* 2007, **18**, 923
12. R. G. Parr, W. Yang, *Proc. Natl. Acad. Sci. U. S. A.* 1985, **82**, 6723..
13. W. Yang, W. J. Mortier, *J. Am. Chem. Soc.* 1986, **108**, 5708.
14. M. K. Harbola, P. K. Chattaraj, R. G. Parr, *Isr. J. Chem.* 1991, **31**, 395.
15. (a) R. K. Roy, S. Krishnamurti, P. Geerlings, S. Pal, *J. Phys. Chem. A* 1998, **102**, 3746. (b) R. K. Roy, F. De. Proft, P. Geerlings, *J. Phys. Chem. A* 1998, **102**, 7035.
16. (a) N. Russo, M. Toscano, A. Grand, T. Mineva, *J. Phys. Chem. A*, 2000, **104**, 4017. (b) S. Krishnamurty, S. Pal, *J. Phys. Chem. A*, 2000, **104**, 7639. (c) T. Mineva, V. Parvanov, I. Petrov, N. Neshev, N. Russo, *J. Phys. Chem.A*, 2001, **105**, 1959.
17. P. Perez, A. Toro-Labbe, A. Aizman, R. Contreras, *J. Org. Chem.*, 2002, **67**, 4747.
18. (a) P. K. Chattaraj, B. Maiti, U. Sarkar, *J. Phys. Chem. A*, 2003, **107**, 4973. (b) P. K. Chattaraj, D. R. Roy, *Chem. Rev.*, 2007, **107**, PR46. (c) P. K. Chattaraj S. Giri, *Annu. Rep. Prog. Chem., Sect. C*, 2009, **105**, 13.
19. (a) S. Saha, R. K. Roy, *J. Phys. Chem. B* 2007, **111**, 9664. (b) S. Saha, R. K. Roy, *J. Phys. Chem. B* 2007, **111**, 9664 (c) S. Saha, R. K. Roy, *J. Phys. Chem. B* 2008, **112**, 1884
20. (a) S. Janssens, A. Borgoo, C. V. Alsenoy, P. Geerlings, *J. Phys. Chem. A* 2008, **112**, 10560. (b) A. Borgoo, P. Jaque, A. Toro-Labbe, C. V. Alsenoy, P. Geerlings, *Phys. Chem. Chem. Phys.* 2009, **11**, 476. (c) P. Jaque, A. Toro-Labbe, P. Geerlings, F. De Proft, *J. Phys. Chem. A* 2009, **113**, 332.
21. (a) S. Pal, K. R. S. Chandrakumar, *J. Am. Chem. Soc.* 2000, **122**, 4145. (b) K. R. S. Chandrakumar, S. Pal, *J. Phys. Chem. A* 2002, **106**, 5737. (c) A. Tanwar, B. Bagchi, S. Pal, *J. Chem. Phys.* 2006, **125**, 214304(1). (d) R. Kar, K. R. S.; Chandrakumar, S. Pal, *J. Phys. Chem. A* 2007, **111**, 375. (d) R. Kar, S. Pal,

-
- Chemical Reactivity Theory: A Density Functional View, Kar, R.; Pal, S.; ed. P. K. Chattaraj. K. CRC Press, 2009.
22. (a) R. K. Roy, *J. Phys. Chem. A* 2004, **108**, 4934. (b) R. K. Roy, V. Usha, J. Paulovic, K. Hirao, *J. Phys. Chem. A* 2005, **109**, 4601. (c) Roy, R. K.; Usha, V.; Patel, B. K.; Hirao, K. *J. Comput. Chem.* 2006, *27*, 773. (d) P. Bagaria, R. K. Roy, *J. Phys. Chem. A* 2008, **112**, 97.
 23. R. G. Parr, R. A. Donnelly, M. Levy, W. E. Palke, *J. Chem. Phys.* 1978, **68**, 3801.
 24. R. S. Mulliken, *J. Chem. Phys.*, 1934, **2**, 782.
 25. A. T. Maynard, M. Huang, W. G. Rice, D. G. Covell, *Proc. Natl. Acad. Sci. U. S. A.* 1998, **95**, 11578.
 26. R. G. Parr, von. L. Szentpaly, S. Liu, *J. Am. Chem. Soc.* 1999, **121**, 1922.
 27. P. W. Ayers, R. G. Parr, *J. Am. Chem. Soc.* 2001, **123**, 2007.
 28. P. Jaramillo, P. Perez, R. Contreras, *J. Phys. Chem. A* 2006, **110**, 8181.
(b) P. Jaramillo, P. Fuentealba, P. Perez, *Chem. Phys. Lett.* 2006, **427**, 421.
 29. A. Cedillo, R. Contreras, M. Galvan, A. Aizman, J. Andres, V. S. J. Safont, *J. Phys. Chem. A* 2007, **111**, 2442.
 30. F. De Vleeschouwer, V. Speybroeck, V. Van, M. Waroquier, P. Geerlings, F. De Proft, *Org. Lett.* 2007, **9**, 2721.
 31. L. R. Domingo, P. Perez, R. Contreras, *J. Org. Chem.* 2003, **68**, 6060.
 32. P. W. Ayers, J. S. M. Anderson, J. I. Rodriguez, Z. Jawed, *Phys. Chem. Chem. Phys.* 2005, **7**, 1918.
 33. P. R. Campodonico, C. Perez, M. Aliaga, M. Gazitua, R. Contreras, *Chem. Phys. Lett.* 2007, **447**, 375.
 34. P. Bagaria, S. Saha, S. Murru, V. Kavala, B. Patel, R. K. Roy, *Phys. Chem. Chem. Phys.* 2009, **11**, 8306
 35. S. Saha, R. K. Roy, S. Pal, *Phys. Chem. Chem. Phys.* 2010, **12**, 9328.
 36. S. F. Boys, F. Bernardi, *Mol. Phys.* 1970, **19**, 553.
 37. S. Simon, M. Duran, J. J. Dannenberg, *J. Chem. Phys.* 1996, **105**, 11204.
 38. Y. Zhao, D. G. Truhlar, *Phys. Chem. Chem. Phys.* 2005, **7**, 2701.
 39. T. A. Koopmans, *Physica*. 1933, **1**, 104.
 40. © 1986-1999 Cambridge Soft Corporation.
 41. (a) C. C. Roothan, *Rev. Mod. Phys.* 1951, **23**, 69. (b) J. A. Pople, R. K. Nesbet, *J. Chem. Phys.* 1954, **22**, 571. (c) R. McWeeny, G. J. Dierksen, *Chem. Phys.* 1968, **49**, 4852.
 42. C. Møller, M. S. Plesset, *Phys. Rev.* 1934, **46**, 618.
 43. G. A. Peterson, M. A. Al-Laham, *J. Chem. Phys.* 1991, **94**, 6081..
 44. W. J. Hehre, R. F. Stewart, J. A. Pople, *J. Chem. Phys.* 1969, **51**, 2657.
 45. G. A. Peterson, A. Bennett, T. G. Tensfeldt, M. A. Al-Laham, W. A. Shirley, J. Mantzaris, *J. Chem. Phys.* 1988, **89**, 2193.
 46. R. Ditchfield, W. J. Hehre, J. A. Pople, *J. Chem. Phys.* 1971, **54**, 724.
 47. M. J. Frisch et .al. GAUSSIAN 03, Revision E.01, Gaussian, Inc., 340 Quinipiac St., Bldg. 40, Wallingford CT 06492.
 48. R. N. Rai, C. W. Lan, *J. Mater. Res.* 2002, **17**, 1587.
 49. (a) R. F. Nalewajski, *J. Am. Chem. Soc.* 1984, **106**, 944. (b) G. L. Gazquez, *Structure and Bonding*, Springer-Verlag: Berlin, 1993. (c) P. W. Ayers, R. G.

Parr, R. G. Pearson, *J. Chem. Phys.* 2006, **124**, 194107. (d) P. W. Ayers, *Faraday Discuss.* 2007, **135**, 161.

Table 7.1 Interaction Energy values of the three probable binary (1:1) structures formed between Urea (U) and m-Nitrobenzoic acid (m-NBA) using HF/6-31G(D,P) and MP2/6-31G(D,P) methods.

Struc.	HF/6-31G(D,P)	MP2/6-31G(D,P)
Struc. Ib	ΔE_{int} -13.5461 kcal/mol	-13.8482 kcal/mol
Struc. IIb	ΔE_{int} -4.6915 kcal/mol	- 4.9388 kcal/mol
Struc. IIIb	ΔE_{int} - 4.8284 kcal/mol	- 4.9441 kcal/mol

Table 7.2 Relevant geometrical and electronic parameters of the three probable H – bonded structures of the binary (1:1) complex using HF/6-31G(D,P) and MP2/6-31G(D,P) methods. See Fig. 7.2 for numbering of atoms.

Atomic Charges			H – bond Distance (Å)			
Struc.		HF	MP2		HF	MP2
Struc. Ib	O_{19}^*	-0.702	-0.721	$O_{19} - H_{15}$	1.727	1.620
	H_{15}	0.441	0.471			
	O_{10}	-0.630	-0.664	$O_{10} - H_{22}$	2.048	1.920
	H_{22}	0.377	0.390			
Struc. IIb	O_{17}	-0.483	-0.4688	$O_{17} - H_7$	2.396	2.207
	H_7	0.321	0.3310			
	O_{16}	-0.470	-0.461	$O_{16} - H_5$	2.315	2.207
	H_5	0.328	0.3324			
Struc. IIIb	O_{17}	-0.480	-0.4684	$O_{17} - H_7$	2.338	2.204
	H_7	0.324	0.3315			
	O_{16}	-0.473	-0.4613	$O_{16} - H_5$	2.355	2.210
	H_5	0.324	0.3316			

*Subscripts are for numbering of atoms

Table 7.3 Energy values of the three probable binary (1:1) structures formed between Urea (U) and m-Nitrobenzoic acid (m-NBA) in presence of solvents (See text for details). Values are given in a.u.

		E_{UNBA}		
Struc.		Methanol	Ethanol	Acetone
Struc. Ib	HF	-845.8625	-845.8561	-845.8461
	MP2	-848.3052	-848.3045	-848.3041
Struc. IIb	HF	-845.8525	-845.8462	-845.8329
	MP2	-848.2975	-848.2970	-848.2964
Struc. IIIb	HF	-845.8525	-845.8461	-845.8330
	MP2	-848.2977	-848.2970	-848.2964

Table 7.4: Charge transfer from Urea (U) to m-Nitrobenzoic acid (m-NBA) in the three probable binary (1:1) structures formed between U and m-NBA in gas phase and in presence of solvents using HF/6-31G(D,P) and MP2/6-31G(D,P) methods. The values are generated by Supermolecular approach.

Struc.		HF/6-31G(D,P)	MP2/6-31G(D,P)
Struc. Ib	(Gas phase)	0.0219	0.0252
	(Methanol)	0.0339	0.0412
	(Ethanol)	0.0336	0.0397
	(Acetone)	0.0335	0.0398
Struc. IIb*	(Gas phase)	-0.0297	-0.0340
	(Methanol)	-0.0373	-0.0435
	(Ethanol)	-0.0377	-0.0431
	(Acetone)	-0.0375	-0.0431
Struc. IIIb*	(Gas phase)	-0.0300	-0.0339
	(Methanol)	-0.0375	-0.0429
	(Ethanol)	-0.0376	-0.0431
	(Acetone)	-0.0375	-0.0432

* Negative ΔN values indicate that the electrons have moved from m-NBA to U.

Table 7.5: DFT-based charge transfer (ΔN) from Urea (U) to m-Nitrobenzoic acid (m-NBA) in the three probable binary (1:1) structures formed between U and m-NBA in gas phase and in presence of solvents using Koopmanns' approximation at HF/6-31G(D,P) and MP2/6-31G(D,P) levels (Fig. 7.1 and Fig. 7.2).

Structures		HF/6-31G(D,P)	MP2/6-
Struc. Ib	(Gas phase)	0.1239	0.1354
	(Methanol)	0.1398	0.1466
	(Ethanol)	0.1395	0.1466
	(Acetone)	0.1370	0.1450
Struc. IIb*	(Gas phase)	-0.1194	-0.1288
	(Methanol)	-0.1351	-0.1397
	(Ethanol)	-0.1346	-0.1397
	(Acetone)	-0.1318	-0.1353
Struc. IIIb*	(Gas phase)	-0.1194	-0.1287
	(Methanol)	-0.1348	-0.1390
	(Ethanol)	-0.1344	-0.1396
	(Acetone)	-0.1318	-0.1380

* Negative ΔN values indicate that the electrons have moved from m-NBA to U.

Table 7.6: DFT-based stabilization energy values (ΔE_{SE}) of the three probable binary (1:1) structures formed between Urea (U) and m-Nitrobenzoic acid (m-NBA) in gas phase and in presence of solvents at HF/6-31G(D,P) and MP2/6-31G(D,P) methods (Fig. 7.1 and Fig. 7.2). Values are given in kcal/mol.

Struc.		HF/6-31G(D,P)	MP2/6-31G(D,P)
Struc. Ib	(Gas phase)	-2.4920	-2.9353
	(Methanol)	-3.2541	-3.5148
	(Ethanol)	-3.2367	-3.5108
	(Acetone)	-3.0845	-3.4003
Struc. IIb	(Gas phase)	-2.3241	-2.6727
	(Methanol)	-3.0477	-3.2143
	(Ethanol)	-3.0237	-3.2135
	(Acetone)	-2.8721	-2.9834
Struc. IIIb	(Gas phase)	-2.3274	-2.6678
	(Methanol)	-3.0363	-3.1778
	(Ethanol)	-3.0160	-3.2063
	(Acetone)	-2.8680	-3.0991

Table 6.7: CDASE-scheme based study of the direction of charge transfer (ΔN) between Urea (U) and m-Nitrobenzoic acid (m-NBA) in the binary (1:1) structure in gas phase as well as in presence of solvents using Koopmanns' approximation. The values are generated at HF/6-31G(D,P) level. Energy values are given in kcal/mol.

B=UREA : A=m-NBA				
	Gas phase	Methanol	Ethanol	Acetone
ΔN	0.1193	0.1294	0.1292	0.1265
$\Delta E_{B(A)}$	9.0434	8.9498	8.9498	9.0936
$\Delta E_{A(B)}$	-11.3808	-11.7723	-11.7620	-11.7672
ΔE_{SE}	-2.3374	-2.8224	-2.8123	-2.6735

B=m-NBA : A=UREA				
	Gas phase	Methanol	Ethanol	Acetone
ΔN	-0.1193	-0.1294	-0.1292	-0.1265
$\Delta E_{B(A)}$	-11.3808	-11.7723	-11.7620	-11.7672
$\Delta E_{A(B)}$	9.0434	8.9498	8.9498	9.0936
ΔE_{SE}	-2.3374	-2.8224	-2.8122	-2.6735

Table 6.8: CDASE-scheme based study of the direction of charge transfer (ΔN) between Urea (U) and m-Nitrobenzoic acid (m-NBA) in the binary (1:1) structure in gas phase as well as in presence of solvents using Koopmanns' approximation. The values are generated at MP2/6-31G(D,P) level. Energy values are given in kcal/mol.

B=UREA : A=m-NBA				
	Gas phase	Methanol	Ethanol	Acetone
ΔN	0.0450	0.1278	0.1291	0.1330
$\Delta E_{B(A)}$	5.4987	9.5481	9.6093	10.0183
$\Delta E_{A(B)}$	-5.7512	-12.2100	-12.3388	-12.9178
ΔE_{SE}	-0.2525	-2.6619	-2.7295	-2.8995
B=m-NBA: A=UREA				
	Gas phase	Methanol	Ethanol	Acetone
ΔN	-0.0450	-0.1278	-0.1291	-0.1330
$\Delta E_{B(A)}$	-5.7512	-12.2100	-12.3388	-12.9178
$\Delta E_{A(B)}$	5.4987	9.5481	9.6093	10.0183
ΔE_{SE}	-0.2525	-2.6619	-2.7295	-2.8995

Chapter VIII

Conclusion and Future Scope

8.1 General conclusion:

An overall summary and conclusions have been included at the end of each chapter. However, to get a systematic overview of the research outcomes it is necessary to draw a general conclusion for the overall thesis. Hence, in the final chapter, I am presenting a brief summary and the relevant future scope of the present thesis.

The present research work is an attempt to develop some computationally cost-effective formalisms based on the conceptual framework of density functional theory (DFT).¹⁻¹¹ In this thesis, we have discussed the application of fundamental DFRT-based concepts in the study of kinetic and thermodynamic aspects of different reactive and non-reactive interactions and also understand the charge transfer process of that particular interaction. To undertake this novel application based study, we have basically considered the use of stabilization energy concept introduced by Parr et al.¹² The entire work encompasses the global reactivity descriptors such as electrophilicity index, proposed by Parr et al.¹² from a qualitative suggestion of Maynard et al.¹³ Chemical science deals with the fundamental process of chemistry, i.e., the bond breaking and bond forming process during a reactive interaction. We have studied how qualitatively these reactivity descriptors can be correlated to the experimental findings to study the reactivity and mechanism of a particular interaction. We have scrutinized the limitations regarding the applicability of the stabilization energy along with global electrophilicity for evaluating electron exchange between the systems of comparable sizes. It is worth mentioning here that, when this descriptor was proposed it was assumed that the donor is a perfect one (normally a very big system in comparison to the acceptor), which will no longer be applicable to evaluate electron exchange when both the donor and the acceptor are of comparable sizes. The limitation of global electrophilicity descriptor is demonstrated through comprehensive decomposition analysis of the stabilization energy (SE) in case of comparable size donor-acceptor system. Claver application of this particular energy decomposition scheme (CDASE) for relatively large system at a reasonable computational cost is the primary concern of the present study. We have systematically analyzed the CDASE scheme based findings, and also tested against the conventional *ab initio* study to ensure the reliability of proposed scheme.

8.2 Specific conclusions:

In this segment, I have included some specific concluding remarks on individual chapters that have been discussed in the earlier sections.

The interaction of well-known anticancer drug with DNA is an extensively explored area in computational chemistry. Although, there are many excellent reviews discussing the origin of anticancer activity for cisplatin drugs¹⁴⁻¹⁸, the proper mechanism behind this phenomenon is yet to be confirmed. We have studied the anticancer activity of cisplatin drug specifically considering its interaction with individual purine bases of DNA. Subsequently, different CDASE scheme based parameters able to produce satisfactory results that complement the experimental observations. It is well known fact that hydrolysis of cisplatin is the very first step in the overall process. Once cisplatin get hydrolyzed it generates two components namely mono-aqua (one Cl has been replaced by a water molecule) and di-aqua (two Cl will be replaced by two water molecules) complexes and these two are the active species.¹⁹⁻²¹ Particularly, binding interaction of hydrolyzed cisplatin with the nucleobases guanine and adenine has been investigated using density functional reactivity theory (DFRT). The energy changes involved in the interaction of both mono-aqua and di-aqua cisplatins with two purine bases are explored using different parameters of CDASE scheme. As observed by earlier experimental and theoretical studies, the present approach also reveals that interaction of cisplatin di-aqua complex is stronger than the corresponding mono-aqua complex and, more importantly, both mono and di-aqua complexes of cisplatin strongly interact with guanine than with adenine. Interestingly, all these observations are based on the charge transfer based energy components and solely depend on the electronic properties of the isolated aqua-cisplatins and nucleobases (i.e., not on the electronic properties of the adduct). Moreover, the sign of the energy components and charge transfer values clearly demonstrate the electron donor and acceptor nature of the purine bases and aqua cisplatins, respectively. The results are also consistent in all the three methods (both *ab-initio* and DFT) adopted in this study.

Although, cisplatin and its analogues has unmatched success rate against different types of cancer cell-lines and recognized as the most widely used anticancer drugs, the associated cytotoxic side-effects of the drug is a major concern in recent years.²²⁻²⁶ We

have introduced a relatively simple theoretical approach to put some new insights on cisplatin therapy to reduce various cytotoxic and nephrotoxic side-effects of cisplatin analogues in cancer treatment through computer aided molecular modeling technique. A better understanding of the interaction between different cisplatin analogues with various protecting agents can be achieved from the descriptors generated by density functional reactivity theory based comprehensive decomposition analysis of stabilization energy scheme. Taking into account of three types of interactions i.e., of (1) Cisplatin analogues with DNA bases and base pairs (2) Cisplatin analogues with protecting agents and (3) Protecting agents with DNA bases, it is possible to develop a strategy (albeit qualitative) that suggests the best possible combinations of these drugs with protecting agents which can cause reduction in the toxic side-effects of cisplatin therapy. The sample set comprises of 96 pairs of cisplatin analogues and rescue agents and the generated data confirms the predictive power of the adopted strategy. By doing proper synchronization of the data generated for three different types of interaction it is possible to propose an application protocol for the protecting agents against a particular cisplatin drug. We have verified the theoretical findings by correlating it to some of the standard experimental observations.²⁷

We have explored the possibility of single walled carbon nanotube (SWCNT) as drug delivery system implementing DFRT based molecular modeling technique.²⁸⁻³⁰ This particular study describes an alternative and computationally cost-effective theoretical approach to explore the interaction of nucleobases with different semi-conducting chiral Single-Walled Carbon Nanotubes (SWCNTs). Application of Density Functional Reactivity Theory (DFRT) based CDASE (Comprehensive Decomposition Analysis of Stabilization Energy) scheme is being extended to understand the kinetic and thermodynamic aspects of the interaction between different DNA bases as well as Watson-Crick base pairs (AT and GC) with SWCNTs. Proposed investigations have been carried out without performing computationally intensive transition state optimization or thermochemistry calculation. The trend of interaction generated by reactivity parameters (based on CDASE scheme) follow the experimentally as well as theoretically verified order, $G > A > C > T > U$, observed earlier.³¹ To determine the reliability of CDASE scheme based findings conventional binding energy calculations is also performed on

some of the selected systems using ONIOM QM:MM approach. Application of ONIOM model in case of large system is a standard practice, where there is flexibility to define different layers in the particular system. In this way, we can generate various zones and assign different level of theories according to our requirement. We will apply higher level of theory at the particular zone where we have the main area of interest. Subsequently, lower levels of theories are adopted for the other zones with the increasing distance from the primary zone. As we have learned from the earlier studies that DNA fragment can be a good precursor for the functionalization of carbon nanotube.³² So, the reported theoretical findings can be exploited as an alternative (albeit qualitative but rapid) technique to understand the CNT functionalization with DNA bases at the electronic level.

With an intention to learn more about the novel aspects of nanosystems, we have extended the application of CDASE scheme to design some hybrid nanostructures on the basis of energetic study. More specifically, we have explored the stability of NanoBud system where a fullerene molecule is covalently attached to the surface of SWCNT.³³ We have rationalized the effect of variation in the symmetry of relatively smaller fullerene (C₃₂) on the mode of its interaction with semi-conducting Single Walled Carbon Nanotubes (SWCNTs) in the process of stable hybrid NanoBud formation. Thermodynamic and kinetic parameters, along with the charge transfer values associated with the interaction between fullerene and SWCNTs, have been evaluated using an unconventional and computationally cost-effective method based on Density Functional Reactivity Theory (DFRT). Conventional *Ab initio* quantum chemical methodologies as well as molecular dynamics studies are also used to support DFRT based understandings on the growth of NanoBud structures formed by the interaction between fullerene and SWCNTs. The outcome of the present study suggests that the kinetic, thermodynamic and structural properties of hybrid carbon NanoBuds are significantly influenced by both symmetry of C₃₂ fullerene and the site of covalent binding.³⁴ In a crude assumption, it is shown that greater stability of the NanoBud structure associated with the higher symmetry of the interacting systems.

It is important to understand the interaction of biological macromolecule such as DNA with a particular metal surface. The characteristic electronic properties of the metal

clusters are modulated to a considerable extent by the attachment of nucleobases on the inorganic surface. The thermodynamic and kinetic aspects associated to the interaction of metal clusters with nucleobases are assessed using Density Functional Reactivity Theory (DFRT) based CDASE scheme. To obtain more details about the complexation between small gold clusters and nucleobases, conventional binding energy (BE) and transition state (TS) calculations are also performed at B3LYP and MP2 level. It is observed that the interaction between Au_n clusters and nucleobases follow the order $G > A > C > T > U$. It is also figured out that, Watson-Crick base pair GC preferentially interact with Au_n cluster than the AT pair. In addition to this, TDDFT calculations are performed for selected clusters to understand the photophysics of this particular interaction. TDDFT analysis predicts significantly important MLCT character in the Au_n -DNA nanocomposite.

Complementarity of the proposed CDASE scheme and the conventional supermolecular approach is also tested in the present study.³⁵ The most stable binary (1:1) molecular complex formed between urea (U) and *m*-nitrobenzoic acid ($m-NBA$) is chosen as a test case. Interaction energy values generated from supermolecular approach show that the most stable binary structure is formed through double H-bonding. One H – bond forms between H_{COOH} (i.e., H atom of the $COOH$ group) of $m-NBA$ and $O_{C=O}$ (i.e., O – atom of the CO group) of U and the other develops between H_{NH_2} (i.e., one of the H – atom of NH_2 group) of U and $O_{C=O}$ (i.e., O – atom of the $C = O$ moiety of $COOH$ group) of $m-NBA$. Stabilization energy values, generated by the CDASE scheme and derived from the conceptual density functional theory (DFT) based reactivity descriptors of the individual components (i.e. Urea and *m*-NBA) in the overall geometry of the molecular complex, fully supports the outcome of the supermolecular approach. Geometrical and the electronic parameters (i.e. bond distances, charges etc.) also support the above results, which are also as observed experimentally. Highest stability of the crystal structure formed between urea and *meta*-nitrobenzoic acid through H-bonding interaction in methanol with a particular orientation is evident from the data generated from two different *ab initio* based approaches.

8.3 Future Scope:

Development and application Density Functional Reactivity Theory (DFRT) based descriptors is a rapidly growing field of theoretical chemistry in recent years. Understanding the profiles (with respect to reaction co-ordinates) of the energy components of DFRT based stabilization energy is not very much clear and yet to be investigated thoroughly to exploit these components in explaining chemical kinetics and thermodynamics. The emerging future prospect of the present Ph.D. thesis can be broadly divided into three different themes,

- (i) Understanding the full profiles of the components of DFRT based stabilization energies.
- (ii) Exploiting these components to explain reaction kinetics and reaction thermodynamics.
- (iii) Inclusion of the electrostatic and dispersion interaction terms in the decomposition scheme to widen the applicability of these two energy components.

It is relevant to determine the exact nature of the energy profile in terms of different energy components (both raising and lowering ones) against reaction co-ordinate. In principle, the nature of the profiles will help to verify whether the conjectures made in the original CDASE scheme are justified or not. During a particular charge transfer interaction, electron exchange taking place between interacting species. Donor will lose a specific amount of electrons and acceptor will gain equal amount of electrons. In the process, losing and gaining of electrons taking place simultaneously. However, in the present formalism of CDASE scheme, the charge transfer is a discrete process and accordingly energy raising and lowering is not simultaneous. Our group is working on this inherent theoretical challenge. Modification of the CDASE scheme based energy profile in terms of rising and lowering component by considering simultaneous charge transfer process is the primary future scope of the present thesis.

We have investigated a verity of kinetic and thermodynamic aspects of various interesting chemical and biological phenomena ranging from drug-DNA interaction to nanocomposites and from small metallic clusters to non-covalently bonded crystal structure. CDASE scheme based energy parameters found to produce reasonable agreement to the experimental findings. However, there are numerous known organic

reactions, where the impact of kinetic and thermodynamic factors in the overall reaction rate is yet to be explored. For example, the mechanism of multicomponent reaction not very certain and it will be an interesting problem from the computational prospect i.e., to provide a plausible mechanism. It is anticipated, that proposed CDASE scheme has the potential to put new shades on the kinetic and thermodynamic aspects of this kind of organic reactions. It is also observed from the earlier examples that if for a particular interaction kinetic stability is more, corresponding thermodynamic stability are also high. However, in principle, which is not always true. Therefore, there is a scope of improvement in the existing formalism of CDASE scheme by introducing relevant scaling factors to the computed results.

Initially, the charge transfer contribution of the stabilization energy was decomposed into raising and lowering components. However, there are lots of interactions (both bonding and non-bonding) in which, apart from charge transfer, electrostatic as well as dispersion interactions are also important. The question is how to include these two contributions in the evaluation of stabilization energy and further how to decompose them? Will the inclusion of these contributions in the energy components change their profile? All these problems remain to be addressed.

References:

1. P. Geerlings, F. De Proft, W. Langenaeker, *Chem. Rev.* 2003, **103**, 1793.
2. R. G. Parr, R. G. Pearson *J. Am. Chem. Soc.* 1983, **105**, 7512.
3. S. K. Ghosh, M. Berkowitz *J. Chem. Phys.* 1985, **83**, 2976.
4. M. K. Harbola, P. K. Chattaraj, R. G. Parr *Isr. J. Chem.* 1991, **31**, 395.
5. S. Saha, R. K. Roy *J. Phys. Chem. B* 2007, **111**, 9664.
6. W. Yang, R. G. Parr, *Proc. Natl. Acad. Sci. U.S.A.* 1985, **82**, 6723.
7. R. G. Parr, W. Yang *J. Am. Chem. Soc.* 1984, **106**, 4049.
8. W. Yang, W. J. Mortier *J. Am. Chem. Soc.* 1986, **108**, 5708.
9. (a) P. Hohenberg, W. Kohn *Phys. Rev. B* 1964, **136**, 864 (b) W. Kohn, L. Sham *J. Phys. Rev. A* 1965, **140**, 1133. (c) R. G. Parr, D. A. Donnelly, M. Levy, W. E. Palke *J. Chem. Phys.* 1978, **68**, 3801.
10. (a) R. K. Roy, S. Krishnamurti, P. Geerlings, S. Pal *J. Phys. Chem. A* 1998, **102**, 3746 (b) R. K. Roy, F. De Proft, P. Geerlings *J. Phys. Chem. A* 1998, **102**, 7035.
11. (a) S. Krishnamurty, S. Pal *J. Phys. Chem. A* 2000, **104**, 7639 (b) N. Russo, M. Toscano, A. Grand, T. Mineva *J. Phys. Chem. A* 2000, **104**, 4017 (c) T. Mineva, V. Parvanov, I. Petrov, N. Neshev, N. Russo *J. Phys. Chem. A* 2001, **105**, 1959.
12. R. G. Parr, L. Von Szentpály, S. Liu *J. Am. Chem. Soc.* 1999, **121**, 1922.
13. A. T. Maynard, M. Huang, W. G. Rice, D. G. Covell *Proc. Natl. Acad. Sci. USA* 1998, **95**, 11578.
14. E. R. Jamieson, S. J. Lippard *Chem. Rev.* 1999, **99**, 2467.
15. M. A. Fuertes, C. Alonso, J. M. Perez *Chem. Rev.* 2003, **103**, 645.
16. S. E. Sherman, S. J. Lippard *Chem. Rev.* 1987, **87**, 1153.
17. R. S. Go, A. Adjei *J. Clin. Oncol.* 1999, **17**, 409.
18. Y. Jung, S. J. Lippard *Chem. Rev.* 2007, **107**, 1387.
19. R. A. Alderden, D. M. Hall, T. W. Hambley *J. Chem. Educ.* **2006**, **83**, 728.
20. Y. Kasherman, S. Sturup, D. Gibson *J. Med. Chem.* 2009, **52**, 4319.
21. H. C. Harder, B. Rosenberg *Int. J. Cancer* 1970, **6**, 207.
22. J. A. Howle, G. R. Gale *Biochem. Pharmacol.* 1970, **19**, 2757.
23. V. Sresht, J. R. Bellare, S. K. Gupta *Ind. Eng. Chem. Res.* 2011, **50**, 12872.
24. M. Yoshida, A. R. Khokhar, Y. Kido, F. Ali-Osman, Z. H. Siddik *Biochem. Pharmacol.* 1994, **48**, 793.
25. M. E. Palm-Espling, P. Wittung-Stafshede *Biochem. Pharmacol.* 2012, **83**, 874.
26. L. Z. Cubeddu, I. S. Horrmann, T. N. Fuenmayor, A. L. Finn *New Engl. J. Med.* 1990, **322**, 810.
27. A. Sarmah, R. K. Roy *J. Comp. Aided Mol. Des.* 2014 (just accepted).
28. M. S. Dresselhaus, G. Dresselhaus, P. Avouris *Carbon Nanotubes: Synthesis, Structure, Properties and Applications*, Springer, Berlin, Germany 2001.
29. R. Satio, G. Dresselhaus, M. S. Dresselhaus *Physical Properties of Carbon Nanotubes*; Imperial College Press: London, UK, 2003.
30. A. Bianco, K. Kostarelos, C. D. Partidos, M. Prato *Chem. Commun.* **2005**, 571.
31. A. Sarmah, R. K. Roy *J. Phys. Chem. C* 2014, **117**, 21539.
32. A. Bianco, M. Prato *Adv. Mater.* **2003**, **15**, 1765.
33. A. G. Nasibulin et al. *Nat. Nanotechnol.* **2007**, **2**, 156.
34. A. Sarmah, R. K. Roy (Manuscript under preparation).
35. A. Sarmah, S. Saha, P. Bagaria, R. K. Roy, *Chem. Phys.* 2012, **394**, 29.

List of Publications:

1. **Sarmah, A.**; Saha, S.; Bagaria, P.; Roy, R. K., “On the complementarity of comprehensive decomposition analysis of stabilization energy (CDASE) – Scheme and supermolecular approach” *Chem. Phys.* 2012, *394*, 29-35.
2. **Sarmah, A.**; Roy, R. K., “Understanding the Interaction of Aqua-cisplatin with Nucleobase Guanine over Adenine: A Density Functional Reactivity Theory Based Approach” *RSC Adv.* 2013, *3*, 2822-2830.
3. **Sarmah, A.**; Roy, R. K., “Understanding the Interaction of Nucleobases with Chiral Semi-conducting Single-Walled Carbon Nanotubes (SWCNTs): An Alternative Theoretical Approach Based on Density Functional Reactivity Theory (DFRT)” *J. Phys. Chem. C* 2013, *117*, 21539-21548.
4. Sonu; Tiwari, A. K.; **Sarmah, A.**; Roy, R. K.; Saha, S. K., “Study on Photophysical Properties and Prototropic Equilibria of trans-2-[4-(N,N′dimethylaminostyryl)]pyridine” *Dyes and Pigments*, 2014, *102*, 114-125.
5. **Sarmah, A.**; Roy, R. K., “A Density Functional Reactivity Theory Based Approach to Understand the Cisplatin Analogues with Protecting Agents” *J. Comp. Aided Mol. Design.* 2014, *28*, 1153-1173.
6. Rakshit, R.; Ghorai, S.; **Sarmah, A.**; Roy, R. K.; Mukherjee, C., “Inter-Ligand Azo (N=N) Unit Formation and Thereafter Stabilization of A Co(II)–Diradical Complex via Metal–to–Ligand d–p back donation: Synthesis, Characterization, and Theoretical Study” *Dalton Trans.* 2015,*44*, 3724-3727 .
7. **Sarmah, A.**; Roy, R. K., “A Comprehensive Study to Understand the Impact of Fullerene Symmetry on the Kinetic, Thermodynamic, Structural and Electronic Properties of NanoBud” (revised manuscript submitted to *JPC-C*).
8. **Sarmah, A.**; Roy, R. K., “A Density Functional Reactivity Theory Based Approach to Explore the Kinetics and Thermodynamics of the Interaction between Small Atom Gold Clusters and Nucleobases” (Manuscript under preparation).
9. Joshi, S., Kumari, S., **Sarmah, A.**, Bhattacharjee, R., Sakhuja, R., Pant, D. D.,

“Estimation of ground and excited state dipole moments of newly synthesized coumarin-triazole derivatives and application as turn off fluorescence sensor: high sensitivity for iron (III) ions: Experimental and theoretical study” (manuscript under preparation).

10. Ghorai, S. **Sarmah, A.**, Roy, R. K., and Mukherjee, C., “Rational Syntheses of Radical-containing Four and Five-Coordinate Co(III) complexes and Their Distinction via Infrared Spectrum: Experimental and Theoretical Studies" (revised manuscript submitted to Dalton Trans.).
11. Ghorai, S. **Sarmah, A.**, Roy, R. K., and Mukherjee, C., “Effect of Geometrical Distortion on the Electronic Structure: Synthesis and Characterization of Monoradical-Coordinated Two Mononuclear Cu(II) Complexes” (manuscript under preparation)

BRIEF BIOGRAPHY OF Prof. RAM KINKAR ROY

Prof. Ram Kinkar Roy is a Professor in the Department of Chemistry at Birla Institute of Technology and Science (BITS), Pilani. He received his Ph. D. degree from National Chemical Laboratory (NCL), Pune in 1996. For his doctoral degree, he worked with Professor Saurav Pal in the research area of theoretical chemistry more precisely conceptual DFT. After his doctorate, he spent a year at National Chemical Laboratory, Pune, working with Prof. Saurav Pal as a Research Associate (CSIR). As a visiting post-doctoral fellow, he worked with Prof. Paul Geerlings for a year (1997-1998) at Vrije Universiteit Brussel, Belgium and with Prof. Kimihiko Hirao in 1998-2001 at the University of Tokyo, Tokyo. He joined BITS, Pilani in 2001 and since then he has been here. He has been involved in research for the last 25 years and in teaching for 14 years. As a result of his research accomplishment, he has around 40 international publications and presently handling a DST project. Currently, Prof. Roy is guiding three Ph. D. students.

BRIEF BIOGRAPHY OF AMRIT SARMAH

Mr. Amrit Sarmah, author of the present thesis, completed his M. Sc. (Hons.) in Chemistry from North-Eastern Hill University, Shillong, Meghalaya in 2009. Subsequently, he has joined Department of Chemistry, BITS Pilani for his doctoral studies under Prof. Ram Kinkar Roy and received DST-JRF and SRF along with UGC-BSR fellowship for his research work. He has been awarded the Royal Society of Chemistry international travel grant to attend the Faradays Discussion meeting 173 in London (unable to attend due to some technical problems). As a Ph. D. scholar, he has received a fully funded trip to Weizmann Institute of Science, Israel to present his research work. During his visit to Israel, he delivered lectures at the Hebrew University, Technion-Israel Institute of Science and Bar-Ilan University. He has published quality research articles in highly reputed international journals and presented papers in a number of national and international conferences/symposiums.